

Coenzyme A biosynthesis and Coenzyme A-dependent redox processes as targets for anti-staphylococcal drug development

Wessel Johannes Albertus Moolman

Dissertation presented for the degree of Doctor of
Philosophy (Biochemistry) in the
Faculty of Natural Sciences at
Stellenbosch University



Supervisor: Prof. Erick Strauss

December 2015

Declaration

By submitting this dissertation electronically, I declare that the entirety of the work contained therein is my own, original work, that I am the owner of the copyright thereof (unless to the extent explicitly otherwise stated), that reproduction and publication thereof by Stellenbosch University will not infringe any third party rights and that I have not previously in its entirety or in part submitted it for obtaining any qualification.

.....

Signature

2015-10-07.....

Date

Summary

Staphylococcus aureus, the bacterium that causes most hospital-acquired infections in humans is rapidly becoming more prevalent in the community and, alarmingly, increasingly resistant to the current arsenal of available antibacterial agents. More than ever, new treatments are urgently needed to combat this threat. In this study we proposed an alternative strategy to current drug development methodologies that entails the identification and targeting of processes that are essential to the survival of pathogenic bacteria in their human host, i.e. where they need to counter the defences of the human immune system. In particular, the focus of this study is the importance of the central metabolic cofactor coenzyme A (CoA) in the defence mechanisms that *S. aureus* employs under such circumstances, and therefore on the targeting of CoA biosynthesis and enzymology as potential antistaphylococcal targets.

The viability of coenzyme A disulfide reductase (CoADR) as a potential antistaphylococcal drug target was evaluated. The *S. aureus* CoADR (SaCoADR) enzyme structures in complex with mechanism-based Michael acceptor-containing inhibitors were examined; specifically how its interaction with these compounds relates to the observed differences in activity between them. Consequently, the observed enzyme inhibition could be adequately explained when taking into account the chemical properties of the inhibitors in combination with their interactions with SaCoADR. Also, the structural data in the study provided a strong starting point for future inhibitor design. The reasons for the poor correlation between the *in vitro* inhibition of SaCoADR by the Michael acceptor-containing CoA analogues and the whole cell inhibition of *S. aureus* by their corresponding pantothenamide precursors were investigated and these results led us to the conclusion that the poor correlation is due to SaCoADR not being essential under normal growth conditions. However, our results suggest that under conditions where CoA levels are sufficiently reduced, CoADR might become relevant, even under normal growth conditions. This opens the door for studies on the possible synergistic effects of CoADR inhibitors and compounds that reduce CoA levels; such combinations most likely hold the most potential for work focused on CoADR as a drug target.

The mechanism of inhibition of phosphopantothenoylcysteine synthetase (PPCS) enzymes by 4'-phospho-CJ-15,801-cytidylate (PCJ-CMP) was investigated by determining the basis for the apparent stability of the inhibitor. We showed that the PPCS protein itself plays no role in the mechanism of inhibition by PCJ-CMP, but that the introduction of the double bond in the β -alanine moiety of the substrate with its extra π -electrons renders the acyl phosphate resistant to nucleophilic attack by introducing new, stable resonance forms. This mechanism of apparent stabilisation *via* resonance was also applied to an unrelated system and we were able to convert substrates of human VNN1 pantetheinase into inhibitors of the enzyme. These studies allowed us to rationalise the tight-binding inhibition observed for PCJ-CMP. Additionally, we uncovered a new strategy whereby β -alanine-containing compounds can be rendered resistant to hydrolysis and/or acyl transfer; this strategy can likely have wide-ranging applications in the design of such small molecule inhibitors and therapeutics.

Opsomming

Staphylococcus aureus, die bakterium verantwoordelik vir die grootste hoeveelheid hospitaalverworwe infeksies in mense, is vinnig besig om meer wydverspreid in die gemeenskap voor te kom terwyl dit besig is om meer weerstandbiedig te raak teen die huidige arsenaal van antimikrobiese middels. Nuwe behandelinge word nou meer as ooit benodig om hierdie bedreiging te bekamp. In hierdie studie stel ons 'n alternatiewe strategie voor teenoor huidige antibiotiese ontwikkelingsmetodologieë wat die indentifisering en teiken van prosesse behels wat essensieël is vir die oorlewing van patogeeniese bakterieë binne hul menslike gasheer; of te wel, waar hulle nodig het om die verdedigingsmeganismes van die menslike immuunsisteem teen te werk. Dienooreenkomstig is die fokus van die studie die belangrikheid van die sentrale metaboliese kofaktor koënsiem A (KoA) in die verdedigingsmeganismes wat *S. aureus* gebruik onder hierdie toestande en gevolglik op die evaluering van KoA-biosintese en ensiemologie as potensiële antistafilokokale teikens.

Die lewensvatbaarheid van koënsiem A disulfied reductase (KoADR) as 'n potensiële antistafilokokale teiken is geëvalueer. Die *S. aureus* KoADR (SaKoADR) ensiemstrukture in kompleks met meganisme-gebaseerde Michael-akseptor-bevattende inhibeerders is ondersoek; spesifiek hoe die interaksie met hierdie verbindings betrekking het tot die waargenome verskille in hul aktiwiteite. Gevolglik kon die waargenome ensieminhibisie voldoende verduidelik word met inagneming van die chemiese eienskappe van die inhibeerders in kombinasie met hul interaksie met SaKoADR. Die strukturele data in die studie verskaf 'n sterk beginpunt vir toekomstige inhibitorontwerp. Die basis vir die swak korrelasie tussen die *in vitro* inhibisie van SaKoADR deur die Michael-akseptorbevattende KoA-analoë en die bakterieële groeiinhibisie van *S. aureus* deur hulle ooreenstemmende pantoteenamied voorlopers is ondersoek en die resultate het aangetoon dat dit te wyte is aan die feit dat SaKoADR nie noodsaaklik onder normale groeitoestande is nie. Desnieteenstaande dui die resultate daarop dat onder omstandighede waar KoA-vlakke voldoende verminder is, KoADR dalk relevant sal word, selfs onder normale groeitoestande. Dit lê die grondslag vir studies op die moontlike sinergistiese effek van KoADR-inhibeerders met verbindings wat KoA-vlakke verminder; sulke kombinasies het waarskynlik die meeste potensiaal vir werk gefokus op KoADR as 'n antistafilokokale teiken.

Die meganisme van inhibisie van fosfopantotenoïelsisteïen-sintetase (FPS) ensieme deur 4'-fosfo-CJ-15,801-sitidilaat (FCJ-SMP) is ondersoek deur die bepaling van die basis vir die oënskynlike stabiliteit van die inhibeerder. Ons het bewys dat die FPS proteïen self geen rol speel in die meganisme van inhibisie deur FCJ-SMP nie, maar dat die invoeging van die dubbelbinding in die β -alanien groep van die substraat met sy ekstra π -elektrone die asielfosfaat weerstandbiedig maak teen nukleofiele-aanval deur die vorming van nuwe, stabiele resonansvorme. Die meganisme van stabilisering deur resonansie is ook toegepas op 'n onverwante stelsel en ons was in staat om substrate van menslike VNN1 pantoteïnase te omskep in inhibeerders van die ensiem. Hierdie studies het ons in staat gestel om die styf-bindende inhibisie waargeneem vir FCJ-SMP te rasionaliseer. Daarbenewens stel ons 'n nuwe strategie bekend waardeur β -alanien-bevattende verbindings bestand gemaak kan word teen hidrolise en / of asiel-oordrag; hierdie strategie kan waarskynlik 'n wye toepassing hê in die ontwerp van sulke klein-molekule inhibeerders en terapieë.

The financial assistance of the National Research Foundation (NRF) towards this research is hereby acknowledged. Opinions expressed and conclusions arrived at, are those of the author and are not necessarily to be attributed to the NRF.

"The mind is not a vessel to be filled, but a fire to be kindled."

— Plutarch

Acknowledgements

Completing a PhD study is no trivial task and entirely impossible by oneself and therefore I need to thank everyone who helped me along the way. First, I'd like to thank my PhD supervisor, Erick Strauss for his continual support, guidance and patience throughout this project. Erick, thank you for taking a chance on me and giving me the opportunity to join your lab. You have put together a great group of people that is a pleasure to work alongside with and you created an excellent environment in which to work successfully, while being constantly challenged. The last five years spent on this project has helped me mature from a hesitant student interested in science, into a critical thinking scientist and has also given me the confidence to pursue a career as a researcher.

All the Strauss-lab members, past and present, thank you all for the encouragement, help with experiments that refuse to work (and the ones that did), chats during coffee time and generally just making me look forward to spending time in the lab.

To all my family and friends, thank you for your encouragement and interest and pretending to understand what I spent most of my waking hours doing over the last few years. Lastly, to Liana Swart, thank you for all your love and support and always believing in me, even the times when I didn't believe in myself.

Additional Acknowledgements

- The University of Stellenbosch for the opportunity to study at this institution.
- Financial assistance from the National Research Foundation (NRF), the Ernst & Ethel Ericksen Trust and Prof. Erick Strauss.
- Dr. D.J. Brand and Ms. Elsa Malherbe of the NMR-unit of the Central Analytical Facility of the University of Stellenbosch.
- Dr. Marietjie Stander of the MS-unit of the Central Analytical Facility of the University of Stellenbosch.
- Prof. Carine Smith and Ms. Kelly Petersen for assistance with neutrophil isolations.

Table of contents

<i>Declaration</i>	<i>ii</i>
<i>Summary</i>	<i>iii</i>
<i>Opsomming</i>	<i>iv</i>
<i>Acknowledgements</i>	<i>vii</i>
<i>Additional acknowledgements</i>	<i>viii</i>
<i>Table of contents</i>	<i>ix</i>
<i>List of abbreviations</i>	<i>xiii</i>

CHAPTER 1: INTRODUCTION AND BACKGROUND	1
1.1 ANTIMICROBIAL RESISTANCE AND THE NEED FOR NEW ANTIMICROBIAL TARGETS	1
1.2 HUMAN INNATE IMMUNE SYSTEM.....	3
1.2.1 <i>Epithelial surfaces help prevent infection</i>	3
1.2.2 <i>Recognition of conserved features of pathogens by human cells</i>	3
1.2.3 <i>Complement activation marks pathogens for phagocytosis or lysis</i>	4
1.2.4 <i>Toll-like proteins are pattern recognition receptors</i>	4
1.2.5 <i>Phagocytic cells engulf and destroy pathogens</i>	4
1.3 <i>S. AUREUS</i> DEFENCE MECHANISMS AGAINST THE HUMAN INNATE IMMUNE SYSTEM	5
1.3.1 <i>Overview</i>	5
1.3.2 <i>Resistance to oxidative stress: Direct elimination of reactive oxygen species</i>	6
1.3.3 <i>Resistance to oxidative stress: Thiol-disulfide interchange reactions</i>	8
1.3.4 <i>Conclusion</i>	16
1.4 RESEARCH QUESTION.....	17
1.5 REFERENCES	17

CHAPTER 2: RECENT ADVANCES IN TARGETING COENZYME A BIOSYNTHESIS AND UTILIZATION FOR ANTIMICROBIAL DRUG DEVELOPMENT	25
2.1 MINI-REVIEW	25
2.2 SUMMARY OF MINI-REVIEW	41
2.3 PREVIOUS COADR RESEARCH	41
2.4 PREVIOUS RESEARCH ON THE INHIBITION OF PPCS BY CJ-15, 801	42
2.5 REFERENCES	42
CHAPTER 3: EVALUATION OF COADR AS AN ANTI-STAPHYLOCOCCAL DRUG TARGET	43
3.1 INTRODUCTION.....	43
3.2 RESULTS	48
3.2.1 <i>Structural characterisation of the SaCoADR–CoA analogue inhibitor interactions</i>	<i>48</i>
3.2.2 <i>Relative importance of conserved Tyr-residues for SaCoADR activity</i>	<i>52</i>
3.2.3 <i>Lack of whole cell inhibition: a case of poor permeability?</i>	<i>53</i>
3.2.4 <i>Confirming the metabolic activation of pantothenamides in S. aureus.....</i>	<i>54</i>
3.2.5 <i>Establishing target-specificity for the Michael acceptor-containing CoADR inhibitors.....</i>	<i>56</i>
3.2.6 <i>Evaluating S. aureus’s resistance to chemically-induced oxidative stress in selected genetic backgrounds.....</i>	<i>58</i>
3.2.7 <i>Evaluating S. aureus’s resistance to neutrophil-induced oxidative stress in selected genetic backgrounds.....</i>	<i>60</i>
3.2.8 <i>Evaluating the effect of reduced CoA levels in selected genetic backgrounds.....</i>	<i>61</i>
3.3 DISCUSSION.....	62
3.4 MATERIALS AND METHODS	65
3.4.1 <i>ADP-coupled Sepharose affinity resin</i>	<i>66</i>
3.4.2 <i>SaCoADR wt and mutants overexpression and purification.....</i>	<i>66</i>
3.4.3 <i>Synthesis of the CoADR substrate (oxidation of CoA to CoA disulfide)</i>	<i>67</i>
3.4.4 <i>SaCoADR activity assay</i>	<i>68</i>
3.4.5 <i>Biosynthesis of CoA analogues from pantothenamide precursors.....</i>	<i>68</i>

3.4.6	<i>Liquid chromatography mass spectrometry (LC–MS) analysis</i>	68
3.4.7	<i>Synthesis of relevant compounds</i>	69
3.4.8	<i>S. aureus whole cell inhibition assay</i>	71
3.4.9	<i>Dose-response of H₂O₂ against S. aureus</i>	71
3.4.10	<i>S. aureus overnight stress test with H₂O₂ and diamide</i>	71
3.4.11	<i>Isolation of human neutrophils</i>	72
3.4.12	<i>Neutrophil bactericidal assay</i>	72
3.5	REFERENCES	72
CHAPTER 4: CHARACTERIZATION OF THE MECHANISM OF INHIBITION OF THE NATURAL PRODUCT CJ-15,801, A SELECTIVE INHIBITOR OF STAPHYLOCOCCUS AUREUS		77
4.1	INTRODUCTION.....	77
4.2	RESULTS	79
4.2.1	<i>A constrained binding pose as a basis for increased inhibitor stability</i>	79
4.2.2	<i>Enzyme structure stabilisation as a basis for inhibition by PCJ-CMP</i>	80
4.2.3	<i>Inhibitor stability based on the inherent electronic properties of the molecule</i>	91
4.2.4	<i>Application of the findings to an unrelated system: hydrolytic stability of modified pantetheinase (Vanin) substrates</i>	93
4.3	DISCUSSION.....	96
4.4	MATERIALS AND METHODS	98
4.4.1	<i>Overexpression and purification of PPCS enzymes</i>	99
4.4.2	<i>Overexpression and purification of His-MtCoaBC</i>	99
4.4.3	<i>Protein Melting Temperature Determinations and Analysis</i>	99
4.4.4	<i>PPCS Inhibition Assays and Data Analyses</i>	100
4.4.5	<i>Progress curve analysis</i>	101
4.4.6	<i>Stopped-flow fluorimetry</i>	102
4.4.7	<i>Fluorescamine assay of pantetheinase activity</i>	103

4.4.8	<i>Continuous enzyme coupled assay of pantetheinase activity</i>	103
4.4.9	<i>Synthesis of model system compounds</i>	104
4.5	REFERENCES	108
CHAPTER 5: GENERAL CONCLUSIONS AND FUTURE WORK		112
5.1	SUMMARY OF RESULTS OBTAINED.....	112
5.1.1	<i>CoADR as an antistaphylococcal drug target</i>	112
5.1.2	<i>Relevance of CoADR, BSH and a putative FDR to survival of S. aureus challenged with oxidative stress conditions</i>	113
5.1.3	<i>Mechanism of inhibition of PPCS by the natural product CJ-15,801</i>	113
5.2	FUTURE STUDIES	114
5.2.1	<i>S. aureus redox balance</i>	114
5.2.2	<i>Hydrolysis resistant substrate analogues</i>	114
5.3	FINAL REMARKS	115
5.4	REFERENCES.....	115
APPENDIX: PUBLICATIONS		116

Abbreviations

aq.	Aqueous	
ADP	Adenosine 5'-diphosphate	
Ahp	Alkylhydroperoxide	
AHR	Alkylhydroperoxide reductase	
Asp	Aspartate	
Asn	Asparagine	
ATP	Adenosine 5'-triphosphate	
Boc	tert-butyl carbonate	
BSH	Bacillithiol	
BSSB	Bacillithiol disulfide (oxidised BSH)	
BuLi	n-butyl lithium	
Cbz	Carbobenzoxy	
CA-MRSA	Community associated MRSA	
CJ	CJ-15,801	
CoA	Coenzyme A	
CoaA	Pantothenate kinase	
CoaB	Phosphopantothenoylcysteine synthetase	
CoaBC	Bifunctional phosphopantothenoylcysteine synthetase/ cysteine decarboxylase	phosphopantothenoyl-
CoaD	Phosphopantetheine adenylyltransferase	
CoaE	Dephospho-coenzyme A kinase	
CoASH	Coenzyme A (reduced)	
(CoAS) ₂	CoA disulfide (oxidised CoA)	
CoADR	CoA disulfide reductase	
CMP	Cytidine 5'-monophosphate	
CTAB	Cetyltrimethylammonium bromide	
CTP	Cytidine 5'-triphosphate	
CSA	10-Camphorsulfonic acid	
Cys	Cysteine	

DCM	Dichloromethane
DMAP	<i>N,N</i> -dimethyl aminopyridine
DMF	<i>N,N</i> -Dimethylformamide
DMSO	Dimethyl sulfoxide
DPCK	Dephospho-coenzyme A kinase
DTNB	5,5-Dithiobis-(2-nitrobenzoic acid)
DTT	Dithiothreitol
<i>E. coli</i>	<i>Escherichia coli</i> (also <i>Ec</i>)
EDC	1-(3-Dimethylaminopropyl)-3-ethylcarbodiimide
Eq	equivalents
ESI-MS	Electrospray Ionisation Mass Spectroscopy
EtOH	Ethanol
EtOAc	Ethyl acetate
EWG	Electron withdrawing group
FAD	Flavin adenine dinucleotide
FDA	United States Food and drug administration
FDR	Flavoprotein disulfide reductases
GSH	Glutathione
GSSG	Glutathione disulfide
GR	Glutathione reductase
H ₂ O ₂	Hydrogen peroxide
HA-MRSA	Hospital-acquired MRSA
His	Histidine
HOBt	<i>N</i> -Hydroxybenzotriazole
HPLC	High Performance Liquid Chromatography
HOCl	Hypochlorite
<i>Hs</i>	<i>Homo sapiens</i>
IC ₅₀	Concentration required for 50% inhibition
IMAC	Immobilized Metal Affinity Chromatography
IPTG	Isopropyl β-D-1-thiogalactopyranoside
KatA	Catalase

k_{cat}	Turnover number
K_i^{app}	Apparent dissociation constant of enzyme inhibitor complex
K_i	Dissociation constant of enzyme inhibitor complex
k_{obs}	Rate of inactivation
K_m	Michaelis constant
LB	Luria Bertani
LC-MS	Liquid Chromatography Mass Spectrometry
LogD	logarithm of the distribution coefficient
LogP	logarithm of the partition coefficient
LMWT	Low molecular weight thiol
LipDH	Lipoamide dehydrogenase
MeCN	Acetonitrile
MerA	Mercuric ion reductase
MeOH	Methanol
MIC	Minimum inhibitory concentration
MR	Mycothione reductase (also Mycothiol disulfide reductase)
MRSA	Methicillin resistant <i>Staphylococcus aureus</i>
MSH	Mycothiol
<i>M. tuberculosis</i>	<i>Mycobacterium tuberculosis</i> (also <i>Mt</i>)
NADH	Nicotinamide adenine dinucleotide (reduced)
NADPH	Nicotinamide adenine dinucleotide phosphate (reduced)
NEM	<i>N</i> -ethyl morpholine
NMR	Nuclear Magnetic Resonance Spectroscopy
NO	Nitric oxide
NO^{3-}	Peroxynitrite
O^{2-}	Superoxide
OD	Optical density
OH·	Hydroxyl radical
Pan	Pantothenic acid (also PanCOOH)
PanK	Pantothenate kinase
PCJ	4'-Phospho-CJ-15,801

PCJ-CMP	4'-Phospho-CJ-15,801-cytidylate
PEP	Phosphoenolpyruvate
PhH	Benzene
PhMe	Toluene
PMB	<i>p</i> -Methoxybenzylidene
PNDOR	Pyridine nucleotide disulfide oxidoreductase
PPan	4'-Phosphopantothenate
PPan-CMP	4'-Phosphopantothenoyl-cytidylate
PPAT	Phosphopantetheine adenylyltransferase
PPCS	Phosphopantothenoylcysteine synthetase
PPCDC/CoaC	Phosphopantothenoylcysteine decarboxylase
PPi	Inorganic pyrophosphate
Prx	Peroxiredoxin
<i>p</i> -TsOH	<i>p</i> -Toluenesulfonic acid
ROS	Reactive oxygen species
RNS	Reactive nitrogen species
rt	Room temperature
<i>S. aureus</i>	<i>Staphylococcus aureus</i> (also <i>Sa</i>)
SaCoADR	<i>Staphylococcus aureus</i> CoA disulfide reductase
SDS PAGE	Sodium dodecyl sulphate polyacrylamide gel electrophoresis
SOH	Sulfenic acid
SO ₂ H	Sulfinic acid
SO ₃ H	Sulfonic acid
<i>Sp</i>	<i>Streptococcus pneumoniae</i>
SPE	Solid phase extraction
TBHP	Tertiary butylhydroperoxide
TFA	Trifluoroacetic acid
TFP	Trx fold class of proteins
THF	Tetrahydrofuran
TLR	Toll-like receptor
<i>T_m</i>	Melting temperature

TR	Trypanothione reductase
Trx	Thioredoxin
TLC	Thin Layer Chromatography
TRIS	Tris(hydroxymethyl)aminomethane
Tyr	Tyrosine
V_{\max}	Maximum reaction rate
VRSA	Vancomycin-resistant <i>S. aureus</i>
wt	wild-type

Chapter 1: Introduction and background

1.1 Antimicrobial resistance and the need for new antimicrobial targets

During the past 75 years of antimicrobial drug use bacteria have developed—and are still developing—incredibly efficient mechanisms to ensure survival in antibiotic-containing environments. The resistance to antimicrobial agents within a wide range of pathogenic organisms is a growing threat to public health. According to a recent global surveillance report by the World Health Organisation, high levels of antimicrobial resistance are already prevalent in all of the 114 countries that submitted data for the study [1]. Consequently, if current trends continue, a post-antibiotic era in which common infections can once again kill, is a very real possibility for the 21st century.

The problem of antimicrobial resistance is two-fold: first, pathogenic organisms—especially bacteria—rapidly acquire immunity against antibiotics *via* random mutation and/or through the exchange of plasmids. Second, the pool of effective antibiotics is diminishing rapidly. What is particularly alarming is that most of the antibiotic classes being used today were discovered before the 1960s and that between 1962 and 2000 no new major classes of antibiotics were discovered (Figure 1.1) [2]. In addition, most of the antibiotic classes introduced since 2000 affect the same targets within pathogenic bacteria as existing antibiotics and are therefore potentially vulnerable against existing resistance mechanisms.

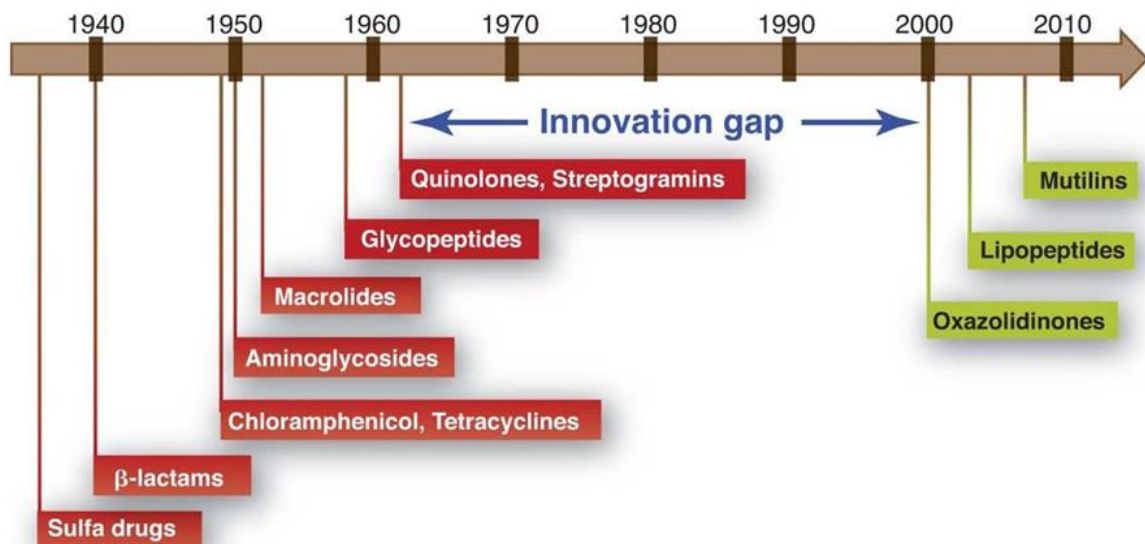


Figure 1.1: No major classes of antibiotics were discovered between 1962 and 2000 [1, 2].

Of particular significance are the so-called “ESKAPE” pathogens (*Enterococcus faecium*, *Staphylococcus aureus*, *Klebsiella pneumoniae*, *Acinetobacter baumannii*, *Pseudomonas aeruginosa*, and *Enterobacter* species) that account for most antibiotic-resistant infections in hospitals [3]. Of special interest to this study is

S. aureus, which historically has rapidly developed resistance against newly introduced anti-staphylococcal agents. Among the most significant of these agents is methicillin, of which resistant *S. aureus* strains were isolated as early as 1961 [4]. More recently resistant *S. aureus* strains have been identified against linezolid in 2001 [5] and daptomycin in 2005 [6]. It is therefore not surprising that resistance to vancomycin (which was discovered in the 1950s and has been the last line of treatment for several years) has also been identified in *S. aureus* [3, 7, 8]. In the United States methicillin-resistant *S. aureus* (MRSA) infections are estimated to be the leading cause of annual fatalities by infectious agents and exceed the number of deaths due to HIV/AIDS [2, 9]. Alarmingly, over the past few years community-associated MRSA (CA-MRSA) has also emerged rapidly and in 2008 it accounted for approximately 60% of clinical *S. aureus* strains isolated from intensive care units in the United States [10]. Fortunately, in May 2014 the United States Food and Drug Administration approved dalbavancin, a new lipoglycopeptide (which puts it in the same class as vancomycin) for the treatment of *S. aureus* and *Streptococcus pyogenes* infections. Dalbavancin has been shown to have activity against a broad range of Gram-positive pathogens, including MRSA [11], which makes it an extremely welcome addition to the current antibiotic arsenal.

The increased prevalence of infections caused by resistant strains of *S. aureus* demands not only a fundamental review of antimicrobial use and development of new agents, but also a reassessment of current research approaches to overcome drug resistance [12]. To achieve this goal, new lead compounds and previously unexploited targets need to be identified to develop novel drugs. Considering that all of the antibiotic classes introduced since 2000 affect the same targets within pathogenic bacteria as existing antibiotics, they may suffer from exactly the same problems as previous ones due to existing antibiotic resistance mechanisms. If a new drug is introduced targeting a previously unexploited process in a pathogenic bacterium, it should require the pathogen far more time to develop resistance against such compounds; since there are no existing resistance mechanisms against the targeted process. This should in turn relieve the pressure on currently available treatments. The main strategies whereby drug development has been approached to date have been to use phenotypic screening to identify lead compounds [13-15], while new targets have been identified through comparative genomics approaches and gene essentiality studies [16-18]. However, an alternative strategy that has not been fully exploited to date would be to identify processes that are essential to the survival of the bacteria in the human host, where they need to counter the defences of the human immune system. As such, this study focuses on the importance of the central metabolic cofactor coenzyme A (CoA) in the defence mechanisms that *S. aureus* employs under such circumstances, and therefore on the targeting of CoA biosynthesis and enzymology as potential antistaphylococcal targets. As background to the experimental work and to provide context for the study as a whole, the remainder of the current chapter summarises the main aspects of the human innate immune system, since this is the most relevant to protect against *S. aureus* infection. An overview of the bacterial defence mechanisms against the human innate immune system is also provided, with a special focus on the role of relevant low molecular weight thiols (LMWTs).

1.2 Human innate immune system

Our ability to avoid infection depends partly on the adaptive immune system, which recognises pathogens with high specificity from previous encounters and destroys them upon subsequent exposure. However, these responses are slow to develop upon first contact with a new pathogen and it can take approximately a week before the responses are effective. The problem is that, by contrast, a single bacterium with a doubling time of one hour can produce almost 20 million progeny, a full-scale infection, within 24 hours. Therefore, during the first critical hours and days of contact with a new pathogen we rely on our innate immune system to protect us from infection. Innate immune responses are not specific to a particular pathogen in the way that the adaptive immune responses are. These are dependent on a group of proteins and phagocytic cells to recognize conserved features of pathogens and become quickly activated to help eradicate invading organisms. Whereas the adaptive immune system evolved less than 500 million years ago exclusively in vertebrates, innate immune responses have been found among both vertebrates and invertebrates (as well as in plants) and the basic mechanisms that regulate them are conserved. Also, the innate immune responses in vertebrates are also required to activate adaptive immune responses [19]. Of particular significance to this study is the interaction of *S. aureus* with the phagocytic cells of the innate immune system as this is crucial for its proliferation of infection [20, 21]. A brief overview of the main parts of the innate immune system is presented below.

1.2.1 Epithelial surfaces help prevent infection

The skin and other epithelial surfaces protect vulnerable cells and organs by providing a physical barrier between the inside of the body and the outside world. These surfaces contain constricted intersections between neighbouring cells that prevent easy entry by potential pathogenic organisms. The interior epithelial surfaces are also covered with a mucus layer that protects against microbial invasion as well as against mechanical and chemical damage. The slimy mucus coating consists of secreted mucin and other glycoproteins, which physically prevent pathogens from adhering to the epithelium. Additionally, it also facilitates their clearance by beating cilia on the epithelial cells. The other significant protection granted by the mucus layer is mediated by substances that kill pathogens or inhibit their growth. The most abundant of these are defensins, which are generally short (12–50 amino acids) and positively charged antimicrobial peptides that also contain hydrophobic or amphipathic domains [22]. The defensins are part of a diverse family with a broad spectrum of antimicrobial activity that is active against Gram-negative and Gram-positive bacteria, fungi, various parasites and even enveloped viruses, such as HIV [19].

1.2.2 Recognition of conserved features of pathogens by human cells

Inevitably, microorganisms manage to occasionally breach the epithelial barriers, which can then lead to infection. The body then relies on the innate and adaptive immune systems to first recognize and subsequently destroy these invading organisms, while causing as little harm as possible to the host cells. The innate immune system recognises specific types of molecules that are common to many pathogens, but

are absent in the host. Once these pathogen-associated molecules are recognised, two types of innate immune responses are stimulated: inflammatory responses and phagocytosis (by cells such as neutrophils and macrophages). Significantly, both of these responses can occur rapidly without the host ever being previously exposed to the invading pathogen [19].

1.2.3 Complement activation marks pathogens for phagocytosis or lysis

The complement system represents a network of about 20 cooperating soluble proteins, produced mainly in the liver, that circulate in the blood and extracellular fluid. Most are inactive and serve as pattern recognition receptors that can be activated directly by pathogen-associated immunostimulants. The early complement components are activated first and consist of three distinct pathways: the classical pathway, the lectin pathway, and the alternative pathway [23]. These early components are all pro-enzymes, which are activated sequentially by proteolytic cleavage. Specifically, the cleavage of each pro-enzyme in the series activates the next component to generate a (serine) protease, which then cleaves the next pro-enzyme in the series one after another. Each activated enzyme cleaves many molecules of the next pro-enzyme in the chain; therefore the activation of the early components leads to an amplifying, proteolytic cascade. Many of these cleavages release biologically active compounds that can promote an inflammatory response, enhance phagocytosis of pathogenic cells or assist with the catalysis of subsequent steps in the complement cascade [19].

1.2.4 Toll-like proteins are pattern recognition receptors

The Toll-like receptor (TLR) family are responsible for triggering host cell gene expression in response to pathogens. Humans express at least ten TLRs, several of which have been shown to play crucial roles in the innate immune recognition of pathogen-associated immunostimulants. TLR activation stimulates the expression of molecules that both initiate an inflammatory response and induce adaptive immune responses [24]. TLRs are found on the surface of macrophages and neutrophils, as well as on the epithelial cells lining the lung and gut. They serve to alert both the innate and adaptive immune systems of an impending infection [19].

1.2.5 Phagocytic cells engulf and destroy pathogens

The previous parts of the innate immune system are involved with either preventing pathogen entry into the body, or recognition of the pathogen for phagocytosis or lysis. The way in which invading pathogens are disposed of shortly after their recognition, is *via* engulfment by a phagocytic cell. There are two major classes of phagocytic cells. Macrophages are long-lived cells that reside in tissues throughout the body and are especially abundant in the lungs and gut, but are also present in large numbers in connective tissues, the liver, and the spleen. These cells are usually among the first to encounter invading pathogens. Neutrophils are short-lived cells, which are abundant in blood but are not found in normal, healthy tissues. They are

rapidly recruited to sites of infection both by activated macrophages and by molecules released by the microbes themselves [19]. Macrophages and neutrophils contain a variety of cell-surface receptors that enable them to recognize and engulf pathogens. Ligand binding to any of these receptors induces actin polymerization at the site of pathogen attachment, causing the phagocyte's plasma membrane to surround the pathogen and engulf it in a large membrane-enclosed phagosome.

Importantly, once the pathogen has been phagocytosed, the macrophage or neutrophil releases a vast array of microbicidal compounds to destroy it. The phagosome is acidified and fuses with lysosomes, which contain lysozyme and acid hydrolases that can degrade bacterial cell walls and proteins. Probably the most important attack is the respiratory (or oxidative) burst. An NADPH oxidase complex is assembled on the phagosomal membrane that catalyses the production of a series of highly toxic reactive oxygen (ROS) and reactive nitrogen species (RNS), including superoxide (O_2^-), hypochlorite (HOCl), hydrogen peroxide (H_2O_2), hydroxyl radicals (OH^\cdot), and nitric oxide (NO). These toxic compounds are produced together with a transient increase in oxygen consumption by the pathogenic cells, which makes this strategy highly effective [19]. However, if the pathogen is not killed by the oxidative burst and manages to escape the phagosome it is free to proliferate and cause infection until the adaptive immune system is able to combat it; at which time it is usually too late to stop the infection and save the host.

1.3 *S. aureus* defence mechanisms against the human innate immune system

1.3.1 Overview

Generally, the human innate immune system is extremely successful at protecting us from infection, but due to co-evolution, pathogenic bacteria have developed numerous efficient systems to circumvent these defences. Gram-positive bacteria have developed proficient strategies to avoid ingestion by phagocytes. For instance, certain bacteria are surrounded by a thick, slimy polysaccharide capsule that is not recognized by the complement system or any phagocyte receptor. *S. aureus* also produces effective anti-inflammatory molecules and employs numerous mechanisms to protect itself against the many aspects of the innate immune system, which include host cationic antimicrobial molecules, defensin-like peptides and bacteriolytic enzymes such as lysozyme. Significantly, certain *S. aureus* genes that assist with escape from innate host defences are conserved in many human pathogens, which suggest that the underlying mechanisms are of general significance in bacterial virulence [20]. However, what sets *S. aureus* apart from many other bacteria is its interaction with the phagocytic cells of the innate immune system and this is also crucial for its proliferation of infection [20, 21]. The success of *S. aureus* to survive and cause infection in its host can mostly be attributed to its ability to detoxify the products of the respiratory burst and ultimately escape the phagosome entirely.

The significance of the oxidative stress resistance of *S. aureus* was illustrated in a previous study on hospital-acquired MRSA (HA-MRSA) and CA-MRSA strains, which showed that even though *S. aureus* was exposed to neutrophil antibacterial components, there was significant survival after phagocytosis [25]. Moreover, not only did the strains show the ability to survive attack by neutrophils, but also caused subsequent neutrophil lysis. A microarray-based assay during the same study evaluated the global changes

in the *S. aureus* transcriptome upon phagocytosis by neutrophils and revealed that the oxidative stress response genes are significantly up-regulated [25]. This provides a basis explaining why this particular pathogen is so effective in surviving the ROS-based killing mechanisms of neutrophils and macrophages. It is therefore necessary to examine the major defences protecting the organism against damage caused by ROS and RNS.

1.3.2 Resistance to oxidative stress: Direct elimination of reactive oxygen species

The first reason why *S. aureus* is incredibly successful at dealing with oxidative stress is due to its highly efficient removal of ROS. The organism responds to oxidative stress directly through the action of enzymes such as the Mn²⁺-dependent superoxide dismutases (SodA and SodM) [26] that neutralize superoxide, and catalase (KatA) [27, 28], peroxiredoxins (Prxs) and other members of the thioredoxin (Trx) fold class of proteins (TFPs) that degrade hydrogen peroxide [29].

Superoxide dismutases (SODs) are metalloproteins that catalyse the dismutation of the superoxide anion (O₂⁻), which is produced by the reduction of oxygen. The conversion of O₂⁻ to H₂O₂ and O₂ not only protects against direct damage caused by the highly reactive O₂⁻, but also against indirect O₂⁻ toxicity by preventing a Fe³⁺-dependent catalytic reaction that leads to the formation of a hydroxyl radical (OH·) *via* the Haber–Weiss reaction [30]. It has also been shown that O₂⁻ can reduce hypochlorous acid (HOCl), a potent oxidant derived from the interaction of H₂O₂ with phagocyte-derived peroxidases, to form OH· [31, 32]. *S. aureus* has two SOD-encoding genes, *sodA* and *sodM*. The proteins expressed by these genes combine to form three active SOD dimers: two homodimers and a heterodimer [33, 34]. *In vitro* data so far indicate that the SodA homodimer is responsible for the majority of the *S. aureus* SOD activity. SodA is a Mn²⁺-dependent enzyme [33], while the metal requirement of SodM has been proposed to be Mn²⁺ also [34]. Both SodA and SodM have been shown to have a role in resisting external O₂⁻ stress, as the absence of both SODs leads to significantly reduced viability and Mn²⁺-supplementation is incapable of restoring resistance [26]. It is becoming apparent in a wide range of organisms that this oxidative stress resistance can be achieved by complementary mechanisms involving enzyme activity and elemental dismutation. These dual systems allow efficient resistance mechanisms to be maintained throughout growth [26].

Catalase is a monofunctional, heme-containing enzyme that degrades two molecules of H₂O₂ to water and oxygen [35, 36]. In *S. aureus* the enzyme is a homotetramer containing one heme group per subunit, and it reacts with H₂O₂ in a two-step process. First, the H₂O₂ molecule oxidizes the heme group and generates water and compound I, an oxyferryl species in which one oxidation equivalent is removed from the iron and one from the porphyrin ring to form a porphyrin cation radical. Second, compound I combines with another molecule of H₂O₂ to regenerate the ferric enzyme and produce molecular oxygen and water. Catalases do not follow Michaelis-Menten kinetics except at very low substrate concentrations. Since both reactions are peroxide-dependent, the simplest model of enzyme activity, by Bonnichsen, Chance, and Theorell [37], predict that the enzyme is never saturated with its substrate and that the turnover of substrate increases indefinitely with an increase in H₂O₂ concentration. Catalases have exceptionally high activities and most of the enzymes in this subgroup only begin to suffer inactivation by H₂O₂ at concentrations above 300–500 mM

and never reach the V_{\max} (as defined by the Michaelis-Menten model) that is predicted by extrapolation from rates at low substrate concentrations [35].

Peroxiredoxins (Prxs), or alkyl hydroperoxide reductases (such as bacterial alkyl hydroperoxide subunit C, AhpC), exert their protective antioxidant role by catalysing the reduction of H_2O_2 , organic hydroperoxides, and peroxynitrite (NO^{3-}) [38-40]. This detoxification function overlaps to some extent with those of catalases, although their catalytic efficiencies ($10^5 M^{-1} \cdot s^{-1}$) are far lower compared with those of catalases ($10^6 M^{-1} \cdot s^{-1}$) [38]. AhpC catalyses the peroxidase reaction without the involvement of bound heme or other metal or non-metal cofactors; and instead it relies on catalytic Cys-residues. Mechanistic studies have clarified the roles of reactive cysteinyl residues in the peroxidatic process and have highlighted the interaction with thiol–disulfide interchange systems that support this process [39] (Figure 1.2). During the first step of the peroxidase reaction a catalytic Cys in the active site of AhpC is oxidised to a sulfenic acid (Cys-SOH) [41]. This conversion is reversible, but the Cys-SOH is susceptible to additional oxidation and can be irreversibly converted to sulfinic (Cys-SO₂H) and sulfonic acids (Cys-SO₃H) [42]. In the next step of the mechanism, the Cys-SOH is attacked by the Cys-thiol(ate) of an adjacent subunit to form an intersubunit disulfide bond [42]. The catalytic cycle is then completed by Prx reductase (PrxR), bacterial alkyl hydroperoxide reductase subunit F (AhpF), which reduces the intersubunit disulfide bond of AhpC [39]. The reduction of the active site Cys-SOH *via* protein disulfide bond formation is characteristic of most, but not all, Prxs. There are mechanistic differences between Prxs at this step, which have led to the outlining of three categories of these proteins. Prxs have been divided into 1-Cys and 2-Cys sub-families and this is based on the conservation and involvement in catalysis of the various Cys-residues [43]. The 2-Cys Prxs have been further divided into two classes labelled as the “typical” (intersubunit disulfide bond-containing) and “atypical” (intrasubunit disulfide bond-containing) 2-Cys Prxs [41].

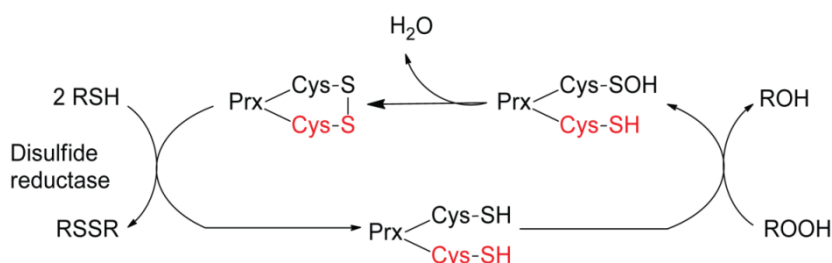


Figure 1.2: During the first step of the peroxidase reaction a catalytic Cys in the active site of AhpC is oxidised to a sulfenic acid (Cys-SOH) [41]. In the next step of the mechanism, the Cys-SOH is attacked by the Cys-thiol(ate) of an adjacent subunit (indicated in red) to form an intersubunit disulfide bond [42]. The catalytic cycle is then completed by a disulfide reductase, Prx reductase (PrxR), bacterial alkyl hydroperoxide reductase subunit F (AhpF), which reduces the intersubunit disulfide bond of AhpC [39].

The mechanism of the Prxs is common to several other proteins that are involved in redox balance. In particular, the two catalytic Cys-residues of Prx form part of a canonical CxxC active site motif that is shared among many of the TFPs [38]. These thiol–disulfide interchange systems are of particular significance to this study and will be explored in more detail in the following sections.

1.3.3 Resistance to oxidative stress: Thiol-disulfide interchange reactions

One of the major challenges that bacteria face when bombarded with ROS is that it causes the oxidation of protein thiol groups to sulfenic acids (RSOH) and disulfides. While this is a process central to the mechanism of ROS neutralization for some Prxs, for most other proteins (including essential enzymes) such changes could prove extremely harmful to their activity. Therefore, the second major mechanism for dealing with oxidative stress (after the efficient removal of ROS) is the reduction of oxidised (macro)molecules, particularly proteins with sulfur-containing active site residues. The reversal of protein-based oxidative damage is accomplished by a tight-knit system of thiol-disulfide interchange reactions that occur between LMWTs, TFPs with CxxC active site motifs [44], and flavoprotein disulfide reductases (FDRs) [45]. On the one hand, the LMWT protects the cell against oxidative damage since it acts as a redox buffer and on the other, its dedicated disulfide reductase (an FDR) reduces the LMWT after oxidation, essentially mediating the reducing potential of NAD(P)H (Figure 1.3A). If any protein-based oxidative damage is incurred, the TFPs then reduce disulfides of oxidised proteins to regenerate catalytic cysteine residues. TFPs can also reduce oxidised LMWTs in the absence of a dedicated FDR for the particular LMWT. For example, in bacteria lacking AhpF their Prxs are generally reduced by TFPs [39]. Then, as above, an FDR reduces the TFP with reducing equivalents that originates from NAD(P)H (Figure 1.3B).

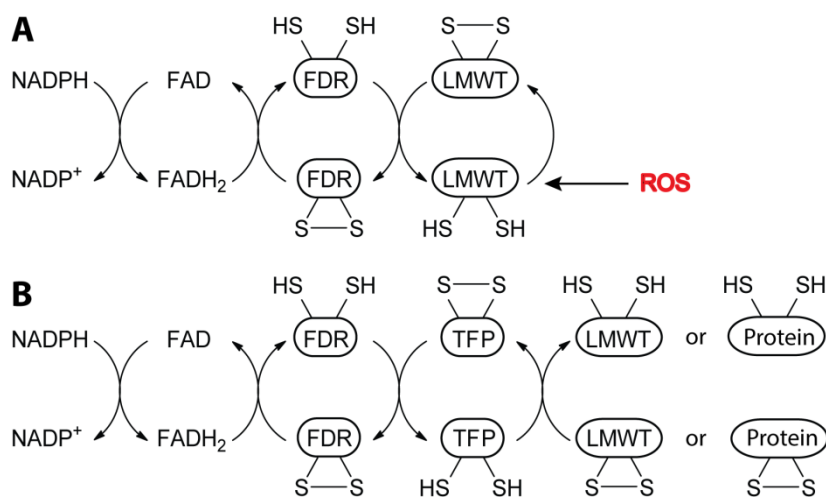


Figure 1.3: Thiol-disulfide interchange systems. Flavoprotein disulfide reductases (FDRs) accept reducing equivalents from NAD(P)H through their flavin group (FAD) and mediates the reduction of low molecular weight thiols (LMWTs) and other thiol-containing proteins either directly (A) or *via* thioredoxin (Trx) fold class proteins (TFPs).

Next, the individual players of the thiol-disulfide interchange systems and the interactions between them will be discussed.

1.3.4.1 Low molecular weight thiols (LMWTs)

LMWTs represent the first line of defence against oxidative stress, since they act as redox buffers. All aerobic organisms maintain high levels of intracellular LMWTs that take part in thiol-disulfide exchange

reactions as part of these organisms' mechanisms to maintain their intracellular redox balance and to defend their cells against oxidative damage [46, 47]. The principal LMWT used to maintain the intracellular redox balance in aerobic eukaryotes—including humans—and Gram-negative bacteria is glutathione (γ -glutamyl-cysteinyl-glycine, GSH, Figure 1.4A). It protects against oxidative damage by providing a reserve of slowly autoxidising cysteine and by acting as a cofactor in the detoxification of epoxides, peroxides and other oxygen reaction products. Significantly, GSH also functions as a cofactor in the reduction of disulfides and ribonucleotides and in the isomerisation of protein disulfides. The FDR enzyme, GR, is responsible for the maintenance of the intracellular redox potential by catalysing the NADPH-dependent reduction of oxidised GSH (glutathione disulfide, GSSG). This is a ubiquitous mechanism where the LMWT acts as a redox buffer and its dedicated disulfide reductase (an FDR) reduces the compound after oxidation with reducing equivalents from NAD(P)H (Figure 1.3). However, several other organisms, including *S. aureus*, do not produce GSH and relies on other LMWT(s) to fulfil the role. Such LMWTs include mycothiol (MSH, Figure 1.4B), coenzyme A (CoA, Figure 1.4C) and bacillithiol (BSH, Figure 1.4D). Indeed, while the importance of the intracellular redox balance and the general mechanisms whereby this is achieved in most organisms are well-known [48], there are many missing pieces in our understanding of the corresponding processes in *S. aureus*.

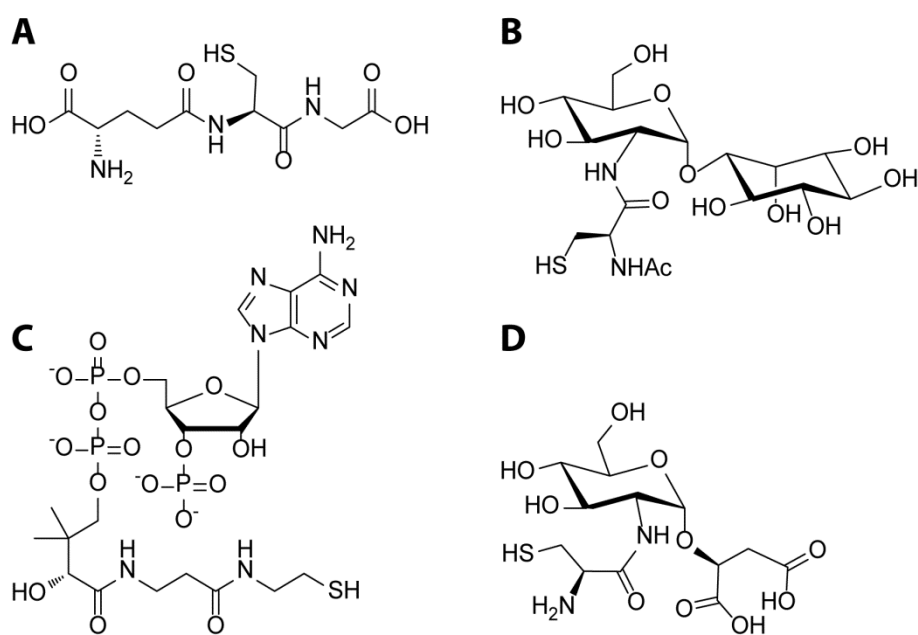


Figure 1.4: Major LMWTs. (A) Glutathione, (B) Mycothiol, (C) coenzyme A and (D) Bacillithiol

CoA was, until recently, believed to be the major LMWT in *S. aureus* [47], since it maintains high levels of this essential metabolic cofactor [49] and also expresses a dedicated disulfide reductase (CoADR, *cdr* gene product). CoA undergoes copper-catalysed autoxidation at a quarter of the rate of GSH [47], making it an appropriate protective thiol for an aerobic organism. A CoA-based redox balancing model has been illustrated in Figure 1.4 and would function as follows: Under conditions of oxidative stress, CoA is sacrificially oxidised to its disulfide (CoAS)₂. The disulfide subsequently needs to be reduced in order for intracellular redox balance, as well as the thiol-disulfide distribution of other thiol-containing molecules, to be

maintained. The free thiol at Cys₄₃ of reduced CoADR nucleophilically attacks one sulphur atom of the substrate and displaces one molecule of CoA to form a mixed Cys₄₃—CoA disulfide. Next, NADPH reduces the mixed disulfide *via* the FAD cofactor to regenerate the reduced form of the enzyme and release another molecule of CoA [47]. In spite of the correlation of this system with the glutathione-based redox system in other organisms, there are factors that cast doubt on the use of CoA and CoADR as the major LMWT /disulfide reductase system in *S. aureus*. First, the cysteine residue in CoA is decarboxylated during biosynthesis; therefore the molecule cannot function as a protected form of cysteine from which cysteine can be regenerated, as is the case with GSH [50]. Also, it has been shown that CoADR is non-essential under normal growth conditions [15] and its expression is not significantly upregulated under oxidative stress conditions [25].

Bacillithiol (BSH) is a fairly recently discovered LMWT produced in *S. aureus*, as well as other *Bacillus* species [50]. It is related to mycothiol (MSH), the major LMWT produced by the Gram-positive Actinomycetes (such as *Mycobacterium tuberculosis*) [51, 52]. Both thiols are based upon the L-Cys-D-glucosamine moiety, but differ with MSH being acetylated at the α -amino group of L-cysteine and the glucosamine-linked $\alpha(1-1)$ to myo-inositol rather than $\alpha(1-2)$ to L-malate in BSH (Figure 1.4). The intracellular concentration of BSH is approximately 30 times less than that of GSH and MSH in other organisms, but it is efficiently maintained in its reduced form in the cell, with a redox ratio comparable to that established for GSH in other organisms [50]. Recent studies have demonstrated the vital role BSH plays in *S. aureus* [53]. *S. aureus* mutants, in which the BSH biosynthesis genes have been disrupted, showed susceptibility to a range of toxins, including oxidants, alkylating agents, and metals [53]. In particular, the bacterium maintains constant BSH levels in response to disulfide stress and oxidative stress from H₂O₂ and cumene hydroperoxide, implying a significant role in oxidative stress defence [53]. BSH has also been shown to play an important role in detoxification and antibiotic resistance [53, 54]. FosB is a divalent-metal-dependent thiol-S-transferase responsible for fosfomycin resistance in many pathogenic Gram-positive bacteria. The *S. aureus* FosB uses BSH as its preferred physiological thiol substrate [54]. These provide convincing arguments for BSH to be the main LMWT in *S. aureus*, however no disulfide reductase has yet been found that can reduce BSH-disulfide (BSSB).

1.3.4.2 Thioredoxin-fold proteins (TFPs)

TFPs forms part of a broad collection of protein superfamilies that share use of the small Trx domain, which consists of a four-stranded β -sheet sandwiched by three α -helices and are differentiated by the many molecular functions catalysed by members of the fold [44]. TFPs are present in every organism and play critical roles in several areas, including protein folding [55], enzymatic detoxification of xenobiotics [56] and particularly defence from oxidative stress [57]. Going beyond the collective use of the Trx domain, class members are associated with one another by a distribution of remnants of the canonical active site and its related catalytic mechanism. In the archetypal catalytic mechanism of the Trx fold class, a disulfide bond in a protein substrate is reduced by means of a dithiol CxxC active site [55] (see Figure 1.2). The first cysteine of this canonical CxxC motif of Trx positions a nucleophilic thiolate at the N-terminus of an α -helix. In the canonical Trx reaction, a disulfide bond is reduced in a substrate protein and the required nucleophilic

thiolate is partially stabilised by proton sharing between the N- and C-terminal cysteine thiols [58]. The TFPs include many classes of proteins involved in the reduction of oxidised substrates, which are relevant to the oxidative defence of *S. aureus* such as Trxs and Prxs.

Thioredoxin (*S. aureus* TrxA) is a relatively low molecular weight oxidoreductase, containing an active thiol-disulfide site, with a variety of functions [29]. The enzyme contains a conserved active-site loop with two redox-active cysteine residues (of the canonical Trx CxxC motif) in the sequence Trp-Cys-Gly-Pro-Cys [59] and is highly efficient at the reduction of disulfide bonds [60], being orders of magnitude faster than dithiothreitol or GSH [61]. In its reduced form Trx is a powerful protein disulfide bond oxidoreductase, with the *S. aureus* enzyme (SaTrxA) exhibiting a redox potential of -268 mV [62]. It is interesting to note that the active site environment is structured to lower the pKa value of the N-terminal Cys (*Ec*Trx pKa ~ 7) to enable Trx to act as a nucleophile and attack disulfides in proteins [63]. During catalysis the two catalytic Cys residues are oxidised to form a disulfide bridge between them. In order to regenerate the active form of the enzyme the disulfide bridge is reduced to a dithiol by TrxR [64] (Figure 1.2B). The Trx-TrxR disulfide interchange system is responsible for the reduction of disulfides of a large amount of oxidised proteins to regenerate their catalytic cysteine residues.

1.3.4.3 Flavoprotein disulfide reductases (FDRs)

The FDRs represent a family of enzymes that catalyse the NAD(P)H-dependent reduction of a diverse range of substrates from disulfides to mercuric ion [65]. They use at least one non-flavin redox centre to transfer electrons from reduced NAD(P)H via a flavin adenine dinucleotide (FAD) prosthetic group [65]. Argyrou and Blanchard defined three different types of FDR based on their reaction mechanisms [65]. Group 1 includes enzymes that use a CXXXXC redox-active disulfide as the non-flavin redox centre. Group 2 comprises enzymes that use two non-flavin redox centres. Bacterial Trx is also included in Group 2 even though it lacks a second non-flavin redox centre; however the transfer of electrons is similar to that of the other members of the group. Group 3 contains enzymes that use a Cys-SOH or a mixed enzyme-substrate disulfide as the non-flavin redox centre. Significantly, all three types rely on catalytic Cys-residues and form disulfides as part of their catalytic mechanism [65]. More recently, Ohja and co-workers performed sequence and structural analysis within the flavoprotein superfamily to identify additional families and subgroups [45]. Based on their observations two major groups were defined with nine subgroups. Three of the subgroups are relevant to this discussion and include: alkylhydroperoxide reductases (AHRs), disulfide reductases (DSRs) and NADH peroxidase/oxidase and CoA-disulfide reductases (PORs) [45]. For the purpose of this study, it is more convenient to discuss the FDRs in the groups by their mechanisms, as defined by Argyrou and Blanchard.

Group 1 FDRs include enzymes such as **lipoamide dehydrogenase (LipDH)**, **glutathione reductase (GR)**, **trypanothione reductase (TR)** and **mycothione reductase (MR)**. They are homodimeric flavoproteins that use a molecule of tightly (non-covalently) bound FAD and one redox-active disulfide per polypeptide chain to catalyse the NAD(P)H-dependent reduction of their disulfide-bonded substrates [65]. The active sites of these enzymes are similar and invariably contain a redox-active disulfide in a CXXXXC motif and therefore this group of enzymes have similar mechanisms. As can be expected, the disulfide substrate-binding sites

differ, since each enzyme has evolved to provide specificity for its own substrate. The complete reaction can be divided into a reductive half reaction and an oxidative half reaction (Figure 1.5). The reductive half reaction begins with reduction of the FAD by NAD(P)H to generate a transitory reduced flavin intermediate [FADH₂-NAD(P)⁺]. Next, intramolecular electrons are transferred to the redox-active disulfide *via* a covalent flavin adduct [66] and NAD(P)⁺ dissociates, regenerating the reduced enzyme [65]. In the oxidative half reaction, the *N*-terminal catalytic Cys of the reduced enzyme forms a mixed-disulfide intermediate with the disulfide substrate. The free thiolate of the *C*-terminal catalytic Cys then nucleophilically attacks the mixed enzyme-substrate disulfide, thereby completing the reduction of the disulfide substrate and regenerating the oxidised enzyme for another round of catalysis.

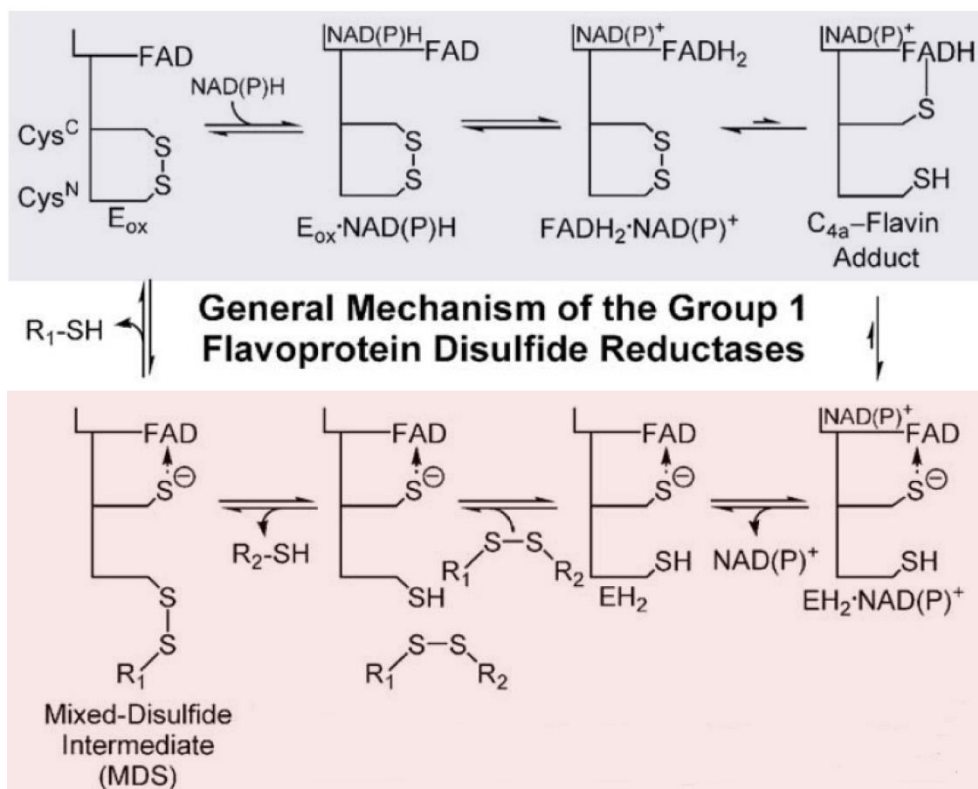


Figure 1.5: The general mechanism of the Group 1 FDRs. The complete reaction can be divided into a reductive half reaction (blue) and an oxidative half reaction (red). The reductive half reaction begins with reduction of the FAD by NAD(P)H to generate a transitory reduced flavin intermediate [FADH₂-NAD(P)⁺]. Next, intramolecular electrons are transferred to the redox-active disulfide *via* a covalent flavin adduct [66] and NAD(P)⁺ dissociates, regenerating the reduced enzyme [65]. In the oxidative half reaction, the *N*-terminal catalytic Cys of the reduced enzyme forms a mixed-disulfide intermediate with the disulfide substrate. The free thiolate of the *C*-terminal catalytic Cys then nucleophilically attacks the mixed enzyme-substrate disulfide, thereby completing the reduction of the disulfide substrate and regenerating the oxidised enzyme for another round of catalysis [65].

AhpF (a PrxR), **TrxR** and **mercuric ion reductase (MerA)** are included with Group 2 FDRs. They catalyse the reduction of disulfides in much larger protein substrates (the 12 kDa Trx and 22 kDa AhpC, respectively) than the first group of FDR enzymes. This poses the problem of active site accessibility. In order to overcome this, TrxR transfers reducing equivalents to the protein surface-through dramatic conformational changes-to affect reduction of its substrate [67]. AhpF employs the same strategy, but also uses a second

non-flavin redox centre [68], which is generally the characterizing feature of Group 2 FDRs. In the case of **TrxR**, the catalytic cycle is initiated by a priming reaction in which NADPH transfers reducing equivalents to FAD [65] (Figure 1.6). NADP⁺ is then released and a domain rotation allows reduction of the enzymatic disulfide by the reduced flavin (FADH₂) [69, 70]. Another domain rotation, this time in the opposite direction, yields a conformation in which the FAD can again be reduced by NADPH [69, 70]. While still in the this conformation, Trx-disulfide (Trx(S)₂) binds and undergoes dithiol-disulfide interchange with the enzymatic dithiol to generate reduced Trx (Trx(SH)₂). Release of Trx(SH)₂ regenerates the initial form of the enzyme for another round of catalysis [65].

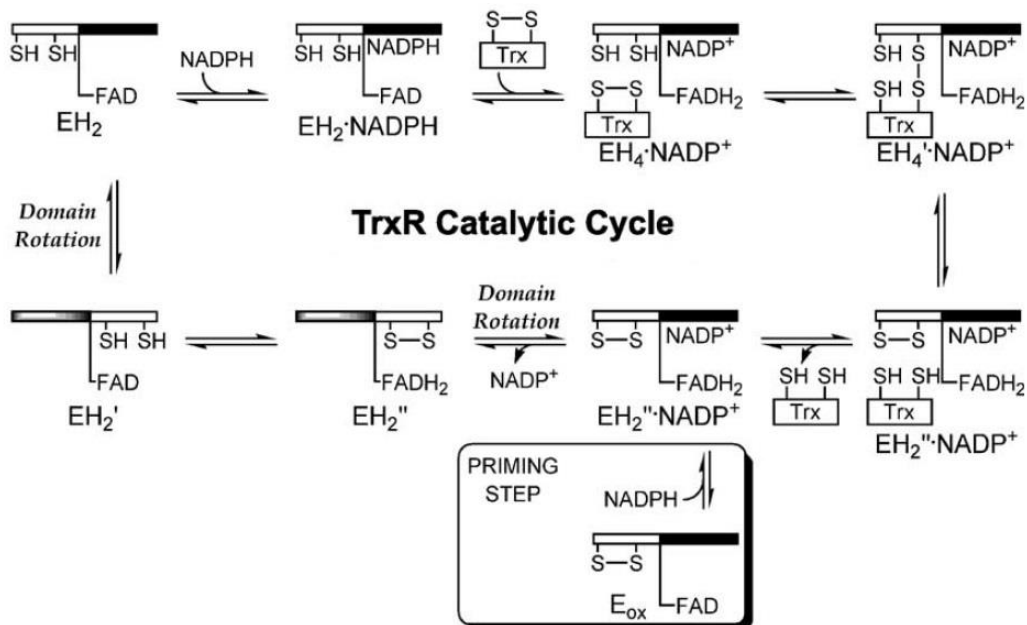


Figure 1.6: Thioredoxin reductase (TrxR) mechanism of action. The catalytic cycle is initiated by a priming reaction in which NADPH transfers reducing equivalents to FAD [65]. NADP⁺ is then released and a domain rotation allows reduction of the enzymatic disulfide by the reduced flavin (FADH₂) [69, 70]. Another domain rotation, this time in the opposite direction, yields a conformation in which the FAD can again be reduced by NADPH [69, 70]. While still in the this conformation, Trx-disulfide (Trx(S)₂) binds and undergoes dithiol-disulfide interchange with the enzymatic dithiol to generate reduced Trx (Trx(SH)₂). Release of Trx(SH)₂ regenerates the initial form of the enzyme for another round of catalysis [65].

Similar to TrxR, **AhpF** enters its catalytic cycle after a priming reaction where NADH transfer reducing equivalents to FAD [71] (Figure 1.7). A domain rotation facilitates the transfer of electrons from FADH₂ to the C-terminal disulfide of AhpF [68]. Another domain rotation, this time in the opposite direction, yields a conformation in which the FAD can again be reduced by NADH [71]. Next, dithiol-disulfide interchange occurs between the C-terminal dithiol and N-terminal disulfide [72]. After this interchange, domain rotation occurs simultaneous with the repositioning of the N-terminal disulfide in a conformation that allows it to reduce the substrate, AhpC. The initial form of the enzyme is thus regenerated for another round of catalysis.

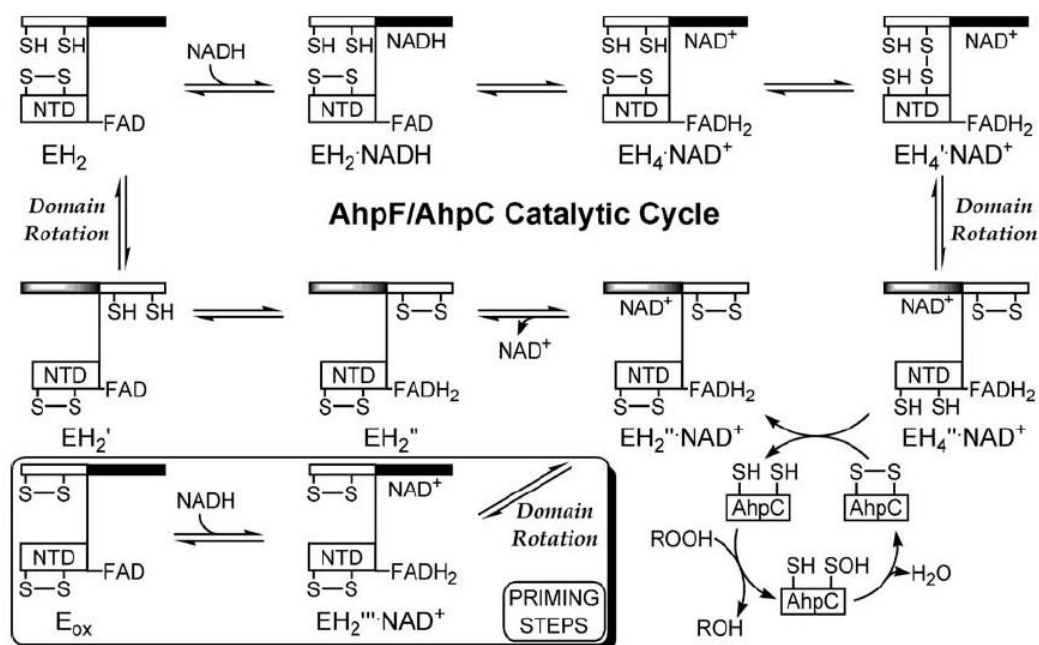


Figure 1.7: Alkyl hydroperoxide subunit F (AhpF) mechanism of action. AhpF enters its catalytic cycle after a priming reaction where NADH transfer reducing equivalents to FAD [71]. A domain rotation facilitates the transfer of electrons from FADH₂ to the C-terminal disulfide of AhpF [68]. Another domain rotation, this time in the opposite direction, yields a conformation in which the FAD can again be reduced by NADH [71]. Next, dithiol-disulfide interchange occurs between the C-terminal dithiol and N-terminal disulfide [72]. After this interchange, domain rotation occurs simultaneous with the repositioning of the N-terminal disulfide in a conformation that allows it to reduce the substrate, AhpC. The initial form of the enzyme is thus regenerated for another round of catalysis [65].

Interestingly, **MerA** is similar in both primary [73] and tertiary structure [74] to Group 1 FDR enzymes, but it contains two additional Cys-residues (Cys₅₅₇ and Cys₅₅₈) at its C-terminus, which are essential for *in vitro* activity with some [75, 76], but not all [77, 78] Hg(II) substrates and also for *in vivo* resistance to mercuric salts [75, 76]. These auxiliary Cys-residues do not cycle between oxidised and reduced states and are also not required for the reduction of Hg(II) in small compounds, such as HgBr₂ and Hg(CN)₂ [75, 76]. However, this supplementary dithiol is necessary to help accommodate more bulky ligands, such as cysteine and GSH, into the active site of the enzyme [77, 78] (Figure 1.8). It has also been shown that mutant MerA with Cys₅₅₇ and Cys₅₅₈ mutated to alanine residues (CCAA) behaves similar to Group 1 FDR enzymes in dithionite titrations [79].

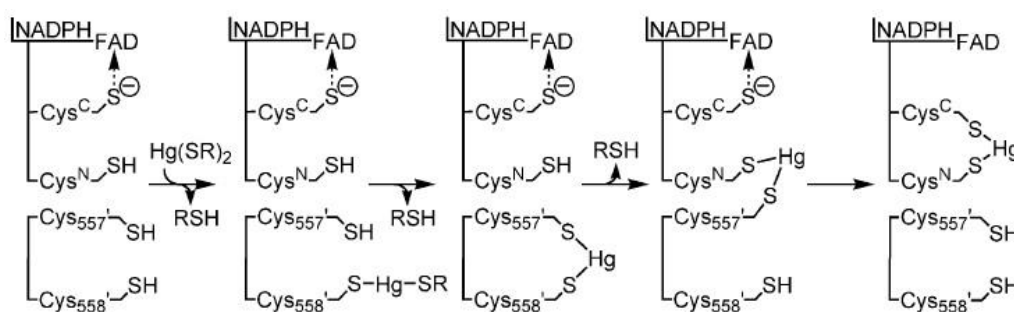


Figure 1.8: Mechanism of entry into the MerA active site of bulky Hg(II) ligands [65].

Contrary to Group 1 FDR enzymes that cycle between the E_{ox} and EH_2 states with each catalytic turnover, MerA cycles between the EH_2 and EH_4 states (Figure 1.9) [80]. Similar to the first reductive half-reaction of Group 1 FDR enzymes (Figure 1.5), MerA undergoes an initial priming step to generate $EH_2 \cdot NADP^+$. A covalent C_{4a} -flavin adduct is formed at a catalytically relevant rate at low pH during this priming reaction both in wild-type MerA [81] and in an ACAA mutant [82], but not in any Group 1 FDR wild-type enzymes. In order to accelerate internal electron transfer from the FAD to the disulfide, it has been suggested that substitution of a histidine residue (His-Glu pair in Group 1 FDR enzymes) to a tyrosine (Tyr₆₀₅) in MerA is responsible for the altered stability of this intermediate. After exchange of $NADP^+$ by NADPH in EH_2 [83] Hg(II) enters the active site (Figure 1.9). The bound NADPH then reduces the FAD to generate the $EH_4 \cdot NADP^+ \cdot Hg(II)$ intermediate, which subsequently reduces Hg(II) to Hg^0 . It should be noted that the mechanism of Hg(II) reduction is unknown. Possibilities proposed include the intermediacy of covalent C_{4a} -flavin adducts with either Cys^C or Hg(II), as well as two single-electron transfers [73]. The exact coordination of Hg(II) in the active site is also unknown.

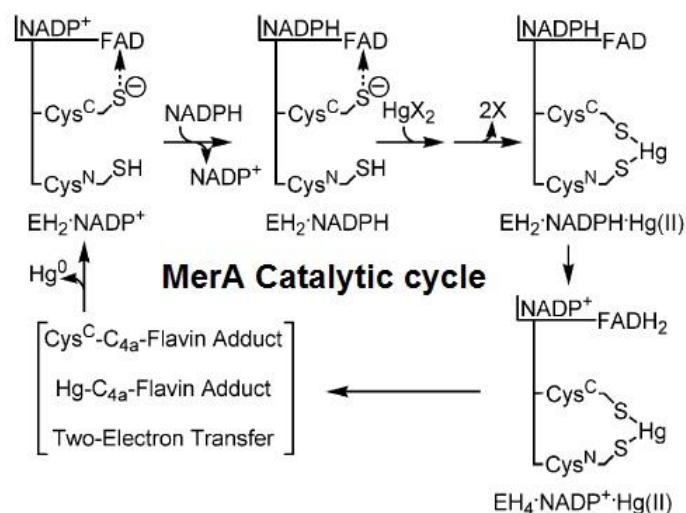


Figure 1.9: MerA catalytic cycle. MerA undergoes an initial priming step to generate $EH_2 \cdot NADP^+$. After exchange of $NADP^+$ by NADPH in EH_2 [83], Hg(II) enters the active site. The bound NADPH then reduces the FAD to generate the $EH_4 \cdot NADP^+ \cdot Hg(II)$ intermediate, which subsequently reduces Hg(II) to Hg^0 [65].

Coenzyme A disulfide reductase (CoADR) is part of the Group 3 FDRs and contains a conserved Cys-residue, which is present in an SFXXC motif [84, 85] at a position in the primary sequence corresponding to the CXXXXC motif in the other FDR enzymes. The reduced CoADR enzyme contains a free thiol at Cys₄₃ [47, 86]. When the enzyme comes into contact with a CoA-disulfide, the Cys₄₃ thiolate anion nucleophilically attacks one sulphur atom of the substrate, thereby displacing one molecule of CoA and forming a mixed Cys₄₃-CoA disulfide [87]. This enzyme-substrate complex has a stable oxidised state and this is also the form in which the enzyme is isolated from cells [86]. Subsequently, NADPH binds the oxidised enzyme and reduces the mixed disulfide *via* the FAD cofactor to regenerate the reduced form of the enzyme and release another molecule of CoA [47]. The SaCoADR mechanism of action is illustrated in Figure 1.10.

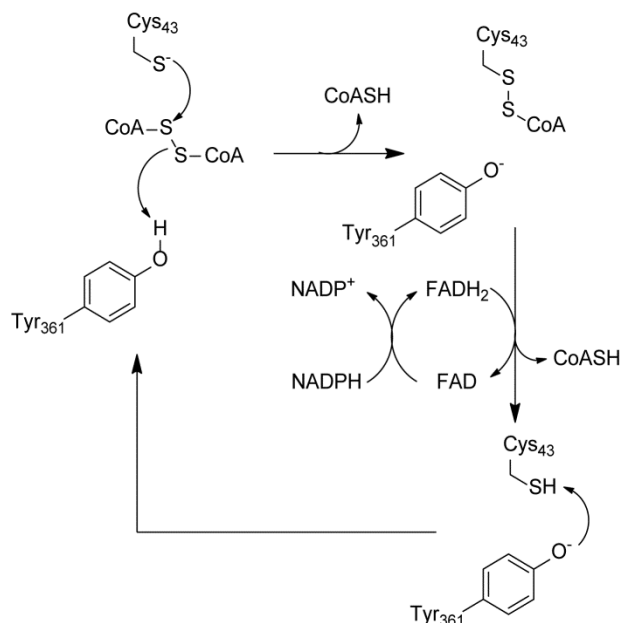


Figure 1.10: SaCoADR reaction mechanism. the Cys₄₃ thiolate anion nucleophilically attacks one sulphur atom of the substrate, (CoAS)₂, thereby displacing one molecule of CoA and forming a mixed Cys₄₃-CoA disulfide [87]. This enzyme-substrate complex has a stable oxidised state and this is also the form in which the enzyme is isolated from cells [86]. Subsequently, NADPH binds the oxidised enzyme and reduces the mixed disulfide *via* the FAD cofactor to regenerate the reduced form of the enzyme and release another molecule of CoA [47].

1.3.4 Conclusion

While the importance of the intracellular redox balance and the general mechanisms whereby this is achieved are well-known [48], there are large gaps in our understanding of the actors involved in this process in *S. aureus*, and the specific interactions between them. In particular, the whole picture of the roles that LMWTs play in *S. aureus* is still not complete. It is possible that both CoA and BSH together are responsible for maintaining intracellular redox balance in the bacterium, which may very well be the reason behind its exceptional resistance to oxidative attack. Also, the TFPs play a significant role in disulfide reduction and it has been proposed that the redox status of BSH may be maintained by the Trx–TrxR system [53, 60, 88], since no disulfide reductase has yet been found that can reduce BSH-disulfide (BSSB). It appears then that the immense success of *S. aureus*'s oxidative stress resistance may be attributed to elaborate systems of both redundancy and interdependence. Even so, the organism relies on a unique system for its thiol redox balance, which presents the opportunity to investigate it as a possible avenue for antistaphylococcal drug development. The fact that *S. aureus* maintains intracellular CoA at millimolar concentrations [49] and that its first CoA biosynthesis enzyme is refractory to feedback inhibition [89] implies a non-trivial role of the cofactor. Also, considering that the redox balancing mechanisms in *S. aureus* have not yet been completely elucidated, the role of CoA as a redox buffer may very well become important under conditions of oxidative stress.

1.4 Research question

At the beginning of this chapter an alternative strategy to current drug development methodologies was proposed that entails the identification of processes that are essential to the survival of the pathogenic bacteria in the human host, where they need to counter the defences of the human immune system. In particular, the focus of this study is the importance of the central metabolic cofactor CoA in the defence mechanisms that *S. aureus* employs under such circumstances, and therefore on the targeting of CoA biosynthesis and enzymology as potential antistaphylococcal targets.

The main research question that needed to be addressed was whether CoA is involved in the maintenance of intracellular redox balance and defence against oxidative damage in *S. aureus*. This was investigated using several approaches:

1. The dedicated disulfide reductase of $(\text{CoAS})_2$ (SaCoADR) was evaluated as a potential antistaphylococcal drug target by building on previous studies with small molecule inhibitors of the enzyme. This work is described in Chapter 3.
2. The importance of several other potential role players in *S. aureus* oxidative stress defence was evaluated and compared to CoA and SaCoADR under normal growth conditions, oxidative stress conditions and under limited intracellular CoA conditions. This work is described in Chapter 3.
3. The mechanism of inhibition of a known CoA biosynthesis inhibitor (CJ-15, 801) was investigated, since insights into its molecular basis of inhibition may be important for drug development against similar bacterial targets. This work is described in Chapter 4.

Taken together, the aim of the study was to provide better insight into the viability of CoA biosynthesis and CoA-dependent redox processes as targets for anti-staphylococcal drug development.

1.5 References

1. World Health Organization. *Antimicrobial Resistance: Global Report on Surveillance*, 2014, WHO: Geneva.
2. Fischbach, M.A. and C.T. Walsh, *Antibiotics for Emerging Pathogens*. *Science*, 2009. **325**(5944): p. 1089-1093.
3. Rice, L.B., *Progress and Challenges in Implementing the Research on ESKAPE Pathogens*. *Infection Control and Hospital Epidemiology*, 2010. **31**(S1): p. S7-S10.
4. M. T. Parker, M.P.J., *A Survey of Methicillin Resistance in Staphylococcus Aureus*. *Postgrad Med J.*, 1964. **40**: p. 170-178.
5. Tsiodras, S., et al., *Linezolid resistance in a clinical isolate of Staphylococcus aureus*. *The Lancet*, 2001. **358**(9277): p. 207-208.

6. Mangili, A., et al., *Daptomycin-Resistant, Methicillin-Resistant Staphylococcus aureus Bacteremia*. *Clinical Infectious Diseases*, 2005. **40**(7): p. 1058-1060.
7. Stefani, S., et al., *Meticillin-resistant Staphylococcus aureus (MRSA): global epidemiology and harmonisation of typing methods*. *International Journal of Antimicrobial Agents*. **39**(4): p. 273-282.
8. Weigel, L.M., et al., *Genetic Analysis of a High-Level Vancomycin-Resistant Isolate of Staphylococcus aureus*. *Science*, 2003. **302**(5650): p. 1569-1571.
9. DeLeo, F.R. and H.F. Chambers, *Reemergence of antibiotic-resistant Staphylococcus aureus in the genomics era*. *The Journal of Clinical Investigation*, 2009. **119**(9): p. 2464-2474.
10. Sakoulas, G. and R.C. Moellering, *Increasing Antibiotic Resistance among Methicillin-Resistant Staphylococcus aureus Strains*. *Clinical Infectious Diseases*, 2008. **46**(Supplement 5): p. S360-S367.
11. Saravolatz, L.D., et al., *Dalbavancin: a Novel Once-Weekly Lipoglycopeptide Antibiotic*. *Clinical Infectious Diseases*, 2008. **46**(4): p. 577-583.
12. Rehm, S.J. and A. Tice, *Staphylococcus aureus: Methicillin-Susceptible S. aureus to Methicillin-Resistant S. aureus and Vancomycin-Resistant S. aureus*. *Clinical Infectious Diseases*, 2010. **51**(Supplement 2): p. S176-S182.
13. Hughes, J.P., et al., *Principles of early drug discovery*. *British Journal of Pharmacology*, 2011. **162**(6): p. 1239-1249.
14. Kurosawa, G., et al., *Comprehensive screening for antigens overexpressed on carcinomas via isolation of human mAbs that may be therapeutic*. *Proceedings of the National Academy of Sciences of the United States of America*, 2008. **105**(20): p. 7287-7292.
15. Fey, P.D., et al., *A Genetic Resource for Rapid and Comprehensive Phenotype Screening of Nonessential Staphylococcus aureus Genes*. *mBio*, 2013. **4**(1).
16. Forsyth, R.A., et al., *A genome-wide strategy for the identification of essential genes in Staphylococcus aureus*. *Molecular Microbiology*, 2002. **43**(6): p. 1387-1400.
17. Le Breton, Y., et al., *Essential Genes in the Core Genome of the Human Pathogen Streptococcus pyogenes*. *Sci. Rep.*, 2015. **5**.
18. Yin, D. and Y. Ji, *Identification of Essential Genes in Staphylococcus aureus by Construction and Screening of Conditional Mutant Library*, in *Microbial Gene Essentiality: Protocols and Bioinformatics*, A. Osterman and S. Gerdes, Editors. 2008, Humana Press. p. 297-305.
19. Alberts, B.J., A; Lewis, J; Raff, M; Roberts, K and Walter, P, *Molecular Biology of the Cell*. 4th edition ed2002, New York: Garland Science.

20. Fedtke, I., F. Götz, and A. Peschel, *Bacterial evasion of innate host defenses – the Staphylococcus aureus lesson*. International Journal of Medical Microbiology, 2004. **294**(2–3): p. 189-194.
21. Kim, H.K., et al., *Recurrent infections and immune evasion strategies of Staphylococcus aureus*. Current Opinion in Microbiology, 2012. **15**(1): p. 92-99.
22. Hancock, R.E.W. and G. Diamond, *The role of cationic antimicrobial peptides in innate host defences*. Trends in Microbiology, 2000. **8**(9): p. 402-410.
23. Dunkelberger, J.R. and W.-C. Song, *Complement and its role in innate and adaptive immune responses*. Cell Res, 2009. **20**(1): p. 34-50.
24. Aderem, A. and R.J. Ulevitch, *Toll-like receptors in the induction of the innate immune response*. Nature, 2000. **406**(6797): p. 782-787.
25. Voyich, J.M., et al., *Insights into Mechanisms Used by Staphylococcus aureus to Avoid Destruction by Human Neutrophils*. Journal of Immunology, 2005. **175**(Copyright (C) 2011 American Chemical Society (ACS). All Rights Reserved.): p. 3907-3919.
26. Karavolos, M.H., et al., *Role and regulation of the superoxide dismutases of Staphylococcus aureus*. Microbiology, 2003. **149**(10): p. 2749-2758.
27. Wolf, C., et al., *Proteomic analysis of antioxidant strategies of Staphylococcus aureus: diverse responses to different oxidants*. Proteomics, 2008. **8**(Copyright (C) 2011 American Chemical Society (ACS). All Rights Reserved.): p. 3139-3153.
28. Pöthner, D.-C., et al., *Diamide triggers mainly S thiolations in the cytoplasmic proteomes of Bacillus subtilis and Staphylococcus aureus*. Journal of Bacteriology, 2009. **191**(Copyright (C) 2011 American Chemical Society (ACS). All Rights Reserved.): p. 7520-7530.
29. Kalinina, E.V., N.N. Chernov, and A.N. Saprin, *Involvement of thio-, peroxi-, and glutaredoxins in cellular redox-dependent processes*. Biochemistry (Moscow), 2008. **73**(Copyright (C) 2011 American Chemical Society (ACS). All Rights Reserved.): p. 1493-1510.
30. Haber, F. and J. Weiss, *The Catalytic Decomposition of Hydrogen Peroxide by Iron Salts*. Proceedings of the Royal Society of London. Series A - Mathematical and Physical Sciences, 1934. **147**(861): p. 332-351.
31. Candeias, L.P., et al., *Free hydroxyl radicals are formed on reaction between the neutrophil-derived species Superoxide anion and hypochlorous acid*. FEBS Letters. **333**(1): p. 151-153.
32. Ramos, C.L., et al., *Spin trapping evidence for myeloperoxidase-dependent hydroxyl radical formation by human neutrophils and monocytes*. Journal of Biological Chemistry, 1992. **267**(12): p. 8307-12.

33. Clements, M.O., S.P. Watson, and S.J. Foster, *Characterization of the Major Superoxide Dismutase of Staphylococcus aureus and Its Role in Starvation Survival, Stress Resistance, and Pathogenicity*. Journal of Bacteriology, 1999. **181**(13): p. 3898-3903.
34. Valderas, M.W. and M.E. Hart, *Identification and Characterization of a Second Superoxide Dismutase Gene (sodM) from Staphylococcus aureus*. Journal of Bacteriology, 2001. **183**(11): p. 3399-3407.
35. Chelikani, P., I. Fita, and P.C. Loewen, *Diversity of structures and properties among catalases*. Cellular and Molecular Life Sciences CMLS, 2004. **61**(2): p. 192-208.
36. Nicholls, P., I. Fita, and P.C. Loewen, *Enzymology and structure of catalases*, in *Advances in Inorganic Chemistry* 2000, Academic Press. p. 51-106.
37. Bonnichsen, R.K.C., B.; Theorell, H., *Catalase Activity*. Acta Chemica Scandinavica, 1947. **1**: p. 685-709.
38. Wood, Z.A., et al., *Structure, mechanism and regulation of peroxiredoxins*. Trends in Biochemical Sciences, 2003. **28**(1): p. 32-40.
39. Poole, L.B., *Bacterial defenses against oxidants: mechanistic features of cysteine-based peroxidases and their flavoprotein reductases*. Archives of Biochemistry and Biophysics, 2005. **433**(1): p. 240-254.
40. Hofmann, B., H.J. Hecht, and L. Flohé, *Peroxiredoxins*, in *Biological Chemistry* 2002. p. 347.
41. Ellis, H.R. and L.B. Poole, *Novel Application of 7-Chloro-4-nitrobenzo-2-oxa-1,3-diazole To Identify Cysteine Sulfenic Acid in the AhpC Component of Alkyl Hydroperoxide Reductase†*. Biochemistry, 1997. **36**(48): p. 15013-15018.
42. Ellis, H.R. and L.B. Poole, *Roles for the Two Cysteine Residues of AhpC in Catalysis of Peroxide Reduction by Alkyl Hydroperoxide Reductase from Salmonella typhimurium†*. Biochemistry, 1997. **36**(43): p. 13349-13356.
43. Chae, H.Z., et al., *Cloning and sequencing of thiol-specific antioxidant from mammalian brain: alkyl hydroperoxide reductase and thiol-specific antioxidant define a large family of antioxidant enzymes*. Proceedings of the National Academy of Sciences, 1994. **91**(15): p. 7017-7021.
44. Atkinson, H.J. and P.C. Babbitt, *An Atlas of the Thioredoxin Fold Class Reveals the Complexity of Function-Enabling Adaptations*. PLoS Comput Biol, 2009. **5**(10): p. e1000541.
45. Ojha, S., E.C. Meng, and P.C. Babbitt, *Evolution of Function in the "Two Dinucleotide Binding Domains" Flavoproteins*. PLoS Comput Biol, 2007. **3**(7): p. e121.
46. Jaeger, T., et al., *The thiol-based redox networks of pathogens: Unexploited targets in the search for new drugs*. BioFactors, 2006. **27**(1): p. 109-120.

47. delCardayré, S.B., et al., *Coenzyme A Disulfide Reductase, the Primary Low Molecular Weight Disulfide Reductase from Staphylococcus aureus*. Journal of Biological Chemistry, 1998. **273**(10): p. 5744-5751.
48. Zuber, P., *Management of Oxidative Stress in Bacillus*. Annual Review of Microbiology, 2009. **63**(1): p. 575-597.
49. Newton, G.L., et al., *Distribution of thiols in microorganisms: mycothiol is a major thiol in most actinomycetes*. Journal of Bacteriology, 1996. **178**(7): p. 1990-1995.
50. Newton, G.L., et al., *Bacillithiol is an antioxidant thiol produced in Bacilli*. Nat Chem Biol, 2009. **5**(9): p. 625-627.
51. Jothivasan, V.K. and C.J. Hamilton, *Mycothiol: synthesis, biosynthesis and biological functions of the major low molecular weight thiol in actinomycetes*. Natural Product Reports, 2008. **25**(6): p. 1091-1117.
52. Newton, G.L., et al., *Distribution of thiols in microorganisms: mycothiol is a major thiol in most actinomycetes*. Journal of Bacteriology, 1996. **178**(7): p. 1990-5.
53. Rajkarnikar, A., et al., *Analysis of mutants disrupted in bacillithiol metabolism in Staphylococcus aureus*. Biochemical and Biophysical Research Communications, 2013. **436**(2): p. 128-133.
54. Roberts, A.A., et al., *Mechanistic studies of FosB: a divalent-metal-dependent bacillithiol-S-transferase that mediates fosfomycin resistance in Staphylococcus aureus*. The Biochemical journal, 2013. **451**(1): p. 69-79.
55. Ito, K. and K. Inaba, *The disulfide bond formation (Dsb) system*. Current Opinion in Structural Biology, 2008. **18**(4): p. 450-458.
56. Armstrong, R.N., *Structure, Catalytic Mechanism, and Evolution of the Glutathione Transferases*. Chemical Research in Toxicology, 1997. **10**(1): p. 2-18.
57. A. Holmgren, C.J., C. Berndt, M.E. Lönn, C. Hudemann and C.H. Lillig, *Thiol redox control via thioredoxin and glutaredoxin systems*. Biochemical Society Transactions, 2005. **33**: p. 1375–1377.
58. Jeng, M.-F., A. Holmgren, and H.J. Dyson, *Proton Sharing between Cysteine Thiols in Escherichia coli Thioredoxin: Implications for the Mechanism of Protein Disulfide Reduction*. Biochemistry, 1995. **34**(32): p. 10101-10105.
59. Eklund, H., F.K. Gleason, and A. Holmgren, *Structural and functional relations among thioredoxins of different species*. Proteins: Structure, Function, and Bioinformatics, 1991. **11**(1): p. 13-28.
60. Holmgren, A., *Thioredoxin*. Annual Review of Biochemistry, 1985. **54**(1): p. 237-271.
61. Arnér, E.S.J. and A. Holmgren, *Physiological functions of thioredoxin and thioredoxin reductase*. European Journal of Biochemistry, 2000. **267**(20): p. 6102-6109.

62. Messens, J., et al., *How Thioredoxin can Reduce a Buried Disulphide Bond*. Journal of Molecular Biology, 2004. **339**(3): p. 527-537.
63. Kallis, G.B. and A. Holmgren, *Differential reactivity of the functional sulfhydryl groups of cysteine-32 and cysteine-35 present in the reduced form of thioredoxin from Escherichia coli*. Journal of Biological Chemistry, 1980. **255**(21): p. 10261-10265.
64. Roos, G., et al., *The Conserved Active Site Proline Determines the Reducing Power of Staphylococcus aureus Thioredoxin*. Journal of Molecular Biology, 2007. **368**(3): p. 800-811.
65. Argyrou, A. and J.S. Blanchard, *Flavoprotein Disulfide Reductases: Advances in Chemistry and Function*, in *Progress in Nucleic Acid Research and Molecular Biology* 2004, Academic Press. p. 89-142.
66. Thorpe, C. and C.H. Williams, *Lipoamide dehydrogenase from pig heart. Pyridine nucleotide induced changes in monoalkylated two-electron reduced enzyme*. Biochemistry, 1981. **20**(6): p. 1507-1513.
67. Williams, C.H., et al., *Thioredoxin reductase*. European Journal of Biochemistry, 2000. **267**(20): p. 6110-6117.
68. Poole, L.B., et al., *AhpF and other NADH:peroxiredoxin oxidoreductases, homologues of low Mr thioredoxin reductase*. European Journal of Biochemistry, 2000. **267**(20): p. 6126-6133.
69. Williams, C.H., *Mechanism and structure of thioredoxin reductase from Escherichia coli*. The FASEB Journal, 1995. **9**(13): p. 1267-76.
70. Lennon, B.W. and C.H. Williams, *Enzyme-Monitored Turnover of Escherichia coli Thioredoxin Reductase: Insights for Catalysis†*. Biochemistry, 1996. **35**(15): p. 4704-4712.
71. Niimura, Y. and V. Massey, *Reaction Mechanism of Amphibacillus xylanus NADH Oxidase/Alkyl Hydroperoxide Reductase Flavoprotein*. Journal of Biological Chemistry, 1996. **271**(48): p. 30459-30464.
72. Wood, Z.A., L.B. Poole, and P.A. Karplus, *Structure of Intact AhpF Reveals a Mirrored Thioredoxin-like Active Site and Implies Large Domain Rotations during Catalysis†,‡*. Biochemistry, 2001. **40**(13): p. 3900-3911.
73. Moore, M.J., et al., *Organomercurial lyase and mercuric ion reductase: nature's mercury detoxification catalysts*. Accounts of Chemical Research, 1990. **23**(9): p. 301-308.
74. Schiering, N., et al., *Structure of the detoxification catalyst mercuric ion reductase from Bacillus sp. strain RC607*. Nature, 1991. **352**(6331): p. 168-172.
75. Miller, S.M., et al., *Evidence for the participation of Cys558 and Cys559 at the active site of mercuric reductase*. Biochemistry, 1989. **28**(3): p. 1194-1205.

76. Moore, M.J., S.M. Miller, and C.T. Walsh, *C-Terminal cysteines of Tn501 mercuric ion reductase*. *Biochemistry*, 1992. **31**(6): p. 1677-1685.
77. Engst, S. and S.M. Miller, *Alternative Routes for Entry of HgX₂ into the Active Site of Mercuric Ion Reductase Depend on the Nature of the X Ligands*. *Biochemistry*, 1999. **38**(12): p. 3519-3529.
78. Engst, S. and S.M. Miller, *Rapid Reduction of Hg(II) by Mercuric Ion Reductase Does Not Require the Conserved C-Terminal Cysteine Pair Using HgBr₂ as the Substrate*. *Biochemistry*, 1998. **37**(33): p. 11496-11507.
79. Moore, M.J. and C.T. Walsh, *Mutagenesis of the N- and C-terminal cysteine pairs of Tn501 mercuric ion reductase: consequences for bacterial detoxification of mercurials*. *Biochemistry*, 1989. **28**(3): p. 1183-1194.
80. Miller, S.M., et al., *Two-electron reduced mercuric reductase binds Hg(II) to the active site dithiol but does not catalyze Hg(II) reduction*. *Journal of Biological Chemistry*, 1986. **261**(18): p. 8081-4.
81. Sahlman, L., A.-M. Lambeir, and S. Lindskog, *Rapid-scan stopped-flow studies of the pH dependence of the reaction between mercuric reductase and NADPH*. *European Journal of Biochemistry*, 1986. **156**(3): p. 479-488.
82. Miller, S.M., et al., *Use of a site-directed triple mutant to trap intermediates: demonstration that the flavin C(4a)-thiol adduct and reduced flavin are kinetically competent intermediates in mercuric ion reductase*. *Biochemistry*, 1990. **29**(11): p. 2831-2841.
83. Sahlman, L., et al., *The reaction between NADPH and mercuric reductase from Pseudomonas aeruginosa*. *Journal of Biological Chemistry*, 1984. **259**(20): p. 12403-12408.
84. delCardayré, S.B. and J.E. Davies, *Staphylococcus aureus Coenzyme A Disulfide Reductase, a New Subfamily of Pyridine Nucleotide-Disulfide Oxidoreductase: SEQUENCE, EXPRESSION, AND ANALYSIS OF cdr*. *Journal of Biological Chemistry*, 1998. **273**(10): p. 5752-5757.
85. Ross, R.P. and A. Claiborne, *Cloning, sequence and overexpression of NADH peroxidase from Streptococcus faecalis 10C1: Structural relationship with the flavoprotein disulfide reductases*. *Journal of Molecular Biology*, 1991. **221**(3): p. 857-871.
86. Mallett, T.C., et al., *Structure of Coenzyme A-Disulfide Reductase from Staphylococcus aureus at 1.54 Å Resolution*. *Biochemistry*, 2006. **45**(38): p. 11278-11289.
87. Luba, J., V. Charrier, and A. Claiborne, *Coenzyme A-Disulfide Reductase from Staphylococcus aureus: Evidence for Asymmetric Behavior on Interaction with Pyridine Nucleotides*. *Biochemistry*, 1999. **38**(9): p. 2725-2737.
88. Mostertz, J., et al., *The role of thioredoxin TrxA in Bacillus subtilis: A proteomics and transcriptomics approach*. *Proteomics*, 2008. **8**(13): p. 2676-2690.

89. Leonardi, R., et al., *A Pantothenate Kinase from Staphylococcus aureus Refractory to Feedback Regulation by Coenzyme A*. *Journal of Biological Chemistry*, 2005. **280**(5): p. 3314-3322.

Chapter 2: Recent advances in targeting coenzyme A biosynthesis and utilization for antimicrobial drug development

2.1 Mini-review

This chapter has been published as a mini-review in *Biochemical Society Transactions* in August 2014 and discusses recent literature (since 2008) regarding CoA biosynthesis and utilisation as possible antimicrobial drug targets. While it presents a fairly broad overview, it sets the stage for the experimental work on the investigation of CoA biosynthesis and CoA-dependent redox processes as targets for anti-staphylococcal drug development as described in the following chapters.

In this review, I wrote the abstract and the section headed “CoA biosynthesis: enzyme-specific inhibitors”. Marianne de Villiers originally wrote the introduction and the section headed “Anti-CoAs”, while Erick Strauss performed the final editing of the manuscript. The paper in its published form is included under Appendices.

Recent advances in targeting coenzyme A biosynthesis and utilization for antimicrobial drug development

Wessel J.A. Moolman, Marianne de Villiers and Erick Strauss*

Department of Biochemistry, Stellenbosch University, Stellenbosch, 7600, South Africa.

***Contact information**

Erick Strauss (contact corresponding author):

e-mail: estrauss@sun.ac.za

Phone: +27-21-808-5866

Fax: +27-21-808-5863

KEY WORDS: coenzyme A, antimicrobial, antimetabolite, biosynthesis, pantothenamide, enzyme inhibitor.

ABBREVIATIONS: ACP, acyl carrier protein; AcpS, ACP-synthase; anti-CoA, CoA antimetabolite; anti-Pan, pantothenate antimetabolite; *BaPanK_{III}*, *Bacillus anthracis* type III PanK; CoA, coenzyme A; CoADR, CoA disulfide reductase; CoASy, CoA synthase; DPCK, dephospho-coenzyme A kinase; dPCoA, dephospho-CoA; FAS-II, type II fatty acid synthase; HoPanAms, homopantothenamide; *HpPPAT*, *Helicobacter pylori* PPAT; *KpPanK_I*, *Klebsiella pneumoniae* type I PanK; MIC, minimal inhibitory concentration; *MtPanK_I*, *Mycobacterium tuberculosis* type I PanK; *MtPanK_{III}*, *Mycobacterium tuberculosis* type III PanK; N5-Pan, *N*-pentyl pantothenamide; Pan, pantothenate; PanAm, *N*-substituted pantothenamide; α -PanAm, α -pantothenamide; PanK, pantothenate kinase; PanK_{III}, type III PanK; PantSH, pantetheine; PPan, 4'-phosphopantothenate; PPantSH, 4'-phosphopantetheine; PPan Δ SH, 4'-phospho-*N*-(1-mercaptomethylcyclopropyl)-pantothenamide; PPAT, phosphopantetheine adenylyltransferase; PPCDC, phosphopantothenoylcysteine decarboxylase; PPCS, phosphopantothenoylcysteine synthetase; *SaPanK_{II}*, *Staphylococcus aureus* type II PanK; SAR, structure-activity relationship.

ABSTRACT

The biosynthesis and utilization of coenzyme A (CoA), the ubiquitous and essential acyl carrier in all organisms, have long been regarded as excellent targets for the development of new antimicrobial drugs. Moreover, bioinformatics and biochemical studies have highlighted significant differences between several of the bacterial enzyme targets and their human counterparts, indicating that selective inhibition of the former should be possible. Over the past decade, a large amount of structural and mechanistic data has been gathered on CoA metabolism and the CoA biosynthetic enzymes, and this has facilitated the discovery and development of several promising candidate antimicrobial agents. These compounds include both target-specific inhibitors, as well as CoA antimetabolite precursors that can reduce CoA levels and interfere processes that are dependent on this cofactor. In this review we provide an overview of the most recent of these studies that, taken together, have also provided chemical validation of CoA biosynthesis and utilization as viable targets for antimicrobial drug development.

INTRODUCTION

The biosynthesis of coenzyme A (CoA)—or more specifically, the utilization of pantothenate (Pan, Figure 1), the vitamin precursor of this essential cofactor—has long been regarded as an excellent target for the development of selective antimicrobials [1]. Studies during the past decade have confirmed that all organisms must obtain CoA through *de novo* biosynthesis from Pan using a conserved pathway consisting of five enzymatic steps [2, 3]. However, in several cases the specific enzymes that catalyze these reactions in humans and pathogenic microorganisms respectively show significant diversity on a sequence, structure and mechanistic level, suggesting that the development of selective inhibitors of microbial CoA biosynthesis should be possible, and highlighting these enzymes as targets for drug development [3, 4].

CoA can also be obtained from pantetheine (PantSH), a product of CoA and acyl carrier protein (ACP) degradation, by means of a shortened pathway consisting of only three of the five biosynthetic enzymes (Figure 1) [3, 5]. Importantly, this pathway can also be hijacked by pantothenate antimetabolites (anti-Pan), compounds that resemble Pan but that do not allow the catalytically essential thiol to be incorporated into the CoA structure. This results in the formation of CoA antimetabolites (anti-CoA) that can interfere and/or inhibit CoA-dependent processes or reduce intracellular CoA levels (Figure 1).

Here we summarize recent advances made in the development of small molecule inhibitors of CoA biosynthesis (and processes dependent on this cofactor) for the discovery of new potent antimicrobials.

COA BIOSYNTHESIS: ENZYME-SPECIFIC INHIBITORS

Pantothenate Kinase (PanK)

PanK (EC 2.7.1.33), which catalyzes the ATP-dependent phosphorylation of Pan to form 4'-phosphopantothenate (PPan), has received the most attention as a potential target for antimicrobial drug development. This is due to several factors: first, the enzyme catalyzes the first and committed step of CoA biosynthesis [3, 6]; second, PanK is believed to be the rate-limiting enzyme of the pathway; and third, PanKs show significant diversity, with two bacterial (types I and III) and one predominantly eukaryotic (type II) PanK types having been described that show differences in sequence homology, structural fold, and catalytic and inhibition properties [7, 8]. Together, these factors have strongly suggested that it should be possible to develop selective small molecule inhibitors of the PanKs of pathogenic microorganisms of interest that show little interaction with the human enzyme.

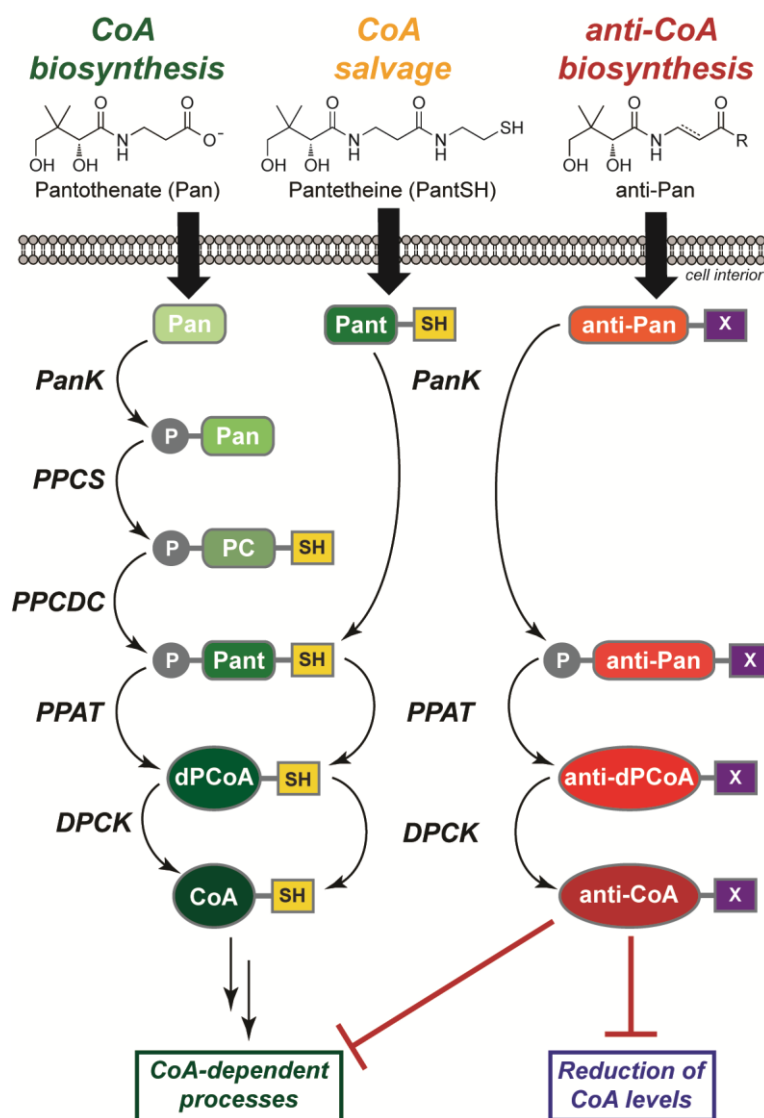


Figure 1. CoA biosynthesis and utilization as an antimicrobial drug target. The biosynthesis of CoA from Pan proceeds in a five-step pathway catalyzed by *PanK* (pantothenate kinase), *PPCS* (phosphopantothenoylcysteine synthetase), *PPCDC* (phosphopantothenoylcysteine decarboxylase), *PPAT* (phosphopantetheine adenyltransferase) and *DPCK* (dephospho-CoA kinase). Of these, *PanK*, *PPCS* and *PPAT* have been successfully targeted in inhibitor development studies aimed at the discovery of new antimicrobials. Additionally, CoA can also be obtained from PantSH (pantetheine, a CoA degradation product) by a shortened salvage pathway that consists of *PanK*, *PPAT* and *DPCK*. This pathway can be hijacked by anti-Pan compounds (a generic structure of such compounds is shown), which are subsequently converted into anti-CoAs that can interfere with CoA-dependent processes and/or reduce CoA levels.

By far the most published studies to date on *PanK* inhibitor discovery have focused on the type I *PanK* enzyme from *Mycobacterium tuberculosis* (*MtPanK_I*) as the target (Figure 2a). *M. tuberculosis* is the causative agent of the debilitating infectious disease tuberculosis (TB), which leads to more than 2 million deaths annually [9]. The enzyme has been crystallized in complex with its substrates, substrate analogues, products and feedback inhibitor (CoA) [10-13]. AstraZeneca identified a range of potent inhibitors of *MtPanK_I*—based on chemical scaffolds of triazoles, thiazoles, quinoline carboxamides and biaryl acetic acid—using a high-throughput screen based on ligand-induced shifts in the protein's melting temperature

[14]. Eight of these compounds based on the triazole and biaryl scaffolds were studied in more detail (the structures of the most potent examples of each scaffold are shown in Figure 2a), with co-crystal structures being obtained to enable correlation of the biochemical and structural data [15]. The triazoles were shown to bind competitive with respect to ATP, while the data obtained for the biaryls suggested a mode of binding that is non-competitive towards ATP. Unfortunately, the compounds described in the study were inactive against *M. tuberculosis* in whole cell inhibition assays, although several showed IC_{50} values (with [ATP] being $\sim K_m$) in the nanomolar range against the enzyme *in vitro*. This result was interrogated further by means of vulnerability studies that used *MtPank_I* over-expression and knockdown strains [16]. These studies showed that a reduction in PanK activity of more than 95% was required to achieve growth inhibition, due to the steady state levels of CoA being far in excess of what is critical for cell survival—a finding that is in agreement with those of previous studies [17, 18]. Consequently, the authors concluded that *MtPank_I* is not an attractive antimycobacterial drug target due to its low vulnerability to inhibition. However, *M. tuberculosis* also expresses a type III PanK enzyme (*MtPank_{III}*), and although studies have shown that this enzyme seems to be non-functional [19], the possibility remains that it is conditionally active and can rescue deficiency in the type I enzyme.

The pantothenamides, a class of PantSH analogues that are mainly considered to exert their antimicrobial activity by acting as CoA antimetabolite precursors, have also been considered as PanK inhibitors in several studies (Figure 2b). A structure-activity relationship (SAR) study showed that these compounds inhibit the Pan phosphorylation activity of several PanK enzymes, although the mode of inhibition was not determined [20]. In a recent structure based study, co-crystal structures of the *Staphylococcus aureus* type II PanK (*SaPank_{II}*) and the type I *Klebsiella pneumoniae* PanK (*KpPank_I*) with *N*-[2-(1,3-benzodioxol-5-yl)ethyl] pantothenamide (N354-Pan, Figure 2b) were solved [21]. These structures revealed that N354-Pan has two distinct conformations in these enzymes. Additionally, both enzymes contained ADP, despite being incubated with ATP for crystallization, and in the case of *SaPank_{II}* phosphorylated N354-Pan was bound in the active site. The authors postulated that *SaPank_{II}* undergoes a conformational change to accommodate N354-Pan, but in doing so locks the enzyme in the closed conformation, preventing the release of phosphorylated N354-Pan and halting the catalytic cycle. By comparison, part of bound N354-Pan was visible through the putative product exit channel in *KpPank_I*, which implied that N354-Pan leaves the active site *via* the channel after phosphorylation and is exchanged for new N354-Pan.

Far less work has been done on type III PanKs (*Pank_{III}*s), since these enzymes were only discovered relatively recently [7]. Currently, the only known inhibitors for *Pank_{III}*s are nucleoside triphosphate mimetics of ATP, which were discovered through the preparation of a library of compounds in which the triphosphate side chain of ATP was replaced by uncharged methylene-triazole linked monosaccharide groups [22]. However, *Pank_{III}*s bind ATP very weakly in an open cavity with no interactions between the enzyme and the adenosine moiety, and the question has been raised as to whether ATP is really the co-substrate of these enzymes [7, 23]. Consequently, the best ATP mimetic (Figure 2c) showed a significant effect on the *Bacillus anthracis* *Pank_{III}* (*BaPank_{III}*) enzyme and competed with ATP binding *in vitro* with a $K_i = 164 \mu\text{M}$ (a threefold decrease of the enzyme's K_M -value for ATP of $510 \mu\text{M}$). Since this value is still too high to be of

pharmaceutical interest, and no whole cell bacterial inhibition was reported, ATP mimetics might not be the most promising avenue to pursue for the discovery of PanK_{III} inhibitors.

In summary, while bacterial PanK enzymes clearly remain valid and important potential targets for antimicrobial drug development, no PanK inhibitor that shows viability in cell growth inhibition tests have been discovered to date.

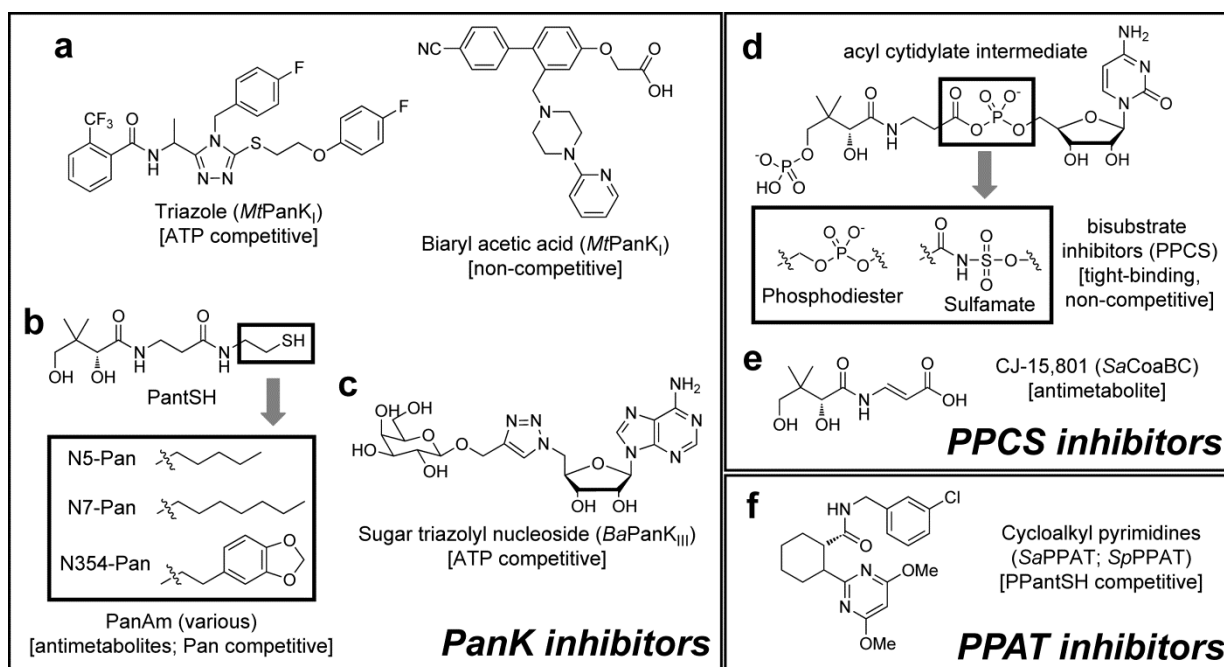


Figure 2. Inhibitor and antimetabolite structures. Structures of the most potent and/or representative inhibitors of the CoA biosynthetic enzymes PanK, PPCS and PPAT; the actual targets and mode of inhibition are also indicated. PanAms (pantothenamides, **b**) are considered to act as antimetabolites, although they could also be Pan competitive inhibitors of PanK enzymes.

Phosphopantothenoylcysteine Synthetase (PPCS)/ Phosphopantothenoylcysteine Decarboxylase (PPCDC)

PPCS (EC 6.3.2.5), the second enzyme of the CoA biosynthetic pathway, catalyzes the Mg^{2+} -dependent formation of 4'-phosphopantothenoylcysteine (PPC) from PPan and L-cysteine using either CTP (in bacteria) or ATP (in eukaryotes) for activation [3, 24, 25]. This difference in the nucleotide triphosphate required for catalysis makes PPCS an excellent target for selective antimicrobial development. Additionally, in bacteria the PPCS enzyme is fused to PPCDC, the enzyme that catalyzes the next step of CoA biosynthesis, to form a bifunctional CoaBC protein (*coaBC* gene product, previously known as *dfp*) [26]. In contrast, the eukaryotic enzymes are typically monofunctional, thereby providing an additional differentiating characteristic [3, 25, 27].

The first reported PPCS inhibitors were compounds that mimicked the structure of the reactive acyl cytidylate intermediate that forms during bacterial PPCS catalysis, but which had the reactive acyl-phosphate moiety replaced by either a phosphodiester or sulfamate isostere (Figure 2d) [28]. These compounds were

found to be non-competitive inhibitors that exhibited slow-onset, tight-binding inhibition with nanomolar IC_{50} and K_i values, and up to 1,000-fold selectivity over the human enzyme. Unfortunately, none of these inhibitors also showed concomitant inhibition of bacterial cell growth, with a lack of cellular penetration being cited as the most probable cause.

More recently, the natural product CJ-15,801 (Figure 2e) was characterized as the precursor to a tight-binding inhibitor of PPCS activity [29]. CJ-15,801 was discovered in 2001 by Pfizer and was shown to inhibit drug-resistant strains of *S. aureus* with micromolar MIC values, but not other bacteria [30]. The compound is a structural analogue of Pan with the notable exception of a trans-substituted double bond in the β -alanine moiety. CJ-15,801 was shown to be phosphorylated by the uniquely selective SaPanK_{II} and subsequently accepted as an alternate substrate for PPCS. Upon cytidylylation, a tight-binding structural mimic of the native reaction intermediate is formed that shows nanomolar K_i values against *E. coli* PPCS (CoaB domain of the CoaBC protein) and *S. aureus* CoaBC [29].

Very little work has been done on the discovery of inhibitors of PPCDC (EC 4.1.1.36), which catalyzes the decarboxylation of PPC's cysteine moiety to give 4'-phosphopantetheine (PPantSH). The only inhibitor described to date is the mechanism-based inactivating agent 4'-phospho-*N*-(1-mercaptomethylcyclopropyl)-pantothenamide (PPan Δ SH) that alkylates a critical catalytic residue at a slow rate ($k_{inact}/K_i \sim 1 \text{ s}^{-1} \cdot \text{M}^{-1}$) [27].

Phosphopantetheine Adenylyltransferase (PPAT)

PPAT (EC 2.7.7.3), the fourth enzyme in the CoA biosynthesis pathway, catalyzes the reversible Mg^{2+} -dependent adenylylation of PPantSH to form dephospho-CoA (dPCoA) and pyrophosphate as products [3]. Typically, the eukaryotic PPAT activity is fused to the last enzyme in the pathway, DPCK, to form a bifunctional PPAT/DPCK protein that is also known as CoA synthase (CoASy) [31-33]. A single enzyme catalyzes the reaction in bacteria, and this activity therefore presents another selective target for antimicrobial development.

A recent high-throughput screening of an AstraZeneca compound library led to the validation of PPAT as a novel target for antibacterial therapy [34], since none of the previously identified PPAT inhibitors exhibited whole cell growth inhibition [35, 36]. The study identified a series of cycloalkyl pyrimidines (Figure 2f) as potential inhibitors of both Gram-positive and Gram-negative species. Further optimization by structure-based design led to substantial improvements against Gram-positive bacteria; these inhibitors were found to be competitive with respect to PPantSH for *S. aureus* and *S. pneumoniae* PPAT. Enzyme inhibition translated to potent growth inhibition against several clinical Gram-positive isolates *in vitro* and in mouse infection models. However, the compounds could not be developed into suitable clinical candidates due to a failure to reconcile their biological activity with drug-like properties.

Another recent study employed an *in silico* screening of the *Helicobacter pylori* PPAT (*HpPPAT*) crystal structure with 407 compound structures retrieved from the PubChem compound database to identify lead compounds that target this enzyme [37]. The screen identified D-amethopterin (methotrexate), a known antimetabolite and anti-cancer drug, as a potential *HpPPAT* inhibitor. The compound exhibited activity

against *HpPPAT in vitro* (as a mixed inhibitor, blocking both PPantSH and ATP binding) and inhibited *H. pylori* viability, but with low potency in both cases. The authors proposed structure optimizations to D-amethopterin to increase binding interaction with *HpPPAT*, although target selectivity would clearly also have to be addressed.

Dephospho-Coenzyme A Kinase (DPCK)

DPCK (EC 2.7.1.24), the final enzyme in the CoA biosynthetic pathway, catalyzes the selective MgATP-dependent phosphorylation of the 3'-hydroxyl of the ribose moiety of dephospho-CoA to form CoA [3]. Unfortunately (from a drug design perspective), bacterial DPCKs show high sequence and structural homology to the DPCK domain of the bifunctional eukaryotic CoASy protein, suggesting that selective inhibition of the bacteria enzyme is unlikely to be achieved [31-33]. Consequently it has not been the focus of any significant inhibitor development study.

COA ANTIMETABOLITES

Anti-CoAs are derived from anti-Pans, compounds that resemble the vitamin precursor of CoA but prevents its catalytically essential thiol to be incorporated and/or that incorporates other reactive moieties that are detrimental to essential CoA-dependent processes. Apart from CJ-15,801, the anti-Pan mentioned above as a precursor to a PPCS inhibitor, the *N*-substituted pantothenamides (PanAms) are by far the best known examples of anti-Pans. These compounds were initially described as growth inhibitors of selected lactic acid bacteria and *Escherichia coli* in 1970 [38], but their potential as antimicrobials have been investigated with renewed interest since it was shown that *N*-pentyl pantothenamide (N5-Pan, Figure 2b), the prototypical example of this class of compounds, is transformed into ethyldethia-CoA, an anti-CoA, by the CoA salvage pathway (Figure 1) [39].

PanAms can exert their inhibitory effects in two ways: first, by reducing the rate of CoA synthesis (since anti-CoAs were found to be produced faster than CoA [39]) and therefore CoA levels, and second, through the formed anti-CoAs inhibiting enzymes and processes dependent on CoA [40]. In regards to the latter, fatty acid biosynthesis has been considered an especially vulnerable target, since the *holo*-acyl carrier protein (*holo*-ACP), which is an essential requirement for type II fatty acid synthase (FAS-II) systems in bacteria, is formed when ACP-synthase (AcpS) transfers the PPantSH group from CoA to *apo*-ACP. However, anti-CoAs can also serve as substrates for this process, leading to the formation of so-called *crypto*-ACPs that lack the ability to act as acyl carriers [18, 41]. The relevance of the two separate inhibition modes, and their relative contributions to PanAm-induced bacterial growth inhibition, still remain a point of debate, as studies supporting either mode have been reported [18, 40, 42].

N5-Pan and its heptyl counterpart, N7-Pan (Figure 2b), remains the most potent bacterial growth inhibitors discovered to date, with N5-Pan exhibiting a minimal inhibitory concentration (MIC) against *E. coli* of 50 μ M, while N7-Pan was found to inhibit *S. aureus* with an MIC of 78 nM (N7-Pan also inhibited *E. coli*,

but its potency was reduced due to TolC-based efflux) [20]. These discoveries were made in a PanAm SAR study conducted on 21 compounds that were tested as competitive substrates of the *E. coli*, *S. aureus*, *Aspergillus nidulans* and mouse PanKs. The compounds were shown to impede PanK activity and to be processed by the *E. coli* CoA salvage enzymes (PanK, PPAT, and DPCK) to form the corresponding anti-CoAs and *crypto*-ACPs, supporting previous findings with N5-Pan in *E. coli* [18]. However, CoA levels in cells treated with these compounds were not determined, and their exact mode of action was thus not pinpointed.

Follow-up studies in which the effect of varying the chain length, oxidation state and functional group composition of the PanAm amide substituent on its ability to inhibit *E. coli* was investigated did not uncover any compound more potent than N5-Pan [43]. Similarly, a study in which variations of the geminal dimethyl groups of the PanAms' pantoic acid moiety were introduced failed to identify a compound showing increased potency against *S. aureus* (both oxacillin-resistant and -sensitive strains) compared to that of N7-Pan [44]. Finally, a small library of 141 pantothenamides was synthesized to evaluate the effects of modifying the PanAm's β -alanine moiety by replacing it with either glycine (yielding a set of α -pantothenamides, α -PanAms) or γ -aminobutyric acid (giving the homopantothenamides, HoPanAms). However, in whole cell inhibition studies on *E. coli* and *S. aureus* N5-Pan and N7-Pan were still found to be the most potent inhibitors respectively [45].

PanAms have also been investigated as antiplasmodial agents, especially since the pathway has been highlighted as an attractive drug target in the malaria parasite *Plasmodium falciparum* based on its essential requirement for Pan and CoA in the blood stage of its life cycle [46]. The first study of the antiplasmodial activity of this class of compounds showed them to have potencies rivaling that of the reference antimalarial chloroquine, with *N*-phenethyl pantothenamide having an IC_{50} of 20 nM [47]. In addition, it was shown that these compounds target Pan and/or CoA utilization and interact with PanK. However, these potency levels were only obtained under conditions in which Vanin pantetheinases—enzymes ubiquitously present in serum that degrade PantSH and its derivatives, and therefore also PanAms—were absent or inactivated. In a follow-up study using the β -alanine modified library synthesized by Van Wyk & Strauss [45], it was demonstrated that pantetheinase does not act on the α -PanAms or HoPanAms series, and these compounds therefore do show antiplasmodial activity even when this enzyme is present, although with a significant reduction in potency (the best candidates had IC_{50} values of ~ 1 – $2 \mu M$) [48].

The discovery of pantetheinase-mediated degradation as a factor in PanAm potency led to the discovery of pantetheinase inhibitors based on Pan as scaffold; using PanAms in combination with these compounds prevented them from being broken down and showed that N5-Pan and N7-Pan have the most potential as antibacterial agents specific for Gram-positive bacteria like *S. aureus*, *Staphylococcus epidermidis*, *S. pneumoniae* and *Streptococcus pyogenes* [49].

Finally, PanAms designed to incorporate dedicated chemical warheads for the inactivation of specific CoA-dependent enzymes have also been developed [50]. In this study, PanAms containing a Michael-acceptor moiety were shown to be converted to the corresponding anti-CoAs, which subsequently inactivated the CoA disulfide reductase (CoADR) enzyme of *S. aureus* that is thought to play a role in this organism's redox regulation. However, the PanAm precursors of the anti-CoAs showing the best CoADR inhibition ($k_{inact}/K_i \sim 40,000 \text{ s}^{-1} \cdot \text{M}^{-1}$) did not show any inhibition of *S. aureus* growth under normal

circumstances, most likely due to poor cell penetration or to CoADR only being essential under oxidative stress conditions (this has not been tested to date).

CONCLUSION

The results of the recent studies of inhibitors of CoA biosynthesis and/or utilization have served to further strengthen the case for these processes being viable and tractable targets for antimicrobial drug development, whether by pursuing an enzyme-focused inhibition strategy, or by exploiting the inhibitory potential of CoA antimetabolites. Considering the dire and pressing need for new antimicrobials acting on novel targets, such studies clearly need to be expanded with the aim of developing the first CoA-directed inhibitor suitable for clinical use.

ACKNOWLEDGMENTS

WJAM and MdV gratefully acknowledge the National Research Foundation (NRF) for an Innovation doctoral scholarship and Innovation postdoctoral fellowship respectively.

FUNDING

This work was supported by grants from the South African Medical Research Council (MRC) and National Research Foundation (NRF).

REFERENCES

- 1 Spry, C., Kirk, K. and Saliba, K. J. (2008) Coenzyme A biosynthesis: an antimicrobial drug target. *FEMS Microbiol. Rev.* **32**, 56-106
- 2 Osterman, A. and Overbeek, R. (2003) Missing genes in metabolic pathways: a comparative genomics approach. *Curr. Opin. Chem. Biol.* **7**, 238-251
- 3 Strauss, E. (2010) Coenzyme A Biosynthesis and Enzymology. In *Comprehensive Natural Products II Chemistry and Biology* (Mander, L. and Liu, H.-W., eds.). pp. 351-410, Elsevier, Oxford
- 4 Genschel, U. (2004) Coenzyme A Biosynthesis: Reconstruction of the Pathway in Archaea and an Evolutionary Scenario Based on Comparative Genomics. *Mol. Biol. Evol.* **21**, 1242-1251
- 5 Leonardi, R., Zhang, Y.-M., Rock, C. O. and Jackowski, S. (2005) Coenzyme A: Back in action. *Prog. Lipid Res.* **44**, 125-153

- 6 Jackowski, S. and Rock, C. O. (1981) Regulation of coenzyme A biosynthesis. *J. Bacteriol.* **148**, 926-932
- 7 Brand, L. A. and Strauss, E. (2005) Characterization of a New Pantothenate Kinase Isoform from *Helicobacter pylori*. *J. Biol. Chem.* **280**, 20185-20188
- 8 Yang, K., Eyobo, Y., Brand, L. A., Martynowski, D., Tomchick, D., Strauss, E. and Zhang, H. (2006) Crystal Structure of a Type III Pantothenate Kinase: Insight into the Mechanism of an Essential Coenzyme A Biosynthetic Enzyme Universally Distributed in Bacteria. *J. Bacteriol.* **188**, 5532-5540
- 9 Dye, C., Watt, C. J., Bleed, D. M., Hosseini, S. and Raviglione, M. C. (2005) Evolution of tuberculosis control and prospects for reducing tuberculosis incidence, prevalence, and deaths globally. *JAMA.* **293**, 2767-2775
- 10 Das, S., Kumar, P., Bhor, V., Surolia, A. and Vijayan, M. (2006) Invariance and variability in bacterial PanK: a study based on the crystal structure of *Mycobacterium tuberculosis* PanK. *Acta Cryst. D.* **62**, 628-638
- 11 Chetnani, B., Das, S., Kumar, P., Surolia, A. and Vijayan, M. (2009) *Mycobacterium tuberculosis* pantothenate kinase: possible changes in location of ligands during enzyme action. *Acta Cryst. D.* **65**, 312-325
- 12 Chetnani, B., Kumar, P., Surolia, A. and Vijayan, M. (2010) *M. tuberculosis* Pantothenate Kinase: Dual Substrate Specificity and Unusual Changes in Ligand Locations. *Journal of Molecular Biology.* **400**, 171-185
- 13 Chetnani, B., Kumar, P., Abhinav, K. V., Chhibber, M., Surolia, A. and Vijayan, M. (2011) Location and conformation of pantothenate and its derivatives in *Mycobacterium tuberculosis* pantothenate kinase: insights into enzyme action. *Acta Cryst. D.* **67**, 774-783
- 14 Venkatraman, J., Bhat, J., Solapure, S. M., Sandesh, J., Sarkar, D., Aishwarya, S., Mukherjee, K., Datta, S., Malolanarasimhan, K., Bandodkar, B. and Das, K. S. (2012) Screening, Identification, and Characterization of Mechanistically Diverse Inhibitors of the *Mycobacterium tuberculosis* Enzyme, Pantothenate Kinase (CoaA). *J. Biomol. Screen.* **17**, 293-302
- 15 Björkelid, C., Bergfors, T., Raichurkar, A. K. V., Mukherjee, K., Malolanarasimhan, K., Bandodkar, B. and Jones, T. A. (2013) Structural and Biochemical Characterization of Compounds Inhibiting *Mycobacterium tuberculosis* Pantothenate Kinase. *J. Biol. Chem.* **288**, 18260-18270
- 16 Reddy, B. K. K., Landge, S., Ravishankar, S., Patil, V., Shinde, V., Tantry, S., Kale, M., Raichurkar, A., Menasinakai, S., Mudugal, N. V., Ambady, A., Ghosh, A., Tunduguru, R., Kaur, P., Singh, R., Kumar, N., Bharath, S., Sundaram, A., Bhat, J., Sambandamurthy, V. K., Björkelid, C., Jones, T. A., Das, K., Bandodkar, B., Malolanarasimhan, K., Mukherjee, K. and Ramachandran, V. (2014) Assessment of *Mycobacterium tuberculosis* Pantothenate kinase vulnerability through target knock down and mechanistically diverse inhibitors. *Antimicrobial. Agents Chemother.*, DOI: 10.1128/aac.00140-00114

- 17 Buchholz, A., Takors, R. and Wandrey, C. (2001) Quantification of Intracellular Metabolites in *Escherichia coli* K12 Using Liquid Chromatographic-Electrospray Ionization Tandem Mass Spectrometric Techniques. *Anal. Biochem.* **295**, 129-137
- 18 Zhang, Y.-M., Frank, M. W., Virga, K. G., Lee, R. E., Rock, C. O. and Jackowski, S. (2004) Acyl Carrier Protein Is a Cellular Target for the Antibacterial Action of the Pantothenamide Class of Pantothenate Antimetabolites. *J. Biol. Chem.* **279**, 50969-50975
- 19 Awasthy, D., Ambady, A., Bhat, J., Sheikh, G., Ravishankar, S., Subbulakshmi, V., Mukherjee, K., Sambandamurthy, V. and Sharma, U. (2010) Essentiality and functional analysis of type I and type III pantothenate kinases of *Mycobacterium tuberculosis*. *Microbiology.* **156**, 2691-2701
- 20 Virga, K. G., Zhang, Y.-M., Leonardi, R., Ivey, R. A., Hevener, K., Park, H.-W., Jackowski, S., Rock, C. O. and Lee, R. E. (2006) Structure-activity relationships and enzyme inhibition of pantothenamide-type pantothenate kinase inhibitors. *Bioorg. Med. Chem.* **14**, 1007-1020
- 21 Hughes, S. J., Antoshchenko, T., Kim, K. P., Smil, D. and Park, H.-W. (2014) Structural characterization of a new N-substituted pantothenamide bound to pantothenate kinases from *Klebsiella pneumoniae* and *Staphylococcus aureus*. *Proteins: Struct., Funct., Bioinf.*, DOI: 10.1002/prot.24524
- 22 Rowan, A. S., Nicely, N. I., Cochrane, N., Wlassoff, W. A., Claiborne, A. and Hamilton, C. J. (2009) Nucleoside triphosphate mimicry: a sugar triazolyl nucleoside as an ATP-competitive inhibitor of *B. anthracis* pantothenate kinase. *Org. Biomol. Chem.* **7**, 4029-4036
- 23 Hong, B. S., Yun, M. K., Zhang, Y.-M., Chohnan, S., Rock, C. O., White, S. W., Jackowski, S., Park, H.-W. and Leonardi, R. (2006) Prokaryotic Type II and Type III Pantothenate Kinases: The Same Monomer Fold Creates Dimers with Distinct Catalytic Properties. *Structure.* **14**, 1251-1261
- 24 Begley, T. P., Kinsland, C. and Strauss, E. (2001) The biosynthesis of coenzyme A in bacteria. *Vitam. Horm.* **61**, 157-171
- 25 Manoj, N., Strauss, E., Begley, T. P. and Ealick, S. E. (2003) Structure of Human Phosphopantothenoylcysteine Synthetase at 2.3 Å Resolution. *Structure.* **11**, 927-936
- 26 Strauss, E., Kinsland, C., Ge, Y., McLafferty, F. W. and Begley, T. P. (2001) Phosphopantothenoylcysteine Synthetase from *Escherichia coli* : Identification and Characterization of the Last Unidentified Coenzyme A Biosynthetic Enzyme in Bacteria. *J. Biol. Chem.* **276**, 13513-13516
- 27 Strauss, E., Zhai, H., Brand, L. A., McLafferty, F. W. and Begley, T. P. (2004) Mechanistic Studies on Phosphopantothenoylcysteine Decarboxylase: Trapping of an Enethiolate Intermediate with a Mechanism-Based Inactivating Agent. *Biochemistry.* **43**, 15520-15533
- 28 Patrone, J. D., Yao, J., Scott, N. E. and Dotson, G. D. (2009) Selective Inhibitors of Bacterial Phosphopantothenoylcysteine Synthetase. *J. Am. Chem. Soc.* **131**, 16340-16341

- 29 van der Westhuyzen, R., Hammons, Justin C., Meier, Jordan L., Dahesh, S., Moolman, Wessel J. A., Pelly, Stephen C., Nizet, V., Burkart, Michael D. and Strauss, E. (2012) The Antibiotic CJ-15,801 Is an Antimetabolite that Hijacks and Then Inhibits CoA Biosynthesis. *Chem. Biol.* **19**, 559-571
- 30 Sugie, Y., Dekker, K.A., Hirai, H., Ichiba, T., Ishiguro, M., Shiomi, Y., Sugiura, A., Brennan, L., Duignan, J., Huang, L.H., Sutcliffe, J. and Kojima, Y. (2001) CJ-15,801, a novel antibiotic from a fungus, *Seimatosporium sp.* *J. Antibiot.* **54**, 1060-1065
- 31 Daugherty, M., Polanuyer, B., Farrell, M., Scholle, M., Lykidis, A., De Crecy-Lagard, V. and Osterman, A. (2002) Complete reconstitution of the human coenzyme A biosynthetic pathway via comparative genomics. *J. Biol. Chem.* **277**, 21431-21439
- 32 Aghajanian, S. and Worrall, D. M. (2002) Identification and characterization of the gene encoding the human phosphopantetheine adenylyltransferase and dephospho-CoA kinase bifunctional enzyme (CoA synthase). *Biochem. J.* **365**, 13-18
- 33 Zhyvoloup, A., Nemazanyy, I., Babich, A., Panasyuk, G., Pobigailo, N., Vudmaska, M., Naidenov, V., Kukhareno, O., Palchevskii, S., Savinska, L., Ovcharenko, G., Verdier, F., Valovka, T., Fenton, T., Rebholz, H., Wang, M.-L., Shepherd, P., Matsuka, G., Filonenko, V. and Gout, I. T. (2002) Molecular Cloning of CoA Synthase: The Missing Link in CoA Biosynthesis. *J. Biol. Chem.* **277**, 22107-22110
- 34 de Jonge, B. L. M., Walkup, G. K., Lahiri, S. D., Huynh, H., Neckermann, G., Utley, L., Nash, T. J., Brock, J., San Martin, M., Kutschke, A., Johnstone, M., Laganas, V., Hajec, L., Gu, R.-F., Ni, H., Chen, B., Hutchings, K., Holt, E., McKinney, D., Gao, N., Livchak, S. and Thresher, J. (2013) Discovery of Inhibitors of 4'-Phosphopantetheine Adenylyltransferase (PPAT) To Validate PPAT as a Target for Antibacterial Therapy. *Antimicrob. Agents Chemother.* **57**, 6005-6015
- 35 Miller, J. R., Thanabal, V., Melnick, M. M., Lall, M., Donovan, C., Sarver, R. W., Lee, D.-Y., Ohren, J. and Emerson, D. (2010) The Use of Biochemical and Biophysical Tools for Triage of High-Throughput Screening Hits – A Case Study with *Escherichia coli* Phosphopantetheine Adenylyltransferase. *Chem. Biol. Drug Design.* **75**, 444-454
- 36 Zhao, L., Allanson, N. M., Thomson, S. P., Maclean, J. K. F., Barker, J. J., Primrose, W. U., Tyler, P. D. and Lewendon, A. (2003) Inhibitors of phosphopantetheine adenylyltransferase. *Eur. J. Med. Chem.* **38**, 345-349
- 37 Cheng, C.-S., Jia, K.-F., Chen, T., Chang, S.-Y., Lin, M.-S. and Yin, H.-S. (2013) Experimentally Validated Novel Inhibitors of *Helicobacter pylori* Phosphopantetheine Adenylyltransferase Discovered by Virtual High-Throughput Screening. *PLoS ONE.* **8**, e74271
- 38 Clifton, G., Bryant, S. R. and Skinner, C. G. (1970) N^1 -(substituted) pantothenamides, antimetabolites of pantothenic acid. *Arch. Biochem. Biophys.* **137**, 523-528

- 39 Strauss, E. and Begley, T. P. (2002) The Antibiotic Activity of *N*-Pentylpantothenamide Results from Its Conversion to Ethyldethia-Coenzyme A, a Coenzyme A Antimetabolite. *J. Biol. Chem.* **277**, 48205-48209
- 40 Thomas, J. and Cronan, J. E. (2010) Antibacterial Activity of *N*-Pentylpantothenamide Is Due to Inhibition of Coenzyme A Synthesis. *Antimicrobial. Agents Chemother.* **54**, 1374-1377
- 41 Mercer, A. C. and Burkart, M. D. (2007) The ubiquitous carrier protein—a window to metabolite biosynthesis. *Nat. Prod. Rep.* **24**, 750-773
- 42 Leonardi, R., Chohnan, S., Zhang, Y.-M., Virga, K. G., Lee, R. E., Rock, C. O. and Jackowski, S. (2005) A Pantothenate Kinase from *Staphylococcus aureus* Refractory to Feedback Regulation by Coenzyme A. *J. Biol. Chem.* **280**, 3314-3322
- 43 Mercer, A. C., Meier, J. L., Hur, G. H., Smith, A. R. and Burkart, M. D. (2008) Antibiotic evaluation and in vivo analysis of alkynyl Coenzyme A antimetabolites in *Escherichia coli*. *Bioorg. Med. Chem. Lett.* **18**, 5991-5994
- 44 Akinnusi, T. O., Vong, K. and Auclair, K. (2011) Geminal dialkyl derivatives of *N*-substituted pantothenamides: Synthesis and antibacterial activity. *Bioorg. Med. Chem.* **19**, 2696-2706
- 45 van Wyk, M. and Strauss, E. (2008) Development of a method for the parallel synthesis and purification of *N*-substituted pantothenamides, known inhibitors of coenzyme A biosynthesis and utilization. *Org. Biomol. Chem.* **6**, 4348-4355
- 46 Spry, C., van Schalkwyk, D. A., Strauss, E. and Saliba, K. J. (2010) Pantothenate utilization by *Plasmodium* as a target for antimalarial chemotherapy. *Infect. Disord. Drug Targets.* **10**, 200-216
- 47 Spry, C., Macuamule, C., Lin, Z., Virga, K. G., Lee, R. E., Strauss, E. and Saliba, K. J. (2013) Pantothenamides Are Potent, On-Target Inhibitors of *Plasmodium falciparum* Growth When Serum Pantetheinase Is Inactivated. *PLoS ONE.* **8**, e54974
- 48 de Villiers, M., Macuamule, C., Spry, C., Hyun, Y.-M., Strauss, E. and Saliba, K. J. (2013) Structural Modification of Pantothenamides Counteracts Degradation by Pantetheinase and Improves Antiplasmodial Activity. *ACS Med. Chem. Lett.* **4**, 784-789
- 49 Jansen, P. A. M., Hermkens, P. H. H., Zeeuwen, P. L. J. M., Botman, P. N. M., Blaauw, R. H., Burghout, P., van Galen, P. M., Mouton, J. W., Rutjes, F. P. J. T. and Schalkwijk, J. (2013) Combination of Pantothenamides with Vanin Inhibitors as a Novel Antibiotic Strategy against Gram-Positive Bacteria. *Antimicrobial. Agents Chemother.* **57**, 4794-4800
- 50 van der Westhuyzen, R. and Strauss, E. (2010) Michael acceptor-containing coenzyme A analogues as inhibitors of the atypical coenzyme A disulfide reductase from *Staphylococcus aureus*. *J. Am. Chem. Soc.* **132**, 12853-12855

2.2 Summary of mini-review

Several aspects highlighted in the review reproduced on the preceding pages are specifically relevant to this study. First, the essential requirement of CoA in all organisms: the cofactor is ubiquitous and must be obtained through *de novo* biosynthesis from Pan using a conserved pathway consisting of five enzymatic steps. Second, the potential for the development of selective inhibitors: in several cases the specific enzymes that catalyse these reactions in humans and pathogenic microorganisms show significant diversity in terms of sequence, structure and on a mechanistic level. Third, the CoA biosynthesis pathway enzymes have been validated as drug targets, with most work having been done on the PanK, PPCS and PPAT enzymes. Taken together, the microbial CoA biosynthetic enzymes are clearly ready for exploitation as new antimicrobial drug targets. This is reinforced by the possible role of CoA in *S. aureus* redox balance under conditions of oxidative stress.

2.3 Previous CoADR research

SaCoADR has been targeted by PanAms designed to incorporate dedicated chemical warheads [1]. In that study, PanAms containing a Michael-acceptor moiety were shown to be converted to the corresponding anti-CoAs, which subsequently inactivated SaCoADR. However, the PanAm precursors of the anti-CoAs showing the best SaCoADR inhibition did not show any inhibition of *S. aureus* growth under normal circumstances, most likely due to poor cell penetration or to CoADR only being essential under oxidative stress conditions [1]. The effect of these compounds (as well as the relevance of SaCoADR) under conditions of oxidative stress remains to be determined.

The crystal structures of SaCoADR bound to the Michael-acceptor-containing inhibitors, synthesised by Van der Westhuyzen [1], has also been solved [2]. These structures highlighted two important features: First, two tyrosine residues (Tyr₃₆₁ and Tyr₄₁₉) in the active site that were previously identified to potentially be important for activity [3], were found to interact with one of the sulfone oxygen atoms of one of the CoA analogue that showed the best inhibition of CoADR. This suggests that these tyrosine residues are very likely to play an important role in the stabilisation of the inhibitors within the active site of SaCoADR, which may also explain the excellent *in vitro* activity of these inhibitors against SaCoADR [1]. The relevance of these interactions needs to be explored further for the development of more effective inhibitors of SaCoADR.

It is clear then that, in terms of the validation of SaCoADR as a drug target, two main questions need to be addressed. First, since it is proposed to be active in the maintenance of redox balance in *S. aureus*, its physiological importance under oxidative stress conditions need to be established. Second, the existing SaCoADR inhibitors must be shown to have an increased effect on the growth of *S. aureus* under oxidative stress conditions.

2.4 Previous research on the inhibition of PPCS by CJ-15, 801

As mentioned in the mini-review above, the natural product CJ-15,801 was characterised as the precursor to a tight-binding inhibitor of PPCS activity [4]. CJ-15,801 was shown to be phosphorylated by the uniquely selective SaPanK_{II} and subsequently accepted as an alternate substrate for PPCS. Upon cytidylylation, a tight-binding structural mimic of the native reaction intermediate is formed that shows nanomolar K_i values against *Escherichia coli* PPCS (CoaB domain of the CoaBC protein) and *S. aureus* CoaBC. It is significant that this inhibitor is seemingly resistant to hydrolysis or acyl transfer, even though it contains an activated acyl phosphate moiety. Investigation of the molecular basis for the increased stability of PCJ-CMP compared to PPan-CMP may provide valuable insights for future drug development and it might serve as a generalised starting point for the development of other β -amino acid-containing tight-binding inhibitors. CJ-15,801 as an inhibitor cannot really be improved, since its mechanism of action relies on its double bond and it fits perfectly into the active site of SaPanK_{II} already. Therefore, structural modification of the compound is unlikely to yield better inhibition of PPCS, but insights into its molecular basis of inhibition may be important for drug development against similar bacterial targets.

2.5 References

1. van der Westhuyzen, R. and E. Strauss, *Michael Acceptor-Containing Coenzyme A Analogues As Inhibitors of the Atypical Coenzyme A Disulfide Reductase from Staphylococcus aureus*. Journal of the American Chemical Society, 2010. **132**(37): p. 12853-12855.
2. Wallace, B.D., et al., *Turnover-Dependent Covalent Inactivation of Staphylococcus aureus Coenzyme A-Disulfide Reductase by Coenzyme A-Mimetics: Mechanistic and Structural Insights*. Biochemistry, 2012. **51**(39): p. 7699-7711.
3. Mallett, T.C., et al., *Structure of Coenzyme A-Disulfide Reductase from Staphylococcus aureus at 1.54 Å Resolution*. Biochemistry, 2006. **45**(38): p. 11278-11289.
4. van der Westhuyzen, R., et al., *The Antibiotic CJ-15,801 Is an Antimetabolite that Hijacks and Then Inhibits CoA Biosynthesis*. Chemistry & Biology, 2012. **19**(5): p. 559-571.

Chapter 3: Evaluation of CoADR as an anti-staphylococcal drug target¹

3.1 Introduction

The pathogenic bacterium *Staphylococcus aureus* is remarkably successful at dealing with oxidative stress, specifically the oxidative bursts of reactive oxygen species (ROS) released as part of its host's innate immune system defences against infection. This is due to the bacterium's highly efficient removal and detoxification of ROS, which allows it to frequently survive such attacks. All organisms maintain redox balance through a ubiquitous mechanism that consists of three sets of actors: 1) low molecular weight thiols (LMWTs), which act as sacrificial reductants [1], 2) thioredoxin-fold proteins (TFPs) that either similarly act as sacrificial reductants or act as intermediaries in the transfer of electrons [2, 3], and 3) dedicated flavin disulfide reductase (FDR) enzymes that reduce the oxidised forms of both LMWTs and TFPs (using NAD(P)H as electron source) to restore these to their original state [4]. While this is also the case in *S. aureus*, significant uncertainty remains about the identity of the major LMWT responsible for redox balance in this organism since it is incapable of producing glutathione (GSH, Figure 3.1, **1b**), the main LMWT in most organisms [5, 6]. Two alternative candidates have been proposed to fulfil this role instead: the essential metabolic cofactor coenzyme A (CoA, Figure 3.1, **1a**) [7], or bacillithiol (BSH, Figure 3.1, **1c**), a unique LMWT recently discovered in the Bacillales and in *Deinococcus* [8, 9]. The latter's candidacy is supported by recent studies highlighting its important role in the oxidative stress response of *S. aureus*, as well as its vital functions in detoxification and antibiotic resistance [8, 10]. However, no dedicated disulfide reductase has been found to date that can reduce bacillithiol disulfide (BSSB), although some candidates have been proposed for this activity based on bioinformatics analysis [9, 11]. In the absence of a BSSB-reductase enzyme, it remains unclear how free BSH would be regenerated. CoA, on the other hand, has long been considered a promising candidate as the main LMWT in *S. aureus* since it is maintained at high concentrations in *S. aureus*, and autoxidises at a quarter the rate of GSH as catalysed by copper [7, 12]. It also has a dedicated disulfide reductase, coenzyme A disulfide reductase (CoADR) [7], which has been characterised and shown to have a unique mechanism among FDRs. However, several factors also cast doubt on the role of CoA as the major LMWT in *S. aureus*. These include the fact that CoA cannot serve as a reservoir of cysteine (it contains cysteamine – decarboxylated cysteine – instead) [13], that CoADR is non-essential under normal growth conditions [14] (also the knockout strain of *cdr*, the gene encoding CoADR, is viable) and that its expression is not significantly upregulated under oxidative stress conditions [15].

¹ The work on the structural characterization of CoADR described in this chapter has been published as part of a bigger study: Wallace, B.D., Edwards, J.S., Wallen, J.R., **Moolman, W.J.A.**, Van der Westhuyzen, R., Strauss, E., Redinbo, M.R. & Claiborne, A. Turnover-Dependent Covalent Inactivation of *Staphylococcus aureus* Coenzyme A-Disulfide Reductase by Coenzyme A-Mimetics: Mechanistic and Structural Insights. *Biochemistry* **51**(39): 7699-7711 (2012). The published version of the article is reproduced in Appendix.

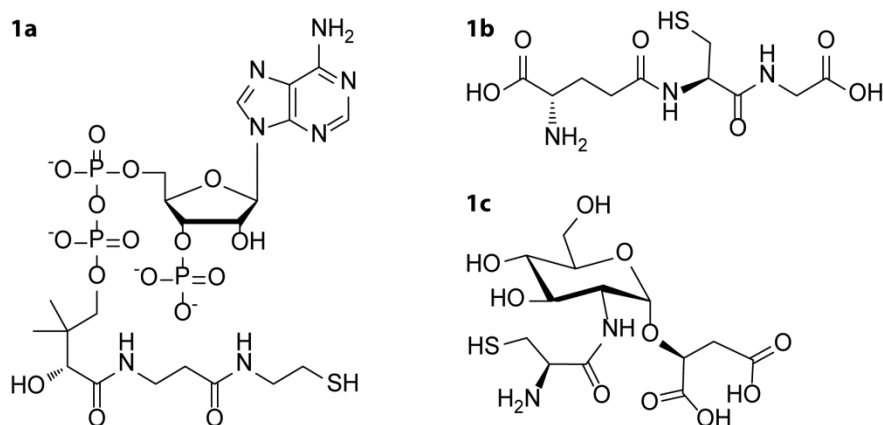


Figure 3.1: Major LMWTs: coenzyme A (CoA, **1a**), Glutathione (GSH, **1b**) and Bacillithiol (BSH, **1c**).

Although several questions therefore remain regarding the redox balancing mechanisms in *S. aureus*, CoADR remains the only known FDR that specifically acts on a LMWT disulfide in this organism. As such, it remains a potentially interesting anti-staphylococcal drug target. Several additional reasons have also prompted us to investigate it further: first, the inhibition of FDRs has previously been proven to be a successful therapeutic strategy with examples that include glutathione reductase (GR) as an anti-cancer treatment [16, 17], trypanothione reductase as target against *Trypanosoma brucei* (sleeping sickness) [18, 19], thioredoxin reductase against *Plasmodium falciparum* (malaria) [20, 21] and both lipamide dehydrogenase and mycothiol disulfide reductase against *Mycobacterium tuberculosis* (TB) [22, 23]. Second, CoADR presents a unique target, since it relies on a different reaction mechanism than most other FDRs, using a single catalytic Cys-residue to form a mixed enzyme-substrate disulfide [24], which is then reduced (Figure 3.2). This is in contrast to other FDRs such as GR, which uses a thiol-disulfide relay with a redox-active disulfide contained in CXXXXC motif as the final electron acceptor [4]. Significantly, humans do not possess a CoADR and uses GSH and GR to maintain redox balance, also making CoADR a selective target. Third, although the gene encoding CoADR has been shown to be non-essential under normal growth conditions, its importance to the survival of *S. aureus* under oxidative stress conditions – when it would be most relevant – has not been determined.

In previous studies our group sought to explore the druggability of CoADR. This was done through the design, synthesis and characterisation of the first known small molecule inhibitors of *S. aureus* CoADR (SaCoADR) [25]. The design strategy behind these inhibitors was to mimic the structure of the enzyme's native substrate, (CoAS)₂, and to irreversibly inhibit SaCoADR in a manner similar to what has previously been done for cysteine protease inhibitors [26-28]. This was possible since, like the cysteine proteases, CoADR also employs nucleophilic attack by a single catalytic cysteine residue during catalysis. In this strategy, a Michael acceptor (α , β -unsaturated ethyl or *tert*-butyl esters, or methyl or phenyl vinyl sulfones) is introduced into each inhibitor in such a manner that its electrophilic centre directly correlates to the position of the disulfide in the native substrate (Figure 3.3A). Since the CoADR mechanism involves a nucleophilic attack of the active site cysteine (Cys₄₃) on the CoA-disulfide (CoAS)₂ (Figure 3.2), this Cys₄₃ is therefore ideally positioned to react with the Michael acceptor to form a covalent link, which subsequently leads to

irreversible inhibition (Figure 3.3B). For both the substrate and the inhibitor a conserved tyrosine residue has been implicated in catalysis by acting as the proton donor of either the departing thiol or the α -carbanion, respectively [29].

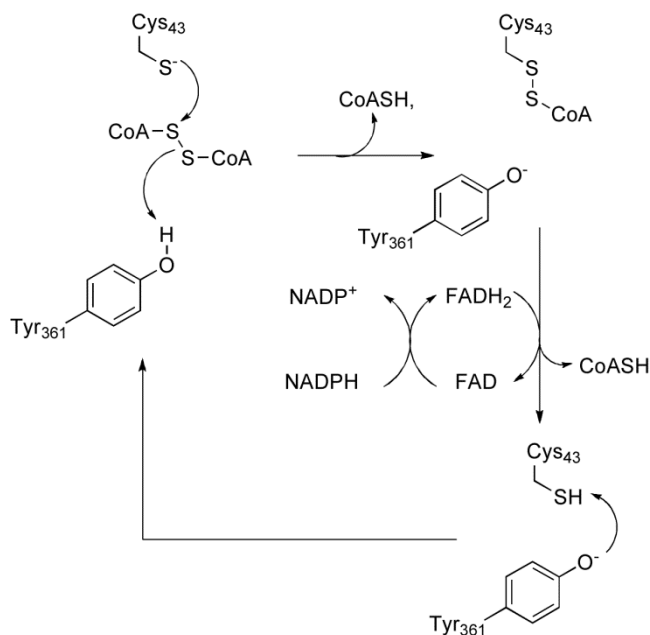


Figure 3.2: SaCoADR reaction mechanism.

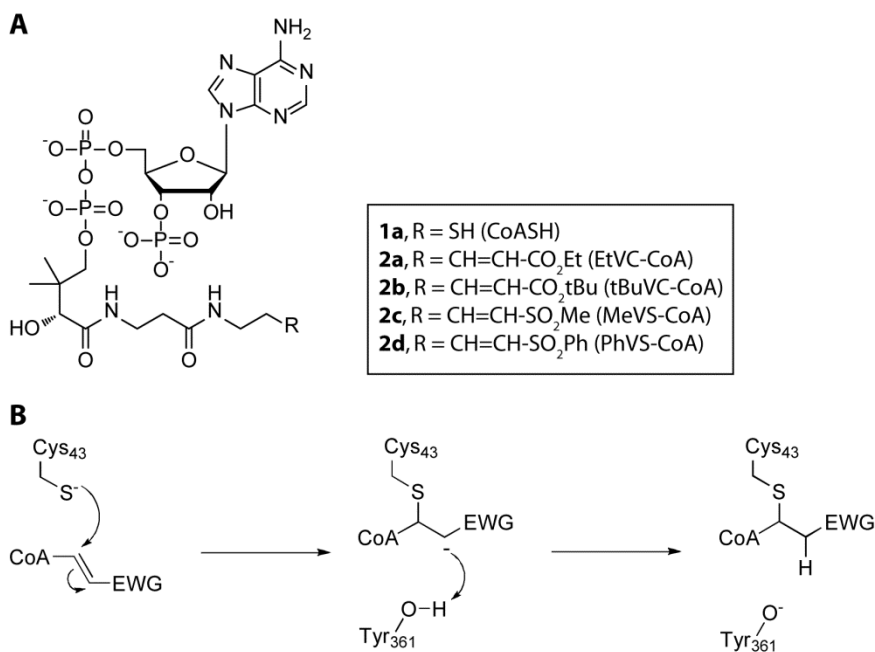


Figure 3.3: (A) Structures of CoA and Michael-acceptor CoA analogues. (B) Irreversible inhibition mechanism of CoADR by Michael-acceptor CoA analogues. EWG = electron withdrawing group.

The CoA analogues (Figure 3.3A, **2a–d**) were prepared *via* chemo-enzymatic synthesis from the corresponding Michael acceptor-containing pantothenamide precursors *in vitro* [25]. This method has been used successfully with several pantothenamides by either using the *E. coli* CoA biosynthetic enzymes pantothenate kinase (PanK), phosphopantetheine adenylyl transferase (PPAT) and dephosphocoenzyme A kinase (DPCK) to convert these to the CoA analogues *in vitro*, or by using the native biosynthetic enzymes by treating bacterial cell cultures with these compounds [30]. The Michael acceptor-containing CoA analogues prepared in this manner were subsequently characterised as inhibitors of SaCoADR *in vitro* (Table 3.1). The Michael acceptor-containing pantothenamide precursors were also tested, but were found not to show any inhibition. This indicated that the adenosine and phosphate moieties of CoA are essential for recognition and binding in the active site of the enzyme, and that the pantothenamides must first be metabolically activated before they can act as CoADR inhibitors [25]. Finally, the pantothenamide precursors were also tested as whole cell growth inhibitors of *S. aureus*, assuming that these compounds would readily enter the targeted bacteria as has been shown to be the case for several other similar pantothenamides [31, 32] (Table 3.1). The predicted pathway for inhibition is summarised schematically in Figure 3.4. The results indicated that although especially the sulfone-containing inhibitors showed excellent *in vitro* inhibition of CoADR (nanomolar range K_i); their corresponding pantothenamide precursors exhibited no whole cell growth inhibition *in vitro*. Conversely, the ester-containing inhibitors were less efficient inhibitors of CoADR *in vitro* than the sulfones, but their pantothenamide precursors did inhibit staphylococcal growth. While these results therefore provided proof-of-concept evidence that Michael acceptor-containing CoA analogues can act as excellent CoADR inhibitors *in vitro*, the lack of a clear correlation between the *in vitro* and whole cell inhibition suggested that the enzyme might not be an ideal anti-staphylococcal drug target.

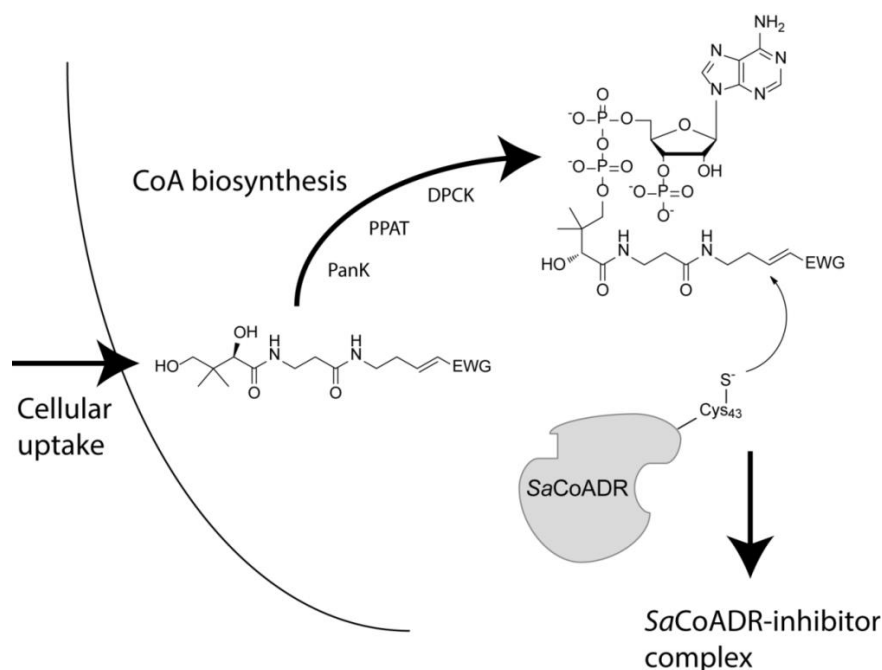


Figure 3.4: A schematic representation of the inhibition of SaCoADR by Michael-acceptor-containing CoA analogues *in vivo*. First a pantothenamide precursor is taken up into the bacterial cell. The compound then enters the CoA biosynthesis pathway and is converted by the PanK, PPAT and DPCK CoA-biosynthesis enzymes to the corresponding CoA analogue. The Michael-acceptor is then the target of nucleophilic attack by the thiolate anion of Cys₄₃ of SaCoADR that causes the active site cysteine to be irreversibly modified. EWG = electron withdrawing group, PanK = pantothenate kinase, PPAT = phosphopantetheine adenylyl transferase, DPCK = dephosphocoenzyme A kinase.

Table 3.1: Enzyme and whole cell inhibition data of SaCoADR inhibitors [25]. The Michael acceptor-containing CoA analogue inhibitors were tested *in vitro* against the SaCoADR enzyme and the Michael acceptor-containing pantothenamide precursors were tested as whole cell growth inhibitors against *S.aureus*. EWG = electron withdrawing group, MIC = minimum inhibitory concentration. *No growth inhibition observed at $\leq 200 \mu\text{M}$ inhibitor concentration.

	<i>In vitro</i> enzyme inhibition (CoA analogue)		Whole cell growth inhibition (Pantothenamide)	
EWG	CoA analogue	K_i (μM)	Pantothenamide	MIC (μM)
CO₂Et	EtVC-CoA	0.66 ± 0.12	EtVC-Pan	55
CO₂tBu	tBuVC-CoA	5.16 ± 0.96	tBuVC-Pan	52
SO₂Me	MeVS-CoA	0.30 ± 0.05	MeVS-Pan	n/a*
SO₂Ph	PhVS-CoA	0.04 ± 0.01	PhVS-Pan	n/a*

In light of our poor knowledge of the physiological role of CoADR – also in the context of the *S. aureus* oxidative stress defence mechanisms – the current study was conducted to further investigate the potential of SaCoADR as an anti-staphylococcal drug target. This was done through the structural characterisation of the interactions between the enzyme and Michael acceptor-containing CoA analogues previously developed in our group, specifically focusing on the role that two conserved Tyr-residues play in locking down the inhibitors. The goal of these studies was to inform any potential future work on the design of improved CoADR inhibitors. Next, we sought to explain the apparent lack of correlation between the *in vitro* inhibition of CoADR by the Michael acceptor-containing CoA analogues and whole cell growth inhibition by their corresponding Michael acceptor-containing pantothenamide precursors. This was done by considering the cell-permeability of the precursors, and the ability of the native *S. aureus* CoA biosynthetic enzymes to convert the pantothenamide precursors to the inhibitory CoA analogues. The specificity of the inhibition shown by the vinyl ester-containing pantothenamide was also investigated by using an equivalent, but non-electrophilic, counterpart in parallel inhibition reactions. Finally, to establish the physiological relevance of SaCoADR, the importance of several actors predicted to be important in *S. aureus* redox balance were investigated under oxidative stress conditions. This was done by comparing the survival of a wild-type MRSA strain (JE2) and strains in which specific genes have been knocked-out in several whole cell assays that specifically test the cells' ability to withstand oxidative stress. Taken together, our results indicate that the poor whole cell inhibition of CoADR-directed inhibitors is most likely tied to the non-essentiality of the target under normal growth conditions, and not to failure of the inhibitors to reach and interact with their target. The preliminary data gathered in this study indicate that this is also the case under oxidative stress conditions, although the physiological importance of CoADR in these circumstances deserves further investigation.

3.2 Results

3.2.1 Structural characterisation of the SaCoADR–CoA analogue inhibitor interactions²

As a first step towards an increased understanding of SaCoADR as a potential drug target, the crystal structures of SaCoADR bound to the ethyl vinyl carboxylate-containing inhibitor **2a** (EtVC-CoA), the methyl vinyl sulfone-containing inhibitor **2c** (MeVS-CoA) or the phenyl vinyl sulfone-containing inhibitor **2d** (PhVS-CoA) were solved [33]. The final refined models each included one FAD and one inhibitor molecule per active site (Figure 3.5A), and showed that the inhibitor was bound in both active sites of the dimeric enzyme, with full occupancy. In all three inhibitor complexes the –dethia-CoA moiety was clearly present in the same site occupied by the Cys₄₃-SSCoA redox centre in oxidised SaCoADR (Figure 3.5B).

Several significant observations were made in terms of improving on future inhibitor design. An unoccupied cleft adjacent to bound CoAS– was also shown to be unoccupied in the inhibitor complexes and provides ample opportunity for the elaboration of inhibitor structures (Figures 3.5B and 3.6). In particular, it is clear that sufficient space is available around the phenyl ring of bound PhVS-CoA to introduce additional moieties that could potentially interact with other parts of the enzyme active site for tighter and more selective inhibitor binding.

²The work described in this section was done in collaboration with Profs. Al Claiborne (Wake Forest University, USA) and Matt Redinbo (University of North Carolina, Chapel Hill) and has been published in modified format. All structures were solved by Bret Wallace and Jonathan Edwards. My major contribution to this work was the purification of enzymes and performing activity assays as described in the next section.

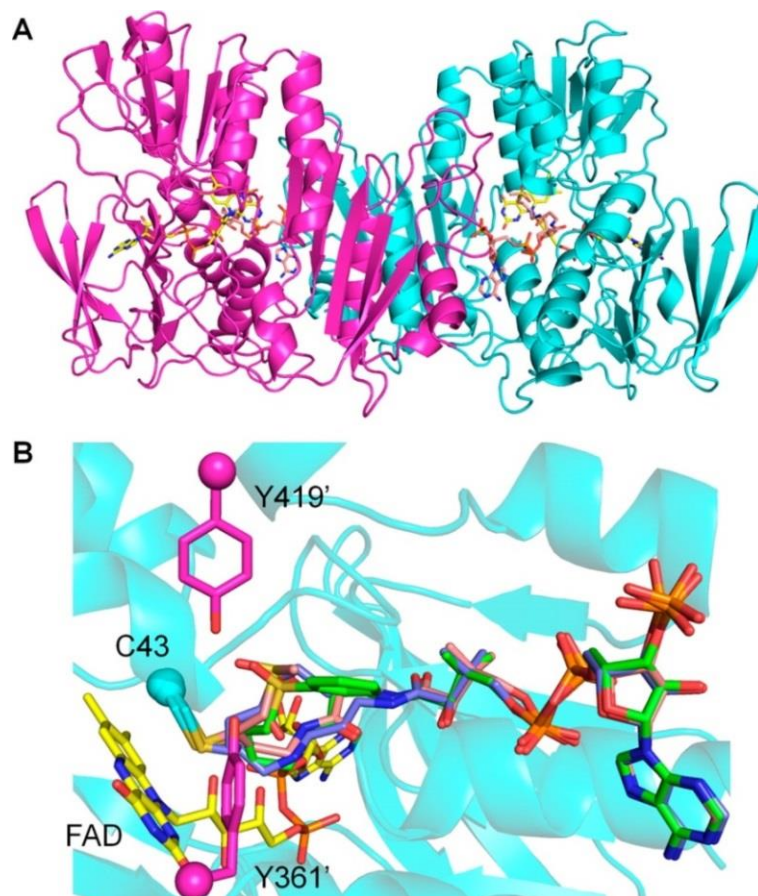


Figure 3.5: (A) The inhibited SaCoADR—MeVS-CoA complex, corresponding to the biological dimer. Each active site includes one Cys43—MeVS-CoA adduct. Protein residues are color-coded, with carbon atoms in cyan and magenta, respectively. FAD and bound MeVS-CoA are color-coded by atom type, with FAD carbon atoms in yellow and MeVS-CoA carbon atoms in orange. (B) Overlay of the three inhibitor-bound SaCoADR complexes, showing covalently bound MeVS-CoA (carbon atoms coloured pink), PhVS-CoA (carbon atoms coloured green), and EtVC-CoA (carbon atoms coloured blue) inhibitors. The MeVS-CoA complex conserves all 12 polar interactions seen with bound CoAS⁻ in wild-type SaCoADR. Tyr361'-OH interacts with one sulfone oxygen in both the MeVS-CoA and PhVS-CoA complexes, while an additional interaction is made by Tyr419'-OH with PhVS-CoA in its complex structure [33].

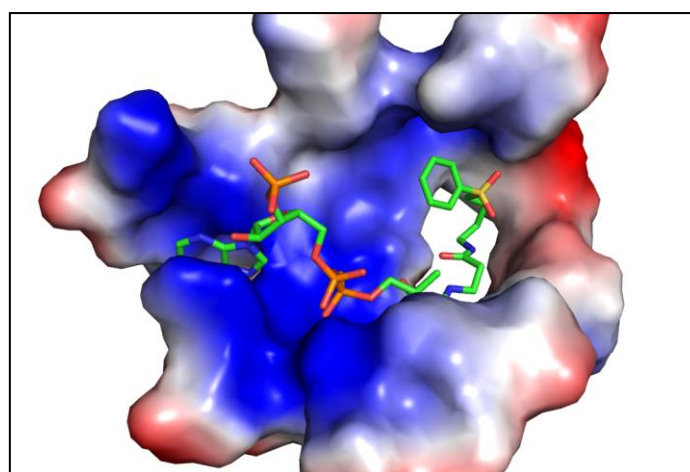


Figure 3.6: A representation of the active site in the crystal structure of SaCoADR with the PhVS-CoA bound. Charge on the protein has been colour-coded: Blue = positive, white = neutral, red = negative.

In the structure of oxidised SaCoADR 12 polar interactions between CoAS⁻ and protein residues were identified and four additional residues provided hydrophobic contacts. There were also 13 solvent waters identified as ligands to CoAS⁻ (Figure 3.7A). These protein interactions were mostly conserved in the inhibitor structures (Figure 3.7B-D). Critically, new electrostatic interactions between one of the sulfone oxygen atoms of both MeVS-CoA and PhVS-CoA and two tyrosine residues, Tyr₃₆₁ and Tyr₄₁₉ were identified. In comparison to the SaCoADR—PhVS-CoA complex (Figure 3.7B), the MeVS-CoA inhibitor conserved all 12 polar interactions found with CoAS⁻ in the oxidised enzyme, but lacked the Tyr₄₁₉-interaction with the sulfone oxygen (Figure 3.7C). Looking at the EtVC-CoA inhibitor, it lacked both the Ser₃₉ and Asn₄₂-interactions of CoAS⁻ and the carboxyl oxygen had no contact with either Tyr₃₆₁ or Tyr₄₁₉ (Figure 3.7D). This decrease in the number of interactions moving down from PhVS-CoA to MeVS-CoA to EtVC-CoA seemed to correlate with their observed K_i -values (Table 3.1), i.e. 0.04 μ M, 0.3 μ M, and 0.66 μ M, respectively [25]. However, it is important to note that although both Tyr₃₆₁ and Tyr₄₁₉-residues were implicated to be playing a role during catalysis, this was determined using substrate-mimics such as methyl methanethiosulfonate (MMTS) and not CoA-substrates.

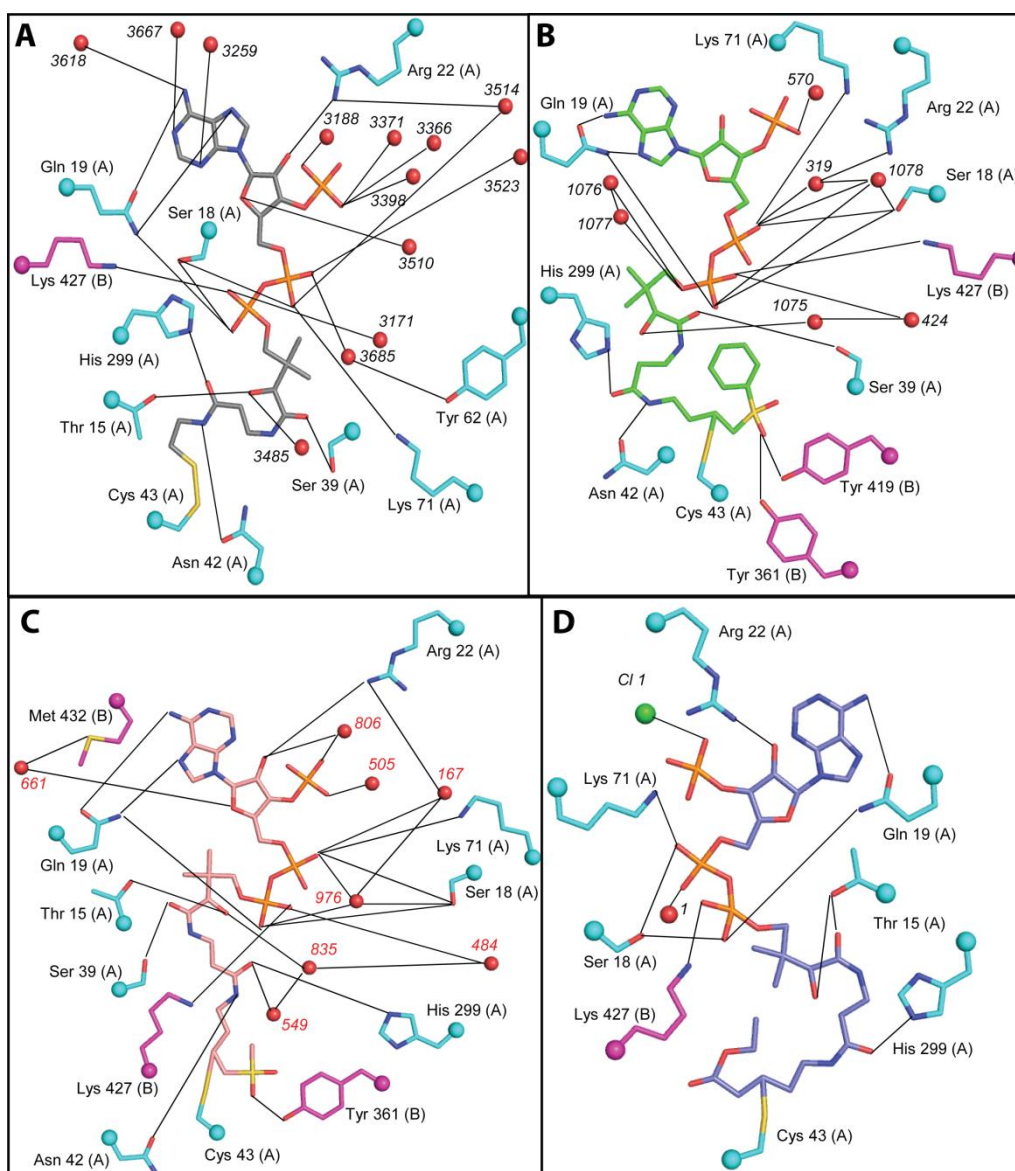


Figure 3.7: LIGPLOT representation of polar protein and solvent water interactions between the SaCoADR and bound substrate and inhibitors within their crystal structures [33]. These interactions are generally conserved in all four (A) CoASH, (B) PhVS-CoA, (C) MeVS-CoA and (D) EtVC-CoA bound complexes. A number of residues lining the active-site cleft provide electrostatic and hydrogen-bonding interactions with the -dethia-CoA moiety and with one sulfone oxygen of the inhibitor. Additional hydrogen-bonding interactions with the -dethia-CoA portion are indicated with ordered water molecules.

The structural data in the study provided a strong starting point for future inhibitor design. Particularly, the next generation inhibitors could be designed to exploit the open space in the CoAS-binding cleft, and in so doing provide increased binding affinity and selectivity for the target enzymes. However, uncertainty remained regarding a possible correlation between the possible catalytic role of Tyr₃₆₁ and Tyr₄₁₉ and their interaction with our Michael acceptor-containing inhibitors. Although it was clear that Tyr₃₆₁ and Tyr₄₁₉ assisted in locking down the inhibitors, we needed to determine their relative importance to SaCoADR catalysis using CoA-substrates, since interaction with these residues might be an important determinant in the design of future inhibitors.

3.2.2 Relative importance of conserved Tyr-residues for SaCoADR activity

To determine the relevance of the two candidate residues (Tyr₃₆₁ and Tyr₄₁₉) implicated in catalysis and inhibitor binding, site-directed mutagenesis was performed to obtain proteins in which these residues have been exchanged for Phe. The two Tyr-residues were mutated both separately (SaCoADR Y361F and SaCoADR Y419F) and in combination (SaCoADR Y361, 419F). In all cases the enzymes lacked any affinity purification tag, and instead were purified on a column packed with ADP-Sepharose resin prepared by coupling ADP to CNBr-activated Sepharose. The resulting proteins, as well as untagged wild-type SaCoADR and His-SaCoADR (with an *N*-terminal His-tag, purified by immobilised metal affinity chromatography), were subsequently assayed with (CoAS)₂ at saturating substrate conditions for the *wt* enzyme using established protocols [34]. The initial reaction rates were determined by following the oxidation of NADPH spectrophotometrically (decrease in absorbance at 340 nm). The catalytic constant (k_{cat}) was determined for each enzyme to give an indication of the effect of each mutation in the SaCoADR active site on the activity of the enzyme. The results are summarised in Figure 3.8.

Compared to the wild-type enzyme, SaCoADR Y361F showed 17% (± 0.35) activity and SaCoADR Y419F showed 28% (± 0.02) activity. The double mutant, SaCoADR Y361, 419F showed only 4% (± 0.04) activity compared to the wild-type. These results confirm that both the Tyr₃₆₁ and Tyr₄₁₉ residues play an important role in the reaction mechanism of SaCoADR, and suggest that this is likely exploited by the most potent inhibitor (PhVS-CoA) which showed a K_i of 0.04 μ M. The design strategies for improved CoADR inhibitors should therefore incorporate groups that engage in interactions with these residues.

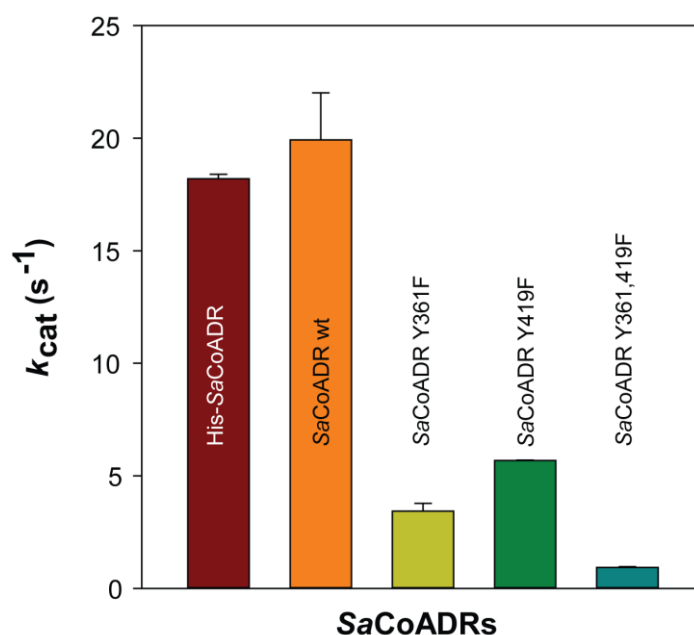


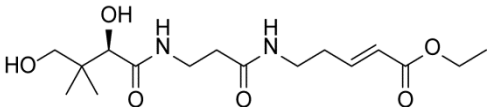
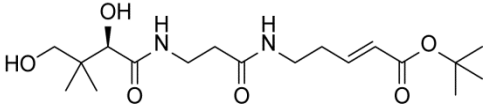
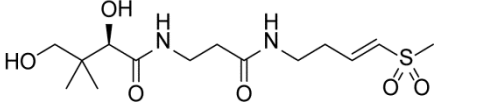
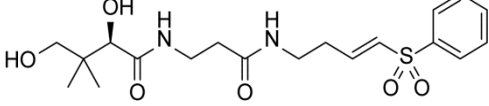
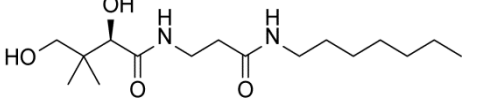
Figure 3.8: Activities of SaCoADR wild-type and mutant enzymes. The figure represents one experiment performed in triplicate for each enzyme and the error bars depict the standard deviation.

3.2.3 Lack of whole cell inhibition: a case of poor permeability?

We next set out to determine the basis for the weak correlation between the excellent *in vitro* inhibition of CoADR by the Michael acceptor-containing inhibitors, and the poor whole cell inhibition results. We first considered the cell permeability of their pantothenamide precursors, since although several different pantothenamide structures have been shown to act as inhibitors of both Gram-negative and Gram-positive bacteria [35-38], none of them incorporated sulfone moieties. A direct method to study the permeability of the bacterial cell membrane to these pantothenamides would be to fluorescently label the compounds and to use microscopy to visually establish if they label CoADR. However, since these molecules are quite small, the attachment of a fluorescent probe would significantly alter their polarity and consequently affect the results of the test. We also considered using electrospray ionisation mass spectroscopy (ESI-MS) to determine if the Michael acceptor-containing pantothenamides can be found in cells treated with them. However, in our experience these compounds show poor sensitivity in MS analysis due to poor ionisation. Also, such experiments would likely not be able to discern between compound bound to the cell envelope and those that have entered the cell.

We therefore decided to calculate several physicochemical properties of each compound in order to compare their hydrophobicity/lipophilicity and to get an indication of their potential to pass through the *S. aureus* cell envelopes. In a recent study, Davis and co-workers performed a systematic and quantitative evaluation of small-molecule permeability in bacteria in order to accurately correlate calculated physicochemical properties of compounds to their real world permeability and bio-availability [39]. The study found positive correlations between hydrophobicity parameters and intracellular compound accumulation for the Gram-positive bacteria *Bacillus subtilis*. These hydrophobicity parameters included the logarithm of the partition coefficient (*LogP*), the logarithm of the distribution coefficient (*LogD*) and Tetko's calculated *LogP* hydrophobicity (*ALogPs*). Accordingly, since *S. aureus* is a Gram-positive bacterium like *B. subtilis*, we decided to calculate these properties for our inhibitor compounds using the exact same methods as used by Davis and co-workers. We also included *N*-pentyl pantothenamide (N7-Pan) for comparison, since it has been well studied and has been shown to act as a potent inhibitor of *S. aureus* [40]. *LogP* is the ratio of concentrations of a compound in a mixture of *n*-octanol and water at equilibrium. *LogD* denotes the ratio of the sum of the concentrations of all forms of the compound, both ionised and non-ionised, in each of the two phases. Both *LogP* and *LogD* were calculated using Instant JChem v15.6.1 from ChemAxon, which uses an algorithm based on that of Viswanadhan [41]. *ALogPs* is also a computed *LogP* hydrophobicity based on the strategy proposed by Tetko and co-workers [42, 43] and the values were calculated using VCCLab's ALOGPS v2.1 online app [44]. All the physicochemical results are summarised in Table 3.2. In all cases higher *LogP* and *LogD* values correlate with increased hydrophobic character, while lower values designates more hydrophilic character.

Table 3.2: Comparison of the structures and several physicochemical values of the pantothenamide inhibitor compounds. Estimation of logarithm of the partition coefficient [*n*-octanol/water] (*LogP*) and the logarithm of the distribution coefficient (*LogD*) were calculated using the cheminformatics tool Instant JChem v15.6.1 from ChemAxon. Tetko's calculated *LogP* hydrophobicity (*ALogPs*) was calculated using VCCLab's ALOGPS v2.1.

Pantothenamide	Structure	<i>LogP</i>	<i>LogD</i>	<i>ALogPs</i>
EtVC-Pan		-0.40 ± 0.49	-0.76 ± 0.52	0.44 ± 0.29
tBuVC-Pan		0.09 ± 0.49	-0.06 ± 0.52	1.06 ± 0.29
MeVS-Pan		-2.44 ± 0.49	-2.59 ± 0.52	-0.24 ± 0.29
PhVS-Pan		-0.38 ± 0.49	-0.48 ± 0.52	0.64 ± 0.29
N7-Pan		0.47 ± 0.49	0.72 ± 0.52	1.99 ± 0.29

The results show that all the compounds analysed are all reasonably polar. MeVS-Pan is clearly the most polar; this could possibly indicate that the compound is potentially unable to cross bacterial cell envelopes. Even so, the absolute values should not be given too much credence as these are still calculated and not experimentally determined. It is more useful to compare the calculated properties of each compound within the series. It is clear then that the calculated hydrophobicity parameters of all the other compounds are quite similar; specifically, in the case of EtVC-Pan which does show growth inhibition and PhVS-Pan which does not, there is no significant difference in any of the parameters. From these calculations we can reasonably conclude that cell permeability is not the reason for the poor correlation between the *in vitro* and whole cell inhibition observed for the Michael acceptor-containing CoADR inhibitors.

3.2.4 Confirming the metabolic activation of pantothenamides in *S. aureus*

An alternative reason for the lack of whole cell inhibition by the Michael acceptor-containing pantothenamides is a failure by the *S. aureus* native CoA biosynthetic enzymes to convert them into inhibitory CoA analogues. Previously, the *in vitro* biotransformation of these pantothenamides was performed with the *E. coli* PanK, PPAT and DPCK enzymes to prepare the CoA analogues that were subsequently

tested on SaCoADR. However, the ability of the corresponding *S. aureus* enzymes to perform these reactions has not been confirmed. Considering that especially the *S. aureus* PanK enzyme has been shown to have a different specificity profile compared to the *E. coli* enzyme [40], we considered it possible that metabolic activation might not occur in *S. aureus*. To determine if this was the case, a biosynthesis reaction was performed *in vitro* using the purified SaPanK, SaPPAT and SaDPCK enzymes to convert the pantothenamides to CoA analogues (Figure 3.9). The enzymes were then precipitated out of each reaction mixture and removed by filtration. The remaining reaction mixtures were subsequently analysed by liquid chromatography mass spectrometry (LC-MS). The components were separated on an ultra-performance liquid chromatography (UPLC) column and each enzyme product was detected by ESI-MS in the positive mode with generation of MS^E fragmentation data. MS^E is an acquisition method used to observe all detectable, eluting species and their corresponding fragment ions. During data acquisition, the ionisation energy is dynamically switched between a low-energy and a high energy state. This produces alternating composite mass spectra of all intact molecular ions, which is then followed by chimeric mass spectra of all precursor molecules. Post-acquisition data analysis methods subsequently extract both the chromatographic and the mass spectrometric information of the generated fragments to provide time-resolved, accurate mass measurements [45]. All the MS results are summarised in Table 3.3 below.

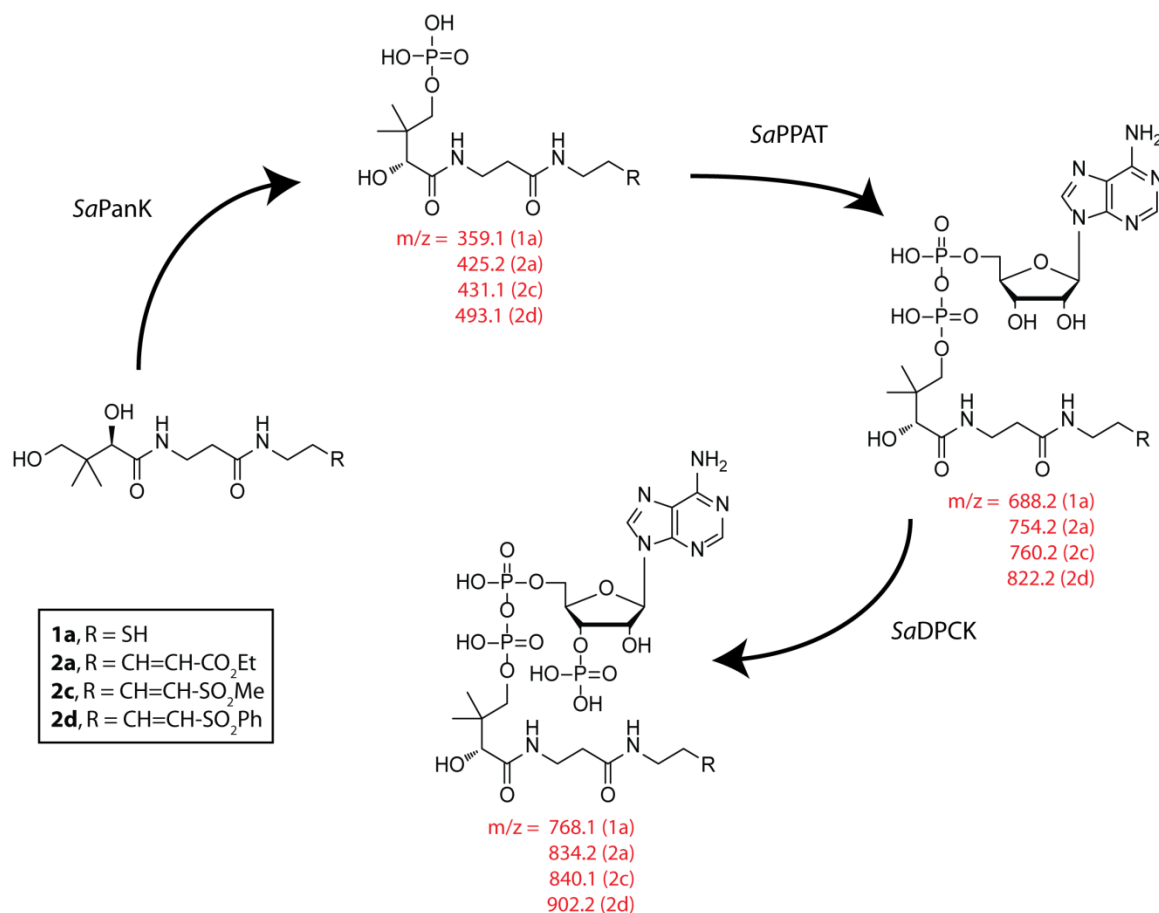


Figure 3.9: Metabolic activation of the Michael acceptor-containing pantothenamides to the corresponding inhibitory CoA analogues by the *S. aureus* PanK (SaPanK), PPAT (SaPPAT) and DPCK (SaDPCK) enzymes. The observed MS mass-to-charge ratios (m/z) are indicated.

All the expected products were observed with LC-MS, including the MS^E fragments resulting from the loss of the ATP-moiety. This was expected, since these compounds are similar to those analysed in a previous

study using analogous detection methods [46]. The results confirmed that the Michael acceptor-containing pantothenamides act as substrates for the CoA biosynthesis enzymes in *S. aureus* and that they would most likely be converted to the corresponding CoA analogues should they cross the cell envelope. Lack of metabolic activation can therefore be excluded as a potential reason for the poor correlation between the *in vitro* and whole cell inhibition data for the Michael acceptor-containing CoADR inhibitors.

Table 3.3: Observed MS parent- and MS^E daughter ions (m/z) of the biosynthetic intermediates of the Michael acceptor-containing CoADR inhibitors.

Pantothenamide	SaPanK product (m/z)	SaPPAT product (m/z)	SaDPCK product (m/z)	MS ^E daughter ion (m/z)
PantSH	359.1	688.2	768.1 (1a)	261.1
EtVC-Pan	425.2	754.2	834.2 (2a)	327.2
MeVS-Pan	431.1	760.2	840.1 (2c)	333.1
PhVS-Pan	493.1	822.2	902.2 (2d)	395.1

3.2.5 Establishing target-specificity for the Michael acceptor-containing CoADR inhibitors

Having established that the Michael acceptor-containing pantothenamides most likely enter *S. aureus* and are converted (i.e. metabolically activated) by the organism's native CoA biosynthesis enzymes to the corresponding CoA analogue inhibitors, we next set out to investigate their target specificity. This was done by synthesising an analogue of EtVC-Pan, the pantothenamide precursor of EtVC-CoA, the only compound that did show growth inhibition of *S. aureus*. This analogue (CO₂Et-Pan) was identical to EtVC-Pan, except that it did not contain the Michael acceptor-moiety (i.e. it contained a single bond instead of a double bond, Figure 3.10). Since this compound had similar structure and polarity to the Michael acceptor-containing inhibitor precursor, it was therefore expected to have a comparable efficiency in cellular uptake. However, since it lacks the Michael acceptor it can bind, but not covalently modify, CoADR. The inhibition of *S. aureus* by both compounds was compared using a whole cell inhibition assay under normal growth conditions without any additional stresses. The compounds were tested against a wild-type MRSA strain (JE2), as well as a mutant MRSA strain (NE1456) in which the *cdr* gene has been knocked out; this mutant strain was provided by the freely accessible NARSA repository. The bacteria were grown in nutrient rich tryptic soy broth (TSB).

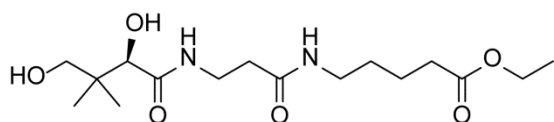


Figure 3.10: CO₂Et-Pan: a non-Michael acceptor-containing inhibitor.

At the outset we expected to see inhibition of staphylococcal growth by both compounds, since metabolic activation of either pantothenamide would lead to the formation of physiologically inactive CoA antimetabolites that lack the catalytically essential thiol of the cofactor [37, 38]. As such, the antimetabolites can interfere with a range of metabolic processes downstream from CoA biosynthesis, including fatty acid biosynthesis [47]. This is a mechanism of action that has been described for other pantothenamides not directed to attack any specific target. However, in the case of the CoADR-directed inhibitors we expected to see strain-based differences in their potency should they act on CoADR as a target: in the strain that lacks *cdr* (the gene encoding CoADR in *S. aureus*) we expected similar potency for both CO₂Et-Pan and EtVC-Pan, because in the absence of CoADR all the observed inhibition would be due to the antimetabolite effects of the compounds. Any differences in potency observed in the wild-type strain would then correlate with the target-specificity of the inhibitors. The results are illustrated in Figure 3.11 and summarised in Table 3.4 below.

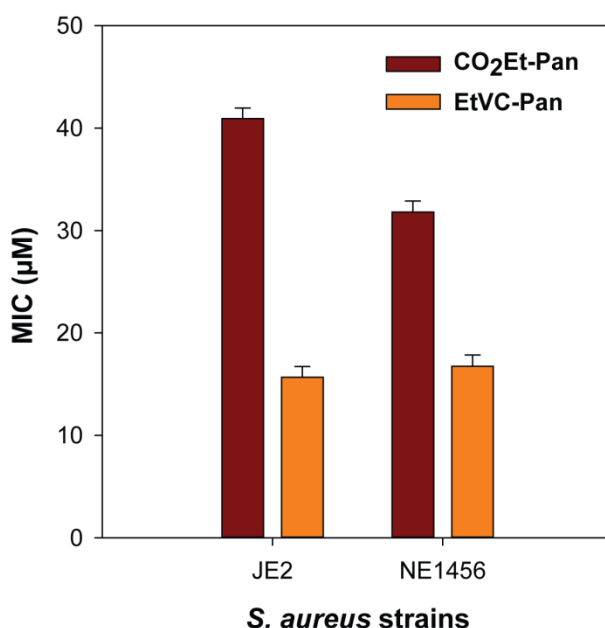


Figure 3.11: Charts comparing the IC₅₀-values (A) and MIC-values (B) of CO₂Et-Pan and EtVC-Pan against *S. aureus* JE2 (*wt*) and *S. aureus* NE1456 (*cdr* knock-out) strains. Data is from one experiment performed in triplicate with error bars indicating the standard error of the fit to calculate the inhibition parameters.

Table 3.4: Whole cell inhibition data of small molecule inhibitors against several *S. aureus* strains.

Compound	<i>Staphylococcus aureus</i> strains			
	JE2 (<i>wt</i>)		NE1456 (<i>cdr</i>)	
	IC ₅₀ (μ M)	MIC (μ M)	IC ₅₀ (μ M)	MIC (μ M)
CO ₂ Et-Pan	20.3	40.9	12.5	31.8
EtVC-Pan	8.0	15.7	6.3	16.7

The results show that the Michael acceptor-containing EtVC-Pan is a more potent inhibitor than the non-Michael acceptor pantothenamide CO₂Et-Pan in not only the wild-type strain, but also in the *cdr* knockout. Additionally, its potency is similar in both strains. This therefore indicates that the observed growth inhibition by EtVC-Pan is not due to CoADR-related effects. The observation that CO₂Et-Pan shows higher potency in the *cdr* knockout background is interesting, suggesting that CoA-dependent processes are more sensitive to inhibition in the absence of this enzyme.

3.2.6 Evaluating *S. aureus*'s resistance to chemically-induced oxidative stress in selected genetic backgrounds

The results presented above indicate that although CoADR is a structurally tractable target for drug design, it could not be validated as a viable physiological target. However, all the whole cell experiments outlined above, as well those directed at determining the essentiality of *S. aureus* genes, have been performed under normal (i.e. optimal) growth conditions. If CoADR plays an important role in oxidative stress resistance, it is more likely that its physiological relevance will also come to light under such conditions. We therefore decided to test the survival of wild-type JE2 *S. aureus*, as well as certain knockout strains, under the influence of the oxidative stressors hydrogen peroxide (H₂O₂) and diamide. Three mutant strains were tested. First was a *cdr* knockout that lacks the gene encoding CoADR (NE1456). Second was a *bshA* knockout that lacks the gene encoding the first enzyme of BSH biosynthesis (NE1728) (previous studies have shown that such strains lack this thiol) [48]. Third was NE785, a strain lacking the gene previously highlighted to be upregulated more than 80-fold in *S. aureus* challenged with neutrophils [15]; this gene (SAUSA300_0576 from MRSA strain USA300) encodes a putative FDR enzyme that shows homology to mercuric ion reductases. For these tests we first performed dose-response assays with H₂O₂ but found that the data did not allow any clear differences between the strains to be distinguished (Figure 3.12A). Next, we carried out overnight stress tests using H₂O₂ (25 mM) and diamide (5 mM) as well as a combination of the two stressors. For these experiments subtle differences were observed, with the wild-type JE2 strain showing slightly more resistance to oxidative stress than the other strains, which all showed similar inhibition (Figure 3.12B). All the strains were highly resistant to the oxidative thiol stress induced by diamide, a

chemical stressor known to induce the formation of disulfide bonds (and which is therefore expected to increase the ratio of oxidised to reduced CoA) [49, 50]. A combination of the two stressors successfully inhibited growth of all the strains, with the *cdr* knockout being the most sensitive. This suggests that under these conditions CoADR plays an important role in oxidative stress resistance.

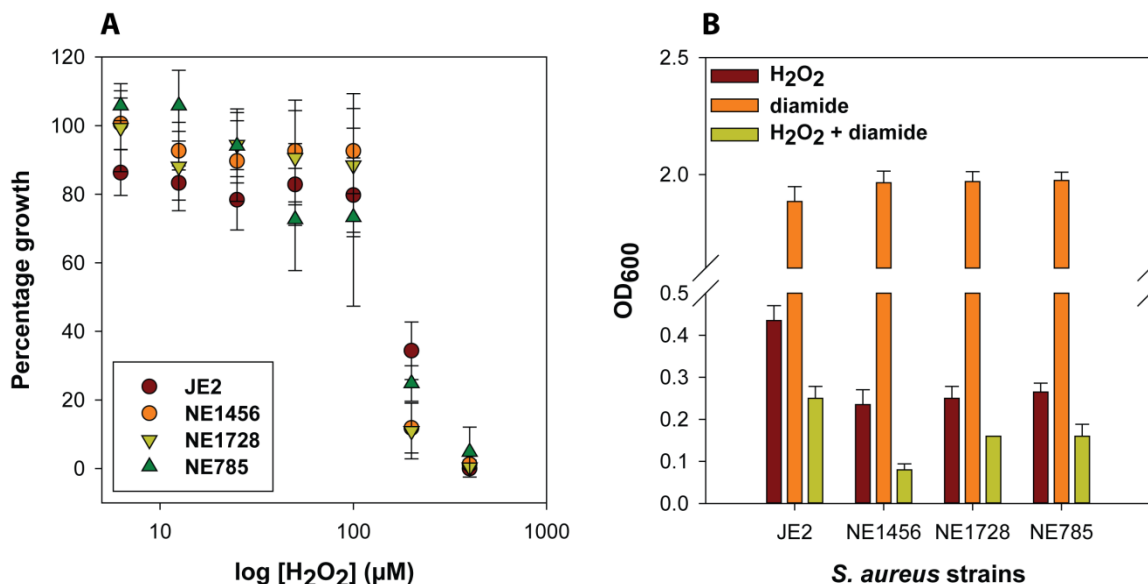


Figure 3.12: (A) Dose response of H₂O₂ against *S. aureus* JE2, NE1456 (*cdr* knockout), NE1728 (*bshA* knockout) and NE785 (knockout of the gene encoding an FDR of unknown function implicated in oxidative stress resistance [15]). The figure represents one experiment performed in triplicate and the error bars depict the standard deviation. (B) Survival of *S. aureus* strains after an overnight (~18 hr) stress test with H₂O₂, diamide and a combination of H₂O₂ and diamide. The figure represents the average of two experiments performed independently and the error bars depict the standard deviation between the two data sets.

Next, the effects of a stressor were assessed at a single concentration over time by performing growth curve analysis (Figure 3.13). The growth curve analysis confirmed that wild-type JE2 shows the most resistance to oxidative stress induced by H₂O₂, with the *cdr* knockout showing intermediate resistance (Figure 3.13A). The remaining two strains showed little growth under these conditions, indicating that BSH and the FDR of unknown function are both important for resistance to H₂O₂. This finding support recent reports on the importance of BSH for the oxidative stress resistance of *S. aureus* [48]. As in the previous experiment, diamide did not reveal any significant differences between the wild-type, *cdr* knockout strain and the strain lacking the FDR of unknown function, while the *bshA* knockout strain showed significant reduced growth at later time points (Figure 3.13B).

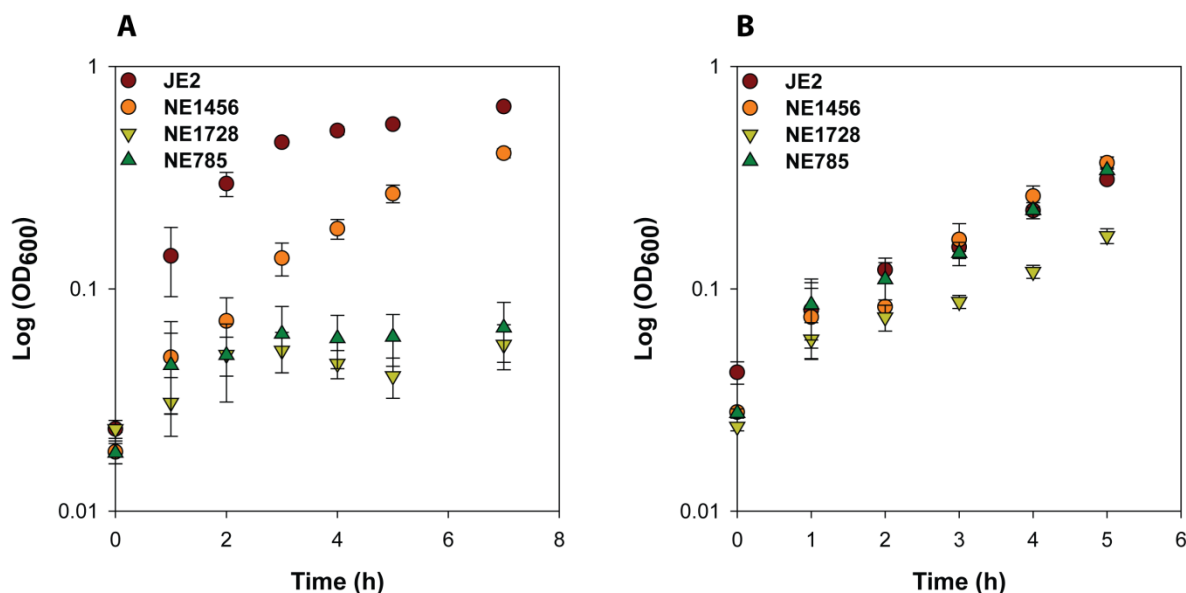


Figure 3.13: Growth curves of *S. aureus* JE2, NE1456 (*cdr* knockout), NE1728 (*bshA* knockout) and NE785 (knockout of the gene encoding an FDR of unknown function implicated in oxidative stress resistance [15]) challenged with (A) 10 mM H₂O₂ and (B) 4 mM diamide. Both figures represent one experiment performed in triplicate and the error bars depict the standard deviation.

The results of the chemically-induced oxidative stress tests therefore seem to indicate that overall, *S. aureus* is quite resistant to H₂O₂ and diamide-induced stress, and that CoADR does not play a significant role in the resistance to the stress induced by these compounds, unless they are used in combination. When measured over time, lack of BSH production and a loss of the FDR of unknown function that has been implicated in resistance to the killing mechanisms of neutrophils have much more pronounced effects on the bacterium's ability to survive. However, it must be noted that we found that the test outcomes showed significant variation on subsequent repetitions. This variation was found to be introduced by performing the test at different growth states (exponential vs. stationary), by using different initial bacterial cell concentrations and by varying the oxidant concentrations that were used. In particular, varying the ratio of bacterial cells to oxidant altered the relative response of the different *S. aureus* strains. However, it became evident from all our results that CoADR did not contribute notably to the oxidative stress resistance of *S. aureus*. Consequently we decided to rather use more physiologically relevant conditions to determine the relative importance of CoADR, BSH and the FDR of unknown function to *S. aureus* oxidative stress resistance.

3.2.7 Evaluating *S. aureus*'s resistance to neutrophil-induced oxidative stress in selected genetic backgrounds

In order to address the variation seen in the chemically-induced oxidative stress experiment, we decided to instead challenge the bacteria with isolated human neutrophils. This would provide more physiologically relevant results, since the bacteria would be subjected to the oxidative burst that these polymorphonuclear leukocytes use to kill phagocytosed bacteria that are encountered during infection. The technique has

previously been applied successfully to the study of processes relevant to the survival of *S. aureus* when challenged by the innate immune system [51, 52]. Also, the ratio of colony-forming units (CFUs) of bacteria to neutrophils could be kept constant for uniformity during each assay.

Neutrophils were successfully isolated from heparinised venous blood and enumerated using a haemocytometer. The white blood cell differential was calculated after staining with Wright-Giemsa stain (see Materials and Methods for details). Briefly, the assay entails the isolation of neutrophils by differential centrifugation and diluting them to the desired concentration in RPMI media. The bacteria are grown to exponential phase in nutrient rich media, then washed and diluted to the desired concentration (CFU/mL) in RPMI media. The neutrophils and bacterial cells are then combined in a 96-well culture plate in a 1:1 ratio (CFU:neutrophil) and gently centrifuged to synchronise phagocytosis in each well. The plate is incubated at 37 °C and at the desired time points samples are taken from the plate, incubated on ice and plated on suitable agar plates in order to determine bacterial survival after neutrophil stress by counting CFUs. Unfortunately, we failed to successfully execute this test even after performing several trials with all the available *S. aureus* strains. In each case the control samples failed to give the expected results: either no viable cells could be isolated in the negative controls, or very little to no killing took place in the positive control samples. This latter observation indicated that the isolated neutrophils were either not viable, or did not stay viable for the duration of the experiment. To address this, we also performed the experiment with whole blood as was done in tests on the importance of BSH for *S. aureus* oxidative stress resistance [48]. However, performing the experiment in this manner also did not give the desired control results. Consequently, we chose to abandon the pursuit of neutrophil-induced oxidative stress tests at this stage of the study, and to finally focus on the impact of specific small molecule inhibitors on *S. aureus* survival instead.

3.2.8 Evaluating the effect of reduced CoA levels in selected genetic backgrounds

Having not been able to unequivocally establish the importance of CoADR to oxidative stress resistance in *S. aureus*, we finally set out to determine the effect of reduced CoA levels in wild-type *S. aureus*, and the three mutant strains lacking CoADR, BSH and the FDR of unknown function. Since CoA levels have been reported to be higher in *S. aureus* than in other bacteria [12], the goal of these experiments were to determine if small molecule inhibitors of CoA biosynthesis had a differentiated effect when these functions were absent. In this manner we hoped to establish whether CoA indeed had a role in *S. aureus* beyond that of acting as a metabolic cofactor.

For these tests three compounds that have been proved to have an effect on CoA biosynthesis or CoA-dependent enzymes were used. N7-Pan is a well-studied inhibitor that inhibits the first CoA biosynthesis enzyme, PanK, in *S. aureus*, but also has effects downstream of the pathway [40], CJ-15,801 forms a tight-binding inhibitor of phosphopantothencysteine synthetase (PPCS), the second CoA biosynthesis enzyme, [53], and Compound D is a recently discovered inhibitor of the fourth CoA biosynthesis enzyme, PPAT [54]. Based on their targets being CoA biosynthetic enzymes, all three compounds are expected to decrease the intracellular levels of available CoA and its esters. The inhibition of *S. aureus* by all three compounds was

compared using a whole cell inhibition assay first performed under normal growth conditions (using nutrient rich tryptic soy broth) without any additional stresses in a manner similar to that described for the tests with EtVC-Pan and CO₂Et-Pan above. The compounds were tested against JE2, NE1456, NE1728 and NE785, and the results are summarised in Figure 3.14.

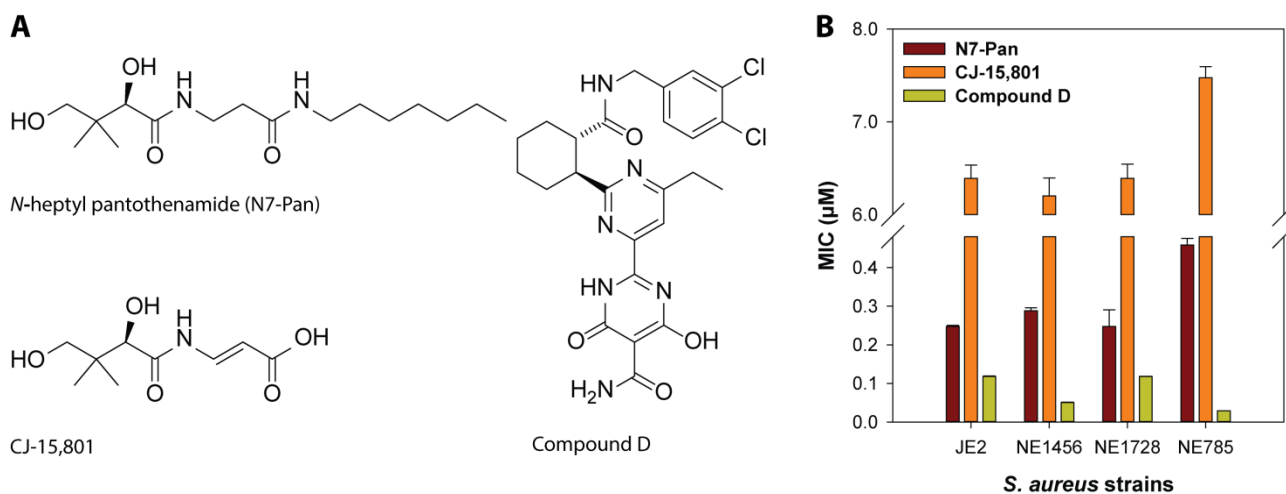


Figure 3.14: (A) Structures of inhibitor compounds used to test against *S. aureus* strains. (B) MICs of N7-Pan, CJ-15,801 and Compound D against *S. aureus* JE2 (wild-type), NE1456 (*cdr* knockout lacking CoADR activity), NE1728 (*bshA* knockout lacking BSH) and NE785 (knockout of the gene encoding an FDR of unknown function implicated in oxidative stress resistance [15]). Each strain was tested once with each inhibitor in triplicate (except CJ-15,801 was tested twice with each strain). The error bars indicate the standard error of the fit to calculate the inhibition parameters from the triplicate values.

The results show that in the case of N7-Pan and CJ-15,801 there is little differentiation between the effects that the inhibitors have on the various strains (taking both the IC₅₀ and MIC data into account simultaneously), although the compounds show a somewhat reduced potency in the SAUSA300_0576 knockout background compared to the other strains. Since this gene encodes an FDR of unknown function, the relevance of this finding is unclear at the moment. Interestingly, Compound D – the most potent inhibitor tested – was found to have increased potency in the *cdr* and the SAUSA300_0576 knockout backgrounds than in the wild-type strain. This suggests that under conditions where CoA levels are sufficiently reduced; CoADR does become relevant – even under normal growth conditions. The fact that the same effect is observed in the absence of the SAUSA300_0576 gene product could imply that it has a function related or dependent on CoA, although this deserves further study.

3.3 Discussion

In this study, we set out to first investigate the viability of CoADR as a potential antistaphylococcal drug target and second, to investigate several other potential role players in *S. aureus* oxidative stress defence. The research was a continuation of previous work on mechanism-based Michael acceptor-containing inhibitors of the SaCoADR enzyme. Particularly, the questions raised by earlier studies were addressed and used in the assessment of the conditions under which this enzyme could be a viable target. We started by

examining the SaCoADR enzyme and specifically how its interaction with the Michael acceptor-containing inhibitors relates to the observed differences in activity between them. We already knew that the sulfones are better Michael acceptors than the esters, which should make them better electrophilic traps for the active site Cys₄₃ of SaCoADR. However, the potency of the various inhibitors was also directly correlated to their interaction with two SaCoADR active site residues, Tyr₃₆₁ and Tyr₄₁₉. Therefore, we could adequately rationalise the observed enzyme inhibition. Also, the structural data in the study provided a strong starting point for future inhibitor design, particularly, the next generation inhibitors could be designed to 1) exploit the open space in the CoAS-binding cleft, and 2) interact with Tyr₃₆₁ and Tyr₄₁₉ of SaCoADR and in so doing provide increased binding affinity and selectivity for the targeted enzyme.

Next, the reasons for the poor correlation between the *in vitro* inhibition of SaCoADR by the Michael acceptor-containing CoA analogues and the whole cell inhibition of *S. aureus* by their corresponding pantothenamide precursors were investigated. As far as we know, no CoA transporter has been found in bacteria and also there is no homolog of the *E. coli* pantothenate transporter (PanF) in *S. aureus*, which could affect the whole cell activity of the inhibitor compounds in terms of uptake into the cell. Therefore, we considered that either the two pantothenamides that showed no inhibition could not cross the *S. aureus* cell envelope or they were not accepted as substrates of the CoA-biosynthesis enzymes inside the cell. We first calculated several physicochemical properties of each compound to compare their relative hydrophobicity/lipophilicity and second, we performed a biosynthesis reaction using the purified SaPanK, SaPPAT and SaDPCK enzymes to convert the pantothenamides to CoA-analogues and detected the enzyme products using LC-MS. Our results confirmed that neither permeability nor biosynthesis is a reason for the poor correlation between the enzyme inhibition of the Michael acceptor-containing CoA analogues and the whole cell inhibition data for their pantothenamide precursors. Additionally we considered the target specificity of the CoADR inhibitors, i.e. that the bacterial growth inhibition of the pantothenamide precursors is mediated *via* a different target than CoADR. The results led us to the conclusion that the poor correlation between the enzyme inhibition and the whole cell growth inhibition is due to SaCoADR not being essential under normal growth conditions.

In spite of our findings suggesting that SaCoADR is not a viable target for antistaphylococcal drug design, it remained possible that it could still be a relevant target under certain non-optimal conditions, i.e. conditions different from those used for the whole cell experiments. It was therefore necessary to evaluate the physiological relevance of CoADR in *S. aureus* under oxidative stress, since it is more likely that its importance will also come to light under such conditions. We also investigated and compared the effects of two other potential role players in *S. aureus* oxidative stress defence, BSH and a putative FDR enzyme that displays homology to mercuric ion reductases. All the chemically induced oxidative stress results indicated that CoADR did not contribute notably to the oxidative stress resistance of *S. aureus*. In contrast, BSH and the FDR of unknown function seemed to have more pronounced contributions to the bacterium's ability to survive (Figure 3.12 and 3.13). Even when evaluated against the background of reduced CoA levels, very little difference was seen between the effects of CoADR, BSH and the FDR of unknown function (Figure 3.14).

Despite the fact that this study could not unequivocally establish the importance of CoADR to oxidative stress resistance in *S. aureus*; several significant findings were made during our evaluation of the potential

drug target. It is noteworthy that while both CoA and BSH are considered as candidates to be the major LMWT responsible for redox balance in *S. aureus*, our results did not reveal any link between the two compounds. Specifically, neither compound appeared to compensate for the absence of the other during our studies with the knockout mutants of *S. aureus*. Also, CO₂Et-Pan showed higher potency in the *cdr* knockout background, suggesting that CoA-dependent processes are more sensitive to inhibition in the absence of this enzyme. This correlated well with our results with the most potent CoA biosynthesis inhibitor tested (Compound D), which was found to have increased potency in the *cdr* and the SAUSA300_0576 knockout backgrounds than in the wild-type strain. This suggests that under conditions where CoA levels are sufficiently reduced, CoADR might become relevant, even under normal growth conditions. Taking these findings into consideration, it would be preferable if the assays with the small molecule inhibitors could be done under oxidative stress conditions, since it would accentuate any effects that are related to redox balance. However, bearing in mind the variability of our chemically-induced oxidative stress results as well as our failure to successfully execute the neutrophil tests, this is currently unfeasible. Also, there is a possibility that CoADR inhibitors could be used synergistically with Compound D, since intracellular levels of reduced CoA would then be significantly lowered due to inhibition of CoA biosynthesis combined with diminished reduction of (CoAS)₂. As it stands, we managed to illuminate several uncertainties regarding CoADR as a potential antistaphylococcal drug target, but also raised important questions regarding the organism's redox balance mechanisms in general. These findings pave the way for further investigation of compounds targeting pathways involved in oxidative stress resistance as potential drugs against in *S. aureus*.

3.4 Materials and methods

Unless otherwise noted, all reagents and chemical compounds were purchased from commercial sources and used without further purification. Lyophilised CNBr-activated Sepharose 4B, Isopropyl β -D-1-thiogalactopyranoside (IPTG), Dextran-500 and Ficoll-Paque Plus were obtained from Sigma. HisTrapFF metal affinity purification columns, HiTrap desalting columns and Vivaspin centrifugal concentrators were from GE Healthcare Life Sciences. Tetrahydrofuran (THF) was distilled under nitrogen from sodium wire using benzophenone as an indicator. Dichloromethane (DCM) was distilled under nitrogen from calcium hydride. *N,N*-Dimethylformamide (DMF) was dried and purified by shaking up over potassium hydroxide followed by distillation under reduced pressure and a nitrogen atmosphere, and was stored over 3 Å molecular sieves. All column chromatography was performed using Merck silica gel 60 (particle size 0.040-0.063 mm) using combinations of hexane, ethyl acetate, DCM and methanol as eluants. Thin layer chromatography (TLC) was carried out on aluminium-backed Merck silica gel 60 F254 plates. Visualisation was performed with a UV lamp followed by spraying with a cerium ammonium molybdate or ninhydrin solution, followed by heating.

Protein purification: All His-tagged protein purification was performed using HisTrapFF metal affinity purification columns on an ÄKTApurification system from GE Healthcare Life Sciences. The purified proteins were desalted using 5 mL HiTrap desalting columns.

Spectrophotometry: All absorbance readings in 96-well plates were measured using a Thermo Scientific Varioskan microplate spectrophotometer. All larger volume measurements were made in an Agilent Technologies Cary 60 UV-Vis Spectrometer using a 1 cm cuvette.

HPLC analyses: High performance liquid chromatography (HPLC) analysis was performed on an Agilent 1100 instrument using a Supelcosil LC-18-T 3 μ C18 column (150 x 4.6 mm) from Supelco.

NMR analyses: All ^1H and ^{13}C nuclear magnetic resonance spectra (NMR) were obtained using 300 MHz Varian VNMRS (75 MHz for ^{13}C), 400 MHz Varian Unity Inova (100 MHz for ^{13}C) or 600 MHz Varian Unity Inova (125 MHz for ^{13}C) instruments at the Central Analytical Facility (CAF) of the University of Stellenbosch. Chemical shifts (δ) were recorded using the residual solvent peak or an external reference. All chemical shifts are reported in ppm and all spectra were obtained at 25 °C. Proton spectral data are reported as follows: chemical shift, multiplicity (ovlp = overlapping, s = singlet, d = doublet, t = triplet, q = quartet, p = pentet, m = multiplet, br = broad), coupling constant (*J*) in Hz, and integration.

MS analyses: All ESI-MS were performed using a Waters Synapt G2 mass spectrometer using a Waters HSS C18 column (2.1 x 150mm) at the CAF of the University of Stellenbosch.

3.4.1 ADP-coupled Sepharose affinity resin

ADP was coupled to Sepharose as follows: Lyophilised CNBr-activated Sepharose 4B (1 g) was weighed out and suspended in HCl (1 mM). The medium swelled immediately and was then washed for 15 minutes with HCl (1 mM) on a sintered glass filter (porosity G3), using approximately 200 ml HCl added in several aliquots. ADP (10 μ mol), the ligand to be coupled, was dissolved in coupling buffer containing 0.1 M NaHCO₃ and 0.5 M NaCl at pH 8.3 (5 mL). The coupling solution containing the ligand was added to the prepared medium suspension in a stoppered vessel. The mixture was rotated gently end-over end overnight at 4 °C. Afterwards, excess ligand was washed away with 5 medium (gel) volumes of coupling buffer. Next, any remaining active groups were blocked. The medium was transferred to 0.1 M Tris-HCl buffer, pH 8.0 and let stand for 2 hours. The medium was washed with five cycles of alternating pH, which consisted of a wash with 0.1 M acetic acid and 0.5 M NaCl, pH 4.0 (5 medium volumes) followed by a wash with 0.1 M Tris-HCl and 0.5 M NaCl, pH 8 (5 medium volumes). A slurry was prepared with binding buffer in a ratio of 75% settled medium to 25% buffer and packed into a column for manual loading and elution of protein. The resin was stored in 60% ethanol at 4 °C.

3.4.2 SaCoADR wt and mutants overexpression and purification

Plasmid vectors encoding the SaCoADR wt, SaCoADR Y361F, SaCoADR Y419F or SaCoADR Y361, 419F proteins were kindly provided by Prof Al Claiborne of Wake Forest University, USA. We also had the plasmid vector encoding the *N*-terminal His-tagged SaCoADR wt (His-SaCoADR wt) protein in the laboratory.

His-SaCoADR wt was expressed and purified using established protocols [25]. The plasmid encoding His-SaCoADR wt (pET-28a-SaCoADR) was transformed into *E. coli* BL21(Star)DE3 for expression. Expression was performed in Luria-Bertani broth supplemented with 30 mg/L kanamycin at 37 °C, and by induction with 1 mM IPTG at OD₆₀₀ = 0.6. Cell growth was continued for a further 3h at 37 °C post-induction, after which the cells were harvested by centrifugation. The obtained cell pellet was suspended in sonication buffer (5 mM imidazole, 500 mM NaCl and 20 mM Tris-HCl, pH 7.9; 10 mL/1 g cell paste) and subsequently sonicated to effect cell lysis. After centrifugation at 15 000 x g for 30 min to collect cell debris, the crude extract (supernatant) was applied to a previously prepared 1 mL HisTrapFF metal affinity purification column using an ÄKTAprime purification system. Weakly bound proteins were removed by washing with sonication buffer, followed by sonication buffer containing 75 mM imidazole. His-SaCoADR wt was eluted by increasing the imidazole concentration to 500 mM. Elution was monitored at A₂₈₀. The purified protein was desalted using a 5 mL HiTrap desalting column (25 mM Tris, 5 mM MgCl₂, pH 8.0). Glycerol was added to the pure protein solution to a final concentration of 5%, after which the protein was aliquoted and stored at -80 °C.

SaCoADR wt, SaCoADR Y361F, SaCoADR Y419F and SaCoADR Y361, 419F was also expressed and purified using established protocols [34]. The plasmid encoding these proteins were transformed into *E. coli* BL21(Star)DE3 for expression. Expression was performed in Terrific Broth supplemented with 100 mg/L ampicillin at 37 °C, and by induction with 1 mM IPTG at OD₆₀₀ = 1.0. Cell growth was continued for a further 3h at 37 °C post-induction, after which the cells were harvested by centrifugation. The obtained cell pellet

was suspended in Tris-EDTA buffer (1 mM EDTA and 20 mM Tris-HCl, pH 7.4; 10 mL/1 g cell paste) and subsequently sonicated to effect cell lysis. After centrifugation at 15 000 x g for 30 min to collect cell debris, unwanted proteins were precipitated from the crude extract (supernatant) with $(\text{NH}_4)_2\text{SO}_4$ up to 50% saturation. After centrifugation at 4 500 x g for 30 min, the precipitated proteins were discarded and SaCoADR was subsequently precipitated from the extract with $(\text{NH}_4)_2\text{SO}_4$ up to 80% saturation. The precipitated SaCoADR was then removed from the extract *via* centrifugation at 4 500 x g for 30 min and resuspended in a minimal volume of Tris-EDTA buffer. Next, after $(\text{NH}_4)_2\text{SO}_4$ was removed by dialysis against 2x 2 L Tris-EDTA buffer, the SaCoADR extract was applied to the ADP-coupled Sepharose affinity resin. Weakly bound proteins were removed by washing with Tris-EDTA buffer and SaCoADR was eluted by increasing concentrations of NaCl (0 – 4 M). The purified protein was desalted using a 6 mL Vivaspinn centrifugal concentrator (50 mM phosphate, 0.5 mM EDTA, pH 7.0). Glycerol was added to the pure protein solution to a final concentration of 5%, after which the protein was aliquoted and stored at -80 °C.

3.4.3 Synthesis of the CoADR substrate (oxidation of CoA to CoA disulfide)

CoA disulfide $(\text{CoAS})_2$ was prepared from CoA by using the established diamide-based oxidation of thiols [49]. To a solution of 50 mM Tris-HCl (pH 7.6) in H_2O (13 mL) was added CoA (final concentration 2.0 mM), followed by diamide (final concentration 1.0 mM). The reaction mixture was stirred for 10 min at room temperature, followed by extraction of diamide with DCM (4 x 4 mL). The concentration of $(\text{CoAS})_2$ in the final solution was determined by preparing five dilutions of the solution, which were each individually analysed spectrophotometrically to determine the absorbance at 260 nm. The $(\text{CoAS})_2$ concentration in each dilution was subsequently calculated using the reported extinction coefficient for CoA disulfide ($\epsilon_{260} = 33600 \text{ M}^{-1} \cdot \text{cm}^{-1}$) [7]. The average value was taken as the $(\text{CoAS})_2$ concentration in the original solution. The purity of $(\text{CoAS})_2$ was confirmed by HPLC analysis. A typical chromatogram is shown below (Figure 3.15).

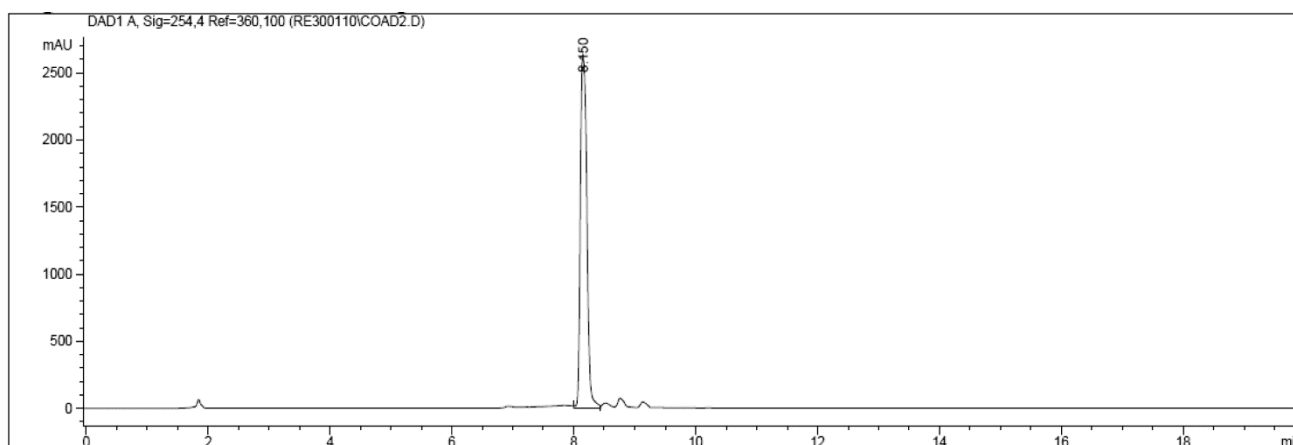


Figure 3.15: HPLC chromatogram of CoA disulfide, $(\text{CoAS})_2$.

HPLC analysis was performed on an Agilent 1100 instrument using a Supelcosil LC-18-T 3μ C18 column (150 x 4.6 mm) from Supelco. The column was equilibrated in 95% solution A (100 mM potassium

phosphate, pH 6.5) and 5% solution B (acetonitrile), followed by elution with 95% A (0 - 5 minutes, isocratic), a linear gradient increasing solution B to 40% (5 - 10 minutes), isocratic elution at 40% (10 - 12 minutes), a linear gradient increasing solution B to 60% (12 - 13 minutes) and finally by an isocratic elution at 60% B (13 - 15 minutes). A flow rate of 1 mL.min⁻¹ was maintained throughout.

3.4.4 SaCoADR activity assay

The SaCoADRs were assayed at saturating substrate conditions using established protocols [34]. Reactions were initiated by adding 450 µL of an enzyme master mix to 50 µL containing (CoAS)₂. CoADR activity was assayed at 25 °C in a total volume of 500 µL containing 50 mM potassium phosphate (pH 7.0), 0.5 mM EDTA, 32 µM NADPH, 20 nM CoADR and 60 µM (CoAS)₂. The initial reaction rates were determined by following the oxidation of the NADPH cofactor spectrophotometrically (decrease in absorbance at 340 nm) at 25 °C. All measurements were made in an Agilent Technologies Cary 60 UV-Vis Spectrometer using a 1 cm cuvette.

3.4.5 Biosynthesis of CoA analogues from pantothenamide precursors

The biosynthesis reactions were initiated by adding 51 µg of each of SaPanK, SaPPAT and SaDPCK to a solution with 16.5 mM ATP, 10 mM MgCl₂, 10 mM pantothenamide and containing 60 mM HEPES (pH 8.0) with a final volume of 500 µL. The reaction mixture was incubated at 37 °C for 2 hours. Afterwards, the reaction mixture was diluted 1:1 with 10 mM NH₄OAc (pH 6.0) and all protein was removed using a Pierce™ 3K MWCO, 0.5 mL protein concentrator.

3.4.6 Liquid chromatography mass spectrometry (LC-MS) analysis

LC-MS analysis was performed on a Waters Synapt G2 instrument using a Waters HSS C18 column (2.1 x 150mm). The column was equilibrated in 98% solvent A (10 mM NH₄OAc, pH 6.5) and 2% solvent B (acetonitrile with 0.1% formic acid), followed by elution with 98% A (0 - 1 minutes, isocratic), a linear gradient increasing solution B to 20% (1 - 10 minutes), a linear gradient increasing solution B to 100% (10 - 15 minutes), an isocratic elution at 100% B (15 - 16 minutes) and finally conditions were returned to 98% A (16 - 20 minutes, isocratic). A flow rate of 0.3 mL.min⁻¹ was maintained throughout.

Electrospray ionisation was applied in the positive mode at a capillary voltage of 2.5 kV, cone voltage of 15 V, desolvation temperature of 275 °C and desolvation gas setting of 650 L/h. The rest of the MS settings were optimised for best sensitivity. The instrument was calibrated with sodium formate and leucine enkephalin was used as lock mass for accurate mass determinations. The MS acquisition method consisted of a low energy function at a trap voltage of 6 V and a high energy function where the trap collision energy was ramped from 15 to 60 V to generate fragmentation data (MS^F).

3.4.7 Synthesis of relevant compounds

All the Michael acceptor-containing inhibitor compounds were synthesised previously by Renier van der Westhuyzen [25]. The synthesis scheme is included in Figure 3.16.

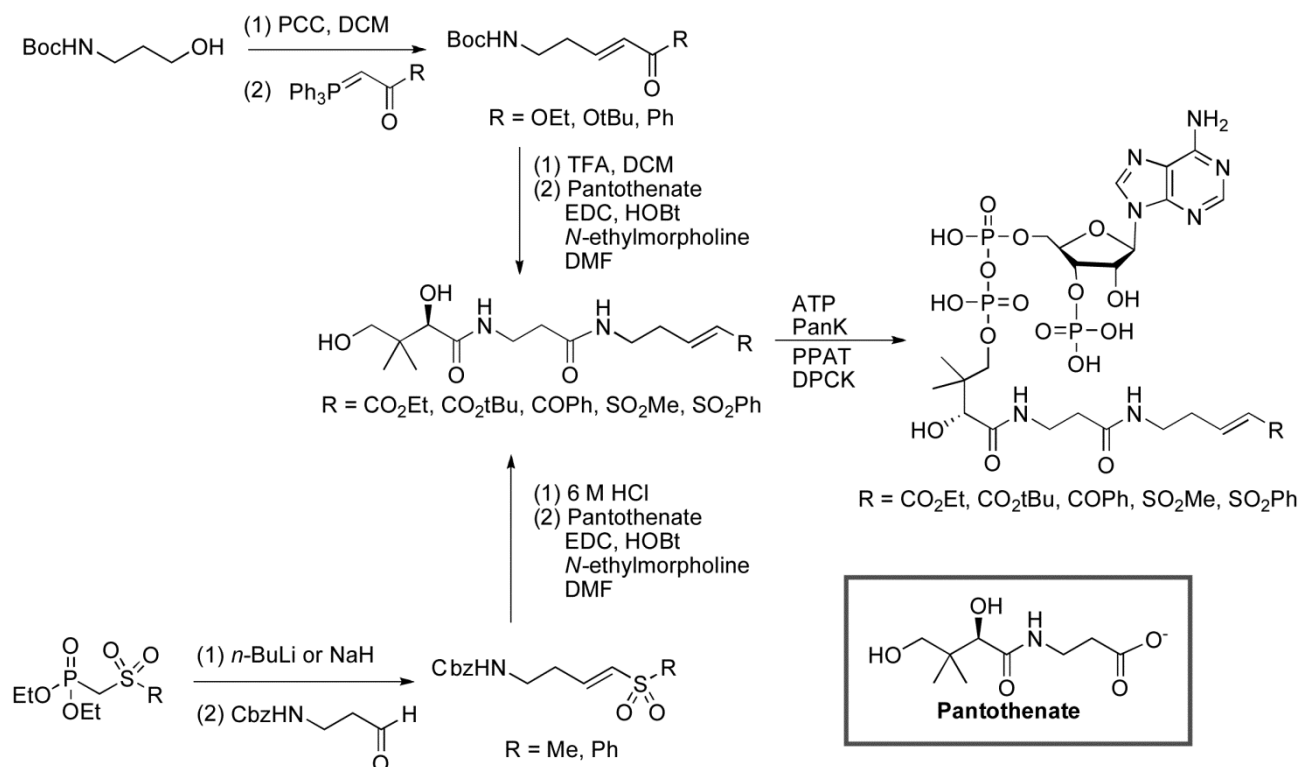
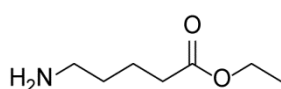
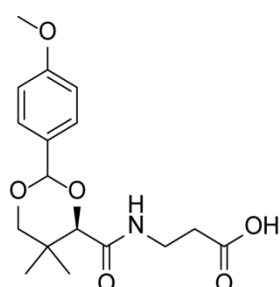


Figure 3.16: Synthesis of the Michael Acceptor-Containing Pantothenamides and CoA-analogues [25].

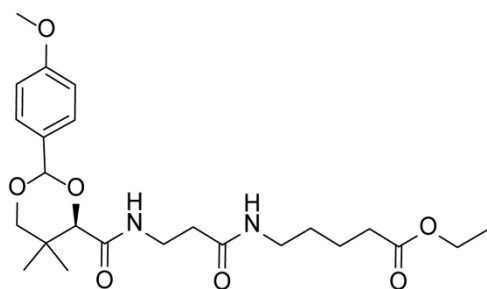


Ethyl 5-aminopentanoate: 5-amino-pentanoic acid was esterified with ethanol using Fischer-esterification to 5-amino-pentanoate as follows. The acid (237.0 mg, 2.02 mmol) was dissolved in excess ethanol (\pm 30 ml, 513 mmol) and concentrated sulphuric acid (0.1 ml) was added as an acid catalyst. The mixture was heated at 80 °C while stirring for 2 hours under reflux. After removing from heat, the unreacted acid was removed by filtration. The mixture was then concentrated *in vacuo* to remove all traces of ethanol and afford pure ethyl 5-amino-pentanoate as a light yellow oil (259.0 mg, 1.78 mmol) at a 88% yield. ¹H NMR (300 MHz, CDCl₃): δ = 4.18 (q, *J* = 7.03, 2H), 2.46 (br, 2H), 1.74-1.72 (m, 2H), 1.70-1.68 (m, 2H), 1.27 (t, *J* = 7.03, 3H).



3-((4R)-2-(4-methoxyphenyl)-5,5-dimethyl-1,3-dioxane-4-carboxamido) propanoic acid: Pantothenic acid was obtained from calcium pantothenate *via* cation exchange. Calcium pantothenate (978.4 mg, 4.1 mmol) was passed through Amberlite IR-120 cation exchange resin (1.1 g) and lyophilised to afford pantothenic acid. The diol-group of the pantothenic acid was then protected using *p*-methoxybenzaldehyde dimethyl acetal (PMB) to prevent any unwanted electrostatic

interactions in the following steps of the synthesis. Pantothenic acid (794.1 mg, 3.62 mmol) was placed under nitrogen flow and crushed molecular sieves (4 Å) was added. Dry THF (10 ml) was added and the mixture was swirled until all the pantothenic acid was dissolved. Camphor-10-sulfonic acid (CSA) (8.41 mg, 0.362 mmol) and PMB (1.24 ml, 7.24 mmol) was added and the reaction mixture was stirred overnight at 25 °C. The molecular sieves were then removed *via* filtration and the THF was removed *in vacuo*. The desired product (PMB-protected pantothenic acid) precipitated as an off-white powder (822.65 mg, 2.44 mmol). The yield was calculated as 67%. ¹H NMR (DMSO-D₆, 400MHz): δ = 0.95 (s, 3H), 1.01 (s, 3H), 2.40 (t, *J* = 7.1 Hz, 2H), 3.35 (m, 2H), 3.63 (dd, *J* = 11.2 Hz, 2H), 3.76 (s, 3H), 4.09 (s, 1H), 5.52 (s, 1H), 6.92 (d, *J* = 8.7 Hz, 2H), 7.43 (d, *J* = 8.9 Hz, 2H), 7.46 (br t, *J* = 6.1 Hz, 1H), 12.30 (br s, 1H).

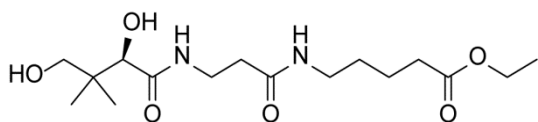


Ethyl 5-(3-((4R)-2-(4-methoxyphenyl)-5,5-dimethyl-1,3-dioxane-4-carboxamido)propanamido)pentanoate:

PMB-protected pantothenic acid was coupled to ethyl 5-amino-pentanoate by *N*-(3-Dimethylaminopropyl)-*N'*-ethylcarbodiimide (EDC)-coupling. The amine, ethyl 5-amino-pentanoate (259.0 mg, 1.78 mmol), was dissolved in dry Dimethylformamide (DMF) (3 mL) and added to a

2-neck round-bottom flask containing the PMB-protected pantothenic acid (600.5 mg, 1.78 mmol), Hydroxybenzotriazole (HOBt) (290.47 mg, 2.15 mmol) and Triethylamine (Et₃N) (550 μl, 3.94 mmol), which were all dissolved in dry DMF (3 mL). The reaction mixture was kept under nitrogen flow. After cooling to 0 °C, EDC (388.0 mg, 2.5 mmol) was dissolved in dry DMF (5 mL) and added to the reaction mixture. The mixture was then stirred for 2 hours at 0 °C after which it was

slowly heated to 25 °C and stirred overnight under nitrogen flow. The DMF was subsequently removed *in vacuo* and the crude product was purified by flash chromatography (5% MeOH/DCM) using a 5 cm silica column. The solvents were then removed *in vacuo* to afford the PMB-protected ethyl pentanoate pantothenamide as a white powder (289.0 mg, 0.62 mmol). The yield was calculated as 34%. ¹H NMR (300 MHz, CDCl₃): δ = 7.44 (d, *J* = 9.37, 1H), 7.41 (d, *J* = 8.59, 1H), 6.93 (d, *J* = 9.37, 1H), 6.90 (d, *J* = 8.59, 1H), 5.45 (s, 1H), 5.30 (s, 1H), 4.15-4.05 (m, 2H), 3.8 (s, 3H), 3.7 (s, 2H), 3.6-3.5 (m, 2H), 3.3-3.15 (m, 2H), 2.41 (t, *J* = 6.25, 2H), 2.28 (t, *J* = 7.42, 2H), 1.66-1.58 (m, 2H), 1.54-1.48 (m, 2H), 1.25 (t, *J* = 7.03, 3H), 1.10 (br, 3H), 1.09 (br, 3H).



Ethyl 5-(pantothenamido) pentanoate:

The final step of the synthesis involved the removal of the PMB-group from PMB-protected ethyl pentanoate pantothenamide. This pantothenamide (289.0 mg, 0.62 mmol) was dissolved in THF (11 mL) and 1 M hydrochloric acid (HCl) (11 mL) was added. The reaction mixture was neutralised after 5 hours with the addition of Amberlite IRA-400 strong basic anion exchange resin until the pH reached 7. The mixture was then filtered and concentrated *in vacuo*. Afterwards the mixture was dissolved in 20% methanol/dichloromethane and purified by flash chromatography using a 4 cm silica column. The solvent was subsequently removed *in vacuo* to afford the final product, ethyl 5-(pantothenamido) pentanoate as a white powder (70.5 mg, 0.204 mmol). The yield was

calculated as 32%. ^1H NMR (300 MHz, CDCl_3): δ = 4.21-4.15 (m, 2H), 4.00 (s, 1H), 3.60-3.48 (m, 4H), 3.20 (t, J = 7.03, 2H), 2.52 (t, J = 6.64, 2H), 2.41 (t, J = 7.42, 2H), 1.68-1.60 (m, 2H), 1.59-1.49 (m, 2H), 1.32-1.24 (m, 3H), 0.93 (s, 3H), 0.89 (s, 3H). $[\text{M}+\text{H}]^+$ calculated for $\text{C}_{16}\text{H}_{31}\text{N}_2\text{O}_6$, 347.2182; found 347.2173.

3.4.8 *S. aureus* whole cell inhibition assay

S. aureus cells were streaked out on TSB-agar plates (no antibiotic for JE2; with erythromycin ($10\ \mu\text{g}\cdot\text{mL}^{-1}$) for all the other strains for selection) and incubated at $37\ ^\circ\text{C}$ overnight. A few (4 or 5) well-isolated colonies were picked from each plate and used to inoculate 5 mL TSB growth medium (with antibiotic where necessary for selection). The cultures were incubated at $37\ ^\circ\text{C}$ for 5 - 6 hours until they reached mid-log phase ($\text{OD}_{600} = 0.4\text{-}0.5$ for *S. aureus*). The mid-log bacterial cultures were diluted 15 000x ($2\ \mu\text{L}$ in 30 mL) in TSB growth media and used to inoculate wells containing TSB in a 96-well cell culture plate. Inhibitor compounds were added in doubling dilutions and the 96-well plate was then incubated at $37\ ^\circ\text{C}$ for 18 hours while shaking, after which the absorbance was read at 600 nm using a Thermo Scientific Varioskan microplate spectrophotometer. The dose response of each compound was then determined and the IC_{50} - and MIC-values were calculated using SigmaPlot 12.0 software (Systat Software).

3.4.9 Dose-response of H_2O_2 against *S. aureus*

S. aureus cells were streaked out on TSB-agar plates (no antibiotic for JE2; with erythromycin ($10\ \mu\text{g}\cdot\text{mL}^{-1}$) for all the other strains for selection) and incubated at $37\ ^\circ\text{C}$ overnight. A few (4 or 5) well-isolated colonies were picked from each plate and used to inoculate 5 mL TSB growth medium (with antibiotic where necessary for selection). The cultures were incubated at $37\ ^\circ\text{C}$ for 5 - 6 hours until they reached mid-log phase ($\text{OD}_{600} = 0.4\text{-}0.5$ for *S. aureus*). The mid-log bacterial cultures were then pipetted into a 96-well cell culture plate. H_2O_2 was added in doubling dilutions and the 96-well plate was then incubated at $37\ ^\circ\text{C}$ for 18 hours after which the absorbance was read at 600 nm using a Thermo Scientific Varioskan microplate spectrophotometer. The dose response of each compound was then determined and the IC_{50} - and MIC-values were calculated using SigmaPlot 12.0 software (Systat Software).

3.4.10 *S. aureus* overnight stress test with H_2O_2 and diamide

For overnight stress assays, cultures were prepared as described above for the H_2O_2 dose-response in 5 ml TSB and grown in triplicate, with one tube containing H_2O_2 (25 mM), the other containing diamide (5 mM) and the last tube containing both compounds at the stated concentrations. The cultures were then incubated at $37\ ^\circ\text{C}$ for 18 hours after which the absorbance was read at 600 nm.

3.4.11 Isolation of human neutrophils

Neutrophils were isolated from heparinised venous blood that was supplied by the Western Province Blood Transfusion Service. Ficoll-Paque Plus (2 mL) at room temperature was pipetted into the bottom of a sterile 15 mL centrifuge tube and blood (4 mL) was then carefully overlaid on top of the Ficoll-Paque Plus. The tubes were then centrifuged at $652 \times g$ for 30 minutes at 21 °C to separate the blood into four different layers. The sediment containing PMNs and erythrocytes were retained and the supernatant layers containing lymphocytes, monocytes and the plasma layer on top were discarded. The sediment was then mixed with an equal volume of 6% Dextran-500 (in 0.9% NaCl) at room temperature and incubated at 37 °C for 45 minutes to allow the sedimentation of erythrocytes. The pellet containing erythrocytes was subsequently discarded and the neutrophil-rich supernatant was collected and mixed with 10 mL of PBS. The PBS-neutrophil mixture was centrifuged at $290 \times g$ for 10 minutes at 4 °C and the pellet containing the neutrophils was collected and the supernatant was discarded. The pellet was then washed twice with 1 mL PBS. The final neutrophil pellet was suspended into the desired volume of RPMI 1640 media (10 mM HEPES buffered at pH 7.4) to achieve the appropriate cell concentration of 2×10^6 cells.mL⁻¹.

3.4.12 Neutrophil bactericidal assay

All *S. aureus* strains were plated on TSB-agar plates (without antibiotic for JE2) containing 10 µg.mL⁻¹ erythromycin for selection for NE785, NE1456 and NE1728 and grown overnight at 37 °C. TSB (5 mL) was inoculated with 4 - 5 single colonies bacteria and grown to mid-log phase (*S. aureus* OD₆₀₀ = 0.4). An aliquot of each culture (1 mL) was then centrifuged briefly (4 min. at 8 000 RPM on a small benchtop centrifuge) to pellet the cells. The cells were then washed twice in PBS and 1 µL of each PBS-cell suspension was diluted into HEPES buffered RPMI at pH 7.4. A sterile 96-well flat-bottom microtiter plate was coated with human serum and washed extensively with PBS. Bacterial cells were then combined with PMNs at a ratio of 1:1 (CFU:PMN ratio) in the 96-well plate in a total volume of 198 µL. Next, the 96-well plate was centrifuged at $456 \times g$ for 7 min to synchronise phagocytosis and afterwards the plate was incubated at 37 °C for up to 120 min. At the desired time points, saponin (22 µl of a 1% solution, 0.1% final concentration) was added to each well to break up any cell clumps and the contents were mixed and then incubated on ice for 15 min. The surviving bacteria were enumerated the following day by CFU-count. Percentage survival was calculated by comparing the numbers of surviving bacteria at each timepoint to those at $t = 0$.

3.5 References

1. Jaeger, T., et al., *The thiol-based redox networks of pathogens: Unexploited targets in the search for new drugs*. BioFactors, 2006. **27**(1): p. 109-120.
2. Atkinson, H.J. and P.C. Babbitt, *An Atlas of the Thioredoxin Fold Class Reveals the Complexity of Function-Enabling Adaptations*. PLoS Comput Biol, 2009. **5**(10): p. e1000541.
3. Holmgren, A., *Thioredoxin*. Annual Review of Biochemistry, 1985. **54**(1): p. 237-271.

4. Argyrou, A. and J.S. Blanchard, *Flavoprotein Disulfide Reductases: Advances in Chemistry and Function*, in *Progress in Nucleic Acid Research and Molecular Biology* 2004, Academic Press. p. 89-142.
5. Fahey, R.C., et al., *Occurrence of glutathione in bacteria*. *Journal of Bacteriology*, 1978. **133**(3): p. 1126-1129.
6. delCardayré, S.B. and J.E. Davies, *Staphylococcus aureus Coenzyme A Disulfide Reductase, a New Subfamily of Pyridine Nucleotide-Disulfide Oxidoreductase: SEQUENCE, EXPRESSION, AND ANALYSIS OF cdr*. *Journal of Biological Chemistry*, 1998. **273**(10): p. 5752-5757.
7. delCardayré, S.B., et al., *Coenzyme A Disulfide Reductase, the Primary Low Molecular Weight Disulfide Reductase from Staphylococcus aureus*. *Journal of Biological Chemistry*, 1998. **273**(10): p. 5744-5751.
8. Rajkarnikar, A., et al., *Analysis of mutants disrupted in bacillithiol metabolism in Staphylococcus aureus*. *Biochemical and Biophysical Research Communications*, 2013. **436**(2): p. 128-133.
9. Helmann, J.D., *Bacillithiol, a New Player in Bacterial Redox Homeostasis*. *Antioxidants & Redox Signaling*, 2010. **15**(1): p. 123-133.
10. Roberts, A.A., et al., *Mechanistic studies of FosB: a divalent-metal-dependent bacillithiol-S-transferase that mediates fosfomycin resistance in Staphylococcus aureus*. *The Biochemical journal*, 2013. **451**(1): p. 69-79.
11. Gaballa, A., et al., *Biosynthesis and functions of bacillithiol, a major low-molecular-weight thiol in Bacilli*. *Proceedings of the National Academy of Sciences*, 2010. **107**(14): p. 6482-6486.
12. Newton, G.L., et al., *Distribution of thiols in microorganisms: mycothiol is a major thiol in most actinomycetes*. *Journal of Bacteriology*, 1996. **178**(7): p. 1990-5.
13. Newton, G.L., et al., *Bacillithiol is an antioxidant thiol produced in Bacilli*. *Nat Chem Biol*, 2009. **5**(9): p. 625-627.
14. Fey, P.D., et al., *A Genetic Resource for Rapid and Comprehensive Phenotype Screening of Nonessential Staphylococcus aureus Genes*. *mBio*, 2013. **4**(1).
15. Voyich, J.M., et al., *Insights into Mechanisms Used by Staphylococcus aureus to Avoid Destruction by Human Neutrophils*. *Journal of Immunology*, 2005. **175**(Copyright (C) 2011 American Chemical Society (ACS). All Rights Reserved.): p. 3907-3919.
16. Freitas, M., et al., *Oxidative stress adaptation in aggressive prostate cancer may be counteracted by the reduction of glutathione reductase*. *FEBS Open Bio*, 2012. **2**(0): p. 119-128.
17. Traverso, N., et al., *Role of Glutathione in Cancer Progression and Chemoresistance*. *Oxidative Medicine and Cellular Longevity*, 2013. **2013**: p. 10.

18. Kumar, S., M.R. Ali, and S. Bawa, *Mini review on tricyclic compounds as an inhibitor of trypanothione reductase*. Journal of Pharmacy & Bioallied Sciences, 2014. **6**(4): p. 222-228.
19. Ferreira, L.G. and A.D. Andricopulo, *Inhibitors of Trypanosoma brucei trypanothione reductase: comparative molecular field analysis modeling and structural basis for selective inhibition*. Future Medicinal Chemistry, 2013. **5**(15): p. 1753-1762.
20. Andricopulo, A.D., et al., *Specific inhibitors of Plasmodium falciparum thioredoxin reductase as potential antimalarial agents*. Bioorganic & Medicinal Chemistry Letters, 2006. **16**(8): p. 2283-2292.
21. Theobald, A.J., et al., *Discovery and Biochemical Characterization of Plasmodium Thioredoxin Reductase Inhibitors from an Antimalarial Set*. Biochemistry, 2012. **51**(23): p. 4764-4771.
22. Mahapatra, A., et al., *Activity of 7-methyljuglone derivatives against Mycobacterium tuberculosis and as subversive substrates for mycothiol disulfide reductase*. Bioorganic & Medicinal Chemistry, 2007. **15**(24): p. 7638-7646.
23. Bryk, R., et al., *Lipoamide Channel-Binding Sulfonamides Selectively Inhibit Mycobacterial Lipoamide Dehydrogenase*. Biochemistry, 2013. **52**(51): p. 9375-9384.
24. Luba, J., V. Charrier, and A. Claiborne, *Coenzyme A-Disulfide Reductase from Staphylococcus aureus: Evidence for Asymmetric Behavior on Interaction with Pyridine Nucleotides*. Biochemistry, 1999. **38**(9): p. 2725-2737.
25. van der Westhuyzen, R. and E. Strauss, *Michael Acceptor-Containing Coenzyme A Analogues As Inhibitors of the Atypical Coenzyme A Disulfide Reductase from Staphylococcus aureus*. Journal of the American Chemical Society, 2010. **132**(37): p. 12853-12855.
26. Powers, J.C., et al., *Irreversible Inhibitors of Serine, Cysteine, and Threonine Proteases*. Chemical Reviews, 2002. **102**(12): p. 4639-4750.
27. Hernandez, A.A. and W.R. Roush, *Recent advances in the synthesis, design and selection of cysteine protease inhibitors*. Current Opinion in Chemical Biology, 2002. **6**(4): p. 459-465.
28. Brinen, L.S., et al., *A target within the target: probing cruzain's P1' site to define structural determinants for the Chagas' disease protease*. Structure, 2000. **8**(8): p. 831-840.
29. Mallett, T.C., et al., *Structure of Coenzyme A-Disulfide Reductase from Staphylococcus aureus at 1.54 Å Resolution*, *†*. Biochemistry, 2006. **45**(38): p. 11278-11289.
30. Strauss, E., M. de Villiers, and I. Rootman, *Biocatalytic Production of Coenzyme A Analogues*. ChemCatChem, 2010. **2**(8): p. 929-937.
31. Clarke, K.M., et al., *In Vivo Reporter Labeling of Proteins via Metabolic Delivery of Coenzyme A Analogues*. Journal of the American Chemical Society, 2005. **127**(32): p. 11234-11235.

32. Meier, J.L., et al., *Synthesis and Evaluation of Bioorthogonal Pantetheine Analogues for in Vivo Protein Modification*. Journal of the American Chemical Society, 2006. **128**(37): p. 12174-12184.
33. Wallace, B.D., et al., *Turnover-Dependent Covalent Inactivation of Staphylococcus aureus Coenzyme A-Disulfide Reductase by Coenzyme A-Mimetics: Mechanistic and Structural Insights*. Biochemistry, 2012. **51**(39): p. 7699-7711.
34. Luba, J., V. Charrier, and A. Claiborne, *Coenzyme A-Disulfide Reductase from Staphylococcus aureus: Evidence for Asymmetric Behavior on Interaction with Pyridine Nucleotides†*. Biochemistry, 1999. **38**(9): p. 2725-2737.
35. Virga, K.G., et al., *Structure–activity relationships and enzyme inhibition of pantothenamide-type pantothenate kinase inhibitors*. Bioorganic & Medicinal Chemistry, 2006. **14**(4): p. 1007-1020.
36. Hughes, S.J., et al., *Structural characterization of a new N-substituted pantothenamide bound to pantothenate kinases from Klebsiella pneumoniae and Staphylococcus aureus*. Proteins: Structure, Function, and Bioinformatics, 2014. **82**(7): p. 1542-1548.
37. Zhang, Y.-M., et al., *Acyl Carrier Protein Is a Cellular Target for the Antibacterial Action of the Pantothenamide Class of Pantothenate Antimetabolites*. Journal of Biological Chemistry, 2004. **279**(49): p. 50969-50975.
38. Strauss, E. and T.P. Begley, *The Antibiotic Activity of N-Pentylpantothenamide Results from Its Conversion to Ethyldethia-Coenzyme A, a Coenzyme A Antimetabolite*. Journal of Biological Chemistry, 2002. **277**(50): p. 48205-48209.
39. Davis, T.D., C.J. Gerry, and D.S. Tan, *General Platform for Systematic Quantitative Evaluation of Small-Molecule Permeability in Bacteria*. ACS Chemical Biology, 2014. **9**(11): p. 2535-2544.
40. de Villiers, M., et al., *Variation in pantothenate kinase type determines the pantothenamide mode of action and impacts on coenzyme A salvage biosynthesis*. FEBS Journal, 2014. **281**(20): p. 4731-4753.
41. Viswanadhan, V.N., et al., *Atomic physicochemical parameters for three dimensional structure directed quantitative structure-activity relationships. 4. Additional parameters for hydrophobic and dispersive interactions and their application for an automated superposition of certain naturally occurring nucleoside antibiotics*. Journal of Chemical Information and Computer Sciences, 1989. **29**(3): p. 163-172.
42. Tetko, I.V., et al., *Internet Software for the Calculation of the Lipophilicity and Aqueous Solubility of Chemical Compounds*. Journal of Chemical Information and Computer Sciences, 2001. **41**(2): p. 246-252.
43. Tetko, I., et al., *Virtual Computational Chemistry Laboratory – Design and Description*. Journal of Computer-Aided Molecular Design, 2005. **19**(6): p. 453-463.

44. Tetko, I.V. *Virtual Computational Chemistry Laboratory*. 2005; Available from: <http://www.vcclab.org>.
45. Silva, J.C., et al., *Simultaneous Qualitative and Quantitative Analysis of the Escherichia coli Proteome: A Sweet Tale*. *Molecular & Cellular Proteomics*, 2006. **5**(4): p. 589-607.
46. Basu, S.S., et al., *Stable Isotope Labeling by Essential Nutrients in Cell Culture for Preparation of Labeled Coenzyme A and Its Thioesters*. *Analytical Chemistry*, 2011. **83**(4): p. 1363-1369.
47. Thomas, J. and J.E. Cronan, *Antibacterial Activity of N-Pentylpantothenamide Is Due to Inhibition of Coenzyme A Synthesis*. *Antimicrobial Agents and Chemotherapy*, 2010. **54**(3): p. 1374-1377.
48. Posada, A.C., et al., *Importance of Bacillithiol in the Oxidative Stress Response of Staphylococcus aureus*. *Infection and Immunity*, 2014. **82**(1): p. 316-332.
49. Kosower, N.S. and E.M. Kosower, [11] *Diamide: An oxidant probe for thiols*, in *Methods in Enzymology*, P. Lester, Editor 1995, Academic Press. p. 123-133.
50. Pöther, D.-C., et al., *Diamide triggers mainly S thiolations in the cytoplasmic proteomes of Bacillus subtilis and Staphylococcus aureus*. *Journal of Bacteriology*, 2009. **191**(Copyright (C) 2011 American Chemical Society (ACS). All Rights Reserved.): p. 7520-7530.
51. Voyich, J.M., et al., *Insights into Mechanisms Used by Staphylococcus aureus to Avoid Destruction by Human Neutrophils*. *The Journal of Immunology*, 2005. **175**(6): p. 3907-3919.
52. Lu, T., et al., *Phagocytosis and Killing of Staphylococcus aureus by Human Neutrophils*. *Journal of Innate Immunity*, 2014. **6**(5): p. 639-649.
53. van der Westhuyzen, R., et al., *The Antibiotic CJ-15,801 Is an Antimetabolite that Hijacks and Then Inhibits CoA Biosynthesis*. *Chemistry & Biology*, 2012. **19**(5): p. 559-571.
54. de Jonge, B.L.M., et al., *Discovery of Inhibitors of 4'-Phosphopantetheine Adenylyltransferase (PPAT) To Validate PPAT as a Target for Antibacterial Therapy*. *Antimicrobial Agents and Chemotherapy*, 2013. **57**(12): p. 6005-6015.

Chapter 4: Characterization of the Mechanism of Inhibition of the Natural Product CJ-15,801, a Selective Inhibitor of *Staphylococcus aureus*³

4.1 Introduction

Staphylococcus aureus, the bacterium that causes most nosocomial and many other opportunistic infections in humans, is rapidly becoming more prevalent in the community and, alarmingly, increasingly resistant to the current arsenal of available antibacterial agents [1]. More than ever, new treatments are urgently needed to combat this threat. One compound that shows promise in this regard is the natural product CJ-15,801 (Figure 4.1, **2**), which was discovered in 2001 by a Pfizer research team when it was isolated from fermenting cultures of a *Seimatosporium* sp. fungus [2]. Subsequently, CJ-15,801 was characterised as an antimetabolite that hijacks the coenzyme A (CoA) biosynthetic pathway in *S. aureus*, being activated by the first enzyme (pantothenate kinase, PanK) before it inhibits the second (phosphopantothenoylcysteine synthetase, PPCS) by forming an inhibitor *in situ* within the active site [3] (Figure 4.1). The inhibitory form of CJ-15,801, 4'-phospho-CJ-15,801-cytidylate (*PCJ-CMP*, **6**), is a structural mimic of 4'-phosphopantothenoyl-cytidylate (*PPan-CMP*, **5**), the natural PPCS reaction intermediate, with the only difference being the introduction of a double bond in its β -alanine moiety (Figure 4.1). Detailed kinetic analysis showed that *PCJ-CMP* acts as a tight-binding inhibitor of PPCS, with a K_i of 13.0 nM.

Mechanistically, PPCS resembles other synthetase enzymes that use ATP to transiently activate the carboxyl group of one substrate for nucleophilic attachment by the amino group of another, forming an amide bond in the process [4, 5]. In all of these cases a tightly bound acyl-adenylate intermediate is formed. This feature has been exploited for inhibitor development in the past through the design and synthesis of non-hydrolysable analogues of these intermediates; such compounds – in which the labile acyl-phosphate moiety is exchanged for other, stable groups such as *N*-acyl sulphonamides [6] or phosphodiester [7] – often show tight binding kinetics with inhibitory constants in the nanomolar range [8]. As such, the discovery of *PCJ-CMP* as an inhibitor of PPCS is not surprising. However, the basis for the apparent resistance of *PCJ-CMP* to hydrolysis or acyl transfer is unclear, since it still contains an activated acyl phosphate moiety. In many respects PPCS show several differences compared to other acyl-adenylate generating synthetases: first, most of these enzymes belong to the ANL superfamily of adenylating enzymes, while PPCS enzymes belong to the ribokinase family [9]. Second, bacterial PPCS enzymes use CTP to activate their substrates' carboxylate groups instead of ATP [10, 11]; while this does not indicate a mechanistic difference, it could imply structural differences are at play in the binding of the inhibitor. Third, the PPCS inhibitor is formed *in situ*, while those characterized for other synthetase enzymes are usually prepared and introduced as the full structural mimics of the respective enzymes' reaction intermediates.

³ The work on the initial characterization of the mechanism of inhibition of *Sa*CoaBC by *PCJ-CMP* has been published as part of a bigger study: Van der Westhuyzen, R., Hammons, J.C., Meier, J.L., Dahesh, S., **Moolman, W.J.A.**, Pelly, S.C., Nizet, V., Burkart, M.D. & Strauss, E. The Antibiotic CJ-15,801 is an Antimetabolite which Hijacks and then Inhibits CoA Biosynthesis. *Chem. Biol.* **19**, 559–571 (2012). The published version of the article is reproduced in the Appendix.

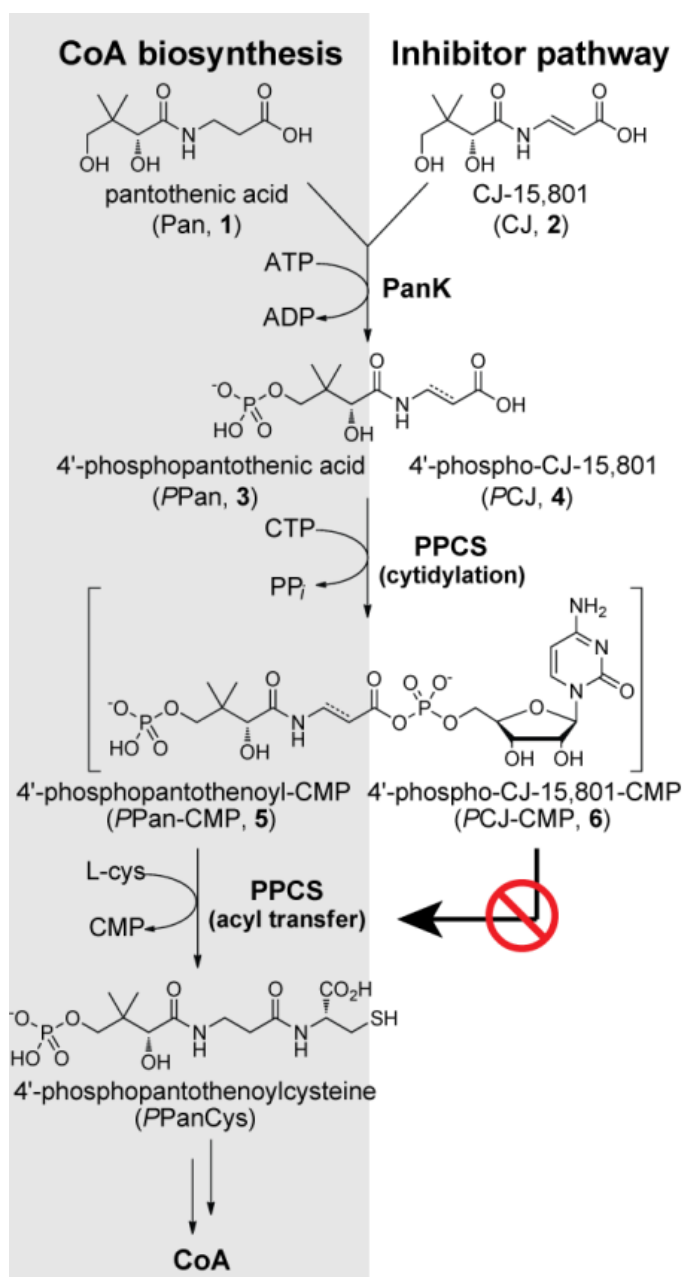


Figure 4.1: Comparison of the differences between pantothenic acid (left) and CJ-15,801 (right) in the coenzyme A (CoA) biosynthesis pathway.

In this study we therefore set out to further investigate the mechanism of inhibition of PPCS enzymes by PCJ-CMP by focusing on the basis for the apparent stability of the inhibitor. Three possible reasons were investigated: first, that the specific interactions between the enzyme and the inhibitor causes the latter to bind in a manner that protects its activated acyl-phosphate moiety from nucleophilic attack; second, that the enzyme undergoes different conformational changes upon binding of the inhibitor compared to the substrate, with the inhibitor inducing a conformation that prevents acyl transfer from taking place; and third, that a specific characteristic innate to the structure of PCJ-CMP molecule endows it with increased stability compared to PPan-CMP, allowing it to act as a tight-binding inhibitor similar to other non-hydrolysable synthetase inhibitors. Our results show that the PPCS protein itself plays no role in the mechanism of

inhibition, but that the presence of the double bond with its extra π -electrons in the inhibitor renders its carboxylate group resistant to nucleophilic attack through the creation of new, stable resonance forms. Apart from shedding light on the mechanism of inhibition of this unique natural product, this finding might also serve as a general starting point for the development of stable variants of other compounds containing β -amino acid moieties.

4.2 Results

4.2.1 A constrained binding pose as a basis for increased inhibitor stability⁴

We first considered if inhibition by *PCJ*-CMP is caused by its planar *N*-acyl vinylogous carbamate functionality imposing restrictions on the rotation of the molecule, thereby preventing it from taking on the optimal binding pose required for attack by cysteine (or water). To establish if *PPan*-CMP and *PCJ*-CMP have different binding modes, we used the only available structure of a PPCS enzyme with its intermediate bound, that of the *E. coli* PPCS Asn210Asp mutant with *PPan*-CMP bound in the active site (PDB ID: 1U7Z). This mutant, which accumulates sufficient amounts of the intermediate to allow direct confirmation of its identity and structure [12, 13], is apparently unable to catalyse the second step of the PPCS reaction (Figure 4.1). However, the molecular basis for this catalytic disability remains speculative since no PPCS structure with cysteine bound has been determined thus far. Nonetheless, the mutation clearly results in tightly-bound *PPan*-CMP in the enzyme's active site. We constructed a model of the native enzyme by computationally reversing the Asn210Asp mutation in the crystal structure, and subsequently used it to dock *PCJ*-CMP in the active site. For the docking, 150 starting conformations were used to ensure sufficient conformational space was sampled considering the complexity of the molecule. The highest scoring docked pose of *PCJ*-CMP very closely mimics the pose of the co-crystallised *PPan*-CMP in the crystal structure (Figure 4.2A), and facilitates all the same hydrogen bonding interactions while maintaining a near planar geometry across the *N*-acyl vinylogous carbamate moiety (Figure 4.2B). This suggests that the basis for inhibition by *PCJ*-CMP is not due to it having a different binding mode, or taking on a potentially unreactive conformation.

⁴ Molecular modelling experiments reported in this section were performed by Dr. Stephen Pelly of the Department of Chemistry and Polymer Science, Stellenbosch University.

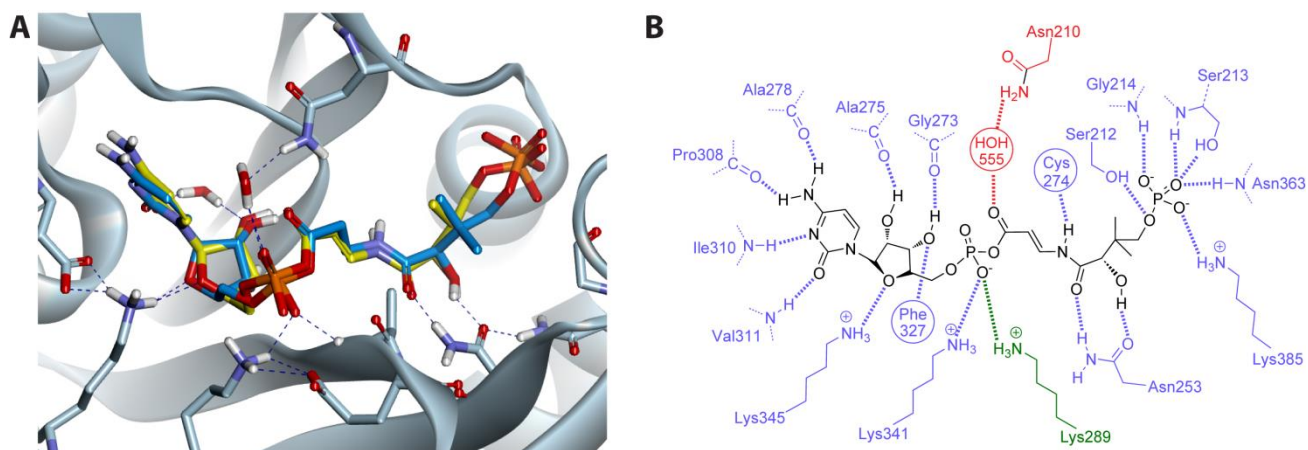


Figure 4.2: (A) Structure of the *PCJ-CMP* inhibitor (stick structure with carbon atoms in yellow) modeled and overlaid on that of the *PPan-CMP* intermediate (stick structure with carbon atoms in blue) bound in the active site of native *EcPPCS*. The model was created from the crystal structure of *EcPPCS* Asn210Asp with co-crystallized *PPan-CMP* bound (PDB: 1U7Z) by reversing the mutation, and docking *PCJ-PMP*. The highest scoring pose of *PCJ-CMP* closely resembles that of *PPan-CMP* and similarly facilitates all hydrogen bonding interactions observed for *PPan-CMP*. Only selected residues are shown for clarity. (B) Schematic view of polar interactions between *PCJ-CMP* and *EcPPCS*. Residues from one monomer are in blue and those from the other monomer in green. The key interaction between Asn₂₁₀ and the acyl phosphate carbonyl, mediated via a bridging water molecule, is shown in red [3].

4.2.2 Enzyme structure stabilisation as a basis for inhibition by *PCJ-CMP*

We next set out to determine if formation of *PCJ-CMP* in the PPCS active site induces formation of a stable conformation of the native protein structure beyond that which would normally be expected for a protein upon binding of a ligand [14-16]. Initial investigation of ligand-induced stabilisation of the structures of *E. coli* PPCS (*EcCoaB*, a dimer) and *S. aureus* CoaBC (*SaCoaBC*, a dodecamer that has both PPCS and phosphopantothencysteine decarboxylase (PPCDC) activities) showed that the former, experienced much less stabilisation as measured by heat-induced denaturation than the latter [3]. Since *EcPPCS* was inhibited by *PCJ-CMP* with an inhibition constant (K_i) of ~160 nM, while the K_i for *SaCoaBC* was ~13 nM, this suggested a correlation between the potency of inhibition and the oligomeric structure of the protein [3].

To establish if this is indeed the case, we increased the sample size and performed the same analysis on several bifunctional dodecameric CoaBC proteins with both PPCS and PPCDC activities [17], as well as several monofunctional, dimeric PPCS enzymes [10]. Among the latter were some – like the human (*HsCoaB*) and *Streptococcus pneumoniae* (*SpCoaB*) enzymes – that naturally occurs in this form, while *EcCoaB* was prepared by expression of the PPCS domain of the bifunctional *E. coli* CoaBC (*EcCoaBC*) protein. This analysis required the ligand-induced stabilisation and inhibition constants for each protein to be determined as described below; the new expanded dataset could then be used to establish if increased inhibition potency only correlates with increased structural stabilisation as would normally be expected [18, 19], or if some deviation or clustering was observed that could be related to the oligomeric structure of the enzymes in question.

4.2.2.1 Melting temperature determination of CoaB and CoaBC enzymes

We used the melting temperatures (T_m) of the proteins to quantify their stability relative to one another. The melting curves of the enzymes were determined in the presence of CTP and either its natural substrate, 4'-phosphopantothenic acid (PPan, **3**), or the inhibitor precursor, 4'-phospho-CJ-15,801 (PCJ, **4**) (Figure 4.1), by following the heat-induced denaturation of these mixtures by circular dichroism (CD). For HsCoaB, ATP was used instead of CTP since eukaryotic PPCS enzymes have different substrate specificity than the bacterial versions. The melting curves of all the proteins are shown in Figure 4.3. We observed a general trend that the enzymes in the presence of inhibitor have higher T_m -values than in the presence of substrate, as demonstrated by calculating the change in T_m -value change ($\Delta\Delta T_m$) between the two conditions. This indicates that the binding of the inhibitor increases protein stability as expected (Figure 4.3A-F, Table 4.1).

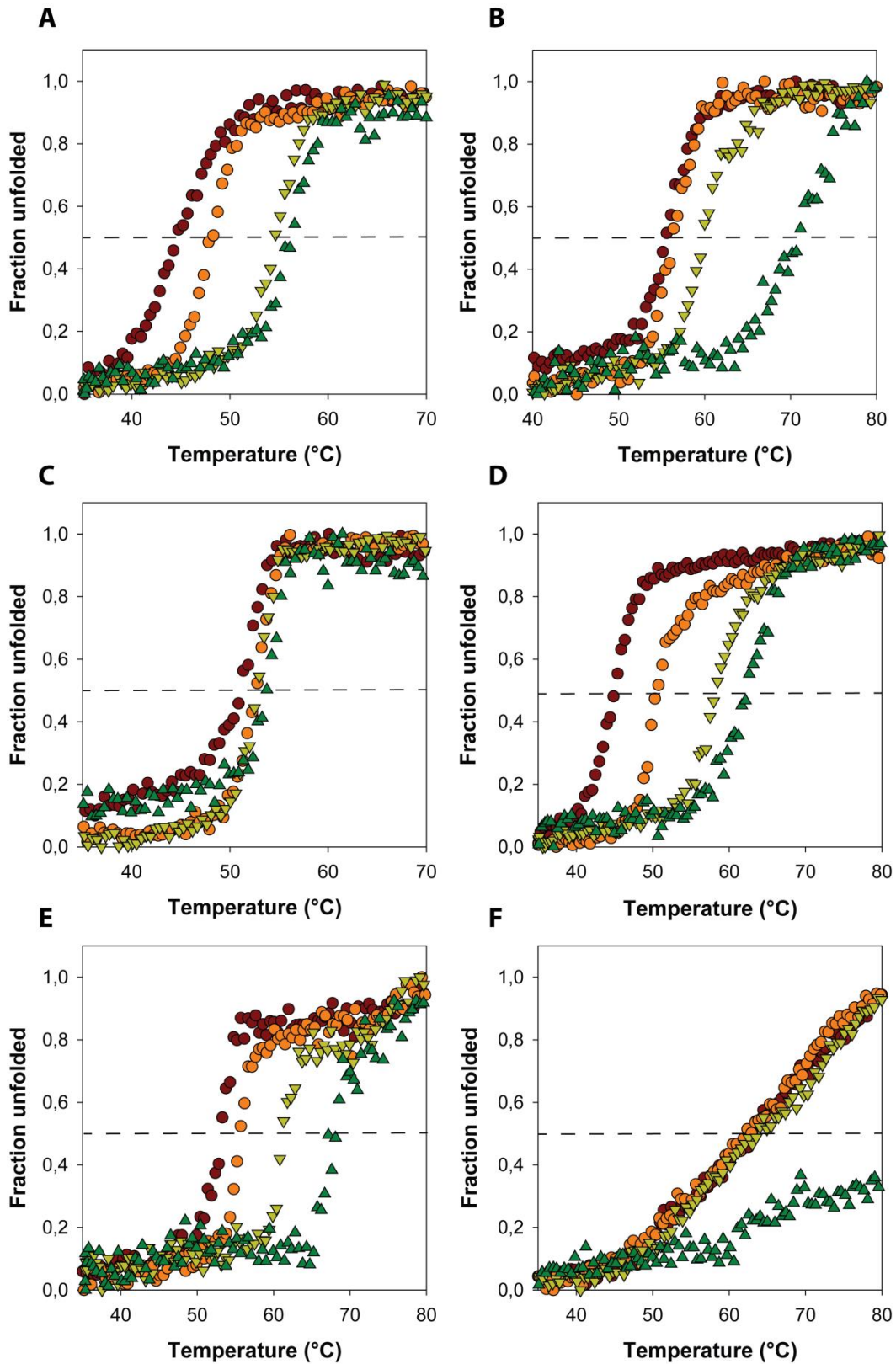


Figure 4.3: Heat-induced protein melting curves for (A) *EcCoaB*, (B) *SpCoaB*, (C) *HsCoaB**, (D) *EcCoaBC*, (E) *MtCoaBC* and (F) *SaCoaBC*. The four curves in each graph represent from left to right: the free protein (●); protein with MgCTP (○); protein with MgCTP and PPan (3) (▽); and protein with MgCTP and PCJ (4) (▲). The curves were determined by following changes in the protein's secondary structure by circular dichroism. *For *HsCoaB* MgATP was used instead of MgCTP since eukaryotic PPCS enzymes have a different substrate specificity than the bacterial versions.

Table 4.1: Summary of the change in melting temperature (ΔT_m) upon addition of either substrate (*PPan*+CTP) or inhibitor (*PCJ*+CTP) to the apo CoaB and CoaBC proteins, as well as the difference between these ($\Delta\Delta T_m$).

PPCS enzyme	Oligomeric state	ΔT_m substrate (°C)	ΔT_m inhibitor (°C)	$\Delta\Delta T_m$ (°C)
<i>EcCoaB</i>	dimer	10.0 ± 0.1	11.4 ± 0.1	1.4 ± 0.2
<i>SpCoaB</i>	dimer	3.8 ± 0.1	16.1 ± 0.8	12.3 ± 0.9
<i>HsCoaB</i>	dimer	1.2 ± 0.1	2.3 ± 0.1	1.1 ± 0.2
<i>EcCoaBC</i>	dodecamer	12.7 ± 0.1	16.9 ± 0.2	4.2 ± 0.3
<i>MtCoaBC</i>	dodecamer	8.0 ± 0.1	15.3 ± 3	7.3 ± 3.1
<i>SaCoaBC</i>	dodecamer	~1	~20	~19

4.2.2.2 Determination of kinetic parameters of CoaB and CoaBC enzymes

The determination of inhibition constants for each protein required that their kinetic parameters (especially K_m) be determined first, since this value is used in the calculation of the inhibition constant of tight-binding inhibitors. PPCS activity was assayed using the pyrophosphate reagent from Sigma-Aldrich that couples the production of pyrophosphate (the product of the first step of the PPCS reaction, see Figure 4.1) to the consumption of NADH, which was followed spectrophotometrically at 340 nm [20]. The initial rates were calculated for each substrate concentration and fitted to the Michaelis-Menten equation (Equation 4.1) for *SaCoaBC*, *MtCoaBC* and *HsCoaB*; interestingly, *EcCoaB*, *EcCoaBC* and *SpCoaB* showed substrate inhibition at high *PPan* concentrations, so in their case the Michaelis-Menten equation that compensates for substrate inhibition (Equation 4.2) was used instead. The results are shown in Figure 4.4 and the kinetic parameters are summarised in Table 4.2.

$$v = \frac{V_{max}[S]}{K_m + [S]} \dots\dots\dots 4.1$$

$$v = \frac{V_{max}}{1 + \frac{K_m}{[S]} + \frac{[S]}{K_i}} \dots\dots\dots 4.2$$

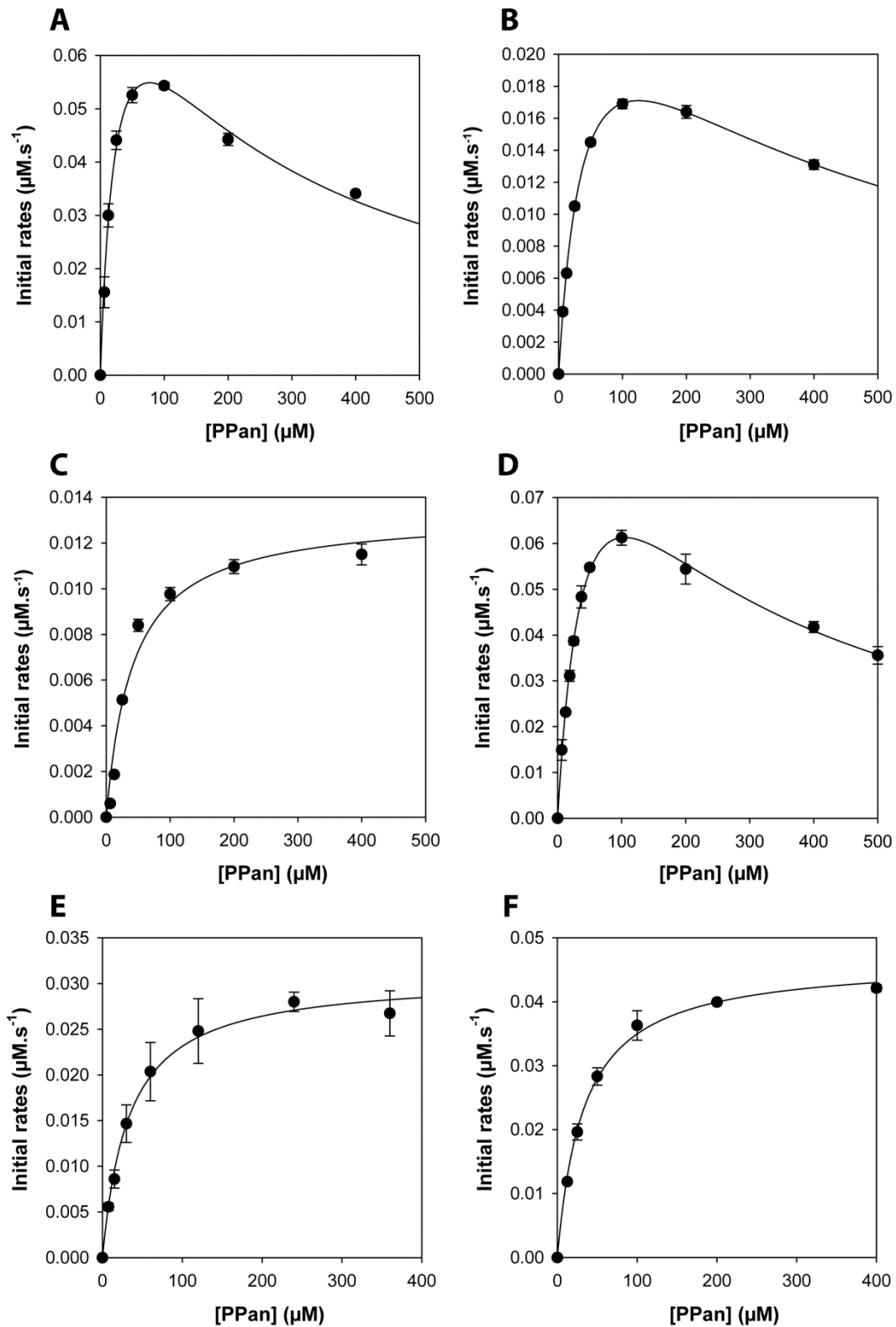


Figure 4.4: Michaelis-Menten plots of (A) *EcCoaB*, (B) *SpCoaB*, (C) *HsCoaB*, (D) *EcCoaBC*, (E) *MtCoaBC* and (F) *SaCoaBC* at 1 mM CTP (ATP for *HsCoaB*) with varying concentrations of *PPan* (3). Initial rates were determined in triplicate at each *PPan* concentration and the error bars indicate the standard deviation between the triplicate values.

Table 4.2: Kinetic parameters of PPCS enzymes. The errors indicate the standard error of the fit to calculate the inhibition parameters (K_m , V_{max} and K_i) from the triplicate values.

PPCS enzyme	[E] (nM)	K_m (μM)	V_{max} ($\text{nM}\cdot\text{s}^{-1}$)	k_{cat} (s^{-1})	k_{cat}/K_m ($\text{s}^{-1}\cdot\text{nM}^{-1}$)	K_i^* (μM)
<i>EcCoaBC</i>	32.8	48.0 \pm 4.7	117.5 \pm 7.1	3.6	75.0	228.3 \pm 27.2
<i>SaCoaBC</i>	25.5	33.2 \pm 1.8	46.6 \pm 0.7	1.8	55.0	<i>n/a</i>
<i>MtCoaBC</i>	38.3	33.2 \pm 4.2	30.8 \pm 1.1	0.80	24.2	<i>n/a</i>
<i>EcCoaB</i>	20.0	25.8 \pm 2.5	91.7 \pm 4.7	4.6	177.7	229.9 \pm 25.5
<i>SpCoaB</i>	10.0	41.9 \pm 1.8	28.6 \pm 0.7	2.9	68.0	372.3 \pm 21.1
<i>HsCoaB</i>	100.0	41.5 \pm 5.2	13.3 \pm 0.5	0.13	3.2	<i>n/a</i>

* K_i for the substrate inhibition by *PPan* in the case of the enzymes for which this was observed.

It should be noted that both the lack of T_m -shift as well as low the levels of activity observed for *HsCoaB* appeared to indicate a lack of proper protein folding. However, the protein was expressed under the same conditions that were used to determine its crystal structure [10] and as such; we consider it an unlikely possibility.

4.2.2.3 K_i determination of PCJ-CMP for each CoaB and CoaBC enzyme

Next, the K_i of PCJ-CMP was determined for each enzyme. PPCS activity was assayed exactly the same as above and, for each enzyme, the fractional activity (v_i/v_0) in the presence of increasing inhibitor concentrations was obtained with the use of progress curves (Figures 4.5-4.10). The first studies on the inhibition of *SaCoaBC* by PCJ-CMP showed it to act as a tight-binding inhibitor. A defining feature of tight-binding inhibitors is the variation of the IC_{50} value observed in relation to the total enzyme concentration at a fixed substrate concentration, as such inhibitors generally interact with their enzymes in nearly stoichiometric fashion [21]. To determine if this was also the case for the other proteins, the assays were performed at two separate enzyme concentrations for additional confirmation of tight-binding inhibition.

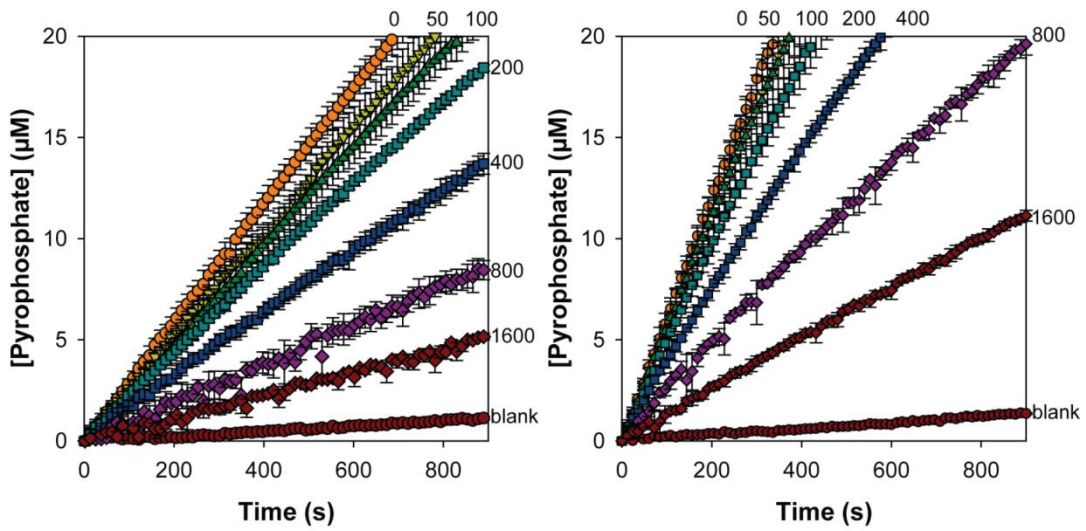


Figure 4.5: Progress curve analysis for the inhibition of *EcCoaBC* (left: 16.4 nM, right: 24.6 nM) in the presence of increasing concentrations of *PCJ*, indicated in nM next to each curve. Reaction rates were determined in triplicate at each *PCJ* concentration and the error bars indicate the standard deviation between the triplicate values.

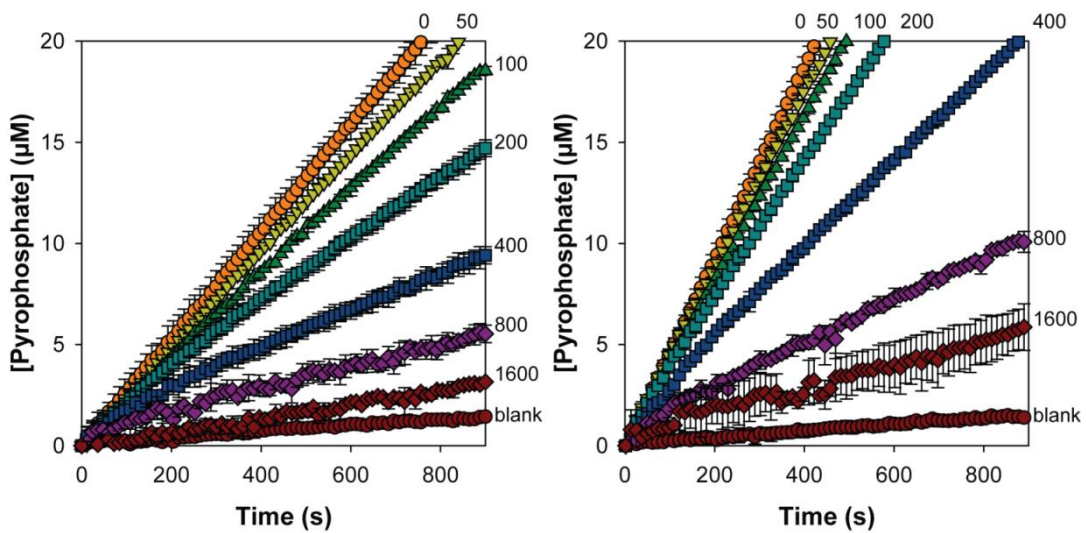


Figure 4.6: Progress curve analysis for the inhibition of *SaCoaBC* (left: 12.8 nM, right: 25.5 nM) in the presence of increasing concentrations of *PCJ*, indicated in nM next to each curve. Reaction rates were determined in triplicate at each *PCJ* concentration and the error bars indicate the standard deviation between the triplicate values.

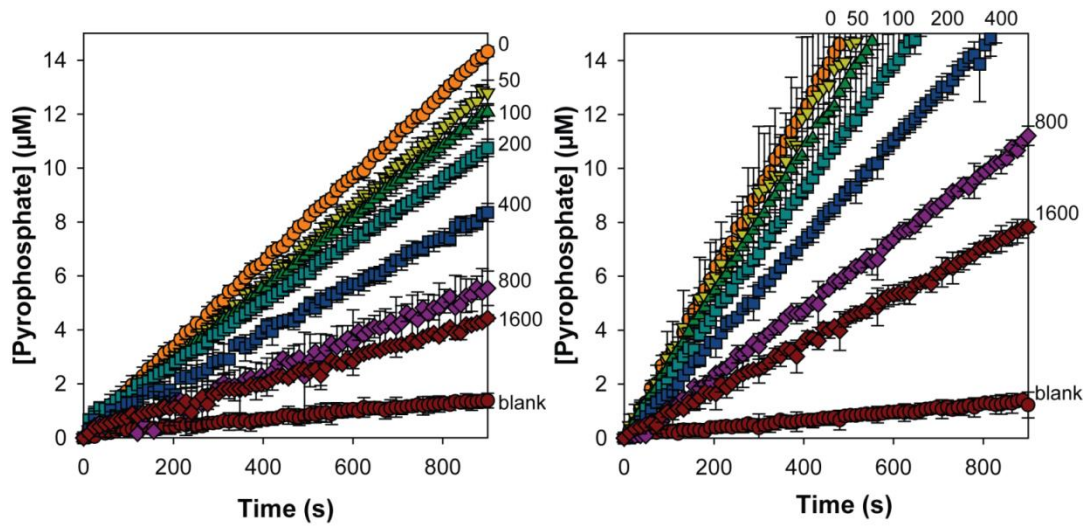


Figure 4.7: Progress curve analysis for the inhibition of *MiCoaBC* (left: 9.6 nM, right: 19.1 nM) in the presence of increasing concentrations of *PCJ*, indicated in nM next to each curve. Reaction rates were determined in triplicate at each *PCJ* concentration and the error bars indicate the standard deviation between the triplicate values.

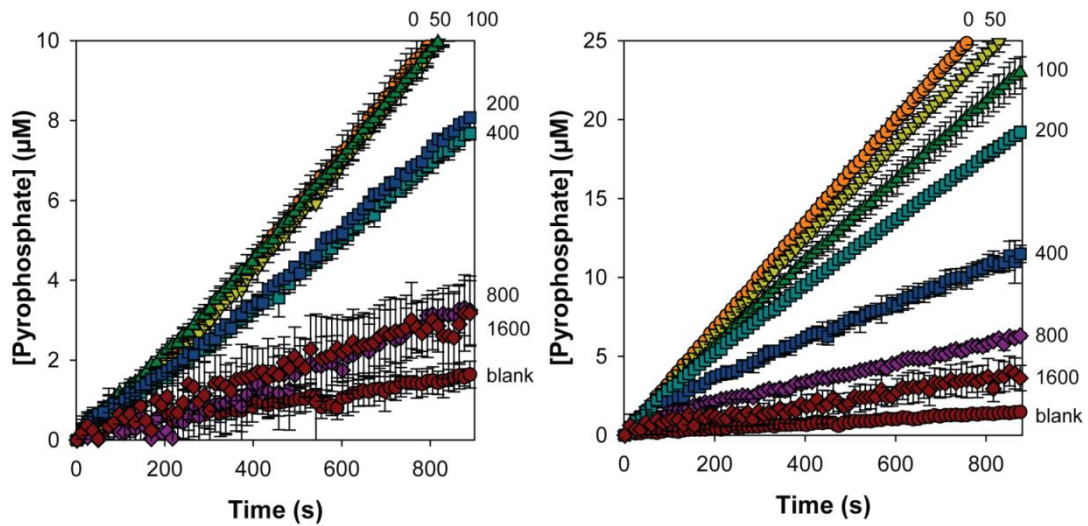


Figure 4.8: Progress curve analysis for the inhibition of *EcCoaB* (left: 15 nM, right: 30 nM) in the presence of increasing concentrations of *PCJ*, indicated in nM next to each curve. Reaction rates were determined in triplicate at each *PCJ* concentration and the error bars indicate the standard deviation between the triplicate values.

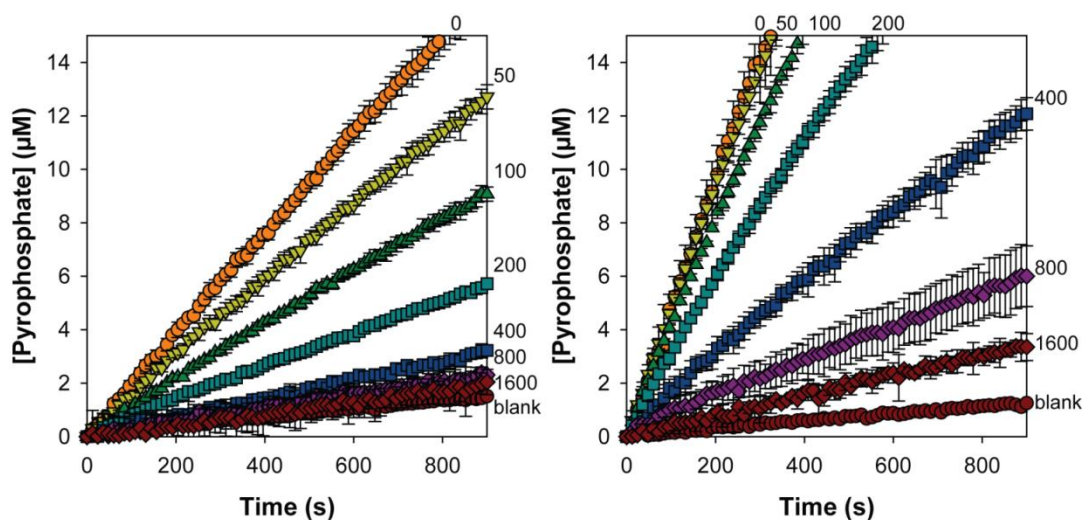


Figure 4.9: Progress curve analysis for the inhibition of *SpCoaB* (left: 10 nM, right: 15 nM) in the presence of increasing concentrations of *PCJ*, indicated in nM next to each curve. Reaction rates were determined in triplicate at each *PCJ* concentration and the error bars indicate the standard deviation between the triplicate values.

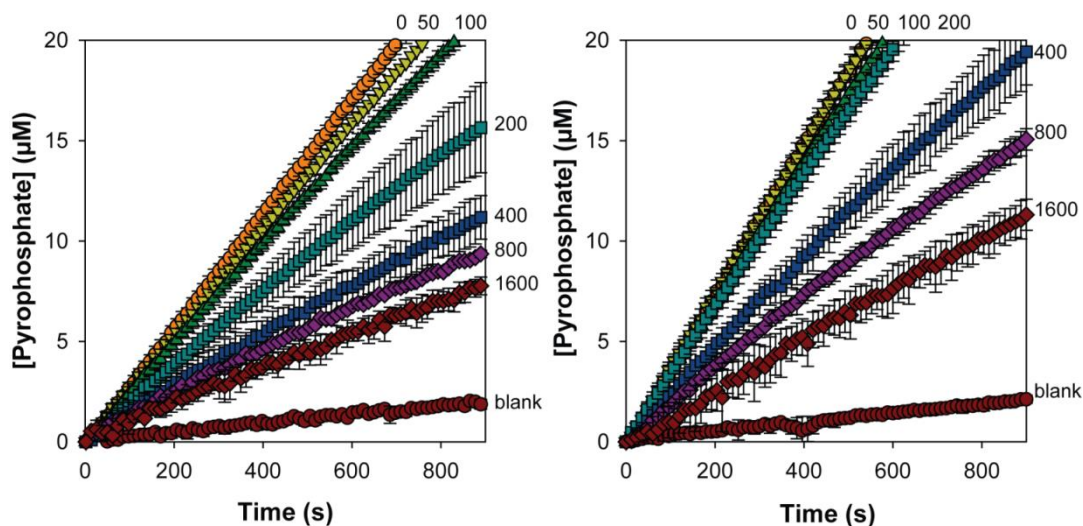


Figure 4.10: Progress curve analysis for the inhibition of *HsCoaB* (left: 150 nM, right: 200 nM) in the presence of increasing concentrations of *PCJ*, indicated in nM next to each curve. Reaction rates were determined in triplicate at each *PCJ* concentration and the error bars indicate the standard deviation between the triplicate values.

From the progress curves presented in Figures 4.5-4.10 the fractional activity at each inhibitor concentration was calculated by linear regression; these values were then plotted against the inhibitor concentration for both enzyme concentrations tested for each protein, generating two plots in each case (Figure 4.11). The fractional activity and inhibitor concentrations were subsequently used to calculate the value of K_i^{app} by fitting the Morrison equation for tight-binding inhibitors (Equation 4.3) to the data. This K_i^{app} was then converted to K_i using the Cheng-Prusoff equation appropriate for competitive inhibitors (Equation 4.4) and the appropriate K_m value (Table 4.2). This was done for both enzyme concentrations tested for each protein, generating a curve for each plot (Figure 4.11).

$$\frac{v_i}{v_0} = 1 - \frac{([E]+[I]+K_i^{app}) - \sqrt{([E]+[I]+K_i^{app})^2 - 4[E][I]}}{2[E]} \dots\dots\dots 4.3$$

$$K_i^{app} = K_i \left(1 + \frac{[S]}{K_m} \right) \dots\dots\dots 4.4$$

These plots made it possible to evaluate the effect of enzyme concentration on IC_{50} to confirm the tight-binding nature of the inhibition. The IC_{50} is indicated by the intersection between the Morrison plot and the dashed line, and clearly shows that the higher enzyme concentration gave a higher IC_{50} -value for all the proteins tested, as expected for tight-binding inhibitors [21]. However, analysis of the fitted curves indicates that the Morrison equation does not describe the observed inhibition profile as well in all cases (errors ~20% of the calculated K_i), pointing to these proteins not having a stoichiometric interaction between inhibitor and protein as would be expected from a tight-binding inhibitor. When the same data obtained for these cases were analysed using equations describing a standard reversible mechanism instead, the obtained fits were worse in all cases. Consequently, we decided to determine the K_i -values in all cases using the Morrison and Cheng-Prusoff equations as described above, although it appears as if PCJ-CMP has more tight-binding character against some PPCS enzymes than others. Performing the analysis in this consistent manner also allowed relative effects to be determined, an important aspect in this study. The K_i -value indicated in each plot is the one obtained from the analysis that gave the smallest error of the fit. Using this methodology we found the K_i of PCJ-CMP with SaCoaBC to be about twice as high as previously reported (27 nM vs 13 nM) [3]. However, such a difference can be reasonably attributed to error and variation in the samples.

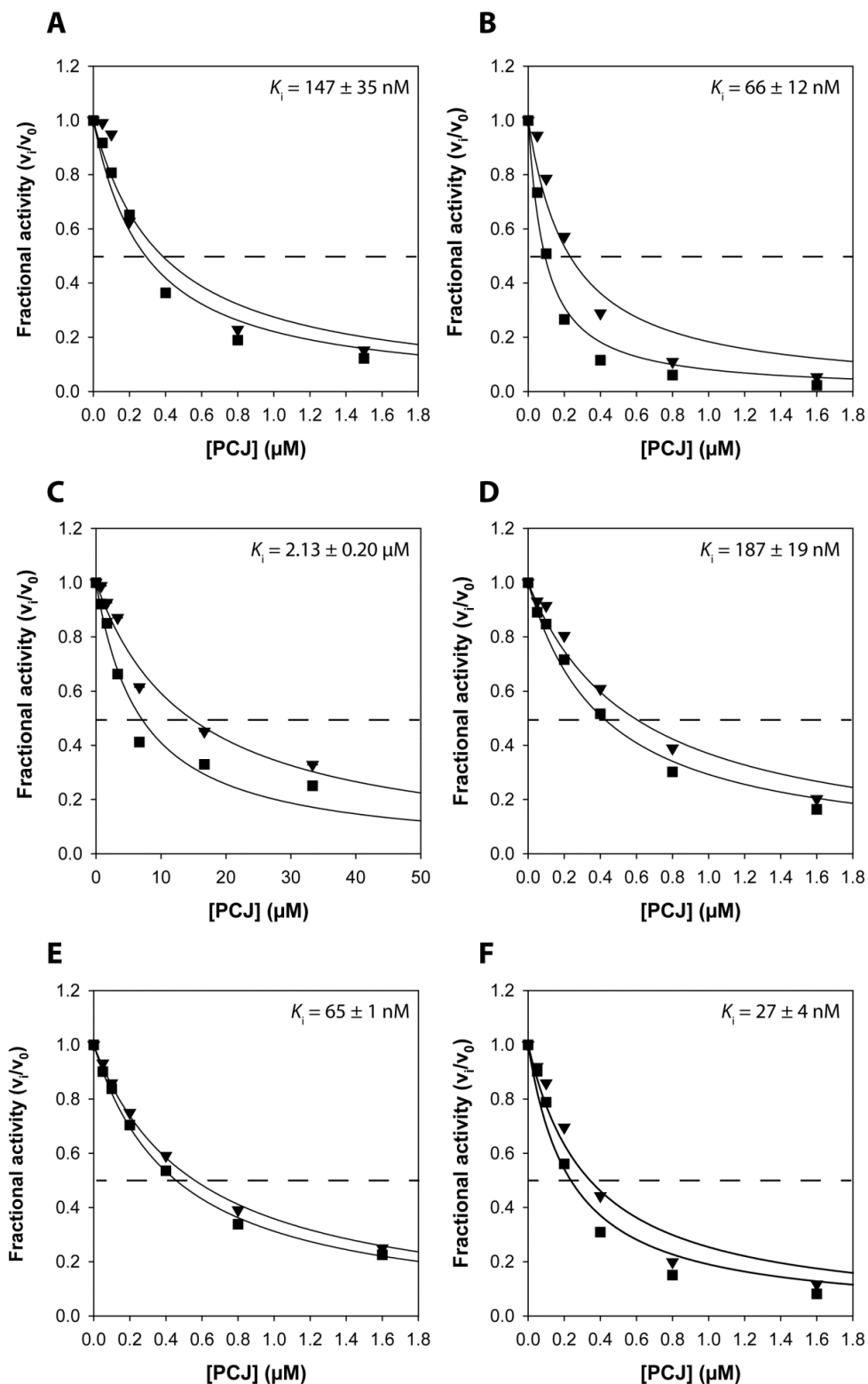


Figure 4.11: The fractional activity of (A) *EcCoaB*, (B) *SpCoaB*, (C) *HsCoaB*, (D) *EcCoaBC*, (E) *MtCoaBC* and (F) *SaCoaBC* at each tested enzyme concentration plotted against inhibitor concentration. The enzyme concentrations are the same as shown in figures 4.5 – 4.10 (\blacktriangledown indicates the higher concentration and \blacksquare denotes the lower enzyme concentration). In each case, the indicated K_i value was determined by fitting the data to the Morrison and Cheng-Prusoff equations for the enzyme concentrations of 15 nM for *EcCoaB*, 15 nM for *SpCoaB*, 150 nM for *HsCoaB*, 25 nM for *EcCoaBC*, 19 nM for *MtCoaBC* and 13 nM for *SaCoaBC*.

4.2.2.4 Comparison between the extent of structure stabilisation and the potency of inhibition

To establish if the correlation between the extent of structure stabilisation (as measured by the increase in T_m) and the potency of inhibition (as embodied in the K_i -values) shows any difference between the dimeric PPCS and the dodecameric CoaBC proteins, the difference in the T_m -values determined in the presence of substrate and inhibitor ($\Delta\Delta T_m$) (Table 4.1) was plotted against the K_i -value obtained in each case (Figure 4.11). The plot obtained in this manner (Figure 4.12) shows that with the exception of *HsCoaB* (the only protein tested that uses ATP and not CTP for the carboxylate activation step), a good correlation exists between the $\Delta\Delta T_m$ and K_i -values ($R^2 = 0.70$), regardless if the protein is a dimeric PPCS or dodecameric CoaBC. This suggests that the protein's oligomeric state plays no role in inhibition, and that the potency of inhibition is only dependent on the nature of the protein itself. Curiously, *EcCoaBC* shows a higher K_i than is expected from a linear trendline; the basis for this is unclear, but it does suggest that this protein might be a poor model for the inhibition of CoaBC enzymes in general. Removing it from the dataset improves the linear correlation ($R^2 = 0.85$) for the remaining data points.

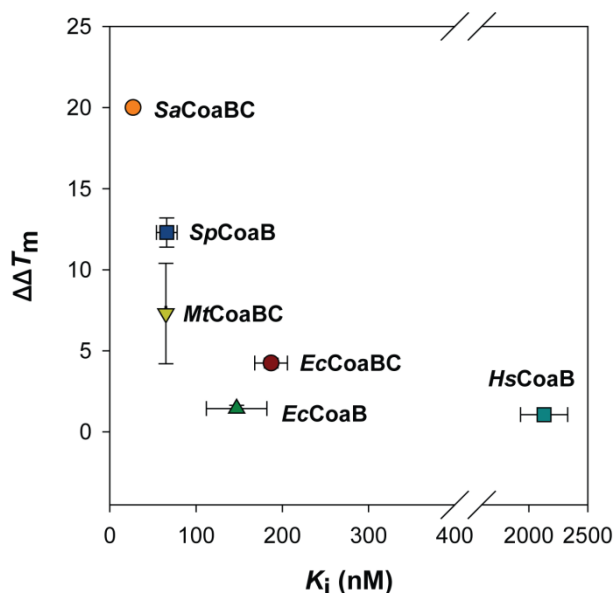


Figure 4.12: Correlation between the extent of structure stabilisation and the potency of inhibition. The difference in the T_m -values determined in the presence of substrate and inhibitor ($\Delta\Delta T_m$) is plotted against the K_i determined for each enzyme. The x-axis error bars indicate the error of the fit for the Morrison equation to calculate the K_i -values and the y-axis error bars indicate the propagated error from the combination of ΔT_m of the substrate and ΔT_m of the inhibitor. Where error bars are not visible they are smaller than the symbols.

4.2.3 Inhibitor stability based on the inherent electronic properties of the molecule

After we established that the basis for inhibition of PPCS by PCJ-CMP is not due to differences in binding mode or to oligomer-dependent stabilisation effects, we shifted our focus to the inherent chemical stability of the molecule itself. As mentioned above, PCJ-CMP is a close structural analogue of the native PPCS substrate, PPan-CMP, with the only difference being the introduction of a double bond in its β -alanine moiety. We hypothesized that this change allows for the introduction of new, stable resonance forms that consequently makes the acyl phosphate of PCJ-CMP more resistant to nucleophilic attack (Figure 4.13). To

test such a hypothesis would require the direct comparative analysis of the hydrolytic stability of pure *PPan*-CMP and *PCJ*-CMP under identical conditions. However, considering the structural complexity of these molecules and the significant synthetic effort that would be required to prepare them (and the additional concern that especially *PPan*-CMP would hydrolyse too fast to allow analysis); we decided to instead use a model system to evaluate the relative chemical stability of the *N*-acyl vinylogous carbamate functionality. We additionally predicted that such a model system would likely give more reproducible results, which would also be more generally applicable to other compounds containing β -amino acid moieties.

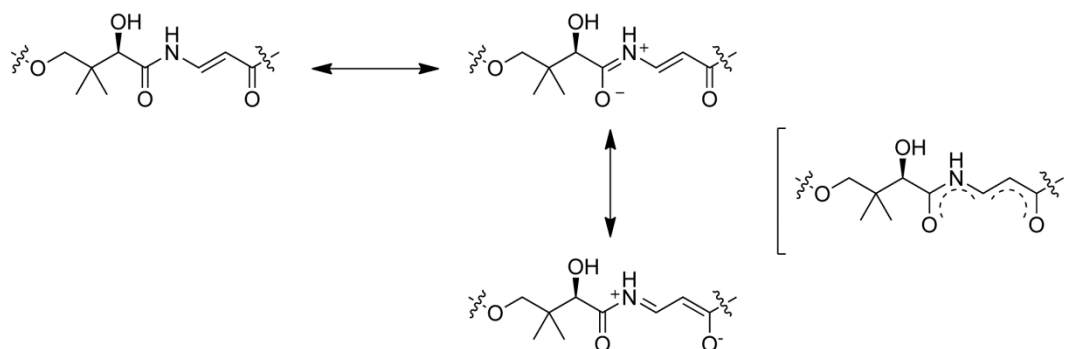


Figure 4.13: Resonance forms of the *N*-acyl vinylogous carbamate functionality illustrating the potential basis of its chemical stability.

For the proposed analysis we designed and synthesised model compounds 4-MU-3-benzamido-propanoate (**7a**) and 4-MU-3-benzamido-acrylate (**7b**) (Figure 4.14A) to represent *PPan*-CMP and *PCJ*-CMP respectively. In these models, the 4'-phosphopantoyl moiety of the two compounds were replaced by a benzoyl group, while the acyl phosphate was replaced by an ester. The benzoyl exchange was chosen to improve the synthetic tractability of the molecules, while the use of an ester instead of an acyl phosphate improved the initial hydrolytic stability of the system to give a bigger dynamic range for analysis. The ester group 4-methyl-umbelliferone (4-MU) was used, since free 4-MU is highly fluorescent, allowing a direct method to detect hydrolysis of the esters. We analysed both compounds by stopped-flow fluorescent spectroscopy and determined their initial rates of hydrolysis (within 60 s of initiating the reaction) using the progress curve method at different buffered pH values. Both **7a** and **7b** were found to be highly stable under low pH conditions (pH 2-8) and did not show any quantifiable hydrolysis for up to 10 h under these conditions (Figure S1). However, at pH 8.5 and above, both compounds showed hydrolysis within a 60 s timeframe, with the β -alanine ester **7a** being significantly more reactive rate than the acrylate **7b** (Figure 4.14B). These results provided compelling evidence that the introduction of a double bond to the β -alanine moiety increases the resistance of the acyl group to nucleophilic attack, most likely due to resonance effects.

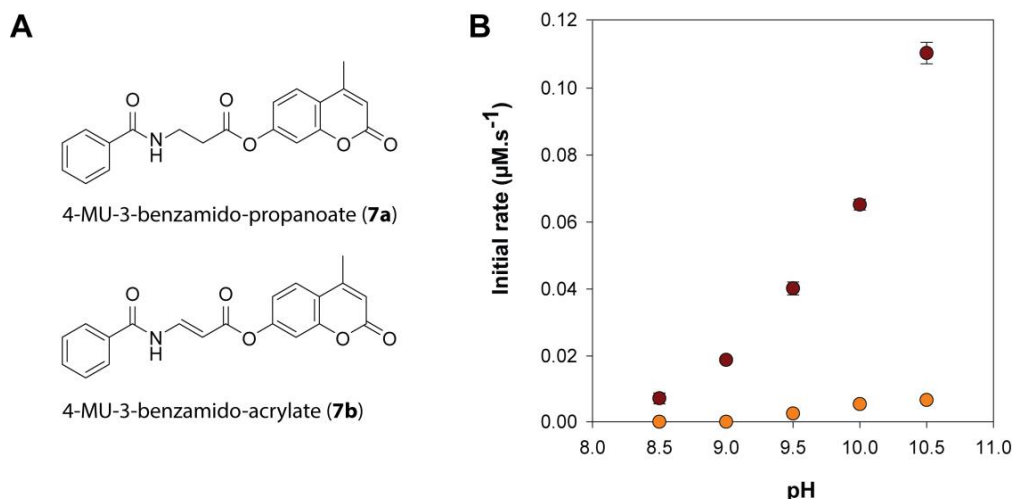


Figure 4.14: (A) Structures of the fluorescent model system compounds: 4-MU-3-benzamido-propanoate (**7a**) and 4-MU-3-benzamido-acrylate (**7b**). (B) The initial rates of hydrolysis of **7a** (●) and **7b** (●) between pH 8.5 – 11. The error bars show the standard deviation between triplicate readings. Some of the bars are not visible behind the symbols.

4.2.4 Application of the findings to an unrelated system: hydrolytic stability of modified pantetheinase (Vanin) substrates

To establish if this mechanism of apparent stabilisation *via* resonance could be applied to other systems for the design of small molecule enzyme inhibitors, the human vanin-1 enzyme (VNN1, pantetheinase) was chosen as test case. The Vanin pantetheinases belong to the nitrilase superfamily, and contain a conserved Glu-Lys-Cys catalytic triad that is responsible for covalent catalysis in the hydrolysis of pantetheine (PantSH) to produce pantothenic acid and cysteamine [22]. The key catalytic step is the nucleophilic attack by the conserved cysteine of the triad on the pantothenoyl amide of its substrate [23]. Mechanistically, the hydrolysis of PantSH by the Vanin pantetheinases is therefore equivalent to the acyl transfer step in the PPCS reaction mechanism, since in both systems the key reaction is nucleophilic attack at the equivalent carbonyl carbon. Importantly, the human VNN1 enzyme has been shown to also use other amide analogues of pantothenic acid (pantothenamides) as substrates [24, 25]. We took advantage of this substrate promiscuity and synthesised *N*-pentyl pantothenamide (N5-Pan, **8a**), *N*-benzyl pantothenamide (Bn-Pan, **8b**), *N*-pentyl-CJ (N5-CJ, **9a**) and *N*-benzyl-CJ (Bn-CJ, **9b**) (Figure 4.15) as potential VNN1 substrates. These structures were chosen to determine if the compounds containing double bonds (i.e. that have an *N*-acyl vinylogous carbamate functionality, namely N5-CJ and Bn-CJ) show increased resistance to pantetheinase-mediated hydrolysis compared to those (N5-Pan and Bn-Pan) having unmodified β -alanine moieties. This analysis required the development of two different assays as described separately below.

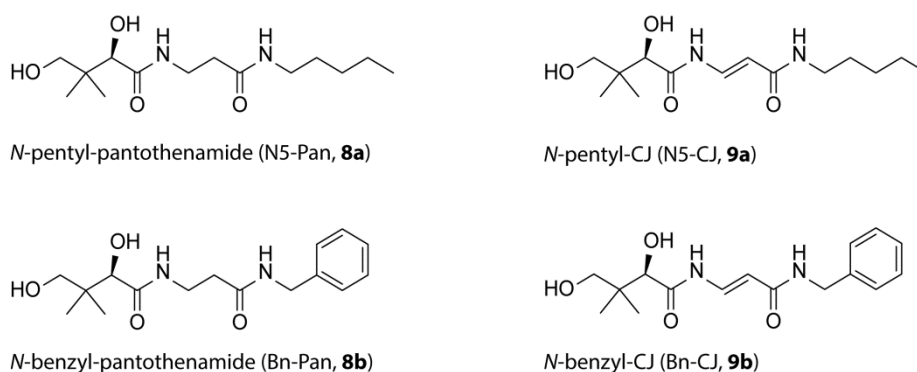


Figure 4.15: Structures of the compounds tested as substrates for VNN1 pantetheinase.

4.2.4.1 Characterisation of pantetheinase activity with alternative substrates: development of a discontinuous assay based on amine formation

In order to perform the stability analyses of our pantetheinase test system, we needed the appropriate assay conditions. First, the pantetheinase-mediated hydrolysis of the test compounds was assayed using fluorescamine derivatisation of the amine-containing reaction products. Fluorescamine is known to readily react with primary amines to form a fluorescent product [24], which can then be detected by fluorimetry. A discontinuous fluorescamine-based assay was developed by adapting an existing method described by Huang and Hernick [26]. After the reaction was initiated by adding enzyme to a substrate mixture, aliquots were removed from the reaction mixture (at the desired time-points) and quenched by the addition of *N*-ethylmaleimide. In the original protocol, the reaction is quenched by using acid precipitation of the enzyme, followed by removal of the precipitated protein *via* centrifugation. We decided to use *N*-ethylmaleimide instead, since it is a small compound that reacts with sulfhydryl groups such as the catalytic cysteine of VNN1 to form stable, covalent thioethers [27]. This leads to rapid inactivation of the enzyme rapidly without the need for an additional centrifugation step. The quenched reaction mixtures are then derivatised with fluorescamine and the resulting fluorescence measured.

4.2.4.2 Characterisation of pantetheinase activity with pantetheine: development of continuous assay based on pantothenate formation

We also required a continuous assay better suited for the characterisation of pantetheinase activity of VNN1 with its natural substrate pantetheine in the presence of the alternative substrates. Therefore, a new enzyme-coupled assay for pantetheinase activity was developed using a type III PanK enzyme. This form of PanK phosphorylates only pantothenic acid (Pan) and not PantSH; this substrate selectivity therefore allows it to be used to discriminate between the substrate and product of the pantetheinase reaction (Figure 4.16). For the assay, the *Bacillus anthracis* PanK (*Ba*PanK) was used, and basing the conditions used by Rowan and co-workers for the activity characterisation of this enzyme [28]. Pantetheinase activity was subsequently characterised in the presence of sufficient amounts of *Ba*PanK so that the coupling reaction was not rate limiting. The reaction rate was determined indirectly by following the oxidation of NADH (produced by

coupling the ADP formed by *BaPanK* to the pyruvate kinase and lactate dehydrogenase reactions) spectrophotometrically at 340 nm.

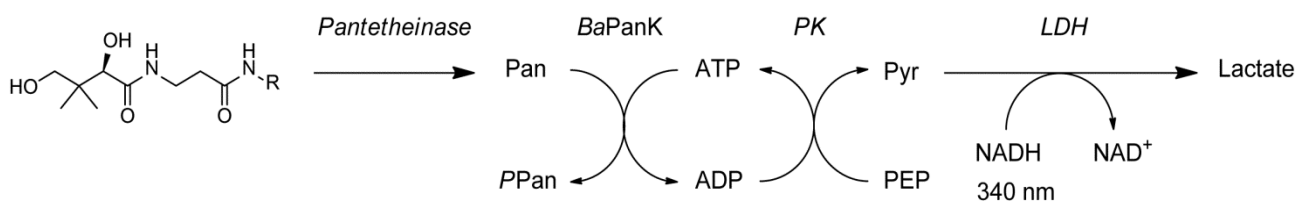


Figure 4.16: A schematic representation of the coupled assay to monitor pantetheinase activity. ATP = adenosine triphosphate, ADP = adenosine diphosphate, PK = pyruvate kinase, LDH = lactate dehydrogenase, PEP = phosphoenol pyruvate, Pyr = pyruvate.

4.2.4.3 Characterisation of *CJ*-amides as pantetheinase substrates (and inhibitors)

All the pantetheinase test compounds were tested with our fluorescamine assay at 20 μM , which is equal to the reported K_m of the native substrate, pantetheine for VNN1 [29]. The reactions for all the test compounds were followed to completion (approximately 2 hours). The results are summarised in Figure 4.17 and show that only N5-Pan and Bn-Pan were converted to product, while no activity was observed with N5-CJ and Bn-CJ.

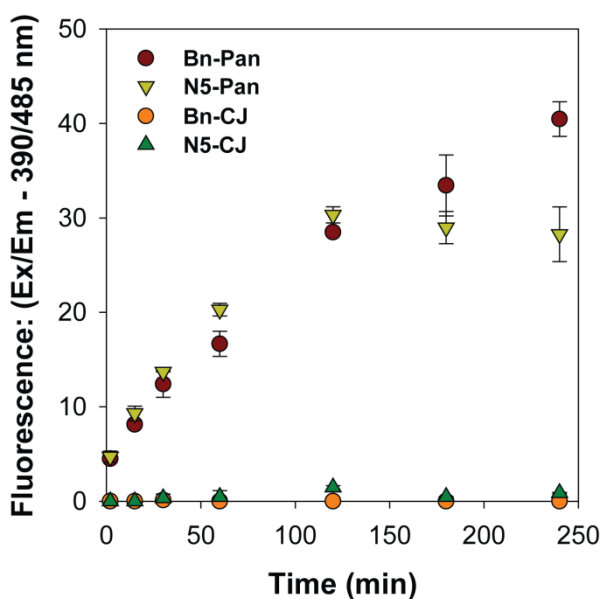


Figure 4.17: Time-course data of the pantetheinase-mediated hydrolysis of the various substrates using fluorescamine derivatisation of their products. *N*-benzyl pantothenamamide (●), *N*-pentyl pantothenamamide (▼), *N*-benzyl-CJ (○) and *N*-pentyl-CJ (▲).

These results suggested that the presence of the double bond in N5-CJ and Bn-CJ increased resistance to hydrolysis by pantetheinase as predicted by the results of the model system. However, one could argue that the restricted rotation introduced by the presence of the double bond prevents these compounds from entering the active site of the enzyme altogether. To demonstrate that this is not the case, we determined if

N5-CJ and Bn-CJ acted as competitive inhibitors of the pantetheinase reaction. First, we characterised the pantetheinase activity of VNN1 with PantSH using our continuous assay. Then we characterised the inhibition of VNN1 by N5-CJ at various concentrations (using the same PantSH concentration each time). The results confirmed that N5-CJ is indeed a competitive inhibitor of pantetheinase (Figure 4.18). This indicates that the lack of pantetheinase activity with the CJ-derived amides is due to their hydrolytic stability, and not to them being excluded from the enzyme.

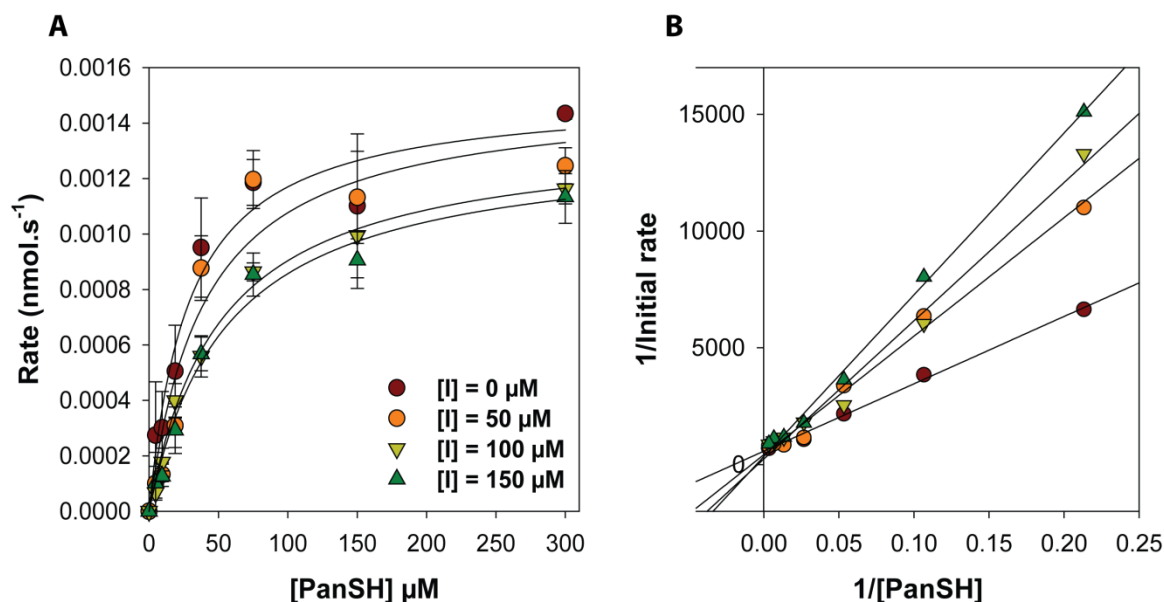


Figure 4.18: Inhibition of VNN1 pantetheinase by *N*-pentyl-CJ (N5-CJ). **(A)** Plots of initial rates of pantetheinase activity against the concentration (at K_m) of pantetheine at various fixed concentrations of N5-CJ. Kinetic parameters for the uninhibited reaction were determined by non-linear regression analysis: $V_{max} = 0.0015 \text{ nmol.s}^{-1}$, $K_m = 25.58 \text{ } \mu\text{M}$. These values correspond to those determined using a discontinuous assay [29]. **(B)** Lineweaver-Burke plot of the data in **A** illustrating competitive inhibition (increase in K_m) of VNN1 pantetheinase by N5-CJ with $K_i = 88.76 \text{ } \mu\text{M}$.

4.3 Discussion

In this study we set out to further investigate the mechanism of inhibition of PPCS enzymes by PCJ-CMP by examining the basis for the apparent stability of the inhibitor. First, we probed any differences between the binding mode of the inhibitor and that of the substrate, which might cause the activated acyl-phosphate in PCJ-CMP to be protected from nucleophilic attack. However, our molecular docking studies showed that the basis for inhibition by PCJ-CMP is not due to it having a different binding mode, or taking on a potentially unreactive conformation. Next, we investigated whether the potency of inhibition by PCJ-CMP is determined by the oligomeric structure of its target enzyme. Since proteins are stabilised upon the binding of a ligand, we searched for a correlation between increased stabilisation (beyond that which would normally be expected) and increased inhibitor potency among a small set of PPCS enzymes, consisting of three dimeric CoaB and three dodecameric CoaBC enzymes. However, when the extent of structure stabilisation (as measured by the increase in T_m) and the potency of inhibition of each enzyme were compared, we found no correlation to oligomeric structure. Interestingly, a good correlation exists between the $\Delta\Delta T_m$ and K_i -values of the prokaryotic enzymes, except for *EcCoaBC*, which shows a higher K_i than what is expected from a linear

trendline. The basis for this is unclear, but it does suggest that this protein might be a poor model for the inhibition of CoaBC enzymes in general. Ideally, more CoaB domains of bifunctional CoaBC enzymes need to be tested for comparison. In fact, since the current sample size is quite small, by including data from additional CoaB and CoaBC proteins more concrete conclusions might be made.

We also investigated if a specific characteristic innate to the structure of *PCJ*-CMP molecule endows it with increased stability compared to *PPan*-CMP, allowing it to act as a tight-binding inhibitor. The relative chemical stability of its *N*-acyl vinylogous carbamate functionality was evaluated by using a model system. The results provided compelling evidence that the introduction of a double bond to the β -alanine moiety increases the resistance of the acyl group to nucleophilic attack, most likely due to resonance effects. It should be noted that the result is not entirely surprising, since we expected that the delocalisation of electrons across the carbamate functionality will decrease the electrophilicity of its carbonyl carbon. This in turn decreases the vulnerability of the carbonyl carbon to nucleophilic attack and increases the resistance of the ester (in the model compound) and acyl phosphate (in *PCJ*-CMP) to acyl transfer. Additionally, the results reinforced that it is not the planar *N*-acyl functionality of *PCJ*-CMP imposing restrictions on the rotation of the molecule that prevents it from taking on the optimal binding pose required for attack by the cysteine, since these compounds displayed increased stability in solution where they may freely rotate. The stabilisation provided by a *trans*-enamine has previously been noted in the study of other antibiotics. Padayatti and co-workers inhibited the SHV-1 β -lactamase by forming a stable, long lived *trans*-enamine intermediate within the active site of the enzyme, which vastly lowered its deacylation efficiency [30]. We went further and applied this mechanism of stabilisation *via* resonance to an unrelated system for the design of small molecule enzyme inhibitors. The human vanin-1 enzyme (VNN1, pantetheinase) was chosen as test case. As before, test compounds were synthesised to evaluate the stability of the *N*-acyl vinylogous carbamate functionality compared to that of the β -alanine moiety as well as the compounds' concomitant resistance to hydrolysis (or lack thereof). All the test compounds were demonstrated to enter the VNN1 active site. The compounds with a double bond, which were consequently stabilised *via* new resonance forms, were shown to be successfully protected against hydrolysis as predicted.

Taken together, our results show that the PPCS protein itself does not provide the basis for the tight-binding mode of inhibition by *PCJ*-CMP, but that the introduction of the double bond in the β -alanine moiety of the substrate with its extra π -electrons renders the acyl phosphate resistant to nucleophilic attack by introducing new, stable resonance forms. This is similar to previous synthetase inhibitor design strategies in which stable intermediate analogues were prepared; however *PCJ*-CMP differs from these as it is generated *in situ*. This is a major advantage, since the inhibitor precursor, *CJ*, can pass through the bacterial cell envelope. It is then selectively activated by *S. aureus*' PanK to form *PCJ*, which is accepted into the active site of the target PPCS enzyme where it forms *PCJ*-CMP as a tight-binding, stable inhibitor. The results of this study have therefore allowed us to rationalise the basis for the tight-binding inhibition previously reported for *PCJ*-CMP. Additionally, our results also uncovered a new strategy whereby the structures of β -amino acid-containing compounds can be rendered stable to hydrolysis. This finding might also serve as a general starting point for the development of stable variants of inhibitors or therapeutics that contain β -amino acid moieties.

4.4 Materials and methods

Unless otherwise noted, all reagents and chemical compounds were purchased from commercial sources and used without further purification. Pyruvate Kinase was from Roche and Inorganic Pyrophosphatase was from Sigma. Dichloromethane (DCM) was distilled under nitrogen from calcium hydride. *N,N*-Dimethylformamide (DMF) was dried and purified by shaking up over potassium hydroxide followed by distillation under reduced pressure and a nitrogen atmosphere, and was stored over 3 Å molecular sieves. All column chromatography was performed using Merck silica gel 60 (particle size 0.040-0.063 mm) using combinations of hexane, ethyl acetate, DCM and methanol as eluants. Thin layer chromatography (TLC) was carried out on aluminium-backed Merck silica gel 60 F254 plates. Visualisation was performed with a UV lamp followed by spraying with a cerium ammonium molybdate or ninhydrin solution, followed by heating.

NMR analyses: All ^1H and ^{13}C nuclear magnetic resonance spectra were obtained using 300 MHz Varian VNMRs (75 MHz for ^{13}C), 400 MHz Varian Unity Inova (100 MHz for ^{13}C) or 600 MHz Varian Unity Inova (125 MHz for ^{13}C) instruments at the Central Analytical Facility (CAF) of the University of Stellenbosch. Chemical shifts (δ) were recorded using the residual solvent peak or an external reference. All chemical shifts are reported in ppm and all spectra were obtained at 25 °C. Proton spectral data are reported as follows: chemical shift, multiplicity (ovlp = overlapping, s = singlet, d = doublet, t = triplet, q = quartet, p = pentet, m = multiplet, br = broad), coupling constant in Hz, and integration.

Protein purification: All His-tagged protein purification was performed using HisTrapFF metal affinity purification columns on an ÄKTApurification system from GE Healthcare Life Sciences. The purified proteins were desalted using 5 mL HiTrap desalting columns.

Spectrophotometry: All absorbance readings in 96-well plates were measured using a Thermo Scientific Varioskan microplate spectrophotometer. All larger volume measurements were made in an Agilent Technologies Cary 60 UV-Vis Spectrometer using a 1 cm cuvette.

NMR analyses: All ^1H and ^{13}C nuclear magnetic resonance spectra (NMR) were obtained using 300 MHz Varian VNMRs (75 MHz for ^{13}C), 400 MHz Varian Unity Inova (100 MHz for ^{13}C) or 600 MHz Varian Unity Inova (125 MHz for ^{13}C) instruments at the Central Analytical Facility (CAF) of the University of Stellenbosch. Chemical shifts (δ) were recorded using the residual solvent peak or an external reference. All chemical shifts are reported in ppm and all spectra were obtained at 25 °C. Proton spectral data are reported as follows: chemical shift, multiplicity (ovlp = overlapping, s = singlet, d = doublet, t = triplet, q = quartet, p = pentet, m = multiplet, br = broad), coupling constant in Hz, and integration.

MS analyses: All high-resolution electrospray ionisation mass spectrometry analyses (HR-ESI-MS) were performed using a Waters Synapt G2 mass spectrometer.

Stopped-flow fluorimetry: All measurements were taken on an Applied Photophysics Chirscan Plus circular dichroism spectrometer using a fluorescence detector and a stopped-flow injector. The total

fluorescence was measured with a long pass cut-off filter installed that blocked all fluorescence below 385 nm. A sample cell pathlength of 2 mm and monochromator bandwidth of 4 nm was used.

4.4.1 Overexpression and purification of PPCS enzymes

The phosphopantothienoyl cysteine synthetase (PPCS) enzymes of *Staphylococcus aureus* (SaCoaBC), *Escherichia coli* (EcCoaBC and EcCoaB), *Streptococcus pneumonia* (SpCoaB) and *Homo sapien* (HsCoaB) were expressed and purified according to published methods using BL21-star (DE3) (Invitrogen) as expression strain [3, 7, 31, 32].

4.4.2 Overexpression and purification of His-MtCoaBC

The plasmid, pET-28a_MtcoaBC, was kindly provided by Michal Blaszczyk (from Prof. Tom Blundell's lab (Dept. of Biochemistry, University of Cambridge), which we transformed into *E. coli* BL21 Star (DE3) (Invitrogen) for expression. Expression was performed in Luria-Bertani broth supplemented with 30 mg/L kanamycin at 37 °C. Cultures were grown until OD₆₀₀ = 0.6, at which point the temperature was lowered to 20 °C before expression was induced by addition of 1 mM IPTG. Cell growth was continued overnight at 20 °C post-induction, after which the cells were harvested by centrifugation. The obtained cell pellet was suspended in sonication buffer (50 mM Tris-HCl, 0.5 M NaCl, 20 mM imidazole, 5% glycerol, pH 7.8; 10 mL/1 g cell paste) and subsequently sonicated to effect cell lysis. After centrifugation at 25 000 rpm for 20 min to collect cell debris, the crude extract (supernatant) was applied to a previously prepared 1 mL HisTrapFF metal affinity purification column (Amersham Biosciences) using an ÄKTAprime purification system. Weakly bound proteins were removed by washing with sonication buffer, followed by sonication buffer containing 75 mM imidazole. His-MtCoaBC was eluted by increasing the imidazole concentration to 500 mM. Elution was monitored at A₂₈₀. The purified protein was desalted with a 5 mL HiTrap desalting column (Amersham Biosciences) using a 50 mM Tris-HCl buffer at pH 8.0, containing 0.15 M NaCl, 0.5 mM TCEP and 5% glycerol. Afterwards, the protein was aliquoted and stored at -80 °C.

4.4.3 Protein Melting Temperature Determinations and Analysis

Protein melting curves were determined by measuring the change in circular dichroism (CD) at 220 nm as the temperature of protein samples were increased from 35 °C to 80 °C at a rate of 1 °C per minute. All measurements were made in an Applied Photophysics Chirascan-Plus CD Spectrometer using a 0.5 mm cuvette.

Determining PPCS temperature melting curves

Four separate samples were prepared of each protein, all of which contained 10 μM PPCS and 1.0 mM MgCl_2 in 50 mM Tris-HCl buffer (pH 7.6). The first sample contained no additional components, while the other three contained 150 μM CTP, 150 μM each of *PPan* and CTP, or 150 μM each of *PCJ* and CTP, respectively. The final volume of all samples was 240 μL . A sampling time of 0.5 s per point was employed. A temperature probe was used in the sample solutions and the preset instrument temperatures were replaced with temperatures measured each minute by the probe for higher accuracy. The T_m were subsequently determined by normalizing the melting curve data, and fitting the resulting curves simultaneously to Equations 4.5, 4.6 and 4.7 (the Gibbs-Helmholtz equation) using SigmaPlot 12.0 software (Systat Software), where lb and rb are the equations for the best linear fits to the left and right baselines of the curves respectively. The following parameter constraints were used for the curve fit: Van't Hoff enthalpy (ΔH_{vH}) > 0; T_m > 0 and ΔC_p > 0.

$$y = FF \times (lb - rb) + rb \dots\dots\dots 4.5$$

$$FF = \frac{1}{1 + \left(\frac{1}{e^{\left(\frac{\Delta G}{1.9872 \times T} \right)}} \right)} \dots\dots\dots 4.6$$

$$\Delta G = \Delta H_{\vartheta H} \left(1 - \frac{T}{T_m} \right) - \Delta C_p \left(T_m - T \ln \frac{T}{T_m} \right) \dots\dots\dots 4.7$$

Determining SaCoaBC temperature melting curves

The same procedure was used for all the PPCS enzymes; however, accurate T_m determinations of SaCoaBC were not possible since the protein was not fully denatured at the highest temperature that can be obtained in the spectrometer. The T_m -values were subsequently estimated by normalizing the melting curve data and determining the first derivatives of the curves.

4.4.4 PPCS Inhibition Assays and Data Analyses

PPCS assays were performed according to the published procedure [3]. The PPCS reaction was observed in the forward reaction *via* an enzyme-linked assay in which the pyrophosphate that is released during transfer of CMP from CTP to the substrate is continuously detected. This is achieved using the commercially available pyrophosphate reagent (PR) from Sigma-Aldrich (P7275). Each vial of PR was resuspended in 4.5

mL dH₂O. The assays were performed on a Thermo Scientific Varioskan microplate spectrophotometer at 37 °C. All curve fitting analyses were performed using SigmaPlot 12.0.

PPCS kinetic parameter determination (with PPan, 3)

A master assay mix containing 50 mM Tris–HCl buffer (pH 7.6), 2.5 mM MgCl₂, 20 mM KCl, 1.0 mM CTP, 1.0 mM L-Cys, 2.5 mM DTT, PPCS enzyme (at varying concentrations for each enzyme) and 60 µL PR was incubated at 37 °C for 15 min and added to a 96-well plate containing PPan (3) (12.5 µM to 500 µM) in different wells to give a final assay volume of 150 µL. All measurements were obtained in triplicate. Initial velocities were calculated for each substrate concentration and fitted to the Michaelis-Menten equation (Equation 4.1) for SaCoaBC, MtCoaBC and HsCoaB; or the Michaelis-Menten equation that compensates for substrate inhibition (Equation 4.2) for EcCoaB, EcCoaBC and SpCoaB using SigmaPlot 12.0. The results are shown in Figure 4.4 and the kinetic parameters are summarised in Table 4.2. The following enzyme concentrations were used: EcCoaBC 32.8 nM, SaCoaBC 25.5 nM, MtCoaBC 38.3 nM, EcCoaB 20.0 nM, SpCoaB 10.0 nM and HsCoaB 100.0nM.

$$v = \frac{V_{max}[S]}{K_m + [S]} \dots\dots\dots 4.1$$

$$v = \frac{V_{max}}{1 + \frac{K_m + [S]}{[S] + K_i}} \dots\dots\dots 4.2$$

4.4.5 Progress curve analysis

To ensure that substrate depletion would not significantly affect the reaction rate, a low enzyme concentration and high substrate concentration (PPan = 250 µM) were used ([21, 33]), which allowed the control experiment (without inhibitor) to proceed linearly over ~15 min. Such a procedure should allow any divergence from linearity, caused by slow onset or irreversible inhibition, to be clearly observable. However, the enzymes that are subject to substrate inhibition were assayed at 100 µM to prevent interference by high substrate concentrations.

Procedure

A master assay mix containing Tris–HCl buffer (50 mM, pH 7.6), MgCl₂ (2.5 mM), KCl (20 mM), CTP (1.0 mM), L-Cys (1.0 mM), DTT (2.5 mM), PPCS (at varying concentrations for each enzyme) and 60 µL PR was incubated at 37 °C for 15 min and added to separate wells of a 96-well plate containing a mixture of 4'-phosphopantothenic acid (100 or 250 µM) and PCJ (in concentrations ranging between 0.025 µM to 1.6 µM),

followed by determination of the activity over a 15 min period. All measurements were obtained in triplicate and the results are shown in Figures 4.5-4.10.

Data analysis

From the progress curves presented in Figures 4.5-4.10 the fractional activity at each inhibitor concentration was calculated by linear regression. The fractional activity and inhibitor concentrations were used to calculate the value of K_i^{app} by fitting the data to the Morrison equation for tight binding inhibitors (Equation 4.3) using SigmaPlot 12.0. This K_i^{app} was then converted to K_i using the Cheng-Prusoff equation appropriate for competitive inhibitors (Equation 4.4) and the appropriate K_m value (Table 4.2). The plots of the Morrison equation for each enzyme are included in Figure 4.11. The K_i -values are included with the T_m -data in Table 4.2.

$$\frac{v_i}{v_0} = 1 - \frac{([E]+[I]+K_i^{app}) - \sqrt{([E]+[I]+K_i^{app})^2 - 4[E][I]}}{2[E]} \dots\dots\dots 4.3$$

$$K_i^{app} = K_i \left(1 + \frac{[S]}{K_m} \right) \dots\dots\dots 4.4$$

4.4.6 Stopped-flow fluorimetry

The measurements were taken on an Applied Photophysics Chirascan Plus circular dichroism spectrometer using a fluorescence detector and a stopped-flow injector. The total fluorescence was measured with a long pass cut-off filter installed that blocked all fluorescence below 385 nm, which could potentially interfere with the sample fluorescence. A sample cell pathlength of 2 mm and monochromator bandwidth of 4 nm was used. The fluorescence excitation wavelength was set to 375 nm and emission was detected by scanning at 440 nm. The stopped-flow sequencer used a manual external trigger for injection and 1000 data points were collected over 60 s.

4-MU standard curves

Separate standard curves were constructed for pH 8.50, pH 9.00, pH 9.50, pH 10.00 and pH 10.50. Glycine-NaOH buffers (50 mM) were made up to buffer the reaction mixtures at each pH-value. A stock solution of 4-MU in DMSO (50 mM) was diluted in water to make up standard solutions of 4-MU: 20 μ M, 10 μ M, and 5 μ M. Each 4-MU solution was injected together with each glycine buffer in triplicate and the resulting fluorescence was measured and used to construct standard curves. No significant differences were observed for 4-MU fluorescence between the various alkaline pH-values. Figure S1A shows the 4-MU standard curve at pH 9.

Fluorimetric analysis of model system compounds

Glycine-NaOH (50 mM) was used to buffer hydrolysis reactions at each pH-value. DMSO stocks of 4-MU-3-benzamido-propanoate (**7a**) and 4-MU-3-benzamido-acrylate (**7b**) were diluted to 200 μM in water. The reactants were loaded into the stopped-flow drive syringes: one with 200 μM 4-MU-amide and one with glycine buffer. Samples were pushed through the flow circuit without collecting data three times to prime the observation chamber. The detector was then calibrated according to the resulting fluorescent signal. Data were then acquired in triplicate with each glycine buffer (Figure S1B).

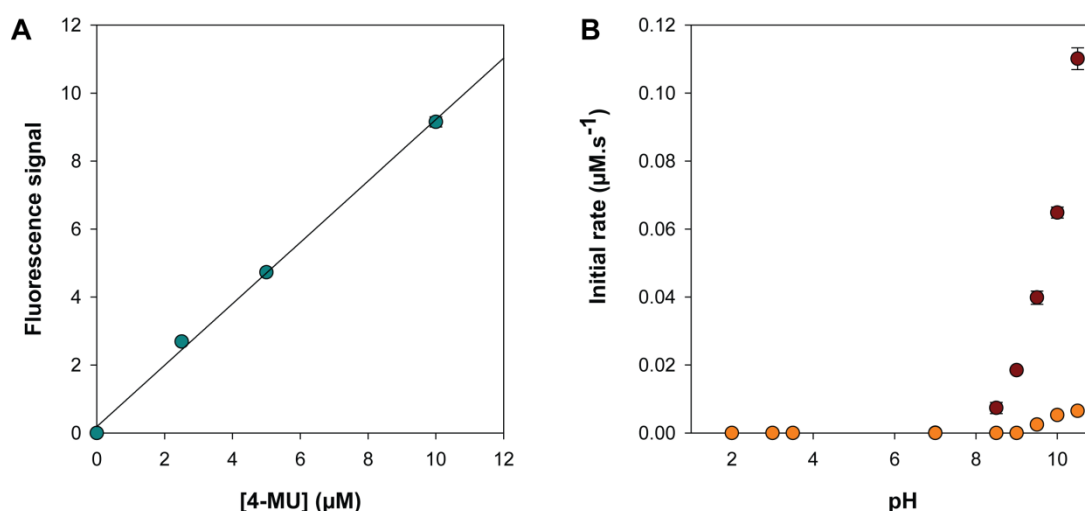


Figure S1: (A) Standard curve of 4-MU at pH 9. (B) pH rate profile of 4-MU-benzamido propanoate (**7a**, ●) and 4-MU-benzamido acrylate (**7b**, ○). The error bars in each figure show the standard deviation between triplicate readings. Some of the bars are not visible behind the symbols.

4.4.7 Fluorescamine assay of pantetheinase activity

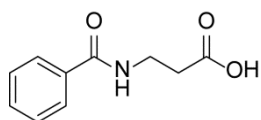
Assay mixtures containing DTT (0.5 mM), BSA (0.01 % (m/v)) and substrate (pantothenamide or CJ-amide, 20 μM) in phosphate buffer (100 mM, pH 7.6) were pre-equilibrated at 37 °C prior to the addition of vanin-1 (18.5 nM) to initiate the reaction. After various times, aliquots (30 μL) were removed from the reaction mixture and quenched by the addition of *N*-ethylmaleimide (10 μL , 1.5 μM). Aliquots of the quenched reaction mixture (25 μL) were transferred into a black 96-well plate, diluted with 1 M borate (pH 9.0, 75 μL), and reacted with fluorescamine (10 mM, 30 μL in CH_3CN). After 10 min the resulting fluorescence was measured (excitation at 395 nm, emission at 485 nm) using a Thermo Scientific Varioskan fluorescent plate reader.

4.4.8 Continuous enzyme coupled assay of pantetheinase activity

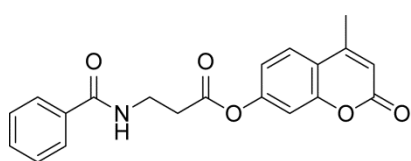
A master assay mix containing HEPES buffer (200 mM, pH 7.6), MgCl_2 (10 mM), NH_4Cl (60 mM), ATP (1 mM), NADH (0.5 mM), PEP (2 mM), PK (7.5 units), LDH (15 units), DTT (500 μM), BSA (50 $\mu\text{g}\cdot\text{mL}^{-1}$), *BaPanK* (44.44 $\mu\text{g}\cdot\text{mL}^{-1}$), and vanin-1 (25 nM) was incubated at 37 °C for 15 min and added to separate

wells of a 96-well plate containing PantSH (4.69 μM – 300 μM) and *N*-pentyl-CJ (0 μM – 50 μM). The reaction was monitored by following the decrease of NADH at 340 nm over a 40 min period at 37 °C. All measurements were obtained in triplicate.

4.4.9 Synthesis of model system compounds⁵



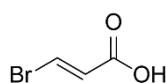
***N*-benzoyl- β -aminopropionic acid (S1):** Prepared according to previously published methods [34].



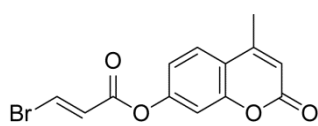
4-methyl-2-oxo-2H-chromen-7-yl 3-benzamido-propanoate (7a): S1

(4.04 mmol, 780 mg) was suspended in 10 mL anhydrous DCM at ambient temperature. 4-methyl-umbelliferone (4.04 mmol, 711.72 mg) and DMAP (0.0018 mmol, 2.24 mg) was added to the acid while stirring.

Next, pivalic anhydride (4.04 mmol, 752.45 mg, 819.66 μL) was added and the reaction mixture was stirred at 50 °C for 48 h. Subsequently, water (9 μL , 0.5 mmol) was added and the mixture was stirred at 50 °C for 1 h. The reaction mixture was then concentrated under vacuum and the product purified on a silica column by eluting with 1 % methanol in DCM. The solvent was removed under vacuum and freeze-dried to afford the product as a white powder (650 mg, 1.85 mmol). The yield was calculated as 45.8% ¹H NMR (600 MHz, DMSO): δ = 2.43 (s, 3H), 2.89 (t, J = 7.03 Hz, 2H), 3.65 (t, J = 7.03 Hz, 2H), 6.39 (s, 1H), 7.21 (d, J = 8.20 Hz, 1H), 7.29 (s, 1H), 7.45 – 7.55 (m, 3H), 7.81 – 7.87 (m, 3H), 8.71 (s, 1H). ¹³C NMR (125 MHz, DMSO): δ = 21.2, 37.2, 38.4, 113.2, 116.8, 120.5, 121.6, 129.9, 130.4, 131.7, 134.3, 137.3, 156.0, 156.5, 162.5, 169.6, 172.9. HRMS (m/z): $[\text{M}+\text{H}]^+$ calculated for $\text{C}_{20}\text{H}_{18}\text{NO}_5$, 352.1185; found 352.1191.



3-bromoacrylic acid (S2): Prepared using previously published methods [35, 36].



(*E/Z*)-4-methyl-2-oxo-2H-chromen-7-yl 3-bromoacrylate (S3.1): S2 (6.62

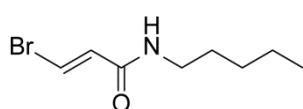
mmol, 1 g) was suspended in anhydrous DCM (10 mL) at ambient temperature. 7-Hydroxy-4-methylcoumarin (6.02 mmol, 1060.78 mg), 4-Dimethylaminopyridine (0.003 mmol, 4.05 mg) and pivalic anhydride (6.62 mmol, 1130.98 mg, 1232 μL) were added to the acid at ambient temperature. The mixture was then stirred at 50 °C for 48h. Water (9 μL , 0.5 mmol) was added and the reaction mixture was stirred for an additional hour at 50 °C. The solvent was removed under reduced pressure and the product purified on a silica column by eluting with 1 %

⁵ The compounds marked with * were previously synthesised by Renier van der Westhuyzen.

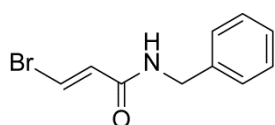
methanol/DCM. The solvent was removed under vacuum and freeze-dried to yield the product as a white powder (1.54 g, 4.98 mmol) The yield was calculated as 82.7%. ^1H NMR (400 MHz, DMSO): δ = 2.43 (s, 3H), 6.39 (s, 1H), 6.92 (d, J = 9.38 Hz, 1H), 7.23 (d, J = 8.59 Hz, 1H), 7.81 (d, J = 9.38, 1H), 8.18 (d, J = 13.28 Hz, 1H). ^{13}C NMR (100 MHz, DMSO): δ = 19.3, 111.2, 114.0, 115.1, 119.0, 119.5, 127.7, 128.7, 132.2, 154.0, 160.8, 162.9. HRMS (m/z): $[\text{M}+\text{H}]^+$ calculated for $\text{C}_{13}\text{H}_{10}\text{O}_4\text{Br}$, 308.9762; found 308.9765.

General procedure for the synthesis of β -bromoacrylamides

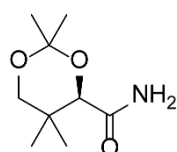
To an oven-dried two neck flask were added **S2** (1.00 g 6.62 mmol) and DMAP (0.162 g, 1.32 mmol). The amine (9.94 mmol) and DCM (13 mL) were then added to the flask using oven-dried syringes. The solution was cooled to 0 °C and DIC (1.13 mL, 7.29 mmol) was added drop-wise with a syringe. The reaction was warmed to rt and stirred for 6 h, after which it was filtered through Celite and concentrated under reduced pressure. After dilution with ethyl acetate, the organic layer was washed with saturated NaHCO_3 (2 x 10 mL), brine (1 x 10 mL) and the organic layer dried over Na_2SO_4 . After filtration and concentration in vacuo the amide was purified using flash chromatography.



***(E)-3-Bromo-N-pentylacrylamide (S3.2):** The acrylamide was prepared according to the general procedure using pentylamine (1.15 mL, 9.94 mmol). A pale yellow solid (0.34 g, 12%) was obtained after purification with flash chromatography (Hexane:EtOAc 8:2). ^1H NMR (300 MHz, CDCl_3): δ = 7.43 (d, J = 13.5 Hz, 1H), 6.46 (d, J = 13.1 Hz, 1H), 5.68 (br s, 1H), 3.34-3.26 (m, 2H), 1.53 (p, J = 14.1, 7.5 Hz, 2H), 1.38-1.28 (m, 4H), 0.90 (t, J = 7.0 Hz, 3H); ^{13}C NMR (CDCl_3 , 75.5 MHz): δ = 163.4, 130.9, 122.4, 39.7, 29.1, 29.0, 22.3, 13.9; HRMS-ESI: m/z $[\text{M}+\text{H}]^+$ calculated for $\text{C}_8\text{H}_{15}\text{BrNO}$: 220.0337; found: 220.0333.



***(E)-N-Benzyl-3-bromoacrylamide (S3.3):** The acrylamide was prepared according to the general procedure using benzylamine (0.982 mL, 9.94 mmol). A white solid (0.774 g, 47%) was obtained after purification with flash chromatography (Hexane:EtOAc 3:1). The ^1H NMR spectrum agreed with the published spectra [37]. ^1H NMR (CDCl_3 , 300MHz): δ = 7.50 (d, J = 13.4 Hz, 1H), 7.37-7.26 (m, 5H), 6.49 (d, J = 13.6 Hz, 1H), 5.85 (br s, 1H), 4.48 (d, J = 5.9 Hz, 2H).

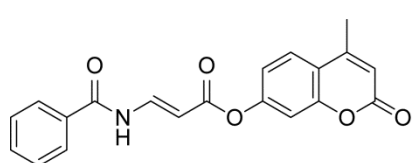


***2,2,5,5-Tetramethyl-[1,3]dioxane-4-carboxylic acid amide (S4):** The synthesis of **S4** was performed according to the literature procedure of Aquino *et al.* [38]. To an oven dried two-neck round bottom flask containing 2,4-dihydroxy-3,3-dimethyl-butylamide (1.58 g, 10.7 mmol) was added anhydrous acetone (27 mL) and DCM (27 mL). To this solution was added dimethoxypropane (2.10 mL, 21.4 mmol) and toluenesulfonic acid (*p*-TsOH) (0.204 g, 1.07 mmol). The resulting mixture was then stirred for 1h at ambient temperature followed by filtration and neutralized by

adding triethyl amine (0.30 mL). The resulting mixture was dried over Na₂SO₄. After filtration the solution was concentrated in vacuo and the amide purified using flash chromatography (Hex/EtOAc 2:1) to afford 4.2 as a yellow oil (1.24 g, 62%) which solidified on standing. The ¹H NMR spectrum agreed with the published spectra.¹⁰ ¹H NMR (DMSO–D₆, 400 MHz): δ = 7.10 (br s, 2H), 5.21 (d, *J* = 6.0 Hz, 1H), 4.47 (t, *J* = 5.5 Hz, 1H), 3.66 (d, *J* = 6.0 Hz, 1H), 3.30 (dd, *J* = 10.2, 5.5 Hz, 1H), 3.18 (dd, *J* = 10.4, 5.4 Hz, 1H), 0.82 (s, 3H), 0.81 (s, 3H).

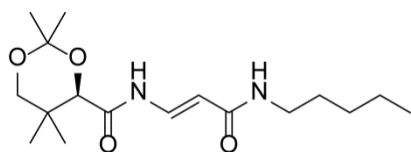
General procedure for Pd-catalyzed couplings

These reactions were conducted according to an adapted procedure of Tanoury *et al.* [23]. To an oven dried Schlenk tube under a nitrogen atmosphere were added Pd(OAc)₂ (0.1 eq), xantphos (0.15 eq), K₂CO₃ (2 eq), CTAB (0.2 eq), the bromide (1.1 eq), the amide (Benzamide or **S4**) (1 eq) and toluene (0.4 M with respect to amide). The suspension was then degassed under high vacuum until no further gas evolution was observed, after which it was warmed to 55 °C. After stirring for 1h, 3 eq of water was added and the reaction stirred for a further 4h at 55 °C. After cooling to rt the reaction was diluted with EtOAc, washed with water and the organic layer dried over Na₂SO₄. After filtration and concentration *in vacuo* the *E* and *Z*-enamides were separated and purified using flash chromatography. The stereochemistry of the products was assigned by comparing the coupling constants of the alkene protons.



(*E/Z*)-4-methyl-2-oxo-2H-chromen-7-yl 3-benzamido-acrylate (**7b**):

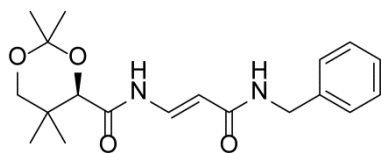
The synthesis was performed according to the general procedure using bromoacrylamide **S3.1** (1514.64 mg, 4.9 mmol). The product precipitated in between the organic and aqueous layers, which was then dissolved in a mixture of DCM and methanol and purified using flash chromatography on a silica column. The solvent was removed under vacuum and freeze-dried to yield the product as a white powder (180 mg, 0.52 mmol). Both *E* and *Z* products were obtained after purification by flash chromatography in a combined yield of 10.6%. ¹H NMR (300 MHz, DMSO): δ = 2.45 (s, 3H), 5.85 (d, *J* = 13.8, 1H), 6.39 (s, 1H), 7.24 (d, *J* = 8.51, 1H), 7.30 (s, 1H), 7.50 – 7.67 (m, 3H), 7.83 (d, *J* = 8.51, 1H), 8.00 – 8.07 (m, 2H), 8.01 (d, *J* = 13.8, 1H). ¹³C NMR (75.5 MHz, DMSO): δ = 18.7, 110.7, 112.5, 114.1, 117.8, 119.1, 126.8, 128.6, 128.7, 129.1, 129.2, 131.7, 132.5, 147.5, 153.5, 153.6, 154.0, 160.2, 165.6, 165.7. HRMS-ESI (*m/z*): [M]⁺ calculated for C₂₀H₁₄NO₅, 348.0872; found 348.0875.



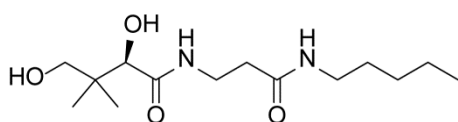
*(*R*)-2,2,5,5-Tetramethyl-*N*-(3-oxo-3-(pentylamino)prop-1-enyl)-1,3-dioxane-4-carboxamide (**S5.1**):

The synthesis was performed according to the general procedure using bromoacrylamide **S3.2** (0.194 g, 0.885 mmol). Both *E* and *Z* products were obtained after purification by flash chromatography (Hexane/EtOAc 1:1 to 1:2) in a combined yield of 49% (*E/Z* ratio of 3:1). (*E*-isomer) ¹H NMR (400 MHz, acetone–D₆): δ = 9.38 (br d, *J* = 10.6 Hz, 1H), 7.80 (dd, *J* = 13.5, 10.9 Hz, 1H), 7.17 (br

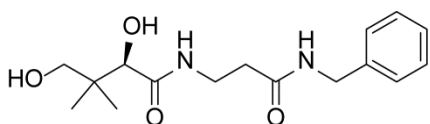
s, 1H), 5.95 (d, $J = 14.1$ Hz, 1H), 4.26 (s, 1H), 3.76 (d, $J = 11.7$ Hz, 1H), 3.28–3.21 (m, 3H), 1.52–1.46 (m, 2H), 1.44 (s, 3H), 1.38 (s, 3H), 1.33–1.26 (m, 4H), 1.00 (s, 3H), 0.98 (s, 3H), 0.87 (t, $J = 7.1$ Hz, 3H); ^{13}C NMR (100 MHz, acetone- D_6): $\delta = 170.3, 168.0, 134.8, 107.9, 101.0, 78.8, 72.8, 72.6, 40.9, 34.8, 34.3, 31.1, 24.0, 23.1, 20.2, 20.0, 15.3$; HRMS–ESI: m/z $[\text{M}+\text{H}]^+$ calculated for $\text{C}_{17}\text{H}_{31}\text{N}_2\text{O}_4$: 327.2284; found: 327.2269.



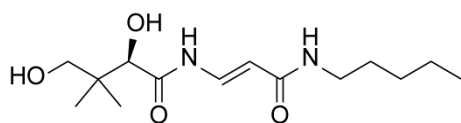
***(R)-N-(3-(Benzylamino)-3-oxoprop-1-enyl)-2,2,5,5-tetramethyl-1,3-dioxane-4-carboxamide (S5.2):** The synthesis was performed according to the general procedure using bromoacrylamide **S3.3** (0.353 g, 1.47 mmol). Both *E* and *Z* products were obtained after purification by flash chromatography (Hexane/EtOAc 1:1 to 1:2) in a combined yield of 52% (*E/Z* ratio of 3:1). (*E*-isomer) The ^1H NMR of matches the literature spectra. ^1H NMR (300 MHz, acetone- D_6): $\delta = 9.46$ (br d, $J = 10.8$ Hz, 1H), 7.89 (dd, $J = 14.2, 11.2$ Hz, 1H), 7.59 (br t, $J = 4.6$ Hz, 1H), 7.30–7.20 (m, 5H), 6.03 (d, $J = 14.1$ Hz, 1H), 4.45 (d, $J = 5.9$ Hz, 2H), 4.27 (s, 1H), 3.76 (d, $J = 11.7$ Hz, 1H), 3.27 (d, $J = 11.7$ Hz, 1H), 1.44 (s, 3H), 1.38 (s, 3H), 1.01 (s, 3H), 0.99 (s, 3H).



***(R)-2,4-dihydroxy-3,3-dimethyl-N-(3-oxo-3-(pentylamino)propyl)butanamide (8a):** Prepared using previously published methods [20, 39].

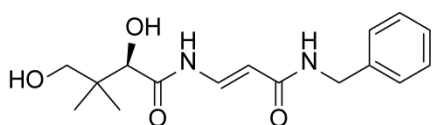


***(R)-N-(3-(benzylamino)-3-oxopropyl)-2,4-dihydroxy-3,3-dimethylbutanamide (8b):** Prepared using previously published methods [20, 39].



***(R,E)-2,4-dihydroxy-3,3-dimethyl-N-(3-oxo-3-(pentylamino)prop-1-en-1-yl)butanamide (9a):** The acetone group was deprotected according to the procedure of Han *et al* [40].

To a round-bottom flask containing **S5.1** (0.088 g, 0.27 mmol), was added BiCl_3 (17 mg, 0.54 mmol), water (97.1 μL , 5.39 mmol) and MeCN (0.24 M). The reaction was then stirred at ambient temperature overnight, filtered and concentrated. The residue was taken up in EtOAc and washed with sat. NaHCO_3 (2 x 10 mL) and the aqueous layer was extracted with EtOAc (1 x 10 mL). The organic layers were combined, dried over Na_2SO_4 , filtered and concentrated *in vacuo*. The crude product was then purified using flash chromatography (EtOAc 100%) to afford the diol **9a** (5 mg, 6%) as a yellow oil. ^1H NMR (400 MHz, CD_3OD): $\delta = 7.81$ (d, $J = 14.1$ Hz, 1H), 5.89 (d, $J = 14.1$ Hz, 1H), 4.00 (s, 1H), 3.48 (d, $J = 10.9$ Hz, 1H), 3.38 (d, $J = 10.9$ Hz, 1H), 3.21 (t, $J = 7.1$ Hz, 2H), 1.55–1.50 (m, 2H), 1.36–1.31 (m, 4H), 0.93–0.89 (m, 9H); HRMS–ESI: m/z $[\text{M}+\text{H}]^+$ calculated for $\text{C}_{14}\text{H}_{27}\text{N}_2\text{O}_4$: 287.1971; found: 287.1973.



(*R,E*)-*N*-(3-(benzylamino)-3-oxoprop-1-en-1-yl)-2,4-dihydroxy-3,3-di-methylbutanamide (9b): The acetonide group was deprotected according to the procedure of Han *et al* [40]. To a round-bottom flask

containing **S5.2** (0.100 g, 0.289 mmol), was added BiCl₃ (18 mg, 0.058 mmol), water (105 μL, 5.78 mmol) and MeCN (0.24 M). The reaction was then stirred at ambient temperature overnight, filtered and concentrated. The residue was taken up in EtOAc and washed with sat. NaHCO₃ (2 x 10 mL) and the aqueous layer was extracted with EtOAc (1 x 10 mL). The organic layers were combined, dried over Na₂SO₄, filtered and concentrated *in vacuo*. The crude product was then purified using flash chromatography (EtOAc 100%) to afford the diol **9b** (30 mg, 34%) as a yellow oil. The ¹H NMR matches the literature spectra [40]. ¹H NMR (300 MHz, acetone-D₆): δ = 9.90 (br d, *J* = 11.1 Hz, 1H), 8.00 (dd, *J* = 13.8, 11.1 Hz, 1H), 7.92 (br t, *J* = 5.9 Hz, 1H), 7.34-7.29 (m, 4H), 7.27-7.19 (m, 1H), 6.11 (d, *J* = 14.2 Hz, 1H), 4.50 (d, *J* = 5.9 Hz, 2H), 4.23 (d, *J* = 5.03 Hz, 1H), 3.51 (d, *J* = 12.1 Hz, 1H), 3.46 (d, *J* = 12.4 Hz, 1H), 0.96 (s, 3H), 0.93 (s, 3H).

4.5 References

1. World Health Organization. *Antimicrobial Resistance: Global Report on Surveillance*, 2014, WHO: Geneva.
2. Sugie, Y., e. al, and et al., *ChemInform Abstract: CJ-15,801, a Novel Antibiotic from a Fungus, Seimatosporium sp.* ChemInform, 2002. **33**(22): p. no-no.
3. van der Westhuyzen, R., et al., *The Antibiotic CJ-15,801 Is an Antimetabolite that Hijacks and Then Inhibits CoA Biosynthesis.* Chemistry & Biology, 2012. **19**(5): p. 559-571.
4. Bollinger, J.M., et al., *Glutathionylspermidine Metabolism in Escherichia coli.: PURIFICATION, CLONING, OVERPRODUCTION, AND CHARACTERIZATION OF A BIFUNCTIONAL GLUTATHIONYLSPERMIDINE SYNTHETASE/AMIDASE.* Journal of Biological Chemistry, 1995. **270**(23): p. 14031-14041.
5. Winter, H.C. and E.E. Dekker, *Purification and characterization of a novel 4-methyleneglutamine synthetase from germinated peanut cotyledons (Arachis hypogaea).* Journal of Biological Chemistry, 1986. **261**(24): p. 11189-11193.
6. Thiagarajan, N., et al., *Functional and structural analyses of N-acylsulfonamide-linked dinucleoside inhibitors of RNase A.* The Febs Journal, 2011. **278**(3): p. 541-549.
7. Patrone, J.D., et al., *Selective Inhibitors of Bacterial Phosphopantothencysteine Synthetase.* Journal of the American Chemical Society, 2009. **131**(45): p. 16340-16341.
8. Koroniak, L., et al., *Synthesis and Characterization of an N-Acylsulfonamide Inhibitor of Human Asparagine Synthetase.* Organic Letters, 2003. **5**(12): p. 2033-2036.

9. Gulick, A.M., *Conformational Dynamics in the Acyl-CoA Synthetases, Adenylation Domains of Non-ribosomal Peptide Synthetases, and Firefly Luciferase*. ACS Chemical Biology, 2009. **4**(10): p. 811-827.
10. Manoj, N., et al., *Structure of Human Phosphopantothencysteine Synthetase at 2.3 Å Resolution*. Structure, 2003. **11**(8): p. 927-936.
11. Yao, J., J.D. Patrone, and G.D. Dotson, *Characterization and Kinetics of Phosphopantothencysteine Synthetase from Enterococcus faecalis*. Biochemistry, 2009. **48**(12): p. 2799-2806.
12. Kupke, T., *Active-site residues and amino acid specificity of the bacterial 4'-phosphopantothencysteine synthetase CoaB*. European Journal of Biochemistry, 2004. **271**(1): p. 163-172.
13. Stanitzek, S., et al., *Structural Basis of CTP-Dependent Peptide Bond Formation in Coenzyme A Biosynthesis Catalyzed by Escherichia coli PPC Synthetase*. Structure, 2004. **12**(11): p. 1977-1988.
14. Schellman, J.A., *Temperature, stability, and the hydrophobic interaction*. Biophysical Journal. **73**(6): p. 2960-2964.
15. Niesen, F.H., H. Berglund, and M. Vedadi, *The use of differential scanning fluorimetry to detect ligand interactions that promote protein stability*. Nat. Protocols, 2007. **2**(9): p. 2212-2221.
16. Privalov, P.L., *Stability of Proteins Small Globular Proteins*, in *Advances in Protein Chemistry*, J.T.E. C.B. Anfinsen and M.R. Frederic, Editors. 1979, Academic Press. p. 167-241.
17. Strauss, E., 7.11 - *Coenzyme A Biosynthesis and Enzymology*, in *Comprehensive Natural Products II*, M. Editors-in-Chief: Lew and L. Hung-Wen, Editors. 2010, Elsevier: Oxford. p. 351-410.
18. Luque, I. and E. Freire, *Structural stability of binding sites: Consequences for binding affinity and allosteric effects*. Proteins: Structure, Function, and Bioinformatics, 2000. **41**(S4): p. 63-71.
19. Leavitt, S. and E. Freire, *Direct measurement of protein binding energetics by isothermal titration calorimetry*. Current Opinion in Structural Biology, 2001. **11**(5): p. 560-566.
20. Strauss, E. and T.P. Begley, *The Antibiotic Activity of N-Pentylpantothenamides Results from Its Conversion to Ethyldeithia-Coenzyme A, a Coenzyme A Antimetabolite*. Journal of Biological Chemistry, 2002. **277**(50): p. 48205-48209.
21. Copeland, R.A., *Enzymes: A Practical Introduction to Structure, Mechanism, and Data Analysis*. 2nd Edition ed2000: John Wiley & Sons.
22. Pace H.C., B.C., *The nitrilase superfamily: classification, structure and function*. Genome Biol., 2001. **2**(1): p. reviews0001.1–reviews0001.9.

23. Duprè, S., et al., *The Enzymatic Breakdown of Pantethine to Pantothenic Acid and Cystamine*. European Journal of Biochemistry, 1970. **16**(3): p. 571-578.
24. Jansen, P.A.M., et al., *Combination of Pantothenamides with Vanin Inhibitors as a Novel Antibiotic Strategy against Gram-Positive Bacteria*. Antimicrobial Agents and Chemotherapy, 2013. **57**(10): p. 4794-4800.
25. Spry, C., et al., *Pantothenamides Are Potent, On-Target Inhibitors of *Plasmodium falciparum* Growth When Serum Pantetheinase Is Inactivated*. PLoS ONE, 2013. **8**(2): p. e54974.
26. Huang, X. and M. Hernick, *A fluorescence-based assay for measuring N-acetyl-1-d-myo-inositol-2-amino-2-deoxy- α -d-glucopyranoside deacetylase activity*. Analytical Biochemistry, 2011. **414**(2): p. 278-281.
27. Partis, M.D., et al., *Cross-linking of protein by ω -maleimido alkanoyl N-hydroxysuccinimido esters*. Journal of Protein Chemistry, 1983. **2**(3): p. 263-277.
28. Rowan, A.S., et al., *Nucleoside triphosphate mimicry: a sugar triazolyl nucleoside as an ATP-competitive inhibitor of *B. anthracis* pantothenate kinase*. Organic & Biomolecular Chemistry, 2009. **7**(19): p. 4029-4036.
29. Wittwer, C., B. Wyse, and R.G. Hansen, *Assay of the enzymatic hydrolysis of pantetheine*. Analytical Biochemistry, 1982. **122**(2): p. 213-222.
30. Padayatti, P.S., et al., *Rational Design of a β -Lactamase Inhibitor Achieved via Stabilization of the trans-Enamine Intermediate: 1.28 Å Crystal Structure of wt SHV-1 Complex with a Penam Sulfone*. Journal of the American Chemical Society, 2006. **128**(40): p. 13235-13242.
31. Strauss, E., et al., *Phosphopantothenoylcysteine Synthetase from *Escherichia coli*: Identification and Characterization of the Last Unidentified Coenzyme A Biosynthetic Enzyme in Bacteria*. Journal of Biological Chemistry, 2001. **276**(17): p. 13513-13516.
32. Yao, J. and G.D. Dotson, *Kinetic characterization of human phosphopantothenoylcysteine synthetase*. Biochimica et Biophysica Acta (BBA) - Proteins and Proteomics, 2009. **1794**(12): p. 1743-1750.
33. Copeland, R.A., *Evaluation of Enzyme Inhibitors in Drug Discovery: A Guide for Medicinal Chemists and Pharmacologists* 2005: John Wiley & Sons. 384.
34. Buijs, W., et al., *Structural and mechanistic studies of the copper(II)-assisted ortho-hydroxylation of benzoates by trimethylamine N-oxide*. Journal of Organometallic Chemistry, 2002. **641**(1-2): p. 71-80.
35. Luo, Y., et al., *Enantioselective Synthesis of Allylboronates and Allylic Alcohols by Copper-Catalyzed 1,6-Boration*. Angewandte Chemie International Edition, 2014. **53**(16): p. 4186-4190.

36. Weir, J.R., B.A. Patel, and R.F. Heck, *Palladium-catalyzed triethylammonium formate reductions. 4. Reduction of acetylenes to cis-monoenes and hydrogenolysis of tertiary allylic amines*. The Journal of Organic Chemistry, 1980. **45**(24): p. 4926-4931.
37. Tanoury, G.J., et al., *Development of a Novel Pd-Catalyzed N-Acyl Vinylogous Carbamate Synthesis for the Key Intermediate of ICE Inhibitor VX-765*. Organic Letters, 2007. **10**(2): p. 185-188.
38. Aquino, F., et al., *A Convenient Dehydration Procedure for the Synthesis of Enantiomerically Pure Cyanohydrins*. Synthesis, 2000. **2000**(05): p. 731-737.
39. van Wyk, M. and E. Strauss, *Development of a method for the parallel synthesis and purification of N-substituted pantothenamides, known inhibitors of coenzyme A biosynthesis and utilization*. Organic & Biomolecular Chemistry, 2008. **6**(23): p. 4348-4355.
40. Han, C., et al., *Copper-Mediated Synthesis of N-Acyl Vinylogous Carbamic Acids and Derivatives: Synthesis of the Antibiotic CJ-15,801*. Organic Letters, 2003. **6**(1): p. 27-30.

Chapter 5: General conclusions and future work

5.1 Summary of results obtained

In this study we proposed an alternative strategy to current drug development methodologies that entails the identification and targeting of processes that are essential to the survival of pathogenic bacteria in their human host, i.e. where they need to counter the defences of the human immune system. In particular, the focus of this study is the importance of the central metabolic cofactor CoA in the defence mechanisms that *S. aureus* employs under such circumstances, and therefore on the targeting of CoA biosynthesis and enzymology as potential antistaphylococcal targets. The research in this study built upon previous investigations that raised several questions in this regard. While we managed to clarify several uncertainties regarding CoADR and CoA redox balance as a potential antistaphylococcal drug target, many of the important questions regarding the organism's redox balance in general remain unanswered.

In addition, the study uncovered the mechanistic basis for the inhibition of PPCS enzymes by a metabolically activated form of the natural product CJ-15,801. This work contributed to our understanding of non-hydrolysable reaction intermediate analogues as inhibitors of important synthetase enzymes.

The achievements in regards to the objectives as outlined at the end of Chapter 1 can be summarised as follows:

5.1.1 CoADR as an antistaphylococcal drug target

In Chapter 3 the evaluation of the viability of CoADR as a potential antistaphylococcal drug target was described. The work in this chapter followed up on previous studies in which our research group explored the druggability of CoADR with small molecule mechanism-based Michael acceptor-containing inhibitors. The SaCoADR enzyme structures in complex with the Michael acceptor-containing inhibitors were examined; specifically how its interaction with these compounds relates to the observed differences in activity between them. Consequently, we could adequately explain the observed enzyme inhibition when taking into account the chemical properties of the inhibitors in combination with their interactions with SaCoADR. Also, the structural data in the study provided a strong starting point for future inhibitor design.

The reasons for the poor correlation between the *in vitro* inhibition of SaCoADR by the Michael acceptor-containing CoA analogues and the whole cell inhibition of *S. aureus* by their corresponding pantothenamide precursors were investigated, since elucidating the basis of this weak correlation should enable us to design potent on target enzyme inhibitors with equivalent bacterial growth inhibition. We were able to show that neither impermeability of the bacterial cell envelope to the inhibitor precursors, nor lack of metabolic activation, are reasons for the poor correlation. While examining the target specificity of the CoADR inhibitors, we found that the bacterial growth inhibition observed for their pantothenamide precursors are due

to mechanisms unrelated to CoADR. These results led us to the conclusion that the poor correlation between the enzyme inhibition and the whole cell growth inhibition is due to SaCoADR not being essential under normal growth conditions. Whether this is due to the CoADR activity not being required under these conditions, or the presence of another protein that is able to reduce sufficient amounts of (CoAS)₂ for survival is not clear at the present moment.

5.1.2 Relevance of CoADR, BSH and a putative FDR to survival of *S. aureus* challenged with oxidative stress conditions

Although our group has previously demonstrated SaCoADR to be a tractable target for inhibition by small molecule inhibitors, its validation as a viable drug target remained uncertain. It was therefore necessary to evaluate the physiological relevance of CoADR in *S. aureus* under oxidative stress, since it is more likely that its importance will also come to light under such conditions. Additionally, we investigated and compared the effects of two other potential role players in *S. aureus* oxidative stress defence, BSH and a putative FDR enzyme shown to be upregulated more than 80-fold in *S. aureus* when challenged with neutrophils [1]. Unfortunately, these results also indicated that CoADR did not contribute notably to the oxidative stress resistance of *S. aureus*. In contrast, BSH and the FDR of unknown function seemed to have more pronounced contributions to the bacterium's ability to survive. When evaluated against the background of reduced CoA levels, very little difference was seen between the effects of CoADR, BSH and the FDR of unknown function.

It is noteworthy that while both CoA and BSH are considered as candidates to be the major LMWT responsible for redox balance in *S. aureus*, our study could not unequivocally support either for such a role. Also, the results did not reveal any link between the two compounds; specifically, neither compound appeared to compensate for the absence of the other during our studies. Of further significance are results which suggested that CoA-dependent processes are more sensitive to inhibition in the absence of SaCoADR. This included CO₂Et-Pan that showed higher potency in the *cdr* knockout background as well as the most potent CoA biosynthesis inhibitor tested (Compound D), which was found to have increased potency in the *cdr* knockout backgrounds than in the wild-type strain. This suggests that under conditions where CoA levels are sufficiently reduced, CoADR might become relevant, even under normal growth conditions. This opens the door for studies on the possible synergistic effects of CoADR inhibitors and compounds that reduce CoA levels; such combinations most likely hold the most potential for work focused on CoADR as a drug target.

5.1.3 Mechanism of inhibition of PPCS by the natural product CJ-15,801

In Chapter 4 we further investigated the mechanism of inhibition of PPCS enzymes by PCJ-CMP by determining the basis for the apparent stability of the inhibitor. We showed that the PPCS protein itself plays no role in the mechanism of inhibition by PCJ-CMP, but that the introduction of the double bond in the β-alanine moiety of the substrate with its extra π-electrons renders the acyl phosphate resistant to nucleophilic

attack by introducing new, stable resonance forms. This mechanism of apparent stabilisation *via* resonance was also applied to an unrelated system and we were able to convert substrates of VNN1 pantetheinase into inhibitors of the enzyme. The inhibition strategy of PCJ-CMP of acting as a non-hydrolysable reaction intermediate is analogous to that used for the development of other synthetase inhibitors [2]; however, since PCJ-CMP is generated *in situ* in the target's active site it offers several major advantages. First, the inhibitor precursor (CJ), which mimics the structure of vitamin B₅ closely, can easily enter the cell. Second, it can then be selectively activated by *S. aureus*' Pank to form PCJ, which is accepted into the active site of the target PPCS enzyme. Taken together, these studies allow us to rationalise the tight-binding inhibition observed for PCJ-CMP. Additionally, we uncovered a new strategy whereby β -alanine-containing compounds can be rendered resistant to hydrolysis and/or acyl transfer; this strategy can likely have wide-ranging applications in the design of such small molecule inhibitors and therapeutics.

5.2 Future studies

5.2.1 *S. aureus* redox balance

The next step in our investigation into the redox balance of *S. aureus* would be to accurately assess the effect of oxidative stress on the organism. This was recently accomplished in a study that targeted the nitric oxide synthase (implicated in oxidative stress defence [3]) for inhibition of MRSA [4]. In the study inhibitors directed against nitric oxide synthase are assayed against *S. aureus* under normal and oxidative stress conditions. The inhibitors are shown to work synergistically with H₂O₂, an oxidative stressor, to significantly limit bacterial growth. By using similar methods and conditions, we would like to compare the effects of all the potential role players in redox balance effectively. Importantly, it will allow us to repeat our assays with the small molecule inhibitors under oxidative stress conditions, since it would accentuate any effects that are related to redox balance. Also, this methodology could potentially open up the possibility to investigate synergism between CoADR inhibitors and CoA biosynthesis inhibitors. We expect to see increased relevance of CoADR when CoA levels are significantly reduced, which could be further accentuated under oxidative stress conditions.

5.2.2 Hydrolysis resistant substrate analogues

We would like to further explore the development of stable variants of other compounds containing β -amino acid moieties and apply it to more biological systems. Also, it should be worthwhile to characterise the thermodynamic differences between the substrates and their stable analogues, since it will provide a quantifiable way to assess their relative stabilities.

5.3 Final remarks

In this study, we were able to demonstrate SaCoADR as a tractable target for drug design, but could not unequivocally validate it as a viable target for antistaphylococcal drug development. However, these findings pave the way for further investigation of redox balance in *S. aureus* as a potential drug target. We also determined the basis of the tight-binding inhibition of PPCS enzymes by PCJ-CMP and in doing so, presented a new form of non-hydrolysable reaction intermediate analogue, which might also serve as a general starting point for the development of stable variants of other compounds containing β -amino acid moieties.

5.4 References

1. Voyich, J.M., et al., *Insights into Mechanisms Used by Staphylococcus aureus to Avoid Destruction by Human Neutrophils*. Journal of Immunology, 2005. **175**(Copyright (C) 2011 American Chemical Society (ACS). All Rights Reserved.): p. 3907-3919.
2. Padayatti, P.S., et al., *Rational Design of a β -Lactamase Inhibitor Achieved via Stabilization of the trans-Enamine Intermediate: 1.28 Å Crystal Structure of wt SHV-1 Complex with a Penam Sulfone*. Journal of the American Chemical Society, 2006. **128**(40): p. 13235-13242.
3. Shatalin, K., et al., *Bacillus anthracis-derived nitric oxide is essential for pathogen virulence and survival in macrophages*. Proceedings of the National Academy of Sciences, 2008. **105**(3): p. 1009-1013.
4. Holden, Jeffrey K., et al., *Nitric Oxide Synthase as a Target for Methicillin-Resistant Staphylococcus aureus*. Chemistry & Biology. **22**(6): p. 785-792.

Appendix: Publications

Publications on which I am a co-author are included in this appendix. First is the mini-review “Recent advances in targeting coenzyme A biosynthesis and utilisation for antimicrobial drug development” included in Chapter 2, in its final published form. *Biochemical Society Transactions* (2014) **42**, 1080–1086; doi:10.1042/BST20140131.

Second is “Turnover-Dependent Covalent Inactivation of *Staphylococcus aureus* Coenzyme A Disulfide Reductase by Coenzyme A Mimetics: Mechanistic and Structural Insights,” referenced in Chapter 3. *Biochemistry* (2012) **51**, 7699–7711; dx.doi.org/10.1021/bi301026c.

Third is “The Antibiotic CJ-15,801 Is an Antimetabolite that Hijacks and Then Inhibits CoA Biosynthesis”, upon which the work in Chapter 4 is based. *Chemistry & Biology* (2012) **19**, 559–571; DOI 10.1016/j.chembiol.2012.03.013.

Recent advances in targeting coenzyme A biosynthesis and utilization for antimicrobial drug development

Wessel J.A. Moolman*, Marianne de Villiers* and Erick Strauss*¹

*Department of Biochemistry, Stellenbosch University, Stellenbosch, 7600, South Africa

Abstract

The biosynthesis and utilization of CoA (coenzyme A), the ubiquitous and essential acyl carrier in all organisms, have long been regarded as excellent targets for the development of new antimicrobial drugs. Moreover, bioinformatics and biochemical studies have highlighted significant differences between several of the bacterial enzyme targets and their human counterparts, indicating that selective inhibition of the former should be possible. Over the past decade, a large amount of structural and mechanistic data has been gathered on CoA metabolism and the CoA biosynthetic enzymes, and this has facilitated the discovery and development of several promising candidate antimicrobial agents. These compounds include both target-specific inhibitors, as well as CoA antimetabolite precursors that can reduce CoA levels and interfere with processes that are dependent on this cofactor. In the present mini-review we provide an overview of the most recent of these studies that, taken together, have also provided chemical validation of CoA biosynthesis and utilization as viable targets for antimicrobial drug development.

Introduction

The biosynthesis of CoA (coenzyme A), or more specifically, the utilization of Pan (pantothenate) (Figure 1), the vitamin precursor of this essential cofactor, has long been regarded as an excellent target for the development of selective antimicrobials [1]. Studies during the past decade have confirmed that all organisms must obtain CoA through *de novo* biosynthesis from Pan using a conserved pathway consisting of five enzymatic steps [2,3]. However, in several cases the specific enzymes that catalyse these reactions in humans and pathogenic micro-organisms show significant diversity on a sequence, structure and mechanistic level, suggesting that the development of selective inhibitors of microbial CoA biosynthesis should be possible, and highlighting these enzymes as targets for drug development [3,4].

CoA can also be obtained from PantSH (pantetheine), by means of a shortened pathway consisting of only three of the five biosynthetic enzymes [3,5] (Figure 1). PantSH is believed to be produced by dephosphorylation of PPantSH (4'-phosphopantetheine), one of the products of nucleotide

diphosphate-catalysed hydrolysis of CoA, and the prosthetic group of the holo-ACP (acyl carrier protein) which is released during recycling of this protein; however, these degradation pathways have not been studied in detail. Nonetheless the so-called CoA salvage pathway can also be hijacked by anti-Pans (pantothenate antimetabolites), compounds that resemble Pan, but that do not allow the catalytically essential thiol to be incorporated into the CoA structure. This results in the formation of anti-CoAs (CoA antimetabolites) that can interfere with and/or inhibit CoA-dependent processes or reduce intracellular CoA levels (Figure 1).

In the present mini-review we summarize the recent advances made in the development of small molecule inhibitors of CoA biosynthesis (and processes dependent on this cofactor) for the discovery of new potent antimicrobials.

CoA biosynthesis: enzyme-specific inhibitors

PanK

PanK (Pan kinase; EC 2.7.1.33), which catalyses the ATP-dependent phosphorylation of Pan to form PPan (4'-phosphopantothenate), has received the most attention as a potential target for antimicrobial drug development. This is due to several factors: first, the enzyme catalyses the first and committed step of CoA biosynthesis [3,6]; secondly, PanK is believed to be the rate-limiting enzyme of the pathway; and thirdly, PanKs show significant diversity, with two bacterial (types I and III) and one predominantly eukaryotic (type II) PanK types having been described that show differences in sequence homology, structural fold, and catalytic and inhibition properties [7,8]. Together, these

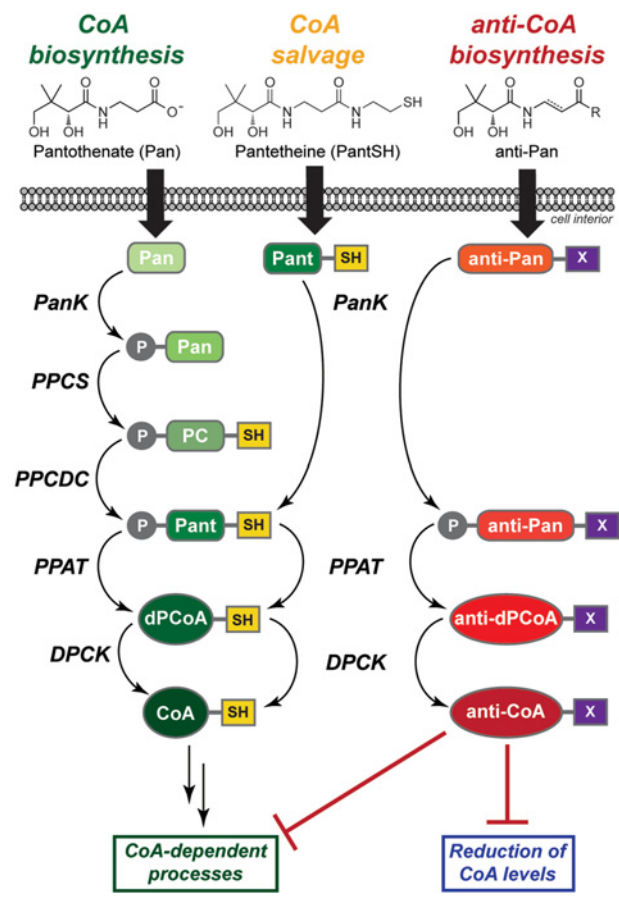
Key words: antimetabolite, antimicrobial, biosynthesis, coenzyme A (CoA), enzyme inhibitor, pantothenamide.

Abbreviations: ACP, acyl carrier protein; anti-CoA, CoA antimetabolite; anti-Pan, pantothenate antimetabolite; CoADR, CoA disulfide reductase; CoASy, CoA synthase; DPCK, dephospho-CoA kinase; HoPanAm, homopantothenamide; HpPPAT, *Helicobacter pylori* PPAT; KpPanK, *Klebsiella pneumoniae* type I PanK; MIC, minimal inhibitory concentration; MtPanK, *Mycobacterium tuberculosis* PanK; N354-Pan, N-[2-(1,3-benzodioxol-5-yl)ethyl]pantothenamide; N5-Pan, N-pentylpantothenamide; N7-Pan, N-heptylpantothenamide; Pan, pantothenate; PanAm, N-substituted pantothenamide; α -PanAm, α -pantothenamide; PanK, Pan kinase; PantSH, pantetheine; PPan, 4'-phosphopantothenate; PPantSH, 4'-phosphopantetheine; PPAT, phosphopantetheine adenyltransferase; PPC, 4'-phosphopantothenoylcysteine; PPCDC, phosphopantothenoylcysteine decarboxylase; PPCS, phosphopantothenoylcysteine synthetase; SoPanK, *Staphylococcus aureus* type II PanK; SAR, structure-activity relationship.

¹To whom correspondence should be addressed (email estrauss@sun.ac.za).

Figure 1 | CoA biosynthesis and utilization as an antimicrobial drug target

The biosynthesis of CoA from Pan proceeds in a five-step pathway catalysed by PanK, PPCS, PPCDC, PPAT and DPCK. Of these, PanK, PPCS and PPAT have been successfully targeted in inhibitor development studies aimed at the discovery of new antimicrobials. Additionally, CoA can also be obtained from PantSH (a CoA degradation product) by a shortened salvage pathway that consists of PanK, PPAT and DPCK. This pathway can be hijacked by anti-Pan compounds (a generic structure of such compounds is shown), which are subsequently converted into anti-CoAs that can interfere with CoA-dependent processes and/or reduce CoA levels.



factors have strongly suggested that it should be possible to develop selective small molecule inhibitors of the PanKs of pathogenic micro-organisms of interest that show little interaction with the human enzyme.

By far the most studies on PanK inhibitor discovery published to date have focused on the type I PanK enzyme from *Mycobacterium tuberculosis* (*MtPanK_I*) as the target (Figure 2a). *M. tuberculosis* is the causative agent of the debilitating infectious disease TB (tuberculosis), which leads to more than 2 million deaths annually [9]. The enzyme has been crystallized in complex with its substrates, substrate analogues, products and feedback inhibitor (CoA) [10–13]. AstraZeneca identified a range of potent inhibitors of

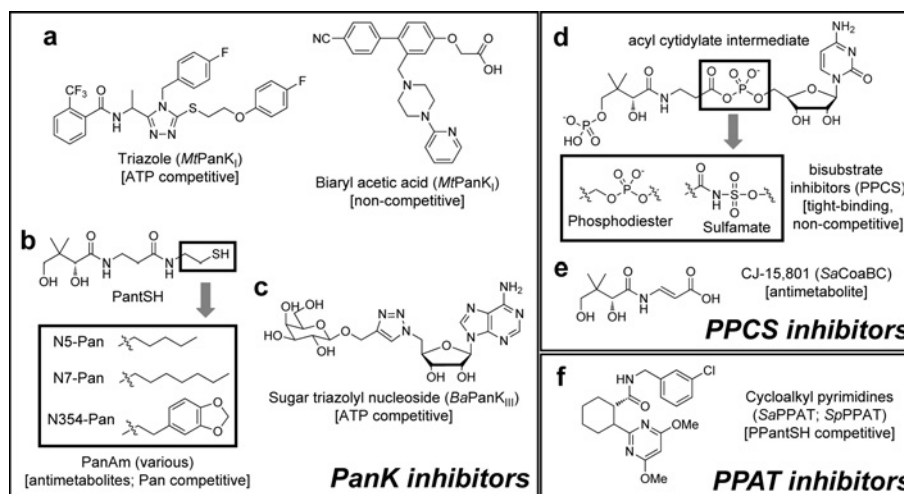
MtPanK_I, based on chemical scaffolds of triazoles, thiazoles, quinoline carboxamides and biaryl acetic acids, using a high-throughput screen based on ligand-induced shifts in the protein's melting temperature [14]. Eight of these compounds based on the triazole and biaryl scaffolds were studied in more detail (the structures of the most potent examples of each scaffold are shown in Figure 2a), with co-crystal structures being obtained to enable correlation of the biochemical and structural data [15]. The triazoles were shown to bind competitively with respect to ATP, whereas the data obtained for the biaryls suggested a mode of binding that is non-competitive towards ATP. Unfortunately, the compounds described in the study were inactive against *M. tuberculosis* in whole cell inhibition assays, although several showed IC₅₀ values against the enzyme in the nanomolar range (at ATP concentration equivalent to the enzyme's *K_m*). This result was interrogated further by means of vulnerability studies that used *MtPanK_I*-overexpression and -knockdown strains [16]. These studies showed that a reduction in PanK activity of more than 95% was required to achieve growth inhibition, due to the steady state levels of CoA being far in excess of what is critical for cell survival, a finding that is in agreement with those of previous studies [17,18]. Consequently, the authors concluded that *MtPanK_I* is not an attractive antimycobacterial drug target due to its low vulnerability to inhibition. However, *M. tuberculosis* also expresses a type III PanK enzyme (*MtPanK_{III}*) and, although studies have shown that this enzyme seems to be non-functional [19], the possibility remains that it is conditionally active and can rescue a deficiency in the type I enzyme.

The pantothenamides, a class of PantSH analogues that are mainly considered to exert their antimicrobial activity by acting as anti-CoA precursors, have also been considered as PanK inhibitors in several studies (Figure 2b). A SAR (structure–activity relationship) study showed that these compounds inhibit the Pan phosphorylation activity of several PanK enzymes, although the mode of inhibition was not determined [20]. In a recent structure-based study, co-crystal structures of the *Staphylococcus aureus* type II PanK (*SaPanK_{II}*) and the type I *Klebsiella pneumoniae* PanK (*KpPanK_I*) with N354-Pan {*N*-[2-(1,3-benzodioxol-5-yl)ethyl]pantothenamide} (Figure 2b) were solved [21]. These structures revealed that N354-Pan has two distinct conformations in these enzymes. Additionally, both enzymes contained ADP, despite being incubated with ATP for crystallization, and in the case of *SaPanK_{II}* phosphorylated N354-Pan was bound in the active site. The authors postulated that *SaPanK_{II}* undergoes a conformational change to accommodate N354-Pan, but in doing so locks the enzyme in the closed conformation, preventing the release of phosphorylated N354-Pan and halting the catalytic cycle. By comparison, part of bound N354-Pan was visible through the putative product exit channel in *KpPanK_I*, which implied that N354-Pan leaves the active site via the channel after phosphorylation and is exchanged for new N354-Pan.

Far less work has been done on type III PanKs (*PanK_{III}*s), since these enzymes were only discovered relatively recently

Figure 2 | Inhibitor and antimetabolite structures

Structures of the most potent and/or representative inhibitors of the CoA biosynthetic enzymes PanK, PPCS and PPAT. The actual targets and mode of inhibition are also indicated. PanAms (**b**) are considered to act as antimetabolites, although they could also be Pan competitive inhibitors of PanK enzymes.



[7]. Currently, the only known inhibitors for PanK_{III}s are nucleoside triphosphate mimetics of ATP, which were discovered through the preparation of a library of compounds in which the triphosphate side chain of ATP was replaced by uncharged methylene-triazole-linked monosaccharide groups [22]. However, PanK_{III}s bind ATP very weakly in an open cavity with no interactions between the enzyme and the adenosine moiety, and the question has been raised as to whether ATP is really the co-substrate of these enzymes [7,23]. Consequently, the best ATP mimetic (Figure 2c) that showed a significant effect on the *Bacillus anthracis* PanK_{III} (*BaPanK_{III}*) enzyme and competed with ATP binding *in vitro* had a K_i value of only 164 μM (a 3-fold decrease in the enzyme's K_m value for ATP of 510 μM). Since this value is still too high to be of pharmaceutical interest, and no whole cell bacterial inhibition was reported, ATP mimetics might not be the most promising avenue to pursue for the discovery of PanK_{III} inhibitors.

In summary, although bacterial PanK enzymes clearly remain valid and important potential targets for antimicrobial drug development, no PanK inhibitor that shows viability in cell growth inhibition tests have been discovered to date.

PPCS/PPCDC

PPCS (phosphopantothencysteine synthetase; EC 6.3.2.5), the second enzyme of the CoA biosynthetic pathway, catalyses the Mg^{2+} -dependent formation of PPC (4'-phosphopantothencysteine) from PPan and L-cysteine using either CTP (in bacteria) or ATP (in eukaryotes) for activation [3,24,25]. This difference in the nucleotide triphosphate required for catalysis makes PPCS an excellent target for selective antimicrobial development. Additionally, in bacteria the PPCS enzyme is fused to PPCDC (phosphopantothencysteine decarboxylase), the enzyme that catalyses the next step of CoA biosynthesis, to

form a bifunctional CoaBC protein (*coaBC* gene product, previously known as *dfp*) [26]. In contrast, the eukaryotic enzymes are typically monofunctional, thereby providing an additional differentiating characteristic [3,25,27].

The first reported PPCS inhibitors were compounds that mimicked the structure of the reactive acyl cytidylate intermediate that forms during bacterial PPCS catalysis, but which had the reactive acyl-phosphate moiety replaced by either a phosphodiester or sulfamate isostere (Figure 2d) [28]. These compounds were found to be non-competitive inhibitors that exhibited slow-onset tight-binding inhibition with nanomolar IC_{50} and K_i values, and up to 1000-fold selectivity over the human enzyme. Unfortunately, none of these inhibitors also showed concomitant inhibition of bacterial cell growth, with a lack of cellular penetration being cited as the most probable cause.

More recently, the natural product CJ-15,801 (Figure 2e) was characterized as the precursor to a tight-binding inhibitor of PPCS activity [29]. CJ-15,801 was discovered in 2001 by Pfizer and was shown to inhibit drug-resistant strains of *S. aureus* with micromolar MIC (minimal inhibitory concentration) values, but not other bacteria [30]. The compound is a structural analogue of Pan with the notable exception of a *trans*-substituted double bond in the β -alanine moiety. CJ-15,801 was shown to be phosphorylated by the uniquely selective *SaPanK_{II}* and subsequently accepted as an alternate substrate for PPCS. Upon cytidylylation, a tight-binding structural mimic of the native reaction intermediate is formed that shows nanomolar K_i values against *Escherichia coli* PPCS (CoaB domain of the CoaBC protein) and *S. aureus* CoaBC [29].

Very little work has been done on the discovery of inhibitors of PPCDC (EC 4.1.1.36), which catalyses the decarboxylation of PPC's cysteine moiety to give PPantSH. The only inhibitor described to date is the

mechanism-based inactivating agent PPan Δ SH [4'-phospho-*N*-(1-mercaptomethylcyclopropyl)-pantothenamide] that alkylates a critical catalytic residue at a low rate ($k_{\text{inact}}/K_i \sim 1 \text{ s}^{-1} \cdot \text{M}^{-1}$) [27].

PPAT

PPAT (phosphopantetheine adenylyltransferase; EC 2.7.7.3), the fourth enzyme in the CoA biosynthesis pathway, catalyses the reversible Mg^{2+} -dependent adenylylation of PPantSH to form dPCoA (dephospho-CoA) and pyrophosphate as products [3]. Typically, the eukaryotic PPAT activity is fused to the last enzyme in the pathway, DPCK (dephospho-CoA kinase), to form a bifunctional PPAT/DPCK protein that is also known as CoASy (CoA synthase) [31–33]. A single enzyme catalyses the reaction in bacteria, and this activity therefore presents another selective target for antimicrobial development.

A recent high-throughput screening of an AstraZeneca compound library led to the validation of PPAT as a novel target for antibacterial therapy [34], since none of the previously identified PPAT inhibitors exhibited whole cell growth inhibition [35,36]. The study identified a series of cycloalkyl pyrimidines (Figure 2f) as potential inhibitors of both Gram-positive and Gram-negative species. Further optimization by structure-based design led to substantial improvements against Gram-positive bacteria; these inhibitors were found to be competitive with respect to PPantSH for *S. aureus* and *S. pneumoniae* PPAT. Enzyme inhibition translated to potent growth inhibition against several clinical Gram-positive isolates *in vitro* and in mouse infection models. However, the compounds could not be developed into suitable clinical candidates due to a failure to reconcile their biological activity with drug-like properties.

Another recent study employed an *in silico* screening of the HpPPAT (*Helicobacter pylori* PPAT) crystal structure with 407 compound structures retrieved from the PubChem compound database to identify lead compounds that target this enzyme [37]. The screen identified D-amethopterin (methotrexate), a known antimetabolite and anti-cancer drug, as a potential HpPPAT inhibitor. The compound exhibited activity against HpPPAT *in vitro* (as a mixed inhibitor, blocking both PPantSH and ATP binding) and inhibited *H. pylori* viability, but with low potency in both cases. The authors proposed structure optimizations to D-amethopterin to increase binding interaction with HpPPAT, although target selectivity would clearly also have to be addressed.

DPCK

DPCK (EC 2.7.1.24), the final enzyme in the CoA biosynthetic pathway, catalyses the selective MgATP -dependent phosphorylation of the 3'-hydroxy of the ribose moiety of dPCoA to form CoA [3]. Unfortunately (from a drug design perspective), bacterial DPCKs show high sequence and structural homology to the DPCK domain of the bifunctional eukaryotic CoASy protein, suggesting that selective inhibition of the bacterial enzyme is unlikely to be achieved [31–33]. Consequently it has not been the focus

of any significant inhibitor development study conducted to date.

Anti-CoAs

Anti-CoAs are derived from anti-Pans, compounds that resemble the vitamin precursor of CoA, but prevent its catalytically essential thiol to be incorporated and/or incorporates other reactive moieties that are detrimental to essential CoA-dependent processes. Apart from CJ-15,801, the anti-Pan mentioned above as a precursor to a PPCS inhibitor, the PanAms (*N*-substituted pantothenamides) are by far the best known examples of anti-Pans. These compounds were initially described as growth inhibitors of selected lactic acid bacteria and *E. coli* in 1970 [38], but their potential as antimicrobials have been investigated with renewed interest since it was shown that N5-Pan (*N*-pentylpantothenamide) (Figure 2b), the prototypical example of this class of compounds, is transformed into ethyldethia-CoA, an anti-CoA, by the CoA salvage pathway [39] (Figure 1).

PanAms can exert their inhibitory effects in two ways: first, by reducing the rate of CoA synthesis (since anti-CoAs were found to be produced faster than CoA [39]) and therefore CoA levels; and secondly, through the formed anti-CoAs inhibiting enzymes and processes dependent on CoA [40]. In regards to the latter, fatty acid biosynthesis has been considered an especially vulnerable target, since *holo*-ACP, which is an essential requirement for FAS-II (type II fatty acid synthase) systems in bacteria, is formed when AcpS (ACP-synthase) transfers the PPantSH group from CoA to *apo*-ACP. However, anti-CoAs can also serve as substrates for this process, leading to the formation of so-called *crypto*-ACPs that lack the ability to act as acyl carriers [18,41]. The relevance of the two separate inhibition modes, and their relative contributions to PanAm-induced bacterial growth inhibition, still remain a point of debate, as studies supporting either mode have been reported [18,40,42].

N5-Pan and its heptyl counterpart, N7-Pan (*N*-heptylpantothenamide) (Figure 2b), remains the most potent bacterial growth inhibitors discovered to date, with N5-Pan exhibiting a MIC against *E. coli* of 50 μM , while N7-Pan was found to inhibit *S. aureus* with an MIC value of 78 nM (N7-Pan also inhibited *E. coli*, but its potency was reduced due to TolC-based efflux) [20]. These discoveries were made in a PanAm SAR study conducted on 21 compounds that were tested as competitive substrates of the *E. coli*, *S. aureus*, *Aspergillus nidulans* and mouse PanKs. The compounds were shown to impede PanK activity and to be processed by the *E. coli* CoA salvage enzymes (PanK, PPAT and DPCK) to form the corresponding anti-CoAs and *crypto*-ACPs, supporting previous findings with N5-Pan in *E. coli* [18]. However, CoA levels in cells treated with these compounds were not determined, and their exact mode of action was thus not pinpointed.

Follow-up studies in which the effect of varying the chain length, oxidation state and functional group composition of the PanAm amide substituent on its ability to inhibit

E. coli was investigated did not uncover any compound more potent than N5-Pan [43]. Similarly, a study in which variations of the geminal dimethyl groups of the PanAms' pantoic acid moiety were introduced failed to identify a compound showing increased potency against *S. aureus* (both oxacillin-resistant and -sensitive strains) compared with that of N7-Pan [44]. Finally, a small library of 141 pantothenamides was synthesized to evaluate the effects of modifying the PanAm's β -alanine moiety by replacing it with either glycine [yielding a set of α -PanAms (α -pantothenamides)] or γ -aminobutyric acid [giving the HoPanAms (homopantothenamides)]. However, in whole cell inhibition studies on *E. coli* and *S. aureus* N5-Pan and N7-Pan were still found to be the most potent inhibitors respectively [45].

PanAms have also been investigated as antiplasmodial agents, especially since the pathway has been highlighted as an attractive drug target in the malaria parasite *Plasmodium falciparum* based on its essential requirement for Pan and CoA in the blood stage of its life cycle [46]. The first study of the antiplasmodial activity of this class of compounds showed them to have potencies rivalling that of the reference antimalarial chloroquine, with *N*-phenethyl pantothenamide having an IC₅₀ value of 20 nM [47]. In addition, it was shown that these compounds target Pan and/or CoA utilization and interact with PanK. However, these potency levels were only obtained under conditions in which Vanin pantetheinases, enzymes ubiquitously present in serum that degrade PantSH and its derivatives, and therefore also PanAms, were absent or inactivated. In a follow-up study using the β -alanine modified library synthesized by Van Wyk and Strauss [45], it was demonstrated that pantetheinase does not act on the α -PanAm or HoPanAm series, and these compounds therefore show antiplasmodial activity even when this enzyme is present, although with a significant reduction in potency (the best candidates had IC₅₀ values of ~ 1 – $2 \mu\text{M}$) [48].

The discovery of pantetheinase-mediated degradation as a factor in PanAm potency led to the discovery of pantetheinase inhibitors based on Pan as scaffold; using PanAms in combination with these compounds prevented them from being broken down and showed that N5-Pan and N7-Pan have the most potential as antibacterial agents specific for Gram-positive bacteria such as *S. aureus*, *Staphylococcus epidermidis*, *S. pneumoniae* and *Streptococcus pyogenes* [49].

Finally, PanAms designed to incorporate dedicated chemical warheads for the inactivation of specific CoA-dependent enzymes have also been developed [50]. In this study, PanAms containing a Michael-acceptor moiety were shown to be converted to the corresponding anti-CoAs, which subsequently inactivated the CoADR (CoA disulfide reductase) enzyme of *S. aureus* that is thought to play a role in this organism's redox regulation. However, the PanAm precursors of the anti-CoAs showing the best CoADR inhibition ($k_{\text{inact}}/K_i \sim 40000 \text{ s}^{-1} \cdot \text{M}^{-1}$) did not show any inhibition of *S. aureus* growth under normal circumstances, most likely due to poor cell penetration or to CoADR

only being essential under oxidative stress conditions (this has not been tested to date).

Conclusion

The results of the recent studies of inhibitors of CoA biosynthesis and/or utilization have served to further strengthen the case for these processes being viable and tractable targets for antimicrobial drug development, whether by pursuing an enzyme-focused inhibition strategy or by exploiting the inhibitory potential of anti-CoAs. Considering the dire and pressing need for new antimicrobials acting on novel targets, such studies clearly need to be expanded with the aim of developing the first CoA-directed inhibitor suitable for clinical use.

Funding

This work was supported by grants from the South African Medical Research Council (MRC) and National Research Foundation (NRF). W.J.A.M. and M.d.V. gratefully acknowledge the National Research Foundation (NRF) for an Innovation doctoral scholarship and Innovation postdoctoral fellowship respectively.

References

- 1 Spry, C., Kirk, K. and Saliba, K.J. (2008) Coenzyme A biosynthesis: an antimicrobial drug target. *FEMS Microbiol. Rev.* **32**, 56–106 [CrossRef PubMed](#)
- 2 Osterman, A. and Overbeek, R. (2003) Missing genes in metabolic pathways: a comparative genomics approach. *Curr. Opin. Chem. Biol.* **7**, 238–251 [CrossRef PubMed](#)
- 3 Strauss, E. (2010) Coenzyme A biosynthesis and enzymology. In *Comprehensive Natural Products II Chemistry and Biology* (Mander, L. and Liu, H.-W., eds), pp. 351–410, Elsevier, Oxford [CrossRef](#)
- 4 Genschel, U. (2004) Coenzyme A biosynthesis: reconstruction of the pathway in archaea and an evolutionary scenario based on comparative genomics. *Mol. Biol. Evol.* **21**, 1242–1251 [CrossRef PubMed](#)
- 5 Leonardi, R., Zhang, Y.-M., Rock, C.O. and Jackowski, S. (2005) Coenzyme A: back in action. *Prog. Lipid Res.* **44**, 125–153 [CrossRef PubMed](#)
- 6 Jackowski, S. and Rock, C.O. (1981) Regulation of coenzyme A biosynthesis. *J. Bacteriol.* **148**, 926–932 [PubMed](#)
- 7 Brand, L.A. and Strauss, E. (2005) Characterization of a new pantothenate kinase isoform from *Helicobacter pylori*. *J. Biol. Chem.* **280**, 20185–20188 [CrossRef PubMed](#)
- 8 Yang, K., Eyobo, Y., Brand, L.A., Martynowski, D., Tomchick, D., Strauss, E. and Zhang, H. (2006) Crystal structure of a type III pantothenate kinase: insight into the mechanism of an essential coenzyme A biosynthetic enzyme universally distributed in bacteria. *J. Bacteriol.* **188**, 5532–5540 [CrossRef PubMed](#)
- 9 Dye, C., Watt, C.J., Bleed, D.M., Hosseini, S. and Raviglione, M.C. (2005) Evolution of tuberculosis control and prospects for reducing tuberculosis incidence, prevalence, and deaths globally. *JAMA* **293**, 2767–2775 [CrossRef PubMed](#)
- 10 Das, S., Kumar, P., Bhor, V., Suroliya, A. and Vijayan, M. (2006) Invariance and variability in bacterial PanK: a study based on the crystal structure of *Mycobacterium tuberculosis* PanK. *Acta Crystallogr. Sect. D Biol. Crystallogr.* **62**, 628–638 [CrossRef](#)
- 11 Chetnani, B., Das, S., Kumar, P., Suroliya, A. and Vijayan, M. (2009) *Mycobacterium tuberculosis* pantothenate kinase: possible changes in location of ligands during enzyme action. *Acta Crystallogr. Sect. D Biol. Crystallogr.* **65**, 312–325 [CrossRef](#)
- 12 Chetnani, B., Kumar, P., Suroliya, A. and Vijayan, M. (2010) *M. tuberculosis* pantothenate kinase: dual substrate specificity and unusual changes in ligand locations. *J. Mol. Biol.* **400**, 171–185 [CrossRef PubMed](#)

- 13 Chetnani, B., Kumar, P., Abhinav, K.V., Chhibber, M., Surolia, A. and Vijayan, M. (2011) Location and conformation of pantothenate and its derivatives in *Mycobacterium tuberculosis* pantothenate kinase: insights into enzyme action. *Acta Crystallogr. Sect. D Biol. Crystallogr.* **67**, 774–783 [CrossRef](#) [PubMed](#)
- 14 Venkatraman, J., Bhat, J., Solapure, S.M., Sandesh, J., Sarkar, D., Aishwarya, S., Mukherjee, K., Datta, S., Malolanarasimhan, K., Bandodkar, B. and Das, K.S. (2012) Screening, identification, and characterization of mechanistically diverse inhibitors of the *Mycobacterium tuberculosis* enzyme, pantothenate kinase (CoaA). *J. Biomol. Screen.* **17**, 293–302 [CrossRef](#) [PubMed](#)
- 15 Björkelid, C., Bergfors, T., Raichurkar, A.K.V., Mukherjee, K., Malolanarasimhan, K., Bandodkar, B. and Jones, T.A. (2013) Structural and biochemical characterization of compounds inhibiting *Mycobacterium tuberculosis* pantothenate kinase. *J. Biol. Chem.* **288**, 18260–18270 [CrossRef](#) [PubMed](#)
- 16 Reddy, B.K.K., Landge, S., Ravishankar, S., Patil, V., Shinde, V., Tantry, S., Kale, M., Raichurkar, A., Menasinakai, S., Mudugal, N.V. et al. (2014) Assessment of *Mycobacterium tuberculosis* pantothenate kinase vulnerability through target knock down and mechanistically diverse inhibitors. *Antimicrob. Agents Chemother.* **58**, 3312–3326 [CrossRef](#) [PubMed](#)
- 17 Buchholz, A., Takors, R. and Wandrey, C. (2001) Quantification of intracellular metabolites in *Escherichia coli* K12 using liquid chromatographic-electrospray ionization tandem mass spectrometric techniques. *Anal. Biochem.* **295**, 129–137 [CrossRef](#) [PubMed](#)
- 18 Zhang, Y.-M., Frank, M.W., Virga, K.G., Lee, R.E., Rock, C.O. and Jackowski, S. (2004) Acyl carrier protein is a cellular target for the antibacterial action of the pantothenamide class of pantothenate antimetabolites. *J. Biol. Chem.* **279**, 50969–50975 [CrossRef](#) [PubMed](#)
- 19 Awasthy, D., Ambady, A., Bhat, J., Sheikh, G., Ravishankar, S., Subbulakshmi, V., Mukherjee, K., Sambandamurthy, V. and Sharma, U. (2010) Essentiality and functional analysis of type I and type III pantothenate kinases of *Mycobacterium tuberculosis*. *Microbiology* **156**, 2691–2701 [CrossRef](#) [PubMed](#)
- 20 Virga, K.G., Zhang, Y.-M., Leonardi, R., Ivey, R.A., Hevener, K., Park, H.-W., Jackowski, S., Rock, C.O. and Lee, R.E. (2006) Structure–activity relationships and enzyme inhibition of pantothenamide-type pantothenate kinase inhibitors. *Bioorg. Med. Chem.* **14**, 1007–1020 [CrossRef](#) [PubMed](#)
- 21 Hughes, S.J., Antoshchenko, T., Kim, K.P., Smil, D. and Park, H.-W. (2014) Structural characterization of a new *N*-substituted pantothenamide bound to pantothenate kinases from *Klebsiella pneumoniae* and *Staphylococcus aureus*. *Proteins* **82**, 1542–1548 [CrossRef](#)
- 22 Rowan, A.S., Nicely, N.I., Cochrane, N., Wlassoff, W.A., Claiborne, A. and Hamilton, C.J. (2009) Nucleoside triphosphate mimicry: a sugar triazolyl nucleoside as an ATP-competitive inhibitor of *B. anthracis* pantothenate kinase. *Org. Biomol. Chem.* **7**, 4029–4036 [CrossRef](#) [PubMed](#)
- 23 Hong, B.S., Yun, M.K., Zhang, Y.-M., Chohnan, S., Rock, C.O., White, S.W., Jackowski, S., Park, H.-W. and Leonardi, R. (2006) Prokaryotic type II and type III pantothenate kinases: the same monomer fold creates dimers with distinct catalytic properties. *Structure* **14**, 1251–1261 [CrossRef](#) [PubMed](#)
- 24 Begley, T.P., Kinsland, C. and Strauss, E. (2001) The biosynthesis of coenzyme A in bacteria. *Vitam. Horm.* **61**, 157–171 [CrossRef](#) [PubMed](#)
- 25 Manoj, N., Strauss, E., Begley, T.P. and Ealick, S.E. (2003) Structure of human phosphopantothienylcysteine synthetase at 2.3 Å resolution. *Structure* **11**, 927–936 [CrossRef](#) [PubMed](#)
- 26 Strauss, E., Kinsland, C., Ge, Y., McLafferty, F.W. and Begley, T.P. (2001) Phosphopantothienylcysteine synthetase from *Escherichia coli*: identification and characterization of the last unidentified coenzyme A biosynthetic enzyme in bacteria. *J. Biol. Chem.* **276**, 13513–13516 [CrossRef](#) [PubMed](#)
- 27 Strauss, E., Zhai, H., Brand, L.A., McLafferty, F.W. and Begley, T.P. (2004) Mechanistic studies on phosphopantothienylcysteine decarboxylase: trapping of an enethiolate intermediate with a mechanism-based inactivating agent. *Biochemistry* **43**, 15520–15533 [CrossRef](#) [PubMed](#)
- 28 Patrone, J.D., Yao, J., Scott, N.E. and Dotson, G.D. (2009) Selective inhibitors of bacterial phosphopantothienylcysteine synthetase. *J. Am. Chem. Soc.* **131**, 16340–16341 [CrossRef](#) [PubMed](#)
- 29 van der Westhuyzen, R., Hammons, Justin, C., Meier, J.L., Dahesh, S., Moolman, Wessel, J.A., Pelly, S.C., Nizet, V., Burkart, M.D. and Strauss, E. (2012) The antibiotic Cj-15,801 is an antimetabolite that hijacks and then inhibits CoA biosynthesis. *Chem. Biol.* **19**, 559–571 [CrossRef](#) [PubMed](#)
- 30 Sugie, Y., Dekker, K.A., Hirai, H., Ichiba, T., Ishiguro, M., Shiomi, Y., Sugiura, A., Brennan, L., Duignan, J., Huang, L.H. et al. (2001) Cj-15,801, a novel antibiotic from a fungus, *Seimatosporium sp.* *J. Antibiot.* **54**, 1060–1065 [CrossRef](#) [PubMed](#)
- 31 Daugherty, M., Polanuyer, B., Farrell, M., Scholle, M., Lykidis, A., De Crecy-Lagard, V. and Osterman, A. (2002) Complete reconstitution of the human coenzyme A biosynthetic pathway via comparative genomics. *J. Biol. Chem.* **277**, 21431–21439 [CrossRef](#) [PubMed](#)
- 32 Aghajanian, S. and Worrall, D.M. (2002) Identification and characterization of the gene encoding the human phosphopantetheine adenyllyltransferase and dephospho-CoA kinase bifunctional enzyme (CoA synthase). *Biochem. J.* **365**, 13–18 [PubMed](#)
- 33 Zhyvoloup, A., Nemazany, I., Babich, A., Panasyuk, G., Pobigailo, N., Vudmaska, M., Naidenov, V., Kukharengo, O., Palchevskii, S., Savinska, L. et al. (2002) Molecular cloning of CoA synthase: the missing link in CoA biosynthesis. *J. Biol. Chem.* **277**, 22107–22110 [CrossRef](#) [PubMed](#)
- 34 de Jonge, B.L.M., Walkup, G.K., Lahiri, S.D., Huynh, H., Neckermann, G., Utley, L., Nash, T.J., Brock, J., San Martin, M., Kutschke, A. et al. (2013) Discovery of inhibitors of 4'-phosphopantetheine adenyllyltransferase (PPAT) to validate PPAT as a target for antibacterial therapy. *Antimicrob. Agents Chemother.* **57**, 6005–6015 [CrossRef](#) [PubMed](#)
- 35 Miller, J.R., Thanabal, V., Melnick, M.M., Lall, M., Donovan, C., Sarver, R.W., Lee, D.-Y., Ohren, J. and Emerson, D. (2010) The use of biochemical and biophysical tools for triage of high-throughput screening hits: a case study with *Escherichia coli* phosphopantetheine adenyllyltransferase. *Chem. Biol. Drug Design.* **75**, 444–454 [CrossRef](#)
- 36 Zhao, L., Allanson, N.M., Thomson, S.P., Maclean, J.K. F., Barker, J.J., Primrose, W.U., Tyler, P.D. and Lewendon, A. (2003) Inhibitors of phosphopantetheine adenyllyltransferase. *Eur. J. Med. Chem.* **38**, 345–349 [CrossRef](#) [PubMed](#)
- 37 Cheng, C.-S., Jia, K.-F., Chen, T., Chang, S.-Y., Lin, M.-S. and Yin, H.-S. (2013) Experimentally validated novel inhibitors of *Helicobacter pylori* phosphopantetheine adenyllyltransferase discovered by virtual high-throughput screening. *PLoS ONE* **8**, e74271 [CrossRef](#) [PubMed](#)
- 38 Clifton, G., Bryant, S.R. and Skinner, C.G. (1970) *N*¹-(substituted) pantothenamides, antimetabolites of pantothenic acid. *Arch. Biochem. Biophys.* **137**, 523–528 [CrossRef](#) [PubMed](#)
- 39 Strauss, E. and Begley, T.P. (2002) The antibiotic activity of *N*-pentylpantothenamide results from its conversion to ethyldethia-coenzyme A, a coenzyme A antimetabolite. *J. Biol. Chem.* **277**, 48205–48209 [CrossRef](#) [PubMed](#)
- 40 Thomas, J. and Cronan, J.E. (2010) Antibacterial activity of *N*-pentylpantothenamide is due to inhibition of coenzyme A synthesis. *Antimicrob. Agents Chemother.* **54**, 1374–1377 [CrossRef](#) [PubMed](#)
- 41 Mercer, A.C. and Burkart, M.D. (2007) The ubiquitous carrier protein: a window to metabolite biosynthesis. *Nat. Prod. Rep.* **24**, 750–773 [CrossRef](#) [PubMed](#)
- 42 Leonardi, R., Chohnan, S., Zhang, Y.-M., Virga, K.G., Lee, R.E., Rock, C.O. and Jackowski, S. (2005) A pantothenate kinase from *Staphylococcus aureus* refractory to feedback regulation by coenzyme A. *J. Biol. Chem.* **280**, 3314–3322 [CrossRef](#) [PubMed](#)
- 43 Mercer, A.C., Meier, J.L., Hur, G.H., Smith, A.R. and Burkart, M.D. (2008) Antibiotic evaluation and *in vivo* analysis of alkynyl coenzyme A antimetabolites in *Escherichia coli*. *Bioorg. Med. Chem. Lett.* **18**, 5991–5994 [CrossRef](#) [PubMed](#)
- 44 Akinnusi, T.O., Vong, K. and Auclair, K. (2011) Geminal dialkyl derivatives of *N*-substituted pantothenamides: synthesis and antibacterial activity. *Bioorg. Med. Chem.* **19**, 2696–2706 [CrossRef](#) [PubMed](#)
- 45 van Wyk, M. and Strauss, E. (2008) Development of a method for the parallel synthesis and purification of *N*-substituted pantothenamides, known inhibitors of coenzyme A biosynthesis and utilization. *Org. Biomol. Chem.* **6**, 4348–4355 [CrossRef](#) [PubMed](#)
- 46 Spry, C., van Schalkwyk, D.A., Strauss, E. and Saliba, K.J. (2010) Pantothenate utilization by *Plasmodium* as a target for antimalarial chemotherapy. *Infect. Disord. Drug Targets* **10**, 200–216 [CrossRef](#) [PubMed](#)
- 47 Spry, C., Macuamule, C., Lin, Z., Virga, K.G., Lee, R.E., Strauss, E. and Saliba, K.J. (2013) Pantothenamides are potent, on-target inhibitors of *Plasmodium falciparum* growth when serum pantothenase is inactivated. *PLoS ONE* **8**, e54974 [CrossRef](#) [PubMed](#)
- 48 de Villiers, M., Macuamule, C., Spry, C., Hyun, Y.-M., Strauss, E. and Saliba, K.J. (2013) Structural modification of pantothenamides counteracts degradation by pantothenase and improves antiplasmodial activity. *ACS Med. Chem. Lett.* **4**, 784–789 [CrossRef](#)

- 49 Jansen, P.A.M., Hermkens, P.H.H., Zeeuwen, P.L.J.M., Botman, P.N.M., Blaauw, R.H., Burghout, P., van Galen, P.M., Mouton, J.W., Rutjes, F.P.J.T. and Schalkwijk, J. (2013) Combination of pantothenamides with vanin inhibitors as a novel antibiotic strategy against Gram-positive bacteria. *Antimicrob. Agents Chemother.* **57**, 4794–4800
[CrossRef](#) [PubMed](#)
- 50 van der Westhuyzen, R. and Strauss, E. (2010) Michael acceptor-containing coenzyme A analogues as inhibitors of the atypical coenzyme A disulfide reductase from *Staphylococcus aureus*. *J. Am. Chem. Soc.* **132**, 12853–12855 [CrossRef](#) [PubMed](#)
-

Received 6 May 2014

doi:10.1042/BST20140131

Turnover-Dependent Covalent Inactivation of *Staphylococcus aureus* Coenzyme A-Disulfide Reductase by Coenzyme A-Mimetics: Mechanistic and Structural Insights

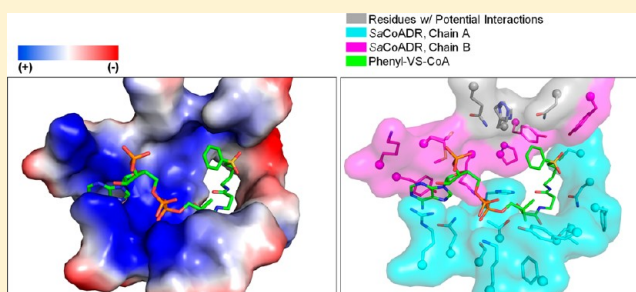
Bret D. Wallace,^{§,||} Jonathan S. Edwards,^{§,||,‡} Jamie R. Wallen,^{#,Δ} Wessel J. A. Moolman,[⊥] Renier van der Westhuyzen,[⊥] Erick Strauss,^{*,⊥} Matthew R. Redinbo,^{*,§} and Al Claiborne^{*,#}

[§]Departments of Chemistry and Biochemistry and Biophysics, University of North Carolina at Chapel Hill, Chapel Hill, North Carolina 27599-3290, United States

[#]Center for Structural Biology, Wake Forest School of Medicine, Winston-Salem, North Carolina 27157, United States

[⊥]Department of Biochemistry, Stellenbosch University, Matieland 7602, South Africa

ABSTRACT: Disruption of the unusual thiol-based redox homeostasis mechanisms in *Staphylococcus aureus* represents a unique opportunity to identify new metabolic processes and new targets for intervention. Targeting uncommon aspects of CoASH biosynthetic and redox functions in *S. aureus*, the antibiotic CJ-15,801 has recently been demonstrated to be an antimetabolite of the CoASH biosynthetic pathway in this organism; CoAS-mimetics containing α,β -unsaturated sulfone and carboxyl moieties have also been exploited as irreversible inhibitors of *S. aureus* coenzyme A-disulfide reductase (SaCoADR). In this work we have determined the crystal structures of three of these covalent SaCoADR-inhibitor complexes, prepared by inactivation of wild-type enzyme during turnover. The structures reveal the covalent linkage between the active-site Cys43-S _{γ} and C _{β} of the vinyl sulfone or carboxyl moiety. The full occupancy of two inhibitor molecules per enzyme dimer, together with kinetic analyses of the wild-type/C43S heterodimer, indicates that half-sites-reactivity is not a factor during normal catalytic turnover. Further, we provide the structures of SaCoADR active-site mutants; in particular, Tyr419'-OH plays dramatic roles in directing intramolecular reduction of the Cys43-SSCoA redox center, in the redox asymmetry observed for the two FAD per dimer in NADPH titrations, and in catalysis. The two conformations observed for the Ser43 side chain in the C43S mutant structure lend support to a conformational switch for Cys43-S _{γ} during its catalytic Cys43-SSCoA/Cys43-SH redox cycle. Finally, the structures of the three inhibitor complexes provide a framework for design of more effective inhibitors with therapeutic potential against several major bacterial pathogens.



The “thiolome” has been referred to as the proteome-wide redox state of cysteine residues.¹ Coenzyme A-disulfide reductase (CoADR), other flavoprotein disulfide reductases, and the thioredoxin fold proteins that include the putative bacilliredoxin, YphP, account for a major portion of the thiolomes in *Staphylococcus aureus* and *Bacillus anthracis*.^{2–6} We extend the definition of the thiolome to apply to the diversity in the structure, function, and distribution of low-molecular-weight thiols — the metabolite-based thiolome. CoASH and the recently identified bacillithiol⁷ function together with the protein-based thiolome to maintain redox homeostasis in these organisms.⁶ Bioinformatics analyses⁸ have classified flavoprotein disulfide reductases into three subgroups: the disulfide reductases that include GR, the alkyl hydroperoxide reductases that include thioredoxin reductase, and the peroxidase-oxidase-reductases that include CoADR, the CoADR-RHD isoform — which contains a C-terminal rhodanese homology domain, as characterized in *B. anthracis*⁹ and *Shewanella loihica*¹⁰ — and the *Pelobacter carbinolicus* “NAD(FAD)-dependent dehydrogenase” isoform encoded by the Pcar_0429 locus.¹¹ In spite of

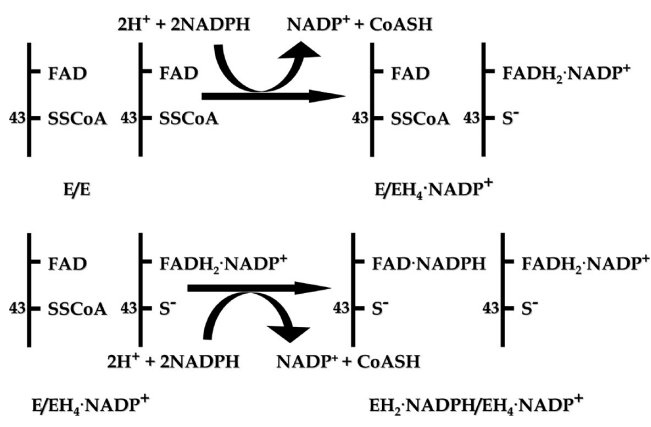
clear similarities with regard to the reactions that they catalyze, the CoADR enzymes are mechanistically distinct from the disulfide reductase subgroup enzymes, in that a single active-site cysteine (SaCoADR Cys43 and BaCoADR Cys42, respectively) reacts with the (CoAS)₂ substrate to form a Cys-SSCoA mixed disulfide redox center, which represents the resting state of the enzyme and is reduced by NAD(P)H via the flavin cofactor in the catalytic cycle.^{12,13}

Kinetic and structural analyses of the SaCoADR and BaCoADR enzymes have revealed several important features relevant to catalysis. Detailed equilibrium titration studies have demonstrated significant asymmetric behavior for both SaCoADR¹³ and BaCoADR,² which occur as homodimeric enzymes. NADPH titrations of SaCoADR lead to an asymmetric EH₂·NADPH/EH₄·NADP⁺ complex in which only one FAD/dimer is reduced (Scheme 1). However, crystal structures of SaCoADR¹⁴ and

Received: July 31, 2012

Revised: September 5, 2012

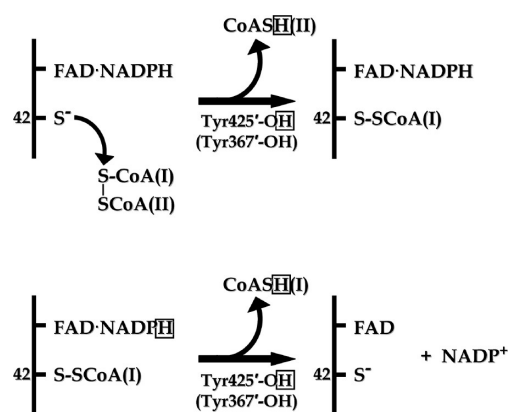
Published: September 6, 2012

Scheme 1. Reductive Intermediates on NADPH Titration of *SaCoADR*

BaCoADR,² in oxidized form and in the reduced *BaCoADR* $\text{EH}_2\cdot\text{CoASH}\cdot\text{NAD(P)H}$ complex, provide no structural basis for such asymmetric behavior with NAD(P)H . In a recent study *CoAS*-mimetics were designed and used to inactivate *SaCoADR* by conjugate addition of the Cys43-thiolate in turnover.¹⁵ However, since the stoichiometry of the modification (i.e., whether full inactivation requires modification of one or both Cys43/dimer) was not determined, these results could not provide additional insight into the apparent asymmetric behavior.

In addition, active-site analyses of the two *CoADR* structures gave clear evidence for intersubunit cooperation, if not cooperativity, in catalysis. In the 1.5 Å structure of oxidized (FAD, Cys43-SSCoA) *SaCoADR*, a well-ordered chloride ion 3.8 Å from the *CoAS*-sulfur (chain A) receives hydrogen bonds from several donors including Tyr361'-OH (chain B, 3.1 Å). The position of this chloride ion was taken as the anchor position for the sulfur of the modeled *CoAS*-II that represents the *CoASH* product formed on attack of $(\text{CoAS})_2$ by Cys43-S⁻. A second conserved Tyr (Tyr419', chain B) is 4.2 Å from Cys43-S_γ (chain A), but the Tyr361'-OH-Cl⁻ interaction, in particular, suggested that the latter served the primary role in protonation of the departing *CoAS*-II thiolate. This working conclusion came into question with the structural analysis of the 2.3 Å *BaCoADR* $\text{EH}_2\cdot\text{CoASH}\cdot\text{NAD(P)H}$ complex, which provides evidence for a reduced enzyme form in which Cys42 adopts an alternate, external conformation. Though not supportive of either Cys42-S⁻ → FAD charge-transfer or in-line nucleophilic attack on the *CoAS*-I sulfur of $(\text{CoAS})_2$, this Cys42-S⁻ interacts strongly with Tyr367'-OH (3.0 Å) and, in particular, Tyr425'-OH (2.9 Å) (equivalent to *SaCoADR* Tyr361' and Tyr419' respectively), suggesting that the latter in fact serves as the primary proton donor.

Given the structural equivalence of Tyr425 and human GR His467, the essential acid-base catalyst in GS-I protonation,¹⁶ kinetic analyses were performed on *BaCoADR* and the corresponding Tyr → Phe mutants to further elucidate the catalytic importance of Tyr367 and Tyr425.² Compared to a wild-type activity of $k_{\text{cat}} = 27 \text{ s}^{-1}$, the Y367F and Y425F mutants exhibited k_{cat} values of 7 s^{-1} (26%) and 0.9 s^{-1} (3%) with NADH and $(\text{CoAS})_2$ respectively, with no activity reported for the Y367,425F double mutant. These data suggest that while Tyr367 (*SaCoADR* Tyr361) does play a cryptic role as alternate proton donor, Tyr425 is the primary acid-base catalyst (Scheme 2).

Scheme 2. Proton Donors and Their Proposed Roles in *BaCoADR*

Kinetic parameters determined by stopped-flow initial velocity are very similar for *Sa*- and *BaCoADR*, with $k_{\text{cat}} = 27\text{--}29 \text{ s}^{-1}$, $K_{\text{m}}(\text{NADPH})$ ca. $1 \mu\text{M}$, and $K_{\text{m}}[(\text{CoAS})_2] = 2\text{--}6 \mu\text{M}$; *BaCoADR* differs primarily in that it exhibits dual NAD(P)H specificity. However, in stopped-flow studies in which an alternate disulfide substrate, MMTS ($K_{\text{m}}^{\text{app}} = 78 \mu\text{M}$ and $k_{\text{cat}} = 6.4 \text{ s}^{-1}$, with wild-type *SaCoADR*), was used,⁹ the Y361F mutant was actually found to be more efficient ($k_{\text{cat}}/K_{\text{m}} = 2.2 \times 10^5 \text{ M}^{-1} \text{ s}^{-1}$) than wild-type enzyme ($k_{\text{cat}}/K_{\text{m}} = 8.2 \times 10^4 \text{ M}^{-1} \text{ s}^{-1}$); Y419F and Y361,419F mutants were only 3–5% as efficient ($k_{\text{cat}}/K_{\text{m}} = 2.1\text{--}4.0 \times 10^3 \text{ M}^{-1} \text{ s}^{-1}$) as wild-type enzyme. It is important to note that only the internal redox step, i.e., the reduction of Cys43-SSCH₃ by $\text{E}(\text{FADH}_2)$ that results in CH₃SH formation requires a proton donor in MMTS turnover (ref 9, Scheme 4); with $(\text{CoAS})_2$ both internal and external (attack of Cys43 on *CoAS*-I) steps require proton donors.

While the case for intersubunit cooperation in *CoADR* is therefore supported by both structural and kinetic studies, the question remains as to whether the redox asymmetry seen with *SaCoADR* in particular is translated to the catalytic mechanism. If it is, are Tyr361 and/or Tyr419 important in intersubunit communication? Early studies on mercuric ion reductase¹⁷ strongly supported active-site communication in the dimeric enzyme and led to an alternating sites hypothesis for catalysis. Although the catalytic core has spectroscopic and NADP(H) binding properties identical to those of the full-length protein, the high-resolution crystal structure was not informative¹⁸ on the mechanism of functional asymmetry. *Plasmodium falciparum* thioredoxin reductase is another disulfide reductase subgroup enzyme for which intersubunit cooperativity was considered in early work.¹⁹ While heterodimers of wild-type enzyme and either C88A or C535A mutants are ca. 50% active with thioredoxin, the wild-type/C88,535A heterodimer is inactive. Recent studies with the flavin oxidoreductase LuxG²⁰ and with three bacterial biotin carboxylases²¹ provide detailed kinetic and structural evidence for half-sites-reactivity.

In the interest of evaluating the roles of the *SaCoADR* Tyr residues, the role of intersubunit cooperativity in catalysis, and the possible link between Tyr361 and/or Tyr419 and this functional asymmetry, we have taken several approaches. First, we determined the catalytic properties of the *SaCoADR* wild-type/C43S heterodimer and the high-resolution structure of the C43S mutant. Second, we performed reductive titrations on each of the Tyr → Phe mutants and determined their crystal structures. Finally, we also determined the crystal structures for

the SaCoADR enzymes as inhibited by each of the three different Michael acceptor-containing CoAS-mimetics used in the recent CoADR inhibition study.¹⁵ Taken together, the results provide a perspective on intersubunit cooperation in CoADR and on inhibition of this as yet unexploited drug target that establishes a platform for probing the thiol-based redox networks in *S. aureus*, *B. anthracis*, and other pathogens.⁶

■ EXPERIMENTAL PROCEDURES

Materials. NADPH and NADP⁺ were purchased from Boehringer Mannheim or Sigma-Aldrich. Adenosine 2',5'-diphosphate agarose was purchased from Sigma. (CoAS)₂ was either purchased from Fluka or prepared as described previously.¹⁵ All other chemicals, as purchased from sources described previously,⁹ were of the best grades available.

Expression and Purification of Wild-Type and Mutant SaCoADRs. Full-length wild-type and mutant (Y361F, Y419F, Y361,419F, and C43S) SaCoADR proteins were expressed and purified as previously described.^{9,13} Standard spectrophotometric SaCoADR activity assays and anaerobic titrations were performed as previously described for BaCoADR.² The following extinction coefficients were used (in M⁻¹ cm⁻¹): NADPH, 6200 at 340 nm; NADP⁺, 18000 at 260 nm; (CoAS)₂, 33600 at 260 nm; and wild-type SaCoADR, 12800 at 452 nm.¹³

Co-Expression and Purification of Wild-Type/C43S SaCoADR Heterodimers in *Escherichia coli* C41(DE3). The procedure for coexpression and purification of SaCoADR homo- and heterodimers followed the general protocol described by Krnajski et al.¹⁹ *E. coli* C41(DE3) cells were transformed with an Amp^r plasmid containing the wild-type *cdr* with an N-terminal *Strep*-tag and a *Cm^r* plasmid encoding the C43S mutant (N-terminal His-tag). The protocol for large-scale growth and expression was essentially as described by Wallen et al.,⁹ but with both Amp and *Cm* supplementation of the growth media. Cell-free extracts were processed as in Luba et al.,¹³ including both ammonium sulfate fractionation and affinity chromatography with adenosine 2',5'-diphosphate agarose. The enriched total SaCoADR pool (ca. 125 mg of SaCoADR, based on A₄₅₀), in 20 mM Tris-HCl, 50 mM sodium phosphate, pH 8.0, containing 4 M NaCl, was applied to a Ni-NTA Superflow (Qiagen) column equilibrated in the sodium phosphate buffer containing 0.5 M NaCl. Some SaCoADR was collected in the flow-through, presumably the *Strep*-tagged wild-type homodimer, and the bound enzyme was eluted with a gradient from 0 → 250 mM imidazole in the phosphate/NaCl buffer. Approximately 90 mg of SaCoADR, presumably heterodimer plus C43S homodimer, resulted at this stage. When this pool was applied directly to a *Strep*Tactin column, a large volume containing presumed C43S homodimer flowed through the column. Elution, with the desthiobiotin-containing buffer provided by the vendor, gave a small amount of presumed wild-type/C43S heterodimer. A yield of ca. 3.6 mg of purified SaCoADR *Strep*/His-tagged wild-type/C43S heterodimer was estimated by A₄₅₂.

Crystallizations. Crystals of C43S, Y361F, Y419F, and Y361,419F SaCoADR were obtained, largely following the protocol for wild-type enzyme.¹⁴ For the C43S mutant, the optimal condition was 31% PEG 600, 0.4 M MgCl₂, and 0.1 M HEPES, pH 7.2, containing 1.3 mM NADP⁺ and 0.4 mM (CoAS)₂. The Tyr361 and Tyr419 mutants behaved similarly, in the absence of (CoAS)₂. Optimal conditions were 35–37% PEG 600, 0.3–0.4 M MgCl₂, and 0.1 M HEPES, pH 7.5, plus 1.3 mM NADP⁺. The best Y361,419F mutant crystals were

obtained in a nearly identical protocol, but with 27% PEG 600 and 0.4 M MgCl₂ at pH 7.2. Growth and handling of crystals for data collection followed the procedures published for wild-type SaCoADR.¹⁴ For preparation of cocrystals of wild-type SaCoADR with the three Michael acceptor-containing CoAS-mimetics [prepared as described previously¹⁵], the enzyme was first reduced using a 10-fold molar excess of NADPH:enzyme to ensure proper inhibitor binding, followed immediately by the addition of a 20:1 molar ratio of each of the respective inhibitors. After a 1-h incubation on ice, the reduced enzyme–inhibitor complex was buffer exchanged into 10 mM HEPES, pH 7.2, using a 30 kDa MWCO Amicon concentrator, and subsequently concentrated to >10 mg/mL. Sitting drop, vapor diffusion crystallization experiments were performed as previously detailed.¹⁴ Crystal nucleation formed within 3 days, growing into large crystals after 5 days. Crystals were looped and flash frozen in liquid nitrogen in preparation for X-ray data collection.

■ Data Collection, Structure Solution, and Refinements.

X-ray diffraction data for all SaCoADR mutants were collected either in-house (C43S, Y361F) on a Rigaku Saturn-92 CCD detector as described for native BaCoADR² or at beamlines X25 (Y419F) and X26C (Y361,419F) of the National Synchrotron Light Source, using ADSC Quantum-315 and Quantum-4 CCD detectors, respectively. Data sets were indexed, integrated, and scaled in d*TREK,²² with model building and refinements being carried out using CNS²³ and the 1.5 Å wild-type SaCoADR structure (PDB entry 1YQZ) as the starting model. Final refinements were performed using TLS²⁴ plus restrained refinement in REFMACS,²⁵ with COOT²⁶ being applied for manual rebuilding and addition of waters. X-ray diffraction data for the inhibitor complexes were collected at the Advanced Photon Source at Argonne National Laboratories using the SER-CAT ID-23 beamline. Crystals were indexed in the space group P2₁, with unit cells of *a* = 76.5 Å, *b* = 64.8 Å, *c* = 94.6 Å, and β = 105°, α, γ = 90.0°. The asymmetric unit was composed of two 51 kDa monomers. Diffraction data were indexed, integrated, and scaled using HKL2000.²⁷ Table 1 summarizes the data collection statistics for all structures. The inhibitor complex structures were phased by molecular replacement using Phaser²⁸ and the wild-type SaCoADR structure. Positive density was found in the F_o – F_c SA-omit maps for the inhibitors which were covalently bound to Cys43 in the active site. Ligand models and parameter files were generated using the ProDRG server and JLigand.²⁹ Structures were refined using simulated annealing, torsion angle, and B-factor refinement using the Phenix software suite.³⁰ Manual refinement of protein residues and inhibitor models was completed using COOT. Refinement statistics for all models are summarized in Table 2.

■ RESULTS

Spectral and Redox Properties of SaCoADR Tyr Mutants. Luba et al.¹³ reported the results for dithionite and NADPH titrations of wild-type and C43S SaCoADR. With dithionite, the first equiv/FAD clearly reduces each Cys43-SSCoA in each subunit of the wild-type dimer as evidenced by a stoichiometric decrease in flavin fluorescence, with only a minor change in the absorbance spectrum. With the second equivalent of dithionite/FAD, the flavin is stoichiometrically reduced. Importantly, it should be noted that no EH₂-like charge-transfer intermediate is observed at 1 equiv of dithionite/FAD. Moreover, the same titration with wild-type BaCoADR²

Table 1. Data Collection Statistics for Wild-type SaCoADR Complexes with the Three Michael Acceptor-Containing CoAS-Mimetics and for SaCoADR C43S and Tyr Mutants

	C43S	Y361F	Y419F	Y361,419F	ErVC-CoA	MeVS-CoA	PHVS-CoA
X-ray source	LAB ^a	LAB	X25 ^b	X26C ^c	APS SER-CAT ID-23 ^d	APS SER-CAT ID-23	APS SER-CAT ID-23
wavelength (Å)	1.5418	1.5418	1.1000	1.1000	1.0000	1.0000	1.0000
space group	P21	P21	P21	P21	P21	P21	P21
Cell dimensions							
a, b, c (Å)	76.0, 65.4, 94.5	75.9, 65.1, 94.4	76.2, 65.4, 94.6	76.2, 65.5, 94.7	76.5, 64.8, 94.6	76.5, 64.8, 94.6	76.5, 64.8, 94.6
α, β, γ (deg)	90, 105, 90	90, 105, 90	90, 105, 90	90, 105, 90	90, 105, 90	90, 105, 90	90, 105, 90
resolution (Å)	53.16–1.70 (1.76–1.70) ^e	53.00–1.80 (1.86–1.80)	51.35–1.50 (1.55–1.50)	53.29–1.50 (1.55–1.50)	50.0–2.40 (2.44–2.40)	50.0–2.00 (2.03–2.00)	50.0–1.83 (1.86–1.83)
unique reflections	98577	82678	137217	140142	33246	62908	79955
completeness (%)	99.9 (99.9)	99.9 (100)	95.4 (79.8)	97.1 (77.5)	98.1 (97.0)	97.2 (85.2)	97.1 (89.9)
redundancy	6.3 (4.3)	7.0 (6.8)	7.3 (6.4)	6.9 (5.2)	7.3 (6.4)	4.1 (2.6)	7.3 (5.6)
I/σ	11.0 (3.1)	7.9 (2.7)	17.1 (4.6)	16.0 (4.1)	38.4 (7.6)	24.1 (2.71)	38.1 (3.98)

^aCollected on a Rigaku Saturn-92 CCD detector using Cu Kα radiation from a MicroMax-007 rotating anode X-ray generator. ^bCollected at beamline X25 of the National Synchrotron Light Source using an ADSC Quantum-315 CCD detector. ^cCollected at beamline X26C of the National Synchrotron Light Source using an ADSC Quantum-4 CCD detector. ^dCollected at beamline ID-23 of the Advanced Photon Source using a Marmosaic 300 CCD detector. ^eNumbers in parentheses represent data for the highest-resolution shell.

also fails to reveal any EH₂-like charge-transfer intermediate at 1 equiv/FAD, giving instead an asymmetric redox intermediate, E(FAD, Cys42-SH)_A/E(FADH₂, Cys42-SSCoA)_B.

The dithionite titration with wild-type SaCoADR also demonstrates that the Cys43-SSCoA redox center is effectively fully reduced before flavin reduction is observed, at equilibrium. The difference in redox potentials, E₂ – E₁, where E₂ represents reduction of oxidized wild-type SaCoADR to the EH₂ (FAD, Cys43-SH) form and E₁ is the redox potential for EH₂ (FAD) → EH₄ (FADH₂),³¹ is ca. 90 mV. In this respect SaCoADR is similar to NADH peroxidase, a peroxidase-oxidase-reductase subgroup enzyme with a Cys42-sulfenic acid (Cys42-SOH) redox center.^{32,33} But, while both nonflavin redox centers (Cys43-SSCoA and Cys42-SOH) are reduced preferentially with dithionite, and with no evidence of intersubunit redox asymmetry, only NADH peroxidase reveals the characteristic EH₂ charge-transfer interaction.

With this in mind, dithionite titrations were performed with SaCoADR Y361F, Y419F, and Y361,419F mutants. Detailed results are presented for the Y419F mutant (Figure 1) and are very similar to those obtained with the double mutant. Both mutants behave quite differently compared to the wild-type enzyme, in that flavin reduction is observed in even early stages of the titration; however, full flavin reduction is only seen at 2 equiv of dithionite/FAD. Flavin reduction is linear with equiv dithionite added through ca. 1.1 equiv/FAD, and 56% of the total ΔA₄₅₄ is seen at 1 equiv/FAD. In contrast with wild-type enzyme, the extents of reduction (at equilibrium) for the flavin and nonflavin centers in Y419F SaCoADR are comparable, demonstrating that Tyr419 plays a major role in contributing to the difference in redox potentials, E₂ – E₁. One explanation, in the absence of a more quantitative analysis, is that Tyr419-OH has a key stabilizing effect on (Cys43-SH + CoASH) in the [Cys43-SSCoA/(Cys43-SH + CoASH)] redox couple, and this is consistent with the structure of the BaCoADR EH₂·CoASH·NAD(P)H complex. In this context, the structure of the reduced BaCoADR Y425F mutant would be quite relevant.

With NADPH, the earlier work of Luba et al.¹³ showed that titration of wild-type SaCoADR was also biphasic, but in a manner strongly supportive of intersubunit redox asymmetry. In contrast to reduction with dithionite, the first equiv of NADPH/FAD clearly gives significant flavin reduction; however, only one flavin/dimer is reduced. The second flavin/dimer is not reduced (at equilibrium) on addition of 2.4 equiv NADPH/FAD. The redox scheme (Scheme 1) proposed to account for these observations is provided above (see the Introduction). NADPH titration of Y419F SaCoADR (Figure 1) also shows flavin reduction in early stages of the experiment. However, in contrast to wild-type SaCoADR, full (100%) formation of the E(FADH₂·NADP⁺, Cys43-SSCoA) intermediate is observed at 1 equiv of NADPH/FAD. The strong FADH₂·NADP⁺ charge-transfer band centered at 750 nm is very similar to that observed with C43S SaCoADR on NADPH titration¹³ and is, at the same time, qualitatively different from that seen in the wild-type SaCoADR experiment. As the second equiv of NADPH/FAD is added, there are saturable, stoichiometric changes in absorbance at 454 and 750 nm, and the presence of excess (beyond 1 equiv/FAD) NADPH is clearly indicated at 340 nm. As NADP⁺ binding to the wild-type SaCoADR EH₂ form is associated with stoichiometric changes in A₄₅₂,¹³ we interpret this phase as representing partial displacement of bound NADP⁺ in the presence of excess NADPH. A similar observation was made in NADPH titrations of C43S SaCoADR. However, it appears as if

Table 2. Crystallographic Refinement Statistics for Wild-type SaCoADR Complexes with the Three Michael Acceptor-Containing CoAS-Mimetics and for SaCoADR C43S and Tyr Mutants

	C43S	Y361F	Y419F	Y361,419F	EtVC-CoA	MeVS-CoA	PhVS-CoA
R-work	0.193 (0.263) ^a	0.185 (0.253)	0.178 (0.272)	0.180 (0.268)	0.164 (0.187)	0.179 (0.262)	0.153 (0.225)
R-free	0.232 (0.318)	0.226 (0.315)	0.201 (0.284)	0.207 (0.275)	0.218 (0.246)	0.226 (0.321)	0.202 (0.362)
molecules per asymmetric unit (AU)	2	2	2	2	2	2	2
no. of amino acids per AU	874 ^b	874	874	874	874	876 ^c	876
no. of waters per AU	939	1216	1268	1285	226	998	1084
average B-factors	22.81	22.24	18.18	16.99	33.67	26.69	20.66
Stereochemical ideality							
bond length rmsd (Å)	0.030	0.006	0.005	0.005	0.02	0.008	0.01
bond angle rmsd (deg)	2.220	1.047	1.032	1.027	1.816	1.719	1.758
Φ,Ψ preferred (%)	98	97	98	98	94.6	97.5	97
Φ,Ψ allowed (%)	1.7	2.6	1.6	1.6	4.4	2.3	2.6
Φ,Ψ outliers (%)	0.23	0.34	0.34	0.34	1.0	0.20	0.34

^aNumbers in parentheses represent data for the highest-resolution shell. ^bSaCoADR dimer. ^cLys438 included in the final refined model.

only a small fraction of enzyme molecules reflect this NADPH effect, as addition of NADPH to 7.6 equiv/FAD gives little if any further change in A_{452} . Two additional observations can be made: (1) there is no spectral evidence for any intersubunit redox asymmetry on NADPH titration of the Y419F mutant, in dramatic contrast to the behavior of wild-type SaCoADR, and (2) while the absorbance changes brought on in the presence of excess NADPH could reflect intramolecular conversion of some E(FADH₂·NADP⁺, Cys43-SSCoA) (EH₂'⁺) to E(FAD·NADPH, Cys43-SH): (a) this would clearly be substoichiometric, and (b) we have no direct evidence for Cys43-SSCoA reduction in the Y419F titration with NADPH; the spectral course is very similar to that for C43S SaCoADR. The crystal structure clearly shows 2 CoAS-/dimer, present as the respective Cys43-SSCoA disulfides, in the Y419F mutant. The NADPH titration behavior of Y361F SaCoADR is quite similar to that of wild-type enzyme, and that of the Y361,419F double mutant is very similar to that described for the Y419F mutant.^a Given that Tyr419 is structurally equivalent with His439, the very important acid-base catalyst required for GS-I protonation in *E. coli* GR,³⁴ the kinetic analysis of the GR H439A mutant also demonstrated an altered, rate-limiting intramolecular electron transfer from that E(FADH₂·NADP⁺) intermediate to the redox-active Cys42-Cys47 disulfide.

Specific Activities of Recombinant SaCoADR Homodimer and Heterodimers. Recombinant wild-type SaCoADR gives specific activities of 29–34 units/mg ($k_{\text{cat}} = 25\text{--}29\text{ s}^{-1}$) in the standard spectrophotometric assay.¹³ The C43S enzyme has only ca. 0.03% activity relative to wild-type SaCoADR. If the intersubunit redox asymmetry observed on NADPH titration is translated to half-the-sites reactivity in the catalytic cycle, the wild-type/C43S heterodimer would be expected to have the same specific activity as wild-type homodimer. Coexpression of wild-type and C43S constructs in *E. coli* C41(DE3) cells resulted in *Strep*-tagged wild-type homodimers, His-tagged C43S homodimers, and *Strep*/His-tagged wild-type/C43S heterodimers. Affinity purification over 2',5'-ADP agarose, Ni-NTA, and *Strep*Tactin resins gave ca. 3.6 mg of wild-type/C43S heterodimer. Specific activities in the standard assay were found to be (1) wild-type homodimer, 25 units/mg; (2) C43S homodimer, 0.3 units/mg; and (3) wild-type/C43S heterodimer, 11 units/mg. The heterodimer is ca. 44% as active as wild-type homodimer; this result is consistent with full-site reactivity in wild-type

SaCoADR. On this basis we conclude that the intersubunit redox asymmetry is not reflected in any half-the-sites catalytic activity.

Crystal Structures of SaCoADR C43S and Tyr Mutants.

The absence of covalently bound CoAS- in C43S CoADR was originally demonstrated by mass spectrometry.¹³ As expected, both dithionite and NADPH titrations led directly to stoichiometric flavin reduction, yielding the E(FADH₂·NADP⁺) complex in the latter case. The structure of C43S SaCoADR has now been determined to 1.7 Å resolution and refined to an R_{free} value of 19.2%. The overall tertiary structures of wild-type and C43S enzyme are very similar, with an all-atom rmsd of 0.12 Å. The prime interest is residue 43 and its environment, including the residues of the CoAS-binding cleft. No density corresponding to CoAS- is observed in the mutant. Figure 2 gives $F_o - F_c$ SA-omit electron density for the C43S SaCoADR active site, including Ser43, Tyr361', Tyr419', and portions of the FAD, together with the refined model. The Ser43 side chain adopts two conformations, and the superposition with the active site of the reduced BaCoADR-CoASH·NADH complex reveals that the primary β ("external") conformation corresponds to that for Cys42-S_γ in the reduced BaCoADR structure,² with optimal Ser43-O_γ—Tyr-OH distances of 2.52 and 2.72 Å, respectively, for Tyr361' and Tyr419'. The secondary α ("internal") conformation gives a proximal Ser43-O_γ to FAD-C4a distance of 2.9 Å but is unfavorable for interactions with either Tyr. In our analysis of the BaCoADR structure, we concluded that the external (now β) conformation resulted from the presence of tightly bound, reduced CoASH (CoAS-I). The present observation with C43S SaCoADR, demonstrating that an external conformation for the isosteric Ser side chain is well populated, indicates that the equivalent Cys43-S_γ conformer may also be populated to a significant extent during catalysis — and in the absence of bound CoASH product. A similar external conformation for Cys44-S_γ in the *E. coli* lipoamide dehydrogenase EH₂ form could correspond to the fluorescent species I identified in dithionite titrations.³⁵ As discussed previously, an α-like conformation for BaCoADR Cys42-S⁻ is required for both the charge-transfer interaction with the flavin and nucleophilic attack on (CoAS)₂.

In the 1.5 Å resolution wild-type SaCoADR structure,¹⁴ a chloride ion was identified in the active site, as confirmed by anomalous dispersion data. A strong interaction with Tyr361'-OH (3.1 Å) was described, and this chloride was taken to

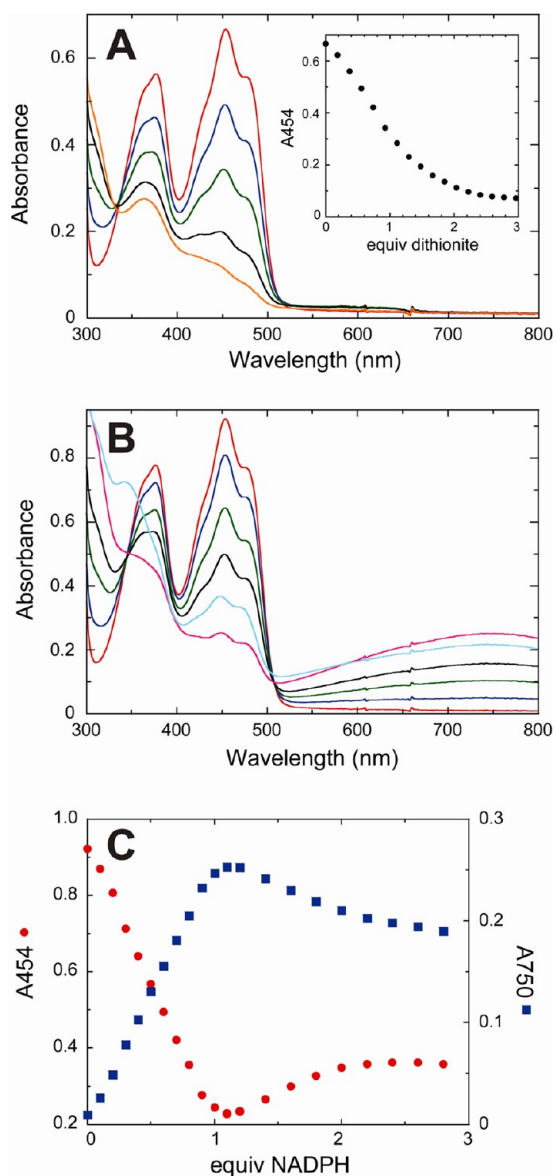


Figure 1. Dithionite and NADPH titrations of Y419F *SaCoADR*. (A) The enzyme (53.6 μM , in 1.0 mL of 50 mM potassium phosphate, pH 7.0, plus 0.5 mM EDTA) was titrated with a 7.5 mM solution of dithionite. Spectra shown, in order of decreasing absorbance at 454 nm, correspond to the addition of 0 (red), 0.56 (blue), 0.93 (green), 1.48 (black), and 2.04 (orange) equiv of dithionite/FAD. Inset: Absorbance change at 454 nm versus added dithionite. The end point corresponds to 1.69 equiv of dithionite/FAD. (B) The enzyme (42.7 μM , prepared as above) was titrated with a 5.4 mM solution of NADPH. Spectra shown, in order of decreasing absorbance at 454 nm, correspond to the addition of 0 (red), 0.2 (blue), 0.4 (green), 0.6 (black), and 1.0 (magenta) equiv of NADPH/FAD. The increase in A_{454} on addition of a second equiv (cyan) of NADPH/FAD corresponds to partial formation of the EH_2NADPH species given in Scheme 1. (C) Absorbance changes at 454 (red circles) and 750 nm (blue squares) versus added NADPH. The end points (ΔA_{454}) correspond to 1.0 and 2.05 equiv of NADPH/FAD.

represent the position of the modeled CoAS-II binding mode. In addition, the external conformation of the Cys42 side chain in the reduced *BaCoADR* complex places Cys42-S γ in contact violation (2.2 Å) with the *SaCoADR* chloride, as determined from a superposition. Though not confirmed by anomalous dispersion, a chloride ion is also found in the same position in

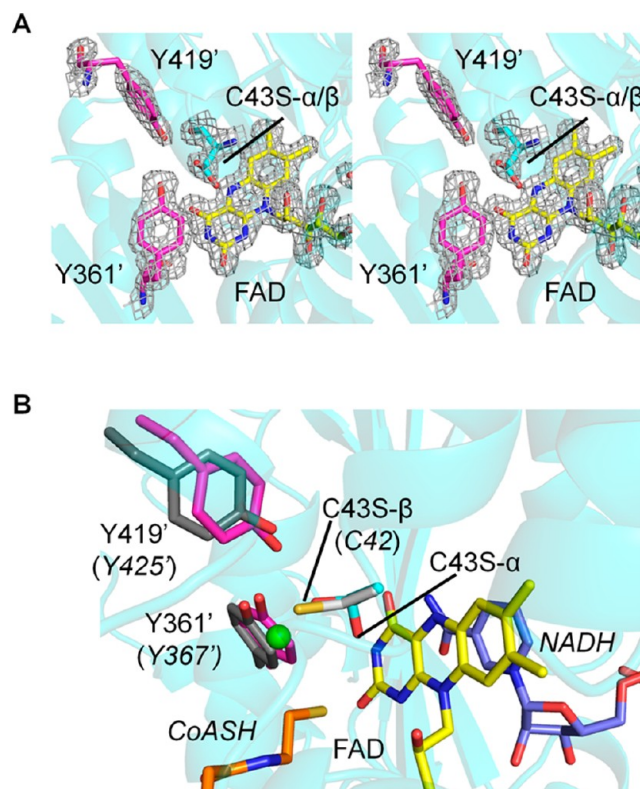


Figure 2. (A) Stereoview of the *SaCoADR* C43S mutant, focusing on the active site. The refined model includes FAD (color-coded by atom type, with portions omitted for clarity), both conformations (α and β) of the Ser43 side chain, and Tyr361' and Tyr419'. An $F_o - F_c$ SA-omit map is shown contoured at 1.5σ . All protein residues are color-coded by atom type, with C α and side chain carbon atoms colored cyan and magenta for chain A and chain B of the homodimer, respectively. Chain A secondary structural elements are rendered as 50% transparent. (B) Superposition of the *SaCoADR* C43S mutant and the *BaCoADR* $\text{EH}_2\text{CoASH}\cdot\text{NADH}$ complex. The refined model for the reduced *BaCoADR* complex includes FAD, CoASH (carbon atoms colored orange), NADH (carbon atoms colored slate blue), Cys42-SH, and active-site Tyr residues 367' and 425'. Color-coding for *SaCoADR* is as in (A), above, with the active-site chloride ion represented as a green sphere. Side chain carbon atoms for *BaCoADR* chain A and chain B residues are colored light gray and dark gray, respectively. Most notable is that the external, β -conformation of the Ser43 side chain in the mutant adopts the same conformation as that of Cys42-SH in the reduced *BaCoADR* structure. Secondary structural elements are rendered as 50% transparent.

each of the mutant structures. While we anticipated that the external β conformer of C43S *SaCoADR* would position Ser43-O γ in contact violation with the chloride, this is not the case. Ser43-O γ in this conformer is shifted relative to Cys42-S γ of the reduced *BaCoADR* complex and is 2.8 Å from the chloride. The observation of this chloride in all mutant structures is generally consistent with the absence of synchrotron reduction — excepting the Y361,419F double mutant — observed with *SaCoADR* versus *BaCoADR*² and *BaCoADR*-RHD⁹ crystals.

The CoAS-binding cleft in wild-type *SaCoADR*¹⁴ consists of residues from both segments of the FAD-binding domain (chain A) as well as from the Interface domain (chain B). In particular, the pantetheine-4'-pyrophosphate component is very important to the CoAS-protein interaction in oxidized wild-type enzyme, with a combination of salt bridges, hydrogen-bonding

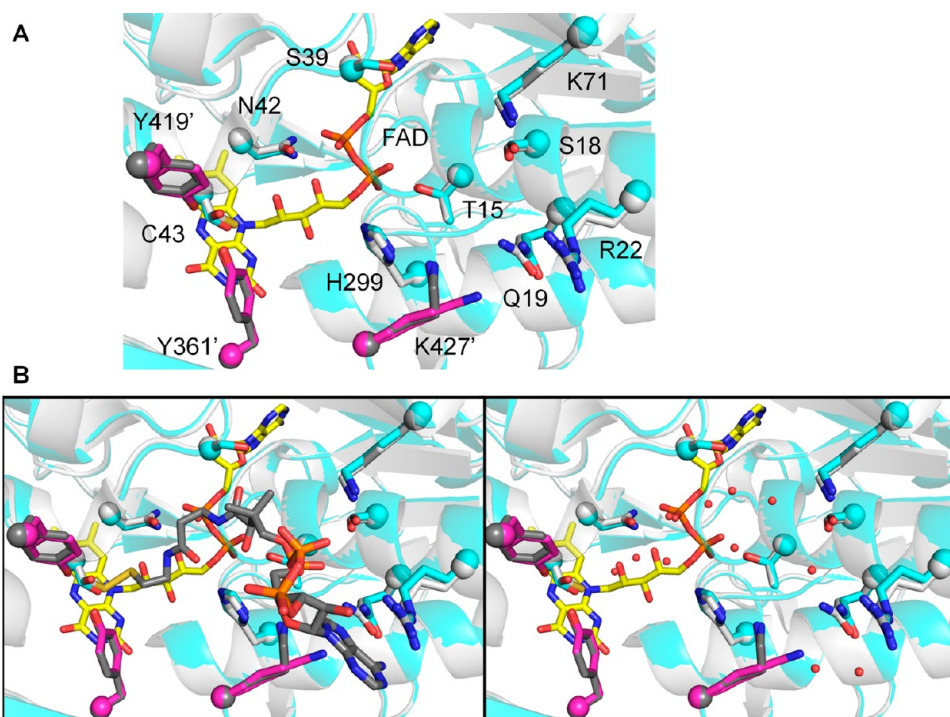


Figure 3. (A) Overlay of the wild-type and C43S mutant *SaCoADR* crystal structures, focusing on the CoAS-binding cleft. In addition to FAD, Cys43-S-, and Tyr361' and Tyr419', key residues known to interact with the CoAS- moiety within the active-site cleft are indicated for the wild-type structure, with carbon atoms colored light gray and dark gray for chains A and B as before. CoAS- has been omitted from the model for clarity. Chain A and B carbon atoms for the mutant are colored cyan and magenta, as before. Notably, side chains lining the cleft maintain the conformations found in the wild-type structure, even in the absence of bound CoAS-. Lys427', however, adopts two conformations in the C43S mutant structure attributed to this absence. Secondary structural elements are rendered as 50% transparent. (B, left) Overlay from (A), above, but including the full Cys43-SSCoA model (CoAS- carbon atoms now in dark gray). (B, right) Same view as in (B, left), but now including the new bound solvent waters (red spheres) that are recruited into the cleft in the absence of CoAS-. CoAS- has been omitted from the wild-type *SaCoADR* model as in (A), above.

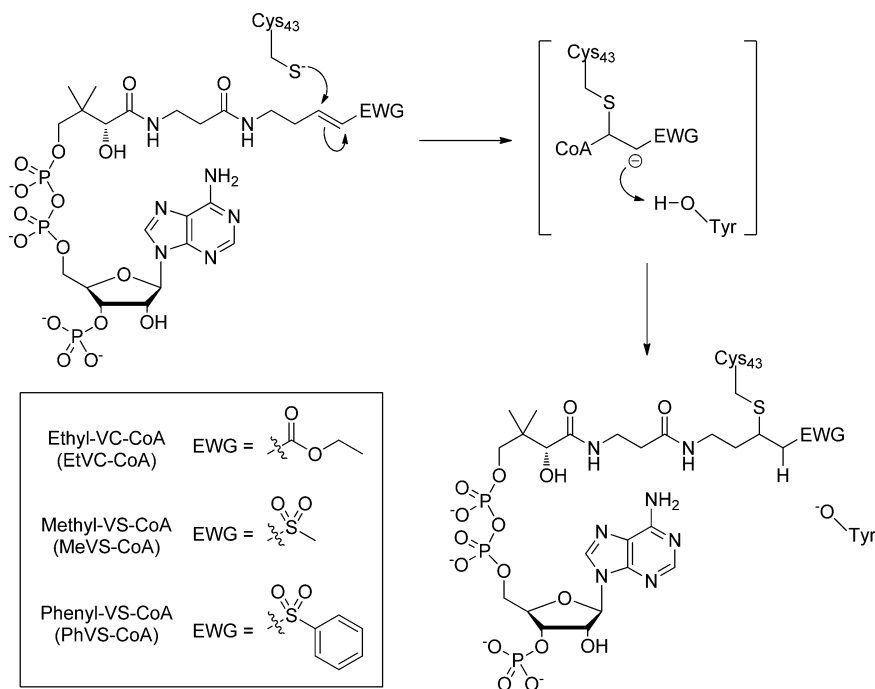
interactions, and hydrophobic contacts involving the pantothenic acid moiety. Even the bound CoASH of the reduced *BaCoADR* complex remains well ordered,² with the analogous protein contacts preserved. We expected that the absence of the large, extended CoAS- in C43S *SaCoADR* could also lead to rearrangements within the cleft, proximal to the FAD in the active site. Figure 3 gives an overlay for wild-type and C43S *SaCoADR*, focusing on several residues known to interact with bound CoAS- in the cleft. There are two significant differences noted within the cleft. The Lys427' side chain normally interacts through a salt bridge with the 4'-phosphopantetheine moiety of bound CoAS-; in the C43S mutant, two conformations are observed for Lys427'. One superimposes very well with the same residue in the wild-type structure, even though CoAS- is absent in the mutant. The second conformer is stabilized by a new hydrogen-bonding interaction with Gln19-O_{ε1}. Second, with similar resolutions of 1.7 and 1.5 Å, there are 11 additional waters in the CoAS-binding cleft of the C43S *CoADR* structure, relative to wild-type. These waters take the place of the bound CoAS-, either replacing the adenosine moiety (two waters) or other CoAS- components (nine waters) more proximal to Ser43. In human erythrocyte GR, a structural analysis showed that NADPH binding physically displaced 14 waters;¹⁶ in both GR and *CoADR*, bound water molecules mimic the polar groups of the respective adenine nucleotide and may contribute to the favorable entropic component for ligand binding.

The structures of Y361F and Y419F *SaCoADR* mutants have been determined to resolutions of 1.8 and 1.5 Å, respectively ($R_{\text{free}} = 21.0$ and 19.7%). All-atom rmsd values are 0.08–0.1 Å

from comparisons with wild-type enzyme, confirming the absence of major structural differences. Both active sites of both asymmetric units contain oxidized Cys43-SSCoA redox centers, even after exposure to synchrotron radiation during data collection. There is no specific perturbation in the juxtaposition of Cys43-SSCoA and FAD that would indicate unfavorable $\text{FADH}_2 \rightarrow \text{Cys43-SSCoA}$ electron transfer. Considering the 40-fold reduction in $k_{\text{cat}}/K_m(\text{MMTS})^9$ and the altered redox properties observed in titrations with the NADPH substrate, both with Y419F *SaCoADR*, and the dramatically reduced activity observed with $(\text{CoAS})_2$ for the equivalent Y425F mutant of *BaCoADR*,² the Y419F *SaCoADR* structure confirms that these are not due to global structural changes in the oxidized enzyme.

The structure of the Y361,419F double mutant, determined to 1.5 Å resolution ($R_{\text{free}} = 20\%$), reveals partial reduction (ca. 50%) of both Cys43-SSCoA per asymmetric unit.⁴ As the behavior of the double mutant in both MMTS reduction kinetics and NADPH titrations is very similar to that of the Y419F mutant, we interpret these catalytic and redox properties as a primary consequence of the Tyr419 replacement. The absence of activity in the $(\text{CoAS})_2$ reduction assay with the equivalent *BaCoADR* double mutant, compared with the residual activity observed with the Y425F mutant, reflects the role of *BaCoADR* Tyr367' as a cryptic proton donor.

Crystal Structures of *SaCoADR*-Inhibitor Complexes. Following on the successful development of irreversible inhibitors of cysteine proteases such as cathepsin K³⁶ and cruzain³⁷ — targeting the respective active-site cysteine residues with electrophilic Michael acceptor-containing substrate analogues — the

Scheme 3. Mechanism-Based Inhibition of SaCoADR by Covalent Modification of the Active Site Cys43 through Nucleophilic Addition to the Michael Acceptor-Containing CoAS-Mimetics


Strauss laboratory recently demonstrated that a similar strategy can be used for the irreversible inhibition of SaCoADR.¹⁵ In their study, Michael acceptor-containing CoAS-mimetics were prepared as electrophilic traps for the active-site Cys43 residue; this was accomplished by replacing the thiol of CoASH with one of three different electron-withdrawing groups, resulting in CoAS-analogues that contained either an α,β -unsaturated ethyl ester (EtVC-CoA), a methyl vinyl sulfone (MeVS-CoA), or a phenyl vinyl sulfone (PhVS-CoA) moiety, respectively (Scheme 3). These mechanism-based inhibitors operate in a two-step process that involves reversible binding (K_i ca. 40 nM for PhVS-CoA) followed by slow (k_{inact} ca. 0.02 s^{-1}) conjugate addition of the SaCoADR Cys43-S⁻ to the inhibitor. As the crystal structures of cathepsin K and cruzain complexed with the respective inhibitors accelerated structure-based drug design programs in both cases,^{36,37} we undertook structural analyses of SaCoADR complexed with each of three CoAS-mimetics. Moreover, we hoped that such complex structures would provide further insight into the roles of Tyr361' and Tyr419' as proton donors in the SaCoADR-catalyzed reaction, considering that protonation of the intermediate that forms on conjugate addition of Cys43-S⁻ to the inhibitor is essential to ensure irreversible, covalent attachment to the enzyme (Scheme 3).

The inhibited enzyme complexes were prepared by incubating SaCoADR with NADPH (10 equiv/FAD) and inhibitor (20 equiv/FAD) on ice for 1 h. Following buffer exchange and crystallization, synchrotron data sets were collected for complexes with PhVS-CoA, MeVS-CoA, and EtVC-CoA. The structures were determined to resolutions of 1.8 Å ($R_{\text{free}} = 20.2\%$), 2.0 Å ($R_{\text{free}} = 22.6\%$), and 2.4 Å ($R_{\text{free}} = 21.8\%$) (Table 2). Again, the overall tertiary structures are very comparable to that of oxidized (Cys43-SSCoA) SaCoADR, with all-atom rmsd values for the respective dimers of 0.11–0.16 Å.

Figure 4 gives the $F_o - F_c$ SA-omit map contoured at 1.2σ , for the active-site region of the SaCoADR—MeVS-CoA complex; this map illustrates the accuracy of the final refined model and

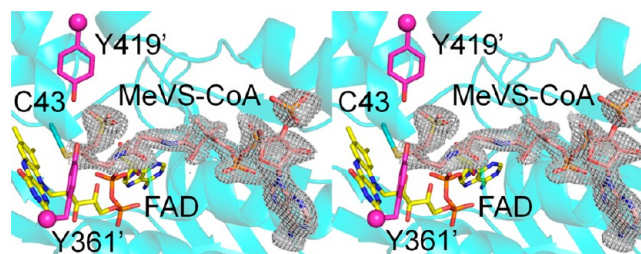


Figure 4. Stereoview of the inhibited SaCoADR—MeVS-CoA complex, focusing on the active site. The presentation is similar to that given in Figure 2A for the C43S mutant but includes Cys43 of the wild-type enzyme as modified with MeVS-CoA. Chain A and B protein residues are color-coded, with carbon atoms in cyan and magenta, respectively. FAD and bound MeVS-CoA are color-coded by atom type, with FAD carbon atoms in yellow and MeVS-CoA carbon atoms in orange. An $F_o - F_c$ SA-omit map contoured at 1.2σ is shown for MeVS-CoA. Secondary structural elements are represented as transparent.

is representative of those calculated for each complex. Each of the final refined models includes one FAD and one inhibitor molecule per active site (Figure 5). As the asymmetric unit corresponds to the biological dimer, it is clear that inhibitor is bound in both active sites per enzyme molecule, with full occupancy. In combination with the activity data for the wild-type/C43S SaCoADR heterodimer presented above, this observation of full inhibitor occupancy in each subunit supports the conclusion that SaCoADR does not operate via half-sites reactivity. Each inhibitor has formed a covalent attachment between its β -carbon (relative to the electron-withdrawing group) and the enzyme Cys43-S _{γ} — as expected for a Michael addition of the Cys residue to the inhibitor. Moreover, in all three inhibitor complexes the -dethia-CoA moiety is clearly present in the CoAS-I site — the same site occupied by the Cys43-SSCoA redox center in oxidized SaCoADR. We earlier identified an unoccupied cleft adjacent to bound

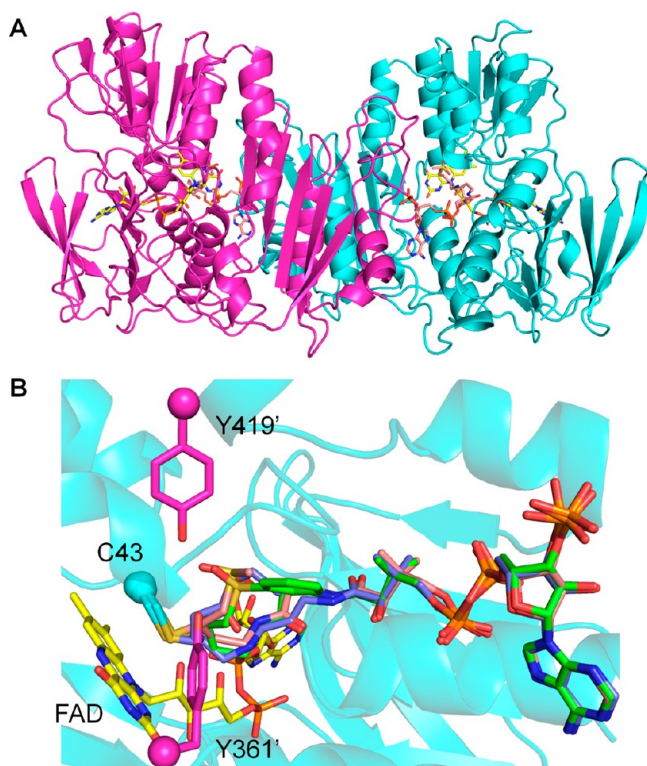


Figure 5. (A) Asymmetric unit for the inhibited *SaCoADR*—MeVS-CoA complex, corresponding to the biological dimer. Each active site includes one Cys43—MeVS-CoA adduct. All elements are color-coded as in Figure 4. (B) Overlay of the three inhibitor-bound *SaCoADR* complexes, showing covalently bound MeVS-CoA (carbon atoms colored pink), PhVS-CoA (carbon atoms colored green), and EtVC-CoA (carbon atoms colored blue) inhibitors. The MeVS-CoA complex conserves all 12 polar interactions seen with bound CoAS- in wild-type *SaCoADR*. Tyr361'-OH interacts with one sulfone oxygen in both MeVS-CoA and PhVS-CoA complexes, and Tyr419'-OH interacts similarly in the PhVS-CoA complex structure.

CoAS-;¹⁴ in the inhibitor complexes this cleft is also unoccupied and provides ample opportunity for the elaboration of inhibitor structures.

One consideration for the exclusive association with the CoAS-I site is whether the polar sulfone or carboxyl moieties of the inhibitors contribute strongly to productive binding and inactivation. In each of the four cruzain-inhibitor complexes,³⁷ including that with a phenyl vinyl sulfone inhibitor (VSI) structurally equivalent to PhVS-CoA, there are four hydrogen bonds between one sulfone oxygen (O35) and the protein. These were noted to outweigh other potential interactions and to lock the inhibitor into the observed orientation. Although unproven, it is likely that these same electrostatic interactions contribute to inhibitor binding to cruzain.^b In all three *SaCoADR*-inhibitor complexes, the respective sulfone and carboxyl moieties occupy the chloride binding site described for oxidized *SaCoADR*, which provides hydrogen-bonding interactions with Cys43-N, Tyr361'-OH, and an active-site water molecule. The 1.5 Å resolution structure of oxidized *SaCoADR* identified 12 polar interactions between CoAS- and protein residues; four additional residues provide hydrophobic contacts.¹⁴ There are also 13 solvent waters identified as ligands to CoAS-. As indicated in Figure 6 and in Table 3, these protein interactions are conserved — with two exceptions — in the 1.8 Å resolution *SaCoADR*—PhVS-CoA structure. There is no

hydrogen bond between Thr15-OH and the pantothenic acid 2'-OH, and Arg22-N_{η2} does not appear to interact directly with the ribose 2'-OH. However, much more significant is the presence of new electrostatic interactions between one of the sulfone oxygen atoms and both Tyr361'-OH (2.5 Å) and Tyr419'-OH (3.2 Å). This environment for the PhVS- moiety resembles that observed in the analogous cruzain-VSI complex. Additionally, there is a hydrophobic interaction between the phenyl ring of the inhibitor and Pro426, which hovers above it. The conformation of the -dethia-CoA moiety of the bound PhVS-CoA inhibitor is essentially identical to that seen for CoAS- in oxidized *SaCoADR*. For example, the adenine base is partially solvent-exposed and interacts via a cation- π stacking mode with the Arg22 guanidinium moiety, and the 3'-phosphate and ribose are entirely solvent exposed.

For the cruzain-VSI complex the position of the phenyl ring was determined solely via the electrostatic lock on oxygen O35 of the sulfone group.³⁷ There is an end-on interaction with the indole ring of Trp177, but there are no π -stacking interactions. In comparison with the *SaCoADR*—PhVS-CoA complex, the MeVS-CoA inhibitor conserves all 12 polar interactions found with CoAS- in the oxidized enzyme but lacks the Tyr419'-OH interaction with the sulfone oxygen. There are eight solvent waters identified in this LIGPLOT analysis. The EtVC-CoA inhibitor lacks both Ser39 and Asn42 interactions, the carboxyl oxygen has no contact with either Tyr, and only one solvent water (at the resolution of 2.4 Å) is identified. The decrease in the number of interactions moving from PhVS-CoA to MeVS-CoA to EtVC-CoA seems to be borne out by competitive inhibition K_i values determined for these three inhibitors (Table 4) — 0.04 μM , 0.3 μM , and 0.66 μM , respectively.¹⁵ The calculated ΔG_i values therefore increase (are less favorable) by 1.7 kcal/mol through the series.

DISCUSSION

CoASH-Based Thiolomes as Targets. The success of *S. aureus* and *B. anthracis* as bacterial pathogens is dependent on the ability of each to circumvent the innate immune system of the human host.^{38,39} Low-molecular-weight thiols such as GSH serve as important intracellular redox buffers in bacteria to counter this challenge.^{40,41} *S. aureus* and *B. anthracis*, however, are known to lack GSH;^{12,42} CoASH and the recently identified bacillithiol (Cys-GlcN-malate) replace it.^{6,7} In *E. coli*, the reduced form of GSH is required for all of its known functions, and the disulfide reductase subgroup enzyme GR is responsible for NADPH-dependent GSSG reduction.⁴³ Similarly, the peroxidase-oxidase-reductase subgroup enzyme CoADR has been characterized in detail in both *S. aureus*¹⁴ and *B. anthracis*² — in our selection of nine NIAID bacterial pathogens, seven have one or more of the CoADR isoforms. Recently, CoADR has also been shown to be essential for infection of the mammalian host by the “newly recognized” NIAID pathogen, *Borrelia burgdorferi*.⁴⁴

Synchrotron Reduction of Cys-SSCoA Redox Centers, Cys-SH Conformations, and Reaction Coordinates. The stability of the *SaCoADR* Cys43-SSCoA center to potential synchrotron reduction may be due to the presence of the well-ordered chloride ion 3.8 Å from the CoAS- sulfur.¹⁴ Although the chain B CoAS- moiety is less well ordered, electron density for the disulfide remains well-defined. In contrast, both *BaCoADR* Cys42-SSCoA and *BaCoADR*-RHD Cys44-SSCoA centers are subject to synchrotron reduction, the latter to an extent of ca. 50%.^{2,9} As described earlier, the naturally reduced

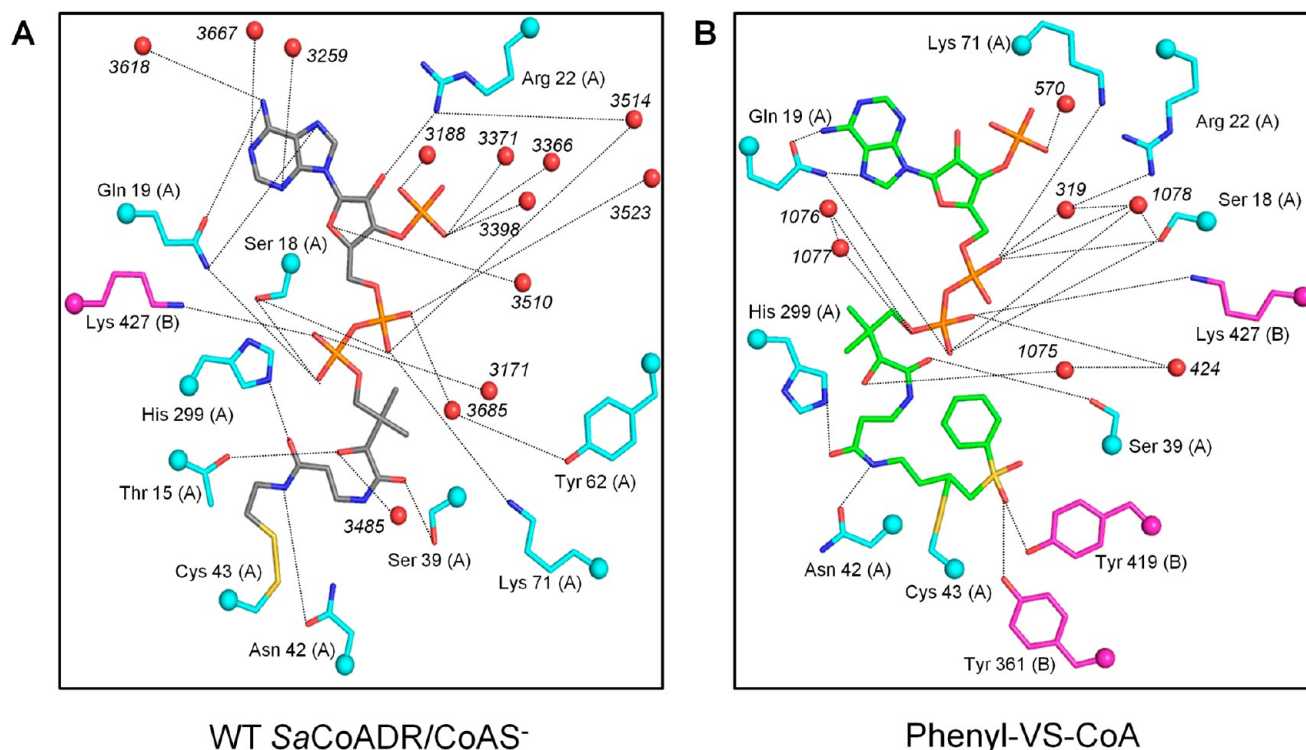


Figure 6. (A) LIGPLOT representation of polar protein and solvent water interactions with CoAS⁻ in the wild-type SaCoADR crystal structure. These interactions are generally conserved in all three (MeVS-CoA, PhVS-CoA, and EtVC-CoA) inhibitor bound crystal structures, as detailed in the text. (B) LIGPLOT representation of polar protein interactions with the PhVS-CoA inhibitor in the structure of that complex. A number of residues lining the active-site cleft provide electrostatic and hydrogen-bonding interactions with the -dethia-CoA moiety and with one sulfone oxygen of the inhibitor. Additional hydrogen-bonding interactions with the -dethia-CoA portion are indicated with ordered water molecules. All color coding is as in Figure 5B.

Table 3. Polar Interactions with CoAS⁻ and PhVS-CoA in Oxidized SaCoADR and the SaCoADR-Inhibitor Complex

oxidized SaCoADR	SaCoADR—PhVS-CoA complex		
protein and CoAS-atoms ^a	D...A (Å)	protein and PhVS-CoA atoms	D...A (Å)
Thr15-O _γ ...CoAS-OAP	2.7	no contact with Thr15	
Ser18-O _γ ...CoAS-O5A	2.8	Ser18-O _γ ...PhVS-CoA-O5A	3.1
Ser18-O _γ ...CoAS-O2A	3.2	Ser18-O _γ ...PhVS-CoA-O2A	3.3
Gln19-N _{e2} ...CoAS-N7A	2.8	Gln19-N _{e2} ...PhVS-CoA-N7A	2.8
Gln19-N _{e2} ...CoAS-O5A	2.8	Gln19-N _{e2} ...PhVS-CoA-O5A	3.2
Gln19-O _{e1} ...CoAS-N6A	2.9	Gln19-O _{e1} ...PhVS-CoA-N6A	2.8
Arg22-N _{η2} ...CoAS-O2B	3.1	Arg22-N _{η2} ...WAT319...PhVS-CoA-O1A	3.0/2.6
Ser39-O _γ ...CoAS-O9P	2.6	Ser39-O _γ ...PhVS-CoA-O9P	3.0
Asn42-O _{δ1} ...CoAS-N4P	3.0	Asn42-O _{δ1} ...PhVS-CoA-N4P	2.6
Lys71-N _ε ...CoAS-O2A	2.9	Lys71-N _ε ...PhVS-CoA-O1A	3.1
His299-N _{e2} ...CoAS-O5P	2.8	His299-N _{e2} ...PhVS-CoA-O5P	2.7
Lys427'-N _ε '...CoAS-O4A	2.7	Lys427'-N _ε '...PhVS-CoA-O4A	2.7
		Tyr361'-O _γ '...PhVS-CoA-SO(O35)	2.5
		Tyr419'-O _γ '...PhVS-CoA-SO(O35)	3.2

^aAtom labeling for CoAS⁻ is derived from the Protein Data Bank ligand summary.⁵⁰ Atom labeling for PhVS-CoA is based directly on that for CoAS⁻, with that for O35 of the sulfone group being taken from that for the equivalent sulfone oxygen in the cruzain-VSI complex,³⁷ as described in the text. See also ref⁵¹.

Cys42-SH side chain of the BaCoADR EH₂-CoASH-NAD(P)H complex adopts a new external conformation in which Cys42-S_γ interacts with both Tyr367'-OH and Tyr425'-OH. While this

conformation has been attributed to the tightly bound CoASH product, it may be populated to some extent during catalysis.

In the inactivated structures of SaCoADR presented in this work, Cys43-S_γ adopts the internal conformation seen in the oxidized Cys43-SSCoA enzyme. While this favorable comparison for Cys43-SSCoA and Cys43-SCHR'/CH₂SO₂Ph (R' = -dethia-CoA) conformations is anticipated, the nucleophilic attack of Cys43-S⁻ in the catalytic cycle, comparing the natural (CoAS)₂ substrate disulfide with the Michael acceptor-containing CoAS-mimetic, reveals insights into the respective transition states. In the former case, both Cys43-S_γ and the CoAS-I sulfur [of (CoAS)₂] represent divalent sulfur; both atoms exhibit sp³ hybridization. In earlier work Rosenfield et al.⁴⁵ analyzed crystal structures of small molecules containing divalent sulfur in order to establish preferred directions of nucleophilic attack (e.g., by Cys43-S⁻ on CoAS-I sulfur). For nonbonded S...S intermolecular contacts, the nucleophilic center tends to approach the complementary sulfur ca. along the extension of one of the covalent bonds to that electrophilic center, i.e., in plane. This S_N2-like displacement involves no change in bond order about CoAS-I sulfur (Scheme 2). The same applies as Cys43-S⁻ attacks the divalent sulfur center of MMTS.

However, the electrophilic carbon center of the Michael acceptor-containing CoAS-mimetics is sp² hybridized with trigonal planar geometry relative to its -dethia-CoA, -H, and =C_α neighbors. This raises several stereochemical and conformational questions for the reaction coordinate. First, does the proton addition to C_α follow a *syn* or *anti* stereochemical course? Second, presuming the -dethia-CoA moiety serves as a conformational anchor in the addition reaction, the =C_α-SO₂Ph moiety will

Table 4. Kinetic Parameters and Associated Free Energies for SaCoADR Catalysis and Inactivation

T = 298 K	K_m	k_{cat}	k_{cat}/K_m	ΔG_s^a	$\Delta G_T^{\ddagger b}$	$\Delta G^{\ddagger c}$
(CoAS) ₂						
wild-type	3 μ M	27 s ⁻¹	9.0×10^6 M ⁻¹ s ⁻¹	-7.5 kcal·mol ⁻¹	8.0 kcal·mol ⁻¹	15.5 kcal·mol ⁻¹
MMTS						
wild-type	78 μ M	6.4 s ⁻¹	8.2×10^4 M ⁻¹ s ⁻¹	-5.6 kcal·mol ⁻¹	10.7 kcal·mol ⁻¹	16.3 kcal·mol ⁻¹
Y361F	47 μ M	10.4 s ⁻¹	2.2×10^5 M ⁻¹ s ⁻¹	-5.9 kcal·mol ⁻¹	10.2 kcal·mol ⁻¹	16.1 kcal·mol ⁻¹
Y419F	575 μ M	1.2 s ⁻¹	2.1×10^3 M ⁻¹ s ⁻¹	-4.4 kcal·mol ⁻¹	12.9 kcal·mol ⁻¹	17.3 kcal·mol ⁻¹
T = 310 K ^d	K_i^e	$k_{inact} (k_2)^f$	$k_{ass} (k_2/K_i^*)^g$	ΔG_i^h	$\Delta G_T^{\ddagger i}$	$\Delta G^{\ddagger j}$
EtVC-CoA	0.66 μ M		219 M ⁻¹ s ⁻¹	-8.8 kcal·mol ⁻¹	14.8 kcal·mol ⁻¹	23.6 kcal·mol ⁻¹
MeVS-CoA	0.3 μ M		500 M ⁻¹ s ⁻¹	-9.3 kcal·mol ⁻¹	14.3 kcal·mol ⁻¹	23.6 kcal·mol ⁻¹
PhVS-CoA	0.04 μ M ^k	(9.4×10^{-3} s ⁻¹) ^k	4.0×10^4 M ⁻¹ s ⁻¹	-10.5 kcal·mol ⁻¹	11.6 kcal·mol ⁻¹	22.1 kcal·mol ⁻¹

^aCalculated assuming $K_m = K_d$. ^bCalculated directly from k_{cat}/K_m . ^cCalculated from $(\Delta G_T^{\ddagger} - \Delta G_s)$. ^dKinetic parameters taken from ref 15. ^eDetermined from competitive inhibition kinetics. ^fThe first-order rate constant, $k_{inact}^{15} = k_2$ (ref S2, Scheme X). ^gThe second-order rate constant, k_{ass} (ref S2, Scheme IX) can be set = k_2/K_i^* in cases where no EI* is observed kinetically. $K_i^* \neq K_i$. ^hCalculated assuming $K_i = K_d$. ⁱCalculated directly from k_{ass} . ^jCalculated from $(\Delta G_T^{\ddagger} - \Delta G_i)$. ^kAs reported by van der Westhuyzen and Strauss,¹⁵ the plot of k_{obs} versus $[I]$ is hyperbolic only for the PhVS-CoA inhibitor, allowing determination of k_2 and K_i^* only in its case. This value of k_2 is given in parentheses. Free energy parameters are defined as in ref 53.

change position in the reaction coordinate, as the C_β electrophilic center assumes tetrahedral, sp³ character. This may contribute additional transition-state stabilization in the conjugate addition reaction, which is 80-fold faster (k_{ass}) for R = -SO₂Ph than for -SO₂Me.¹⁵ The inactivation kinetics with R = -CO₂Et, -SO₂Me, and -SO₂Ph can be compared with the reaction kinetics for SaCoADR with both (CoAS)₂¹³ and with MMTS (Table 3).⁹ From the individual kinetic parameters and specificity constants (inhibitor potencies), values for the binding energies and free energies of activation have been calculated for these reactions.

Nucleophilic Additions of Thiols to Disulfides versus Michael Acceptors. For the inactivation of cruzain with one series of phenyl-containing vinyl sulfone inhibitors, Brinen et al.³⁷ reported values for k_{ass} (see Table 4) ranging from 10⁵–10⁷ M⁻¹ s⁻¹ at room temperature. In complexes with each of four inhibitors, the electrostatic contributions of hydrogen bond interactions with at least one sulfone oxygen lock each inhibitor in the observed orientation. For the VSI inhibitor, $k_{ass} = 3.2 \times 10^5$ M⁻¹ s⁻¹ corresponds to $\Delta G_T^{\ddagger} = 9.9$ kcal/mol; increasing length for the spacer connecting the sulfone component with the P1' phenyl appears to have a favorable effect on k_{ass} . To the extent that reported IC₅₀ values represent competitive K_i parameters, this also reflects a favorable effect on ΔG_i for increased inhibitor length. The reaction between cruzain Cys25 and VSI in fact mimics that for the formation of the "tetrahedral intermediate" in protease catalysis.⁴⁶ While the VSI phenyl group is proximal to the P1' binding site, with the addition of atoms between the phenyl ring and the sulfone moiety contributing favorably to k_{ass} (and thus, to ΔG_T^{\ddagger}), these observations suggest that the peptidyl component must move in the transition state. Although direct evidence that the sulfone group is locked in place on VSI binding is lacking, this remains the working conclusion.^b

The k_{ass} values determined for cruzain (Cys25)³⁷ and SaCoADR (Cys43)¹⁵ to similar phenyl vinyl sulfone-based Michael acceptor-containing mimetics (VSI and PhVS-CoA, respectively, as corrected for different reaction temperatures) differ by ca. 16-fold in favor of the cruzain reaction. This corresponds to a $\Delta \Delta G_T^{\ddagger}$ of ca. 2 kcal/mol, in part reflecting the non-natural conformational change about C_β of the PhVS-CoA electrophilic center in the reaction coordinate for SaCoADR Cys43 reaction. The k_{ass} value of 4×10^4 M⁻¹ s⁻¹ determined for SaCoADR and PhVS-CoA at 37 °C is ca. 2 orders of

magnitude lower than $k_{cat}/K_m[(CoAS)_2]$ (9.0×10^6 M⁻¹ s⁻¹) measured at 25 °C. While this corresponds to a $\Delta \Delta G_T^{\ddagger}$ of ca. 3.6 kcal/mol (not correcting for different reaction temperatures) favoring reduction of (CoAS)₂ over reaction with the CoAS-mimetic, the calculated ΔG_i for PhVS-CoA is 3 kcal/mol more favorable than ΔG_s calculated for (CoAS)₂.

The rates of reaction for an organic thiol with compounds similar to those in the cruzain series have been reported, but only as relative rates.⁴⁷ Szajewski and Whitesides⁴⁸ have analyzed the reactions of organic thiols, both with free GSSG and with protein-SSCH₃ (and other) disulfides. The observed correlation between thiol pK_a and rate of nucleophilic attack on GSSG was interpreted in support of a simple S_N2 transition state, as suggested by crystallographic analyses cited previously,⁴⁵ yielding a preferred direction of approach for a sulfur nucleophile to a disulfide along that S–S axis. There is significant negative charge on all three S atoms in this transition state ($S_{nuc} \cdots S_c \cdots S_{lg}$), but it is concentrated on S_{nuc} and S_{lg}. While rates of GSSG reduction in these model studies are generally slow, the reaction rates of thiols with papain Cys25-SSCH₃, for example, approach 8300 M⁻¹ s⁻¹ (= k_1) for 2-mercaptoethanol.⁴⁹ There is no evidence from this work to suggest deviation from the S_N2 displacement reaction previously described for thiol-disulfide interchange; local factors contributing to Cys-S⁻ leaving group acidity, rather than steric effects of protein structure, dominate the reactivity as observed.

Inhibitor Design Potential. The observation that the covalent inhibitors — detailed in the cocrystal structures reported here with *S. aureus* CoADR — leave unoccupied space in the CoAS-II binding cleft has been noted. Additionally, it is clear that Tyr361' and Tyr419' assist in locking down the inhibitors, as outlined in Figures 5B and 6B. Thus, there is good evidence that the existing compounds provide a strong starting point for novel inhibitor design. Indeed, next generation inhibitors could be designed to exploit the open space in the CoAS-II binding cleft, and in so doing provide increased binding affinity and selectivity for the target enzymes in a range of host organisms. If such compounds could be developed and validated, they could contribute both basic and translational leads in the search for new clinical approaches to several NIAID priority pathogens, such as *S. aureus*, *B. anthracis*, and *B. burgdorferi*.

■ ASSOCIATED CONTENT

Accession Codes

Coordinates have been deposited with the Protein Data Bank under the file names 4EQX, 4EQR, 4EQS, 4EQW, 4EM4, 4EM3, and 4EMW.

■ AUTHOR INFORMATION

Corresponding Author

*Tel.: +27-21-808-5866, Fax: +27-21-808-5863. E-mail: estrauss@sun.ac.za (E.S.); Tel.: (919) 843-8910, Fax: (919) 962-2388. E-mail: redinbo@unc.edu (M.R.R.); Tel.: (336) 716-3914, Fax: (336) 713-1283. E-mail: alc@csb.wfu.edu (A.C.).

Present Addresses

[‡]Department of Biological Engineering, Massachusetts Institute of Technology, Cambridge, MA 02139.

^ΔDepartment of Biochemistry and Molecular Biophysics, Washington University School of Medicine, St. Louis, MO 63110.

Author Contributions

^{||}These authors contributed equally to this work.

Funding

This work was supported by National Institutes of Health (NIH) Grant AI-078924 (M.R.R.), by North Carolina Biotechnology Center Grant 2011-MRG-1116 (A.C.), by National Research Foundation (NRF) Grant CPR20110726000022216 (E.S.), and by a grant from the Medical Research Council (E.S.). W.J.A.M. and R.v.d.W. were recipients of NRF Scarce Skills scholarships.

Notes

The authors declare no competing financial interest.

■ ACKNOWLEDGMENTS

We especially thank Dr. Conn Mallett and Dr. Derek Parsonage for their leading roles in protein expression and crystallography with the SaCoADR mutants.

■ ABBREVIATIONS

CoADR, coenzyme A-disulfide reductase; GR, glutathione reductase; SaCoADR, *Staphylococcus aureus* coenzyme A-disulfide reductase; BaCoADR, *Bacillus anthracis* coenzyme A-disulfide reductase; (CoAS)₂, coenzyme A-disulfide; EH₂, two-electron reduced enzyme; CoAS-I and GS-I, assigned halves of coenzyme A-disulfide and GSSG corresponding to the second CoASH and GSH products, respectively, during catalytic reduction; MMTS, methyl methanethiolsulfonate; EtVC-CoA, α,β -unsaturated ethyl ester-containing CoAS-mimetic inhibitor; MeVS-CoA, methyl vinyl sulfone-containing CoAS-mimetic inhibitor; PhVS-CoA, phenyl vinyl sulfone-containing CoAS-mimetic inhibitor; VSI, phenyl vinyl sulfone-containing inhibitor of cruzain

■ ADDITIONAL NOTES

^aThe crystal structure of the Y361,419F double mutant indicates that both Cys43-SSCoA per asymmetric unit are partially reduced (ca. 50%). As with the BaCoADR and BaCoADR-RHD structures, however, this is attributed to synchrotron reduction. The Y361,419F enzyme as purified contains two Cys43-SSCoA disulfides per dimer.

^bW.R. Roush, personal communication.

■ REFERENCES

- (1) www.narcis.nl/research/RecordID/OND1345442/Language/en.
- (2) Wallen, J. R., Paige, C., Mallett, T. C., Karplus, P. A., and Claiborne, A. (2008) Pyridine nucleotide complexes with *Bacillus anthracis* coenzyme A-disulfide reductase: a structural analysis of dual NAD(P)H specificity. *Biochemistry* 47, 5182–5193.
- (3) Argyrou, A., and Blanchard, J. S. (2004) Flavoprotein disulfide reductases: advances in chemistry and function. *Prog. Nucleic Acid Res. Mol. Biol.* 78, 89–142.
- (4) Atkinson, H. J., and Babbitt, P. C. (2009) An atlas of the thioredoxin fold class reveals the complexity of function-enabling adaptations. *PLoS Comput. Biol.* 5, e1000541.
- (5) Chi, B. K., Gronau, K., Maeder, U., Hessling, B., Becher, D., and Antelmann, H. (2011) S-bacillithiolation protects against hypochlorite stress in *Bacillus subtilis* as revealed by transcriptomics and redox proteomics. *Mol. Cell. Proteomics* 10, M111.009506.
- (6) Parsonage, D., Newton, G. L., Holder, R. C., Wallace, B. D., Paige, C., Hamilton, C. J., Dos Santos, P. C., Redinbo, M. R., Reid, S. D., and Claiborne, A. (2010) Characterization of the N-acetyl- α -D-glucosaminyl L-malate synthase and deacetylase functions for bacillithiol biosynthesis in *Bacillus anthracis*. *Biochemistry* 49, 8398–8414.
- (7) Newton, G. L., Rawat, M., La Clair, J. J., Jothivasan, V. K., Budiarto, T., Hamilton, C. J., Claiborne, A., Helmann, J. D., and Fahey, R. C. (2009) Bacillithiol is an antioxidant thiol produced in *Bacilli*. *Nat. Chem. Biol.* 5, 625–627.
- (8) Ojha, S., Meng, E. C., and Babbitt, P. C. (2007) Evolution of function in the “two dinucleotide binding domains” flavoproteins. *PLoS Comput. Biol.* 3, e121.
- (9) Wallen, J. R., Mallett, T. C., Boles, W., Parsonage, D., Furdui, C. M., Karplus, P. A., and Claiborne, A. (2009) Crystal structure and catalytic properties of *Bacillus anthracis* CoADR-RHD: implications for flavin-linked sulfur trafficking. *Biochemistry* 48, 9650–9667.
- (10) Warner, M. D., Lukose, V., Lee, K. H., Lopez, K., Sazinsky, M. H., and Crane, E. J., III. (2011) Characterization of an NADH-dependent persulfide reductase from *Shewanella loihica* PV-4: implications for the mechanism of sulfur respiration via FAD-dependent enzymes. *Biochemistry* 50, 194–206.
- (11) Haveman, S. A., DiDonato, R. J., Jr., Villanueva, L., Shelobolina, E. S., Postier, B. L., Xu, B., Liu, A., and Lovley, D. R. (2008) Genome-wide gene expression patterns and growth requirements suggest that *Pelobacter carbinolicus* reduces Fe(III) indirectly via sulfide production. *Appl. Environ. Microbiol.* 74, 4277–4284.
- (12) delCardayre, S. B., Stock, K. P., Newton, G. L., Fahey, R. C., and Davies, J. E. (1998) Coenzyme A disulfide reductase, the primary low molecular weight disulfide reductase from *Staphylococcus aureus*. Purification and characterization of the native enzyme. *J. Biol. Chem.* 273, 5744–5751.
- (13) Luba, J., Charrier, V., and Claiborne, A. (1999) Coenzyme A-disulfide reductase from *Staphylococcus aureus*: evidence for asymmetric behavior on interaction with pyridine nucleotides. *Biochemistry* 38, 2725–2737.
- (14) Mallett, T. C., Wallen, J. R., Karplus, P. A., Sakai, H., Tsukihara, T., and Claiborne, A. (2006) Structure of coenzyme A-disulfide reductase from *Staphylococcus aureus* at 1.54 Å resolution. *Biochemistry* 45, 11278–11289.
- (15) van der Westhuyzen, R., and Strauss, E. (2010) Michael acceptor-containing coenzyme A analogues as inhibitors of the atypical coenzyme A disulfide reductase from *Staphylococcus aureus*. *J. Am. Chem. Soc.* 132, 12853–12855.
- (16) Karplus, P. A., and Schulz, G. E. (1989) Substrate binding and catalysis by glutathione reductase as derived from refined enzyme-substrate crystal structures at 2 Å resolution. *J. Mol. Biol.* 210, 163–180.
- (17) Miller, S. M., Massey, V., Williams, C. H., Jr., Ballou, D. P., and Walsh, C. T. (1991) Communication between the active sites in dimeric mercuric ion reductase: an alternating sites hypothesis for catalysis. *Biochemistry* 30, 2600–2612.

- (18) Ledwidge, R., Patel, B., Dong, A., Fiedler, D., Falkowski, M., Zelikova, J., Summers, A. O., Pai, E. F., and Miller, S. M. (2005) NmerA, the metal binding domain of mercuric ion reductase, removes Hg²⁺ from proteins, delivers it to the catalytic core, and protects cells under glutathione-depleted conditions. *Biochemistry* 44, 11402–11416.
- (19) Krnajska, Z., Gilberger, T. W., Walter, R. D., and Müller, S. (2000) Intersubunit interactions in *Plasmodium falciparum* thioredoxin reductase. *J. Biol. Chem.* 275, 40874–40878.
- (20) Nijvipakul, S., Ballou, D. P., and Chaiyen, P. (2010) Reduction kinetics of a flavin oxidoreductase LuxG from *Photobacterium leiognathi* (TH1): half-sites reactivity. *Biochemistry* 49, 9241–9248.
- (21) Mochalkin, I., Miller, J. R., Evdokimov, A., Lightle, S., Yan, C., Stover, C. K., and Waldrop, G. L. (2008) Structural evidence for substrate-induced synergism and half-sites reactivity in biotin carboxylase. *Protein Sci.* 17, 1706–1718.
- (22) Pflugrath, J. W. (1999) The finer things in X-ray diffraction data collection. *Acta Crystallogr. D55*, 1718–1725.
- (23) Brunger, A. T., Adams, P. D., Clore, G. M., DeLano, W. L., Gros, P., Grosse-Kunstleve, R. W., Jiang, J. S., Kuszewski, J., Nilges, M., Pannu, N. S., Read, R. J., Rice, L. M., Simonson, T., and Warren, G. L. (1998) Crystallography & NMR system: a new software suite for macromolecular structure determination. *Acta Crystallogr. D54*, 905–921.
- (24) Winn, M. D., Isupov, M. N., and Murshudov, G. N. (2001) Use of TLS parameters to model anisotropic displacements in macromolecular refinement. *Acta Crystallogr. D57*, 122–133.
- (25) Murshudov, G. N., Vagin, A. A., and Dodson, E. J. (1997) Refinement of macromolecular structures by the maximum-likelihood method. *Acta Crystallogr. D53*, 240–255.
- (26) Emsley, P., and Cowtan, K. (2004) Coot: model-building tools for molecular graphics. *Acta Crystallogr. D60*, 2126–2132.
- (27) Otwinowski, Z., and Minor, W. (1997) Processing of X-ray diffraction data collected in oscillation mode. *Methods Enzymol.* 276, 307–326.
- (28) McCoy, A. J., Grosse-Kunstleve, R. W., Adams, P. D., Winn, M. D., Storoni, L. C., and Read, R. J. (2007) Phaser crystallographic software. *J. Appl. Crystallogr.* 40, 658–674.
- (29) Schuttelkopf, A. W., and van Aalten, D. M. (2004) PRODRG: a tool for high-throughput crystallography of protein-ligand complexes. *Acta Crystallogr. D60*, 1355–1363.
- (30) Adams, P. D., Afonine, P. V., Bunkoczi, G., Chen, V. B., Davis, I. W., Echols, N., Headd, J. J., Hung, L. W., Kapral, G. J., Grosse-Kunstleve, R. W., McCoy, A. J., Moriarty, N. W., Oeffner, R., Read, R. J., Richardson, D. C., Richardson, J. S., Terwilliger, T. C., and Zwart, P. H. (2010) PHENIX: a comprehensive Python-based system for macromolecular structure solution. *Acta Crystallogr. D66*, 213–221.
- (31) Matthews, R. G., and Williams, C. H., Jr. (1976) Measurement of the oxidation-reduction potentials for two-electron and four-electron reduction of lipoamide dehydrogenase from pig heart. *J. Biol. Chem.* 251, 3956–3964.
- (32) Poole, L. B., and Claiborne, A. (1986) Interactions of pyridine nucleotides with redox forms of the flavin-containing NADH peroxidase from *Streptococcus faecalis*. *J. Biol. Chem.* 261, 14525–14533.
- (33) Poole, L. B., and Claiborne, A. (1989) The non-flavin redox center of the streptococcal NADH peroxidase. I. Thiol reactivity and redox behavior in the presence of urea. *J. Biol. Chem.* 264, 12322–12329.
- (34) Rietveld, P., Arscott, L. D., Berry, A., Scrutton, N. S., Deonarain, M. P., Perham, R. N., and Williams, C. H., Jr. (1994) Reductive and oxidative half-reactions of glutathione reductase from *Escherichia coli*. *Biochemistry* 33, 13888–13895.
- (35) Wilkinson, K. D., and Williams, C. H., Jr. (1979) Evidence for multiple electronic forms of two-electron-reduced lipoamide dehydrogenase from *Escherichia coli*. *J. Biol. Chem.* 254, 852–862.
- (36) McGrath, M. E., Klaus, J. L., Barnes, M. G., and Bromme, D. (1997) Crystal structure of human cathepsin K complexed with a potent inhibitor. *Nat. Struct. Biol.* 4, 105–109.
- (37) Brinen, L. S., Hansell, E., Cheng, J., Roush, W. R., McKerrow, J. H., and Fletterick, R. J. (2000) A target within the target: probing cruzain's P1' site to define structural determinants for the Chagas' disease protease. *Structure* 8, 831–840.
- (38) Kobayashi, S. D., and DeLeo, F. R. (2009) An update on community-associated MRSA virulence. *Curr. Opin. Pharmacol.* 9, 545–551.
- (39) Passalacqua, K. D., and Bergman, N. H. (2006) *Bacillus anthracis*: interactions with the host and establishment of inhalational anthrax. *Future Microbiol.* 1, 397–415.
- (40) Fahey, R. C. (2001) Novel thiols of prokaryotes. *Annu. Rev. Microbiol.* 55, 333–356.
- (41) Zuber, P. (2009) Management of oxidative stress in *Bacillus*. *Annu. Rev. Microbiol.* 63, 575–597.
- (42) Nicely, N. I., Parsonage, D., Paige, C., Newton, G. L., Fahey, R. C., Leonardi, R., Jackowski, S., Mallett, T. C., and Claiborne, A. (2007) Structure of the type III pantothenate kinase from *Bacillus anthracis* at 2.0 Å resolution: implications for coenzyme A-dependent redox biology. *Biochemistry* 46, 3234–3245.
- (43) Toledano, M. B., Kumar, C., Le Moan, N., Spector, D., and Tacnet, F. (2007) The system biology of thiol redox system in *Escherichia coli* and yeast: differential functions in oxidative stress, iron metabolism and DNA synthesis. *FEBS Lett.* 581, 3598–3607.
- (44) Eggers, C. H., Caimano, M. J., Malizia, R. A., Kariu, T., Cusack, B., Desrosiers, D. C., Hazlett, K. R. O., Claiborne, A., Pal, U., and Radolf, J. D. (2011) The coenzyme A disulphide reductase of *Borrelia burgdorferi* is important for rapid growth throughout the enzootic cycle and essential for infection of the mammalian host. *Mol. Microbiol.* 82, 679–697.
- (45) Rosenfield, R. E., Parthasarathy, R., and Dunitz, J. D. (1977) Directional preferences of nonbonded atomic contacts with divalent sulfur. I. Electrophiles and nucleophiles. *J. Am. Chem. Soc.* 99, 4860–4862.
- (46) Brak, K., Kerr, I. D., Barrett, K. T., Fuchi, N., Debnath, M., Ang, K., Engel, J. C., McKerrow, J. H., Doyle, P. S., Brinen, L. S., and Ellman, J. A. (2010) Nonpeptidic tetrafluorophenoxymethyl ketone cruzain inhibitors as promising new leads for Chagas disease chemotherapy. *J. Med. Chem.* 53, 1763–1773.
- (47) Reddick, J. J., Cheng, J., and Roush, W. R. (2003) Relative rates of Michael reactions of 2'-(phenethyl)thiol with vinyl sulfones, vinyl sulfonate esters, and vinyl sulfonamides relevant to vinyl sulfonyl cysteine protease inhibitors. *Org. Lett.* 5, 1967–1970.
- (48) Szajewski, R. P., and Whitesides, G. M. (1980) Rate constants and equilibrium constants for thiol-disulfide interchange reactions involving oxidized glutathione. *J. Am. Chem. Soc.* 102, 2011–2026.
- (49) Shaked, Z., Szajewski, R. P., and Whitesides, G. M. (1980) Rates of thiol-disulfide interchange reactions involving proteins and kinetic measurements of thiol pK_a values. *Biochemistry* 19, 4156–4166.
- (50) www.rcsb.org/pdb/ligand/ligandsummary.do?hetId=COA.
- (51) www.rcsb.org/pdb/ligand/ligandsummary.do?hetId=VS1&sid=1F29.
- (52) Bieth, J. G. (1995) Theoretical and practical aspects of proteinase inhibition kinetics. *Methods Enzymol.* 248, 59–84.
- (53) Fersht, A. (1999) *Structure and Mechanism in Protein Science*, W.H. Freeman and Company, New York.

The Antibiotic CJ-15,801 Is an Antimetabolite that Hijacks and Then Inhibits CoA Biosynthesis

Renier van der Westhuyzen,^{1,5} Justin C. Hammons,^{3,5} Jordan L. Meier,³ Samira Dahesh,⁴ Wessel J.A. Moolman,¹ Stephen C. Pelly,² Victor Nizet,⁴ Michael D. Burkart,^{3,*} and Erick Strauss^{1,*}

¹Department of Biochemistry

²Department of Chemistry and Polymer Science

Stellenbosch University, Stellenbosch 7600, South Africa

³Department of Chemistry and Biochemistry

⁴Division of Pharmacology and Drug Discovery, Department of Pediatrics, and Skaggs School of Pharmacy and Pharmaceutical Sciences

University of California San Diego, La Jolla, CA 92093, USA

⁵These authors contributed equally to this work

*Correspondence: mburkart@ucsd.edu (M.D.B.), estrauss@sun.ac.za (E.S.)

DOI 10.1016/j.chembiol.2012.03.013

SUMMARY

The natural product CJ-15,801 is an inhibitor of *Staphylococcus aureus*, but not other bacteria. Its close structural resemblance to pantothenic acid, the vitamin precursor of coenzyme A (CoA), and its Michael acceptor moiety suggest that it irreversibly inhibits an enzyme involved in CoA biosynthesis or utilization. However, its mode of action and the basis for its specificity have not been elucidated to date. We demonstrate that CJ-15,801 is transformed by the uniquely selective *S. aureus* pantothenate kinase, the first CoA biosynthetic enzyme, into a substrate for the next enzyme, phosphopantothenoylcysteine synthetase, which is inhibited through formation of a tight-binding structural mimic of its native reaction intermediate. These findings reveal CJ-15,801 as a vitamin biosynthetic pathway antimetabolite with a mechanism similar to that of the sulfonamide antibiotics and highlight CoA biosynthesis as a viable antimicrobial drug target.

INTRODUCTION

The antibiotic CJ-15,801 (**1**; Figure 1A) was discovered in 2001 by a Pfizer research team when it was isolated from fermenting cultures of a *Seimatosporium* sp. fungus (Sugie et al., 2001). Structural analysis showed the compound to resemble pantothenic acid (vitamin B₅, **2**; Figure 1B), the natural precursor of the essential metabolic cofactor coenzyme A (CoA, **3**) (Strauss, 2010), with the notable exception of a *trans*-substituted double bond in the β -alanine moiety. This feature imparts an *N*-acyl vinyllogous carbamic acid functionality to **1**, an uncommon motif that is also present in the anticancer agent palytoxin and lipopeptide antibiotics such as enamidonin (Han et al., 2004; Nicolaou and Mathison, 2005). Subsequently, CJ-15,801 was shown to inhibit the growth of drug-resistant strains of *Staphylococcus aureus* (MRSA) with minimum inhibitory concentration (MIC) values ranging between 6.25 and 50 μ g/ml (30–230 μ M). Interestingly, other bacteria, including *Escherichia coli*, *Haemo-*

philus influenzae, and several *Streptococcus* species, were not inhibited. In a later study, Saliba and Kirk determined that CJ-15,801 also inhibits the intraerythrocytic growth stage of the malaria parasite *Plasmodium falciparum* with an IC₅₀ value of 39 μ M, while leaving rat hepatoma tissue culture (HTC) cells unaffected (Saliba and Kirk, 2005). Moreover, the malarial inhibition was reversed when the concentration of pantothenic acid in the medium was increased. Taken together, these findings all pointed to CJ-15,801 targeting CoA biosynthesis, or an enzyme or process dependent on this cofactor (Spry et al., 2008, 2010). However, such a proposal has not been confirmed experimentally in any of the organisms sensitive to CJ-15,801, nor does it provide a satisfactory explanation for this antibiotic's peculiar selectivity.

The presence of the *N*-acyl vinyllogous carbamic acid functionality in CJ-15,801, combined with a knowledge of the chemical and biological reactivity of other inhibitors with similar reactive moieties, suggests that **1** most probably acts as an irreversible inhibitor of its biological target. Two mechanisms for such inhibition can be proposed: first, the α,β -unsaturated carbonyl moiety can act as a Michael-acceptor that would trap an active site nucleophile (Figure 1C); such a mechanism of action is seen in the structurally related daptamide family of antibiotics (Hollenhorst et al., 2011; Kucharczyk et al., 1990) and has also been exploited in the development of irreversible inhibitors of CoA disulfide reductase (van der Westhuyzen and Strauss, 2010). Second, if the carboxylate of CJ-15,801 were functionalized in an enzymatic transformation with an appropriate leaving group, this may provide sufficient activation for the formation of a reactive ketene intermediate that could similarly act as an electrophilic trap (Figure 1D). Importantly, both of these mechanisms would remain equally viable if the 4'-OH group of CJ-15,801 is phosphorylated or otherwise functionalized, suggesting it could be transformed by the CoA biosynthetic enzymes into an inhibitory CoA analog with a target downstream of the pathway. Such a mechanism of action has been demonstrated for the pantothenamides, a class of pantothenic acid analogs in which its carboxylate has been functionalized by amidation (Clifton et al., 1970; van Wyk and Strauss, 2008). For example, *N*-pentylpantothenamide (*N*5-Pan, **4**), which acts as a bacteriostatic agent in both *E. coli* and *S. aureus* (Choudhry et al., 2003), is transformed by three of the five CoA biosynthetic

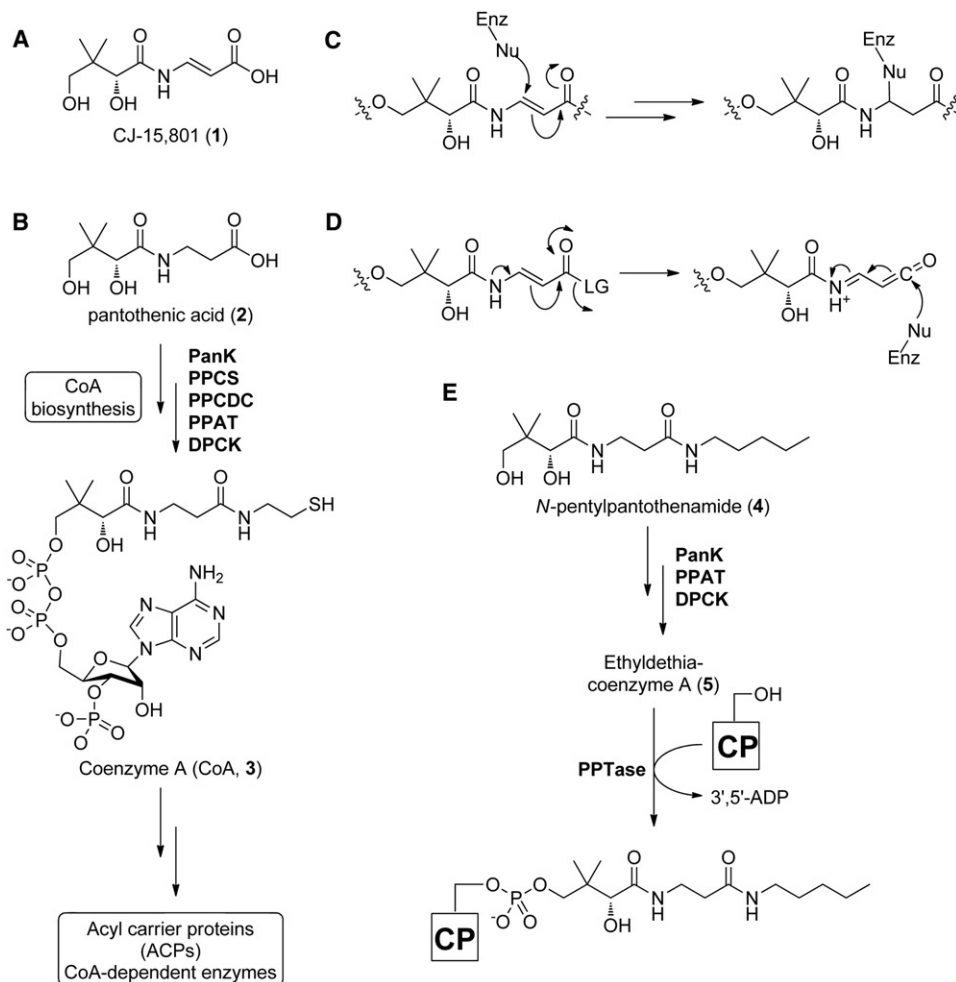


Figure 1. Structures of the Antibiotic CJ-15,801 (1), Selected Coenzyme A Biosynthetic Intermediates, Antimetabolites, and Intermediate Mimics

(A) Structure of the CJ-15,801 (1).

(B) Biosynthesis of CoA (3) from pantothenic acid (2). PanK, pantothenate kinase; PPCS, phosphopantothenoylcysteine synthetase; PPCDC, phosphopantothenoylcysteine decarboxylase; PPAT, phosphopantetheine adenylyltransferase; DCPK, dephospho-coenzyme A kinase.

(C) Proposed mechanism for irreversible inhibition by CJ-15,801 acting as an electrophilic trap.

(D) Proposed mechanism for irreversible inhibition by CJ-15,801 after its transformation into a ketene intermediate.

(E) Biotransformation of the pantothenic acid analog *N*-pentylpantothenamide (4) to the CoA antimetabolite ethyldethia-CoA (5), which has the catalytically essential thiol of the cofactor replaced by a propyl group. The antimetabolite subsequently serves as donor in the phosphopantetheinyl transferase (PPTase)-catalyzed posttranslational modification of acyl and peptidyl carrier proteins (CPs), which results in similarly inactive *crypto*-CPs.

enzymes into ethyldethia-CoA (5), a CoA antimetabolite that lacks the thiol required for the cofactor's acyl carrier functions (Figure 1E) (Strauss and Begley, 2002). This analog subsequently serves as donor in the posttranslational modification of the *apo*-acyl carrier protein (ACP), leading to the formation of catalytically inactive *crypto*-ACP (Leonardi et al., 2005; Mercer and Burkart, 2007; Zhang et al., 2004). The resulting loss of function and subsequent impact on fatty acid metabolism is believed to be the major cause for bacteriostasis, although a recent study pointed to an impact on CoA biosynthesis as well (Thomas and Cronan, 2010).

Interestingly, like CJ-15,801, the pantothenamides also exhibit organism-based specificity. While the basis for this specificity may partially reflect differences in the targeted organism's cell

permeability and/or the nature of potential drug efflux pumps, the most important factor relates to the nature of the pantothenate kinase (PanK) enzyme present in the cell. PanK catalyzes the first step of CoA biosynthesis, namely the ATP-dependent phosphorylation of pantothenic acid (2) to form 4'-phosphopantothenic acid (P-Pan, 6) (Figure 3A). This reaction is unique because it is catalyzed by three distinct types of PanK, referred to as type I, type II, and type III, respectively. These different PanK types can be distinguished based on their sequence, structure, the extent to which they experience feedback inhibition by CoA, and importantly, their ability to act on pantothenamides as alternative substrates (Brand and Strauss, 2005; Hong et al., 2006; Strauss, 2010; Strauss et al., 2010; Yang et al., 2008). Only type I and II PanKs (PanK_I and PanK_{II})

Chemistry & Biology

Mode of Action of the Antibiotic CJ-15,801

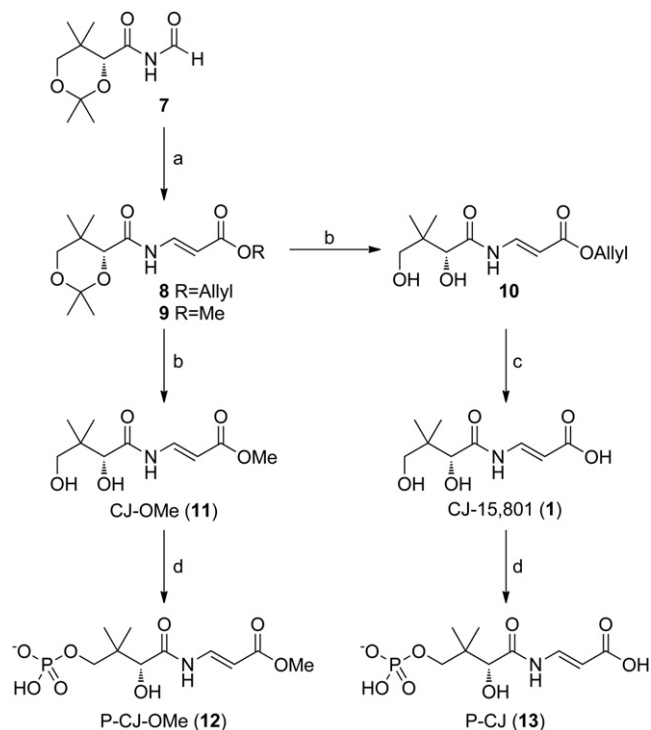


Figure 2. Synthesis of CJ-15,801, Its Methyl Ester and Their Respective Phosphorylated Versions

The respective reaction conditions are as follows: (a) Allyl- or methylacetyl-triphenylphosphonium bromide, Et₃N, toluene, 90° C, 75% (Villa et al., 2007); (b) BiCl₃, H₂O, CH₂CN, room temperature, 5 hr, 75%; (c) Pd(PPh₃)₄, pyrrolidine, THF, 81%; (d) SaPanK, ATP, MgCl₂, Tris-HCl (pH 7.5), 98% (for **12**); 79% (for **13**).

See also Figure S3.

phosphorylate pantothenamides, thereby allowing the formation of CoA antimetabolites. Organisms like *Pseudomonas aeruginosa* that have type III PanK (PanK_{III}) enzymes that exclude these compounds from their active sites are therefore refractory to the effects of *N*-pentylpantothenamide and similar analogs (Balibar et al., 2011). This suggests that the basis for CJ-15,801's unique specificity for *S. aureus* and *P. falciparum* may also be based on the type specificity of their PanKs, both of which have been characterized as atypical type II enzymes (Hong et al., 2006; Leonardi et al., 2005; Spry et al., 2010).

In this study, we set out to identify the target of CJ-15,801's antibiotic action in bacteria, to elucidate its mechanism of action, and to establish the basis for its specificity. Our results reveal that CJ-15,801 acts as an antimetabolite by using the first enzyme of the CoA biosynthesis as gateway to the pathway, after which it inhibits the second CoA biosynthetic enzyme, phosphopantothenoylcysteine synthetase (PPCS). This mode of action is reminiscent of the sulfonamide antibiotics, which block folic acid biosynthesis using a similar strategy. However, contrary to expectations, detailed analysis of the inhibition mechanism failed to provide any evidence of irreversible inhibition. Instead, our results show that CJ-15,801 is transformed into a tight-binding mimic of the PPCS enzyme's natural reaction intermediate, a mechanism also utilized by other known natural

product inhibitors of adenylyating enzymes, such as ascamycin and mupirocin (May et al., 2005; Pope et al., 1998). Taken together, these findings not only provide insight into the basis of CJ-15,801's antibiotic action, but also suggest a new and potentially general strategy for the development of synthetase inhibitors with in vivo efficacy.

RESULTS

Synthesis of CJ-15,801 and Its Esters

The synthesis of CJ-15,801 and its related analogs presents several challenges, the first of which relates to the preparation of the *N*-acyl vinylogous carbamic acid moiety. In fact, several groups have used the synthesis of CJ-15,801 to showcase new methodologies developed specifically for the preparation of this functionality (Han et al., 2004; Lee et al., 2006; Nicolaou and Mathison, 2005). However, we found these methods to be unsuitable for this study as they are either optimized for small-scale synthetic preparations, or led to the preferential formation of the unwanted (*Z*)-double bond configuration. We therefore utilized the more recent method of Villa et al., which installs the required *N*-acyl vinylogous carbamic acid moiety mainly with an (*E*)-configuration via Wittig-type chemistry, for preparation of the protected esters **8** and **9** (Figure 2) (Villa et al., 2007). A second challenge derives from the sensitivity of the *N*-vinyl amide moiety to both acid and base, which severely restricts the options for the protection and deprotection of the synthetic intermediates. In this case, established protocols that make use of neutral conditions were used to remove the acetal protecting groups from **8** and **9** to, respectively, obtain CJ-15,801's allyl (**10**) and methyl (**11**) esters, and to remove the allyl ester from **10** to provide CJ-15,801 itself. The (*Z*)-configured analog of CJ-15,801 (**Z-1**) was obtained by similar deprotection of the minor constituent of the Wittig coupling reaction product mixture.

Recently, an updated report of the Wittig-based synthesis of CJ-15,801 appeared in which several other options for deprotection of its carboxyl group are also provided (Sewell et al., 2011).

A Bacterium's Susceptibility to CJ-15,801 Correlates with Its PanK Type

The original Pfizer discovery group found that in standard susceptibility tests conducted using cation adjusted Mueller-Hinton broth as growth medium CJ-15,801 is uniquely and peculiarly selective for *S. aureus*, with none of the other organisms tested showing inhibition at 100 μg/ml (460 μM) (Sugie et al., 2001). These resistant organisms included both Gram-positive (*Staphylococcus*, *Enterococcus*, and *Streptococcus* spp.) and Gram-negative (*H. influenzae*, *Moraxella catarrhalis*, and *E. coli*) bacteria, indicating that cell envelope type alone does not determine selectivity. However, the panel of test organisms also comprised bacteria expressing all three known pantothenate kinase (PanK; Figure 3A) types: the enterococci, streptococci, *H. influenzae*, and *E. coli* are known or predicted to have PanK_I enzymes, while *M. catarrhalis* is predicted to have a PanK_{III} (Yang et al., 2006). Importantly, the staphylococci are the only known bacteria to have an active PanK_{II}, suggesting that the presence of this PanK type is a prerequisite for inhibition by CJ-15,801.

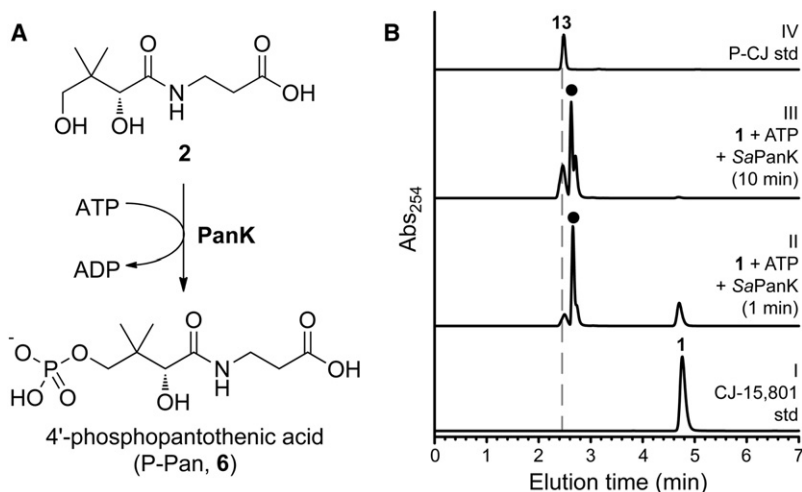


Figure 3. Evaluation of PanK as a Potential Gatekeeper to CJ-15,801's Inhibitory Action

(A) The ATP-dependent phosphorylation of pantothenic acid (**2**) catalyzed by PanK enzymes.

(B) HPLC analysis of the putative ATP-dependent phosphorylation of CJ-15,801 by SaPanK. The traces represent: I, a synthetically prepared standard of CJ-15,801 (**1**); II, a reaction mixture containing CJ-15,801, ATP and SaPanK that had been incubated for 1 min; III, the same after 10 min of incubation; and IV, a synthetic P-CJ (**13**) standard. The peak labeled with (●) represents ATP and ADP.

See also Table S2.

To test this hypothesis, we repeated the CJ-15,801 susceptibility tests against a panel of organisms representing all combinations of cell envelope and PanK type. Since the original tests were conducted in growth medium rich in pantothenic acid, these experiments were conducted in 1% tryptone (that contains essentially no pantothenic acid) instead to exclude any potential antagonistic effects that the presence of the vitamin could have on inhibition. The results show that the PanK_{II}-containing *S. aureus* (MRSA strain TCH1516) was the most sensitive to the inhibitory effects of CJ-15,801, showing an MIC of 15 μ M (Table S1 available online). This value is 2-fold lower than the lowest MIC reported in the previous susceptibility tests, suggesting that pantothenate does affect inhibition similar to what was seen in the experiments with malaria parasites (Saliba and Kirk, 2005). Moreover, under these test conditions some of the other organisms (most notably *P. aeruginosa*) also showed low levels of inhibition (MIC \sim 60 μ M).

To determine which aspects of CJ-15,801's structure are required for inhibition, we evaluated the inhibitory activity of the (Z)-configured analog (**Z-1**) and CJ-15,801's methyl ester (CJ-OME, **11**) against *S. aureus*. Neither compound showed any inhibition, indicating that the configuration of the double bond and the availability of the free carboxylate of CJ-15,801 are both important determinants for its mechanism of inhibition.

Only PanK_{II} Enzymes Accept CJ-15,801 as Substrate

To confirm that the observed inhibition results can indeed be correlated with PanK type and activity, we performed in vitro activity analyses using purified PanK enzymes. Based on the inhibition results, we first used the most likely candidate, the PanK_{II} enzyme from *S. aureus* (SaPanK_{II}), to determine if it converts CJ-15,801 to phospho-CJ,15,801 (P-CJ, **13**) when incubated with ATP. High-performance liquid chromatography (HPLC) analysis of the reaction mixture confirmed this to be the case, based on the time-dependent formation of P-CJ (Figure 3B). Next, the activity of the PanK_I from *E. coli* (EcPanK_I), SaPanK_{III}, and the PanK_{III} from *P. aeruginosa* (PaPanK_{III}) toward CJ-15,801 were fully characterized kinetically. The resulting data indicate that EcPanK_I and PaPanK_{III} only show activity toward pantothenic acid and not CJ-15,801;

moreover, neither enzyme was inhibited by 100 μ M CJ-15,801 (Table S2). However, SaPanK_{II} shows little distinction between CJ-15,801 and pantothenic acid, exhibiting

specificity constants (k_{cat}/K_m) of $13.8 \pm 4.2 \text{ mM}^{-1}\cdot\text{s}^{-1}$ and $30.2 \pm 8.7 \text{ mM}^{-1}\cdot\text{s}^{-1}$ for the two compounds, respectively, with the difference being mainly due to an elevated K_m value. The enzyme also acts on CJ-OME, indicating that the lack of inhibition seen for this analog is due to effects downstream of PanK.

Taken together, these results indicate that PanK acts as a gatekeeper to the inhibitory effects of CJ-15,801 in *S. aureus*.

CJ-15,801's Antistaphylococcal Activity Is Affected by Pantothenic Acid and Pantetheine

The observation that *S. aureus*'s susceptibility to inhibition by CJ-15,801 is apparently affected by pantothenic acid (**2**), as well as the finding that SaPanK_{II} accepts both the inhibitor and the vitamin as substrates, led us to perform checkerboard assays to quantify these effects (Figure 4A). The same assay was also conducted with pantetheine (**17**), the precursor to the CoA salvage pathway that bypasses the PPCS and phosphopantothenoylcysteine decarboxylase (PPCDC) enzymes (Strauss, 2010; Strauss et al., 2010) (Figure 4B). The results show that the presence of either compound reduces the potency of CJ-15,801, most likely through competition with SaPanK_{II}. However, their interaction with the natural product is complex, since increasing the concentration of either compound above a certain level (\sim 7.5 μ M for **2**, and \sim 15 μ M for **17**) leads to inhibition being reestablished. While the basis for this observation is currently unknown, the results confirm that the point of CJ-15,801's inhibitory action is a process dependent on pantothenic acid (or pantetheine).

Pantothenamides Increase the Potency of CJ-15,801's Antistaphylococcal Activity

Previous studies have shown that treatment of *S. aureus* with N5-Pan (and its analog, N-heptylpantothenamide, N7-Pan) results in growth inhibition by formation of inactive carrier proteins (Figure 1E) (Leonardi et al., 2005; Zhang et al., 2004). To determine if the points of action of the pantothenamides and CJ-15,801 overlap, a checkerboard assay with N5-Pan (**4**) and CJ-15,801 was performed in 1% tryptone media (Figure 4C). The results show that when combined, CJ-15,801 and N5-Pan exhibited significantly reduced MICs of 3.75 μ M and \sim 1.0 μ M,

Chemistry & Biology

Mode of Action of the Antibiotic CJ-15,801

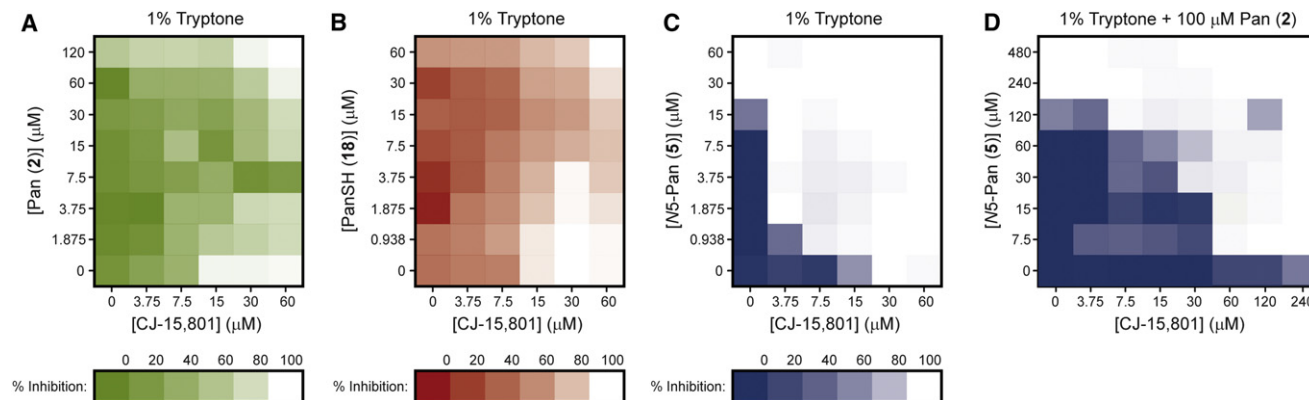


Figure 4. Synergism in the Antibacterial Action of CJ-15,801 and N5-Pan

(A) Checkerboard assay of the growth inhibition of *S. aureus* by CJ-15,801 (1) when grown in the presence of pantothenic acid (2) in 1% tryptone shows that increasing the amount of vitamin (up to a certain concentration) reverses the inhibition. MIC value for CJ-15,801 is 15 μ M.

(B) As for (A), but with pantetheine (17) added instead of pantothenic acid.

(C) Checkerboard assay of the growth inhibition of *S. aureus* grown in 1% tryptone by CJ-15,801 (1) and N5-Pan (4) demonstrates the synergism between these compounds (FICI < 0.5). MIC value for N5-Pan is 30 μ M.

(D) As for (C), but determined in the presence of 100 μ M pantothenic acid (2), demonstrating that the combination of CJ-15,801 and N5-Pan can overcome the antagonism caused by an excess of the natural substrate of the CoA biosynthetic pathway, but at the expense of converting the synergism to an additive effect (0.5 < FICI < 1.0).

See also Tables S1 and S3.

respectively, with a fractional inhibitory concentration index (FICI) of 0.25, indicating synergism (Table S3). Importantly, when the same assay was performed in the presence of 100 μ M pantothenic acid, the inhibition was not as adversely affected as in the case of the individual compounds (Figure 4D). Instead, the MIC values were slightly elevated and the previously observed synergism was converted to an additive inhibitory effect (FICI \sim 0.5–1.0) (Table S3). This finding suggests that CJ-15,801 and N5-Pan does not have the same mode of action and indicates that in combination these compounds can counter the antagonism caused by pantothenic acid.

Synthesis of the 4'-Phosphates of CJ-15,801 and Its Methyl Ester

The discovery that SaPanK phosphorylates both CJ-15,801 and CJ-OMe (11) provided us with a convenient biocatalytic method by which their 4'-phosphorylated versions could be prepared. P-CJ (13) and its methyl ester, 12 (P-CJ-OMe), were therefore obtained by milligram-scale biotransformations using recombinant SaPanK and ATP, followed by purification by either preparative HPLC (for P-CJ) or solid-phase extraction (SPE) (for P-CJ-OMe) (Figure 2).

PPCS Accepts P-CJ as Substrate and Is Then Inhibited by It

With the knowledge that CJ-15,801 can be converted to P-CJ within *S. aureus*, we set out to determine if PPCS, the next enzyme in the pathway, is the target for the antibiotic's inhibitory action. PPCS catalyzes the condensation of P-Pan (6) with L-cysteine to form 4'-phosphopantothencysteine (PPC, 15) using a two-step acyl transfer mechanism common to most synthetase (C-N ligase) enzymes, including all the amino acid tRNA synthetases and the adenylation domains of the modular nonribosomal peptide synthetases (NRPSs) (Figure 5A)

(Schimmel et al., 1998; Sieber and Marahiel, 2005). While all known PPCSs follow this general scheme, bacterial enzymes are unique in that they use CTP instead of ATP as nucleotide source for the activation reaction, and therefore form 4'-phosphopantothencyl-CMP (P-Pan-CMP, 14) as intermediate (Kupke, 2002, 2004; Manoj et al., 2003; Stanitzek et al., 2004; Strauss, 2010; Strauss et al., 2001).

In most bacteria PPCS activity is located on one domain of the bifunctional CoaBC protein (which also carries PPCDC activity), although monofunctional PPCS enzymes do occur in certain enterococci (such as *Enterococcus faecalis* [Yao et al., 2009]) and streptococci. Among all bacterial PPCS enzymes the PPCS activity of *E. coli*'s bifunctional CoaBC protein is by far the best studied: its mechanism has been established through trapping and isolation of P-Pan-CMP (14), and the structure of the N210D mutant with the trapped intermediate 14 bound in the active site has been determined (Kupke, 2002, 2004; Stanitzek et al., 2004). Moreover, many of these studies were performed using the separate PPCS domain (*EcPPCS*) expressed and purified on its own, showing that the two activities of the bifunctional CoaBC protein are independent. This conclusion is also supported by kinetic isotope studies of the PPCDC activity of *E. coli*'s CoaBC (Strauss and Begley, 2001). We therefore decided to use the *EcPPCS* domain to perform the initial tests on the interaction of PPCS and P-CJ.

To determine if P-CJ is accepted as an alternate substrate by PPCS and forms the corresponding P-CJ-CMP intermediate 16 (Figure 5B), mixtures of P-CJ and CTP were incubated with increasing concentrations of *EcPPCS*. A clear correlation between the rate of pyrophosphate release and enzyme concentration was evident in such reactions (Figure 5C). Moreover, HPLC analysis of the reaction mixture containing the highest *EcPPCS* concentration (24 μ M) showed the formation of a peak absent in native reaction mixtures, or in mixtures

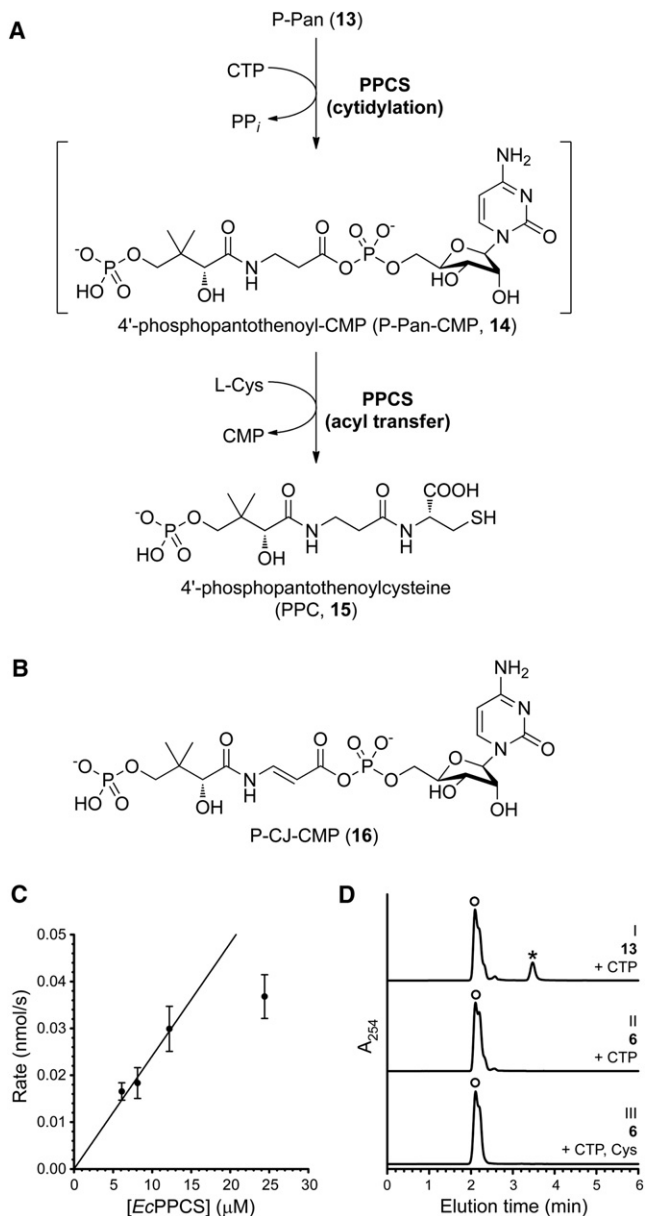


Figure 5. Evaluation of PPCS Activity with P-CJ (13) as Substrate

(A) The reaction catalyzed by PPCS, showing the two steps of its mechanism and the P-Pan-CMP (14) reaction intermediate.

(B) The structure of P-CJ-CMP (16) resulting from the putative cytidylation of P-CJ (13) by PPCS.

(C) The rate of pyrophosphate release from a reaction mixture containing P-CJ (13), CTP, and *EcPPCS* correlates with enzyme concentration. Experiments were run in duplicate; the shown data points are the average of duplicate assays (error bars indicate the SD).

(D) HPLC analysis of a reaction mixture containing P-CJ (13), CTP, and *EcPPCS* (24 μ M) (trace I) show the formation of a new peak (indicated with an asterisk) that represents P-CJ-CMP (16) based on LC-MS analysis. This peak is not present when P-CJ is replaced with P-Pan (6) (trace II) or in native reaction mixtures containing P-Pan, CTP and L-cysteine. Note that the retention time of pure P-CJ is \sim 2.4 min (see Figure 2B). The broad peak labeled with (○) represents CTP and CMP.

See also Figure S1.

containing P-Pan (6) instead of P-CJ, suggesting the formation of P-CJ-CMP (Figure 5D). Note that P-Pan-CMP is usually not observed under these conditions, as was previously reported (Kupke, 2002, 2004). Liquid chromatography-tandem mass spectrometry (LC-MS) analysis was subsequently conducted on the same mixture. While the P-CJ-CMP-derived molecular ion was not observed, the corresponding mass spectrum did show mass peaks that are in agreement with the fragmentation of P-CJ-CMP (Figure S1). The same experiment was subsequently repeated with the bifunctional CoaBC protein from *S. aureus* (SaCoaBC). A similar result was obtained, although the apparent rate of conversion of P-CJ into P-CJ-CMP was significantly slower than for *EcPPCS* (Figure S1).

In combination, these results indicate that P-CJ is accepted as an alternate substrate by PPCS, which cytidylylates its carboxylate to form P-CJ-CMP.

PPCS Transform P-CJ into P-CJ-CMP, which Inhibits Its Activity

Subsequent activity analysis of PPCS in the presence of P-CJ, CTP, and L-cysteine failed to show catalytic turnover. Moreover, when P-CJ was added to PPCS reaction mixtures containing the enzyme's native P-Pan substrate, the rate of the reaction was reduced compared to mixtures without it, suggesting inhibition by P-CJ. To confirm that such inhibition is dependent on the reaction catalyzed by PPCS, an inhibition screen was performed in which CJ-15,801, CJ-OMe, P-CJ, or P-CJ-OMe was added to native PPCS reaction mixtures at a concentration of 100 μ M. The results showed that among these compounds, only P-CJ inhibited *EcPPCS* (data not shown). The lack of inhibition by P-CJ-OMe indicated that the free carboxylate group is required for inhibition, while the inability of CJ-15,801 to affect enzyme activity highlights the necessity of the phosphate group for binding. Taken together with the results described above, these findings reveal PPCS as CJ-15,801's target of inhibitory action, which is achieved through formation of P-CJ-CMP 16 as an apparent dead-end inhibitor.

Kinetic Characterization Reveals P-CJ-CMP as a Tight-Binding Inhibitor of PPCS

Inhibition by P-CJ-CMP could potentially occur by either of the proposed irreversible inhibition mechanisms (Figures 1C and 1D), or by a completely unrelated mechanism. To elucidate the actual mechanism of inhibition, detailed kinetic analyses were performed. First, dose-response curves were used to evaluate the inhibition of the cytidyl-transfer reaction catalyzed by *EcPPCS*. The resulting IC_{50} value of 2.66 ± 0.16 μ M, determined using saturating concentrations of CTP and 100 μ M P-Pan (note that *EcPPCS* experiences substrate inhibition, see Figure S2), was less than 10-fold the concentration of enzyme used in these assays (240 nM). This indicated that P-CJ-CMP acts as either a tight-binding or irreversible inhibitor of *EcPPCS* (Copeland, 2000). The inhibition of *EcPPCS* was next studied by the progress curve method. The resulting curves increased in a linear fashion, showing a decreased rate at increased concentrations of P-CJ (Figure 6A). Surprisingly, this indicated that the inhibition was tight binding and not irreversible (which would have led to the steady-state rates approaching zero) as predicted (Copeland, 2005). This finding was confirmed by showing that

Chemistry & Biology

Mode of Action of the Antibiotic CJ-15,801

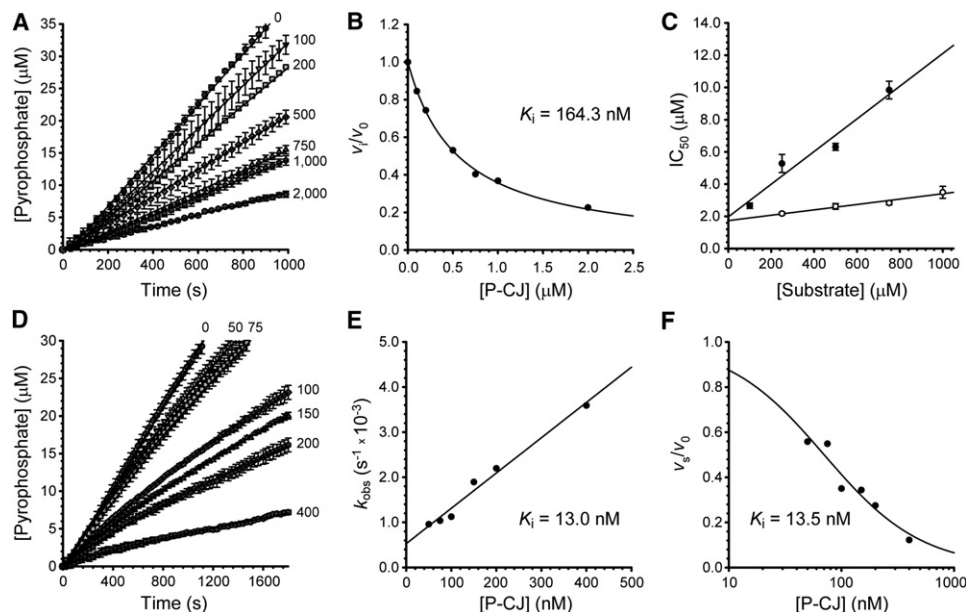


Figure 6. Kinetic Characterization of the CJ-15,801-Based Inhibition of PPCS

(A) Progress curves analysis for the inhibition of *EcPPCS* in the presence of increasing concentrations of P-CJ (**13**), indicated in nM next to each curve.

(B) Plot of the fractional activity (initial velocity v_i relative to the inhibited velocity v_0), as determined from the progress curves in (A), against inhibitor concentration. The indicated K_i value is determined by fitting the data to the Morrison and Cheng-Prusoff equation.

(C) Determination of the inhibition modality of *EcPPCS* by P-CJ (**13**) by calculation of the IC_{50} values in the presence of increasing concentrations of P-Pan (**6**) (●), and CTP (○).

(D) Progress curves analysis for the inhibition of *SaCoaBC* in the presence of increasing concentrations of P-CJ (**13**), indicated in nM next to each curve.

(E) Plot of the first order rate of inactivation constants (k_{obs}), as determined from the data presented in (D), against inhibitor concentration. The indicated K_i value is determined by fitting the data to the equation for a straight line.

(F) Plot of the fractional activity (steady-state velocity v_s relative to the inhibited velocity v_0), as determined from the progress curves in (D), against inhibitor concentration. The indicated K_i value is determined by fitting the data to a Langmuir isotherm.

All progress curve analyses were performed in triplicate (error bars represent the SD).

See Supplemental Experimental Procedures for details on calculations, as well as Figure S2 for the determination of *EcPPCS* and *SaCoaBC* kinetic parameters.

removal of the inhibitor by gel filtration was sufficient to restore the activity of a sample of *EcPPCS* that had been pretreated with P-CJ and CTP.

The K_i^{app} (apparent inhibition constant) was subsequently calculated by plotting the fractional activity versus inhibitor concentration, fitting the data to the Morrison equation (Figure 6B), and converting the obtained value to the true K_i by applying the appropriate Cheng-Prusoff equation (Copeland, 2000, 2005). The mode of inhibition was established using a method specifically developed for tight-binding inhibitors in which IC_{50} values are determined at a fixed enzyme concentration, but in the presence of increasing concentrations of either P-Pan (**6**) or CTP (Figure 6C). A linear increase in IC_{50} values with increasing concentration of P-Pan but not CTP indicates that inhibition is competitive toward P-Pan but noncompetitive toward CTP (Copeland, 2000, 2005). This observation agrees with previous studies of the *E. faecalis* and human PPCS enzymes that determined an ordered Bi Uni Uni Bi Ping-Pong kinetic mechanism with CTP binding first, followed by P-Pan (**6**) (Yao and Dotson, 2009; Yao et al., 2009). In this manner, a K_i of 164.3 nM was determined for P-CJ's inhibition of *EcPPCS*.

While *EcPPCS* is a convenient and well-studied model to use for characterization of CJ-based inhibition, *E. coli* is not affected

by CJ-15,801 due to the gatekeeping activity of its PanK (Tables S1 and S2). We therefore performed the same kinetic analysis on *SaCoaBC*, which is expected to be the natural target for CJ-15,801's observed antistaphylococcal action. A progress curve analysis similar to that conducted on *EcPPCS* showed that *SaCoaBC* experiences time-dependent inhibition, since the curves showed a fast initial velocity (v_i) phase and a slower steady-state velocity (v_s) phase (Figure 6D). The first order rate of inactivation constants (k_{obs}) were subsequently determined and plotted against the inhibitor concentration. The resulting plot (Figure 6E) showed a linear relationship between k_{obs} and $[I]$, which points to a one-step inhibition mechanism (Copeland, 2005). However, it is more likely that the true mechanism consists of two steps, with P-CJ **13** binding first in a reversible manner, followed by the slow formation of P-CJ-CMP. Such a mechanism would be kinetically indistinguishable from a one-step mechanism.

The K_i value for the inhibition of *SaCoaBC* by P-CJ-CMP can be determined from the slope and y-intercept of the linear plot shown in Figure 6E. The K_i value can also be calculated by using the progress curves to determine the steady-state velocity (v_s) at each inhibitor concentration; a plot of the fractional activity against inhibitor concentration yields an isotherm curve with the K_i at its midpoint (Figure 6F) (Copeland, 2005). In this manner,

K_i values of 13.0 and 13.5 nM were determined, respectively. These values are nearly an order of magnitude lower than that determined for EcPPCS, clearly showing that the nature of the actual target protein also plays an important role in the extent of inhibition. Taken together, these data show that P-CJ-CMP acts as a tight-binding inhibitor of PPCS enzymes.

Analysis of the Mechanistic Basis for the Tight-Binding Inhibition of P-CJ-CMP

The close structural homology between P-Pan-CMP (**14**) and P-CJ-CMP (**16**), and the fact that both compounds contain reactive acyl phosphate moieties, raises a question regarding the mechanistic basis for the inhibition by P-CJ-CMP. We considered three possible explanations: first, inhibition is based on differences in the electrophilicity of the carbonyl carbon of the acyl phosphate moieties of P-Pan-CMP and P-CJ-CMP, respectively; second, inhibition is caused by the two compounds having different binding modes in the active site, due to the structural nature of the planar *N*-acyl vinylogous carbamate functionality of P-CJ-CMP; and third, inhibition is caused by P-Pan-CMP and P-CJ-CMP having different effects on any conformational changes that occur during catalysis through stabilization of the protein's quaternary structure. While the significant synthetic effort that is required to prepare P-Pan-CMP and P-CJ-CMP precluded a direct experimental comparison of their respective reactivities, we were able to perform tests to assess whether the latter two proposed mechanisms contribute to inhibition.

To establish if P-Pan-CMP (**14**) and P-CJ-CMP (**16**) have different binding modes, we used the only available structure of a PPCS enzyme with its intermediate bound, that of the EcPPCS Asn210Asp mutant with P-Pan-CMP bound in the active site (PDB ID: 1U7Z). This mutant, which accumulates sufficient amounts of the intermediate to have allowed direct confirmation of its identity and structure (Kupke, 2004; Stanitzek et al., 2004), is apparently unable to catalyze the second step of the PPCS reaction. However, the molecular basis for this catalytic disability remains speculative since no PPCS structure with cysteine bound has been determined thus far. Nonetheless, the mutation clearly results in tightly bound P-Pan-CMP in the enzyme's active site.

We constructed a model of the native enzyme by reversing the Asn210Asp mutation in the crystal structure and used it to dock P-CJ-CMP (**16**) in the active site using 150 starting conformations to ensure sufficient conformational space was sampled considering the complexity of the molecule. The highest scoring docked pose of P-CJ-CMP very closely mimics the pose of the cocrystallized P-Pan-CMP in the crystal structure (Figure 7A), and facilitates all the same hydrogen bonding interactions while maintaining a near planar geometry across the *N*-acyl vinylogous carbamate moiety (Figure 7B). This suggests that the basis for inhibition by P-CJ-CMP is not due to it having a different binding mode, or taking on a potentially unreactive conformation.

Members of the ANL superfamily of adenylating enzymes, such as the adenylation domains of the NRPSs, use a large domain rotation event to facilitate the catalysis of their two-step reactions (Gulick, 2009). While it is currently unknown whether PPCS enzymes, which belong to the ribokinase family, undergo similar large conformational changes during catalysis, the determined crystal structures of the *E. coli* and human

proteins show that they occur as dimers, with the dimer interface partially occluding the active site (Manoj et al., 2003; Stanitzek et al., 2004). To evaluate the effect of different ligands on the enzyme's overall stability, the melting temperatures (T_m) of the EcPPCS protein in the presence of its native substrates or the inhibitor were determined by following the heat-induced denaturation of these mixtures by circular dichroism (CD). The results show that the T_m increases from 47.7°C (for the free enzyme) to 49.7°C (for the enzyme bound to CTP) to 54.3°C (for the enzyme bound to P-Pan-CMP, formed in situ from P-Pan and CTP), highlighting the many stabilizing interactions the protein has with its native ligands (Figure 7C). Importantly, the T_m of EcPPCS bound to P-CJ-CMP (formed in situ from P-CJ and CTP) shows an even larger increase to 57.3°C. When the same experiment was conducted with the bifunctional SaCoaBC, the protein showed increased stability compared to EcPPCS (CoaBC proteins exist as higher order oligomers, usually dodecamers [Manoj et al., 2003]), but only small differences in the T_m values for the protein in the absence and presence of its native ligands. However, the T_m showed an impressive improvement from ~65°C to 85°C for the proteins bound to P-Pan-CMP and P-CJ-CMP, respectively (Figure 7D). Taken together, these findings indicate that the binding of the conformationally more rigid ligand **16** results in an increased stabilization of the PPCS oligomers and the trapping of the ligand in the active site. This stabilization, which may be due to interactions between the ligand and residues of the adjacent monomer (such as Lys289, see Figure 7B) contained in a disordered loop that partially covers the entrance to the active site (Figure 7E), is therefore most likely an important contributor to the mechanism of inhibition by P-CJ-CMP.

DISCUSSION

One of the biggest obstacles to elucidation of the CJ-15,801 mode of action is scarcity of the natural product. The original discoverers shared the bulk of the isolated material with the authors of a malaria parasite inhibition study (Spry et al., 2008), but new stocks are unlikely to be obtained in this manner since the CJ-producing *Seimatosporium* strain can currently not be traced due to closure of the laboratory in which it was characterized (Y. Sugie, personal communication). New developments in the synthesis of CJ-15,801 have certainly improved the situation, but the unique sensitivity of the *N*-acyl vinylogous carbamic acid functionality still presents a significant challenge to the synthesis of this antibiotic.

The original finding that CJ-15,801 is highly selective in its antibiotic action, affecting only *S. aureus* strains among a range of other Gram-positive bacteria including *Streptococcus* and *Enterococcus* spp. (Sugie et al., 2001), provoked curiosity in regards to its mechanism of action. Here, we show that the primary reason for this selectivity is the substrate specificity of the host organism's PanK enzyme. Only the PanK_{II} of *S. aureus* accepts CJ-15,801 and phosphorylates it, thereby allowing it to enter the CoA biosynthetic pathway. Interestingly, SaPanK_{II} is the only known active bacterial representative of a type II PanK; all other examples occur in eukaryotes. However, an earlier study showed that CJ-15,801 does not inhibit rat hepatoma cells, suggesting that typical eukaryotic PanKs do not act as

Chemistry & Biology

Mode of Action of the Antibiotic CJ-15,801

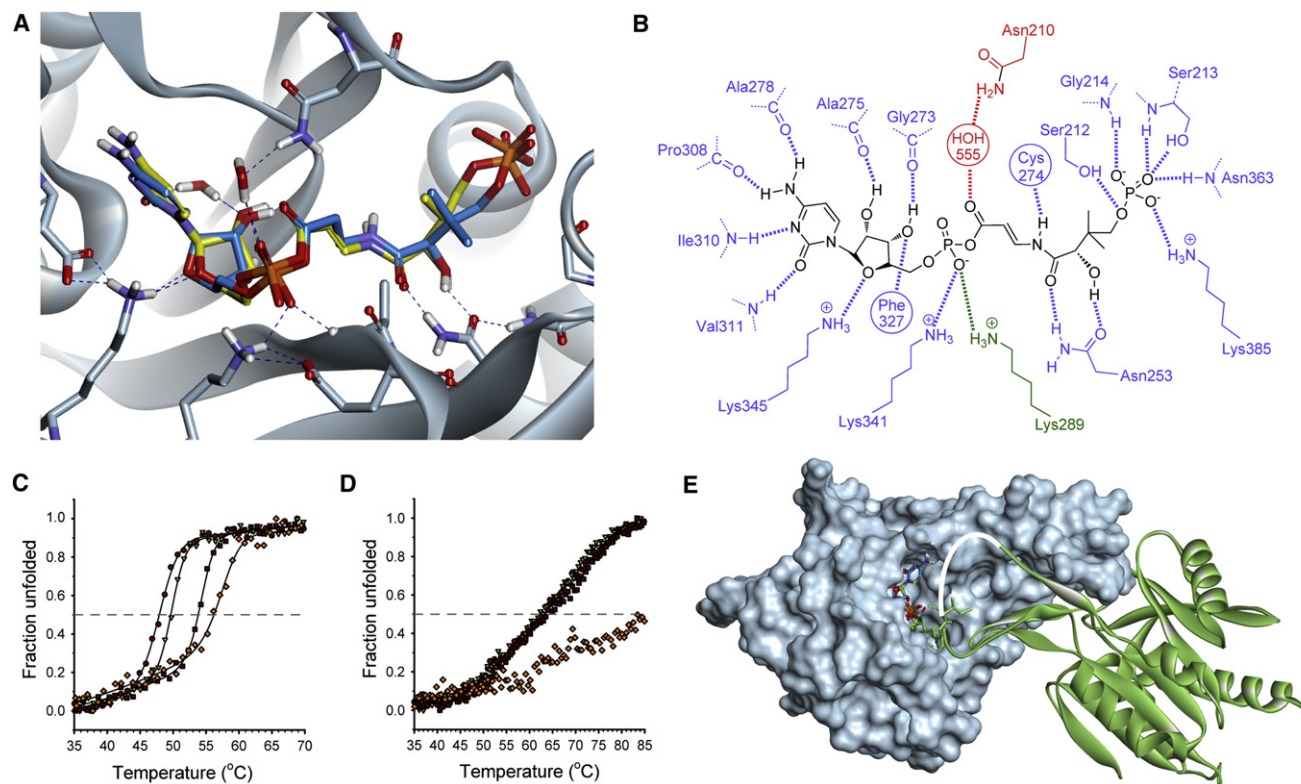


Figure 7. Structural Basis for the Tight-Binding Inhibition of the CJ-15,801-Derived Inhibitor

(A) Structure of the P-CJ-CMP inhibitor **16** (stick structure with carbon atoms in yellow) modeled and overlaid on that of the P-Pan-CMP intermediate **14** (stick structure with carbon atoms in blue) bound in the active site of native EcPPCS. The model was created from the crystal structure of EcPPCS Asn210Asp with cocrystallized P-Pan-CMP **14** bound (PDB: 1U7Z) by reversing the mutation, and docking P-CJ-PMP. The highest scoring pose of P-CJ-CMP closely resembles that of P-Pan-CMP and similarly facilitates all hydrogen bonding interactions observed for P-Pan-CMP. Only selected residues are shown for clarity.

(B) Schematic view of polar interactions between P-CJ-CMP and EcPPCS. Residues from monomer A are in blue and those from monomer B in green. The key interaction between Asn210 and the acyl phosphate carbonyl, mediated via a bridging water molecule, is shown in red.

(C) Heat-induced protein melting curves for EcPPCS. The four curves represent from left to right: the free protein (●); protein with MgGTP (▽); protein with MgGTP and P-Pan (**2**) (■); and protein with MgGTP and P-CJ (**13**) (■ ■ ■). The curves were determined by following changes in the protein's secondary structure by circular dichroism.

(D) Heat-induced protein melting curves for SaCoaBC determined as for EcPPCS in (B).

(E) Structure of the EcPPCS dimer (PDB: 1U7Z) with one monomer shown as a solvent-accessible surface (in cyan) and the other as ribbon structure (in green). The overlaid P-Pan-CMP and P-CJ-CMP stick structures are shown docked in the active site. Note that residues 291–298, which form part of a loop (shown in white) that cover the active site, is normally disordered and is absent in all crystal structures of PPCS enzymes (Manoj et al., 2003; Stanitzek et al., 2004). See also Figure S4.

gateways to its antibiotic action (Saliba and Kirk, 2005). Such a conclusion is supported by the results of a structure-activity relationship study of the inhibition of EcPanK_I and the PanK_{II}s from *Aspergillus nidulans*, *Mus musculus* (mouse), and *S. aureus* by the pantothenamides, which showed a clear differentiation between eukaryotic PanK_{II}s and SaPanK_{II}, and even between the eukaryotic PanK_{II}s themselves (Virga et al., 2006). The varied selectivity of PanK_{II}s have clearly not been fully explored, since *P. falciparum* (which is also sensitive to inhibition by CJ-15,801) is also predicted to have a PanK_{II} (Spry et al., 2010).

The evolution of CJ-15,801 as a natural product that specifically targets the *S. aureus* CoA biosynthetic pathway may reflect this organism's unique redox physiology. Like some other Gram-positive bacteria, including *Bacillus anthracis* (Nicely et al., 2007), *S. aureus* does not contain glutathione but instead relies on the sacrificial oxidation of CoA and a specific NADPH- and flavin-

dependent CoA disulfide reductase (CoADR) enzyme to maintain its intracellular redox balance (delCardayre and Davies, 1998; Mallett et al., 2006). This causes *S. aureus* to maintain high intracellular levels of reduced CoA (Newton et al., 1996), which imparts an additional unique characteristic to SaPanK_{II}: unlike other eukaryotic PanK_{II}s, it is refractory to feedback inhibition by CoA and its thioesters (Choudhry et al., 2003; Hong et al., 2006; Leonardi et al., 2005). The combination of *S. aureus*'s distinctive reliance on CoA biosynthesis and the unique characteristics of its SaPanK_{II} enzyme have seemingly created an ideal target for antibacterial action that was eventually exploited through the production of CJ-15,801.

The interaction between CJ-15,801 and pantothenic acid and its analogs is complex, and warrants further study (Figures 4A and 4B). The observation that inhibition by CJ-15,801 is alleviated in the presence of either pantothenic acid or pantetheine

is expected in light of its determined mode of action; however, it is unclear why the inhibition returns when the concentrations of the vitamin is increased beyond a certain level. It is possible that the susceptibility to CJ-15,801 under these circumstances is due to the high concentrations of pantothenic acid stimulating CoA biosynthesis, as this would result in increased amounts of P-CJ-CMP being formed. The low levels of inhibition seen in the absence of pantothenic acid in organisms such as *P. aeruginosa* that cannot form P-CJ (and which therefore should not experience any inhibition by the mechanism proposed here) is probably due to similar effects on the regulation of pantothenic acid biosynthesis and/or utilization. However, such effects are clearly weak, as they are completely abolished in the presence of increased concentrations of the vitamin.

The finding that CJ-15,801 and members of the pantothenamide class of antibiotics work in a synergistic fashion supports most studies that have indicated that the pantothenamides have a target downstream of CoA biosynthesis (Figure 4C) (Leonardi et al., 2005; Mercer et al., 2009; Thomas and Cronan, 2010; Zhang et al., 2004). Moreover, such a combination can apparently maintain its inhibitory effects even in the presence of pantothenic acid (Figure 4D). This indicates that it is possible to increase the modest antistaphylococcal activity of CJ-15,801 and even counteract the antagonism caused by pantothenic acid by combining it with other appropriate inhibitors, especially those that also affect CoA-based metabolism.

The finding that P-CJ-CMP acts as a tight-binding inhibitor of the PPCS enzyme can be rationalized in light of the findings of previous studies that have shown that nonhydrolyzable mimics of acyl nucleotidylate intermediates are often potent (tight-binding) inhibitors of enzyme activity (Cisar and Tan, 2008; Kim et al., 2003; Schimmel et al., 1998). In fact, this strategy was also successfully applied to PPCS in a study in which the phosphodiester analog of P-Pan-CMP was shown to be a potent inhibitor of the PPCS of *E. faecalis* (Patrone et al., 2009). However, the finding that P-CJ-CMP does not undergo attack by cysteine in spite of having an activated acyl phosphate moiety remains surprising. Of the three possible mechanisms that were considered for the inhibition by P-CJ-CMP, the most likely is that the introduction of the conjugated system in the β -alanine moiety reduces the reactivity of the acyl phosphate carbonyl toward nucleophilic attack. Such a reduced activity could be based on electronic effects, or be due to the potential tautomerization of the carbonyl enamine function of the inhibitor to an enol imine. Such a modification in reactivity has been noted in similar systems, as in the case of the vinylogous carbamate ester that forms as a result of the mechanism of action of the β -lactamase inhibitor clavulanate (and penam sulfones), and which has been reported to be stable toward hydrolysis (Imtiaz et al., 1993). However, structural studies have indicated that this stability is partly due to interactions with active site residues, and that it can be enhanced by manipulation of these interactions (Padayatti et al., 2005, 2006). Our model of P-CJ-CMP docked in the active site of EcPPCS does not show the formation of any new active site-ligand interactions that are not present with P-Pan-CMP, suggesting that such factors are not at play in the inhibition of PPCS by P-CJ-CMP.

Our experiences with the synthetic preparation of CJ-15,801 (Figure 2) indicated that the conjugation provided by the unsatu-

rated β -alanine moiety does deactivate this center. Specifically, all chemical attempts to hydrolyze the methyl esters **9** and **11** en route to **1** proved difficult and inefficient, which necessitated the use of an allyl ester protection strategy that deprotects via nonhydrolytic mechanisms. However, direct evidence for the difference in reactivities between P-CJ-CMP and P-Pan-CMP will have to be obtained through experimentation with model systems; these studies are currently under way.

Nonetheless, the results of the temperature melting curve analyses clearly show that P-CJ-CMP also significantly improves the overall stabilization of PPCS oligomers compared to the natural intermediate P-Pan-CMP, indicating that the stabilization of certain conformations of the enzyme could also be an important factor causing inhibition. The finding that the extent of apparent stabilization is much larger for SaCoaBC than EcPPCS (which is in agreement with the significantly lower K_i observed in the case of the former protein) could be due to the increase in stability being compounded in the bifunctional CoaBC proteins that usually form dodecamers instead of the dimers formed by most PPCS enzymes. We conclude that this stabilization prevents further reaction by cysteine by protecting the potentially reactive P-CJ-CMP intermediate, resulting in its trapping in the active site and the observed inhibition. This analysis is supported by the available EcPPCS structures, which show significant differences in the active site architectures of the CTP (PDB: 1U7W), P-Pan-CMP (PDB: 1U7Z), and CMP-bound (PDB: 1U70) forms of the enzyme, indicating that the enzyme undergoes significant movement during catalysis.

In conclusion, we have demonstrated that the natural product CJ-15,801 hijacks the CoA biosynthetic pathway, and inhibits its second enzyme by forming a tight-binding inhibitor in situ within the active site. This mechanism is highly reminiscent of that of the sulfonamide antibiotics, which inhibit the biosynthesis of another vitamin—folic acid—in a similar manner. The mechanism is also complementary to that employed by an adenosine sulfamate inhibitor of ubiquitin-like protein conjugation pathways, which also forms a nonhydrolyzable mimic of its target's reaction intermediate in situ (Brownell et al., 2010; Chen et al., 2011). Taken together, these findings provide important new insights into inhibitors that target CoA biosynthesis and CoA-utilizing enzymes. They also highlight an alternative strategy for inhibitor development—one based on the stabilization of certain protein conformations—that may also hold significant potential for drug design efforts targeting other medicinally relevant synthetase enzymes.

SIGNIFICANCE

The antibiotic CJ-15,801 was found to be a selective inhibitor of CoA biosynthesis in *S. aureus* due to the unique selectivity of SaPanK, the first enzyme of the CoA pathway, which currently is the only known example of an active bacterial PanKII enzyme. This demonstrates that the diversity of PanK enzymes can be exploited for selective inhibition or, as in this case, specific gatekeeping functions. The phospho-CJ-15,801 product that forms as a result of the phosphorylation by PanK subsequently acts as a substrate for PPCS, which transfers a cytidyl group to its carboxylate to form P-CJ-CMP. Surprisingly, this reaction does not result

Chemistry & Biology

Mode of Action of the Antibiotic CJ-15,801

in the formation of an electrophilically reactive intermediate; instead P-CJ-CMP acts as a potent tight-binding inhibitor of the enzyme. The results of temperature-dependent stability studies indicate that this inhibition is at least partly due to stabilization of the interactions between the adjacent monomers in the PPCS dimer, which seemingly prevents the reaction of cysteine—the second substrate in the PPCS reaction—with the activated acyl group of P-CJ-CMP. These findings indicate that the inhibition of synthetase enzymes by nonreactive analogs of their intermediates may have an alternative mechanistic basis in some cases, which is the stabilization of certain structural conformations, and that this should be considered as a potential new strategy for the inhibition of these enzymes. The findings also reveal CJ-15,801 as an antimetabolite of a vitamin biosynthetic pathway, similar to the sulfonamide antibiotics. Finally, we show that the potency of CJ-15,801 is significantly improved in combination with a pantothenamide, a known CoA antimetabolite precursor, confirming that these antimicrobials have different points of action and establishing the potential of drug development strategies that are focused on enzymes involved in CoA biosynthesis and utilization.

EXPERIMENTAL PROCEDURES

See Supplemental Experimental Procedures for full details of all synthetic procedures (including characterization data for all compounds), antibacterial activity assays, procedures for the preparation of proteins, enzyme assays and accompanying data analyses, and protein melting temperature determinations and analysis.

Synthesis of CJ-15,801 and Its Analogs

The inhibitor and its analogs were prepared by modification of published procedures (Figure S3) (Nicolaou and Mathison, 2005; Sewell et al., 2011; Villa et al., 2007).

Inhibition Assays and Analysis

The activity of CJ-15,801 against test strains of *S. aureus*, *Streptococcus agalactiae*, *E. coli*, *P. aeruginosa*, and *Bacillus subtilis* was assessed by MIC assays performed by microbroth dilution in 96-well microtiter plates and turbidometric analysis at OD₆₀₀. The effect of pantothenate and its analogs on the antibiotic activity of CJ-15,801 against *S. aureus* was assessed in a checkerboard assay to calculate FICI indicative of synergy, additivity, indifference, or antagonism (Orhan et al., 2005).

PanK Assay and Data Analysis

Pantothenate kinase activity was determined using a continuous spectrophotometric assay that coupled the production of ADP to the consumption of NADH as described previously (Brand and Strauss, 2005; Strauss and Begley, 2002). All enzyme assays were based on decrease of NADH concentration, as monitored by change in absorbance at 340 nm. An extinction coefficient of 6,220 M⁻¹·cm⁻¹ was used for NADH. Assays were performed in 96-well UV transparent plates (Greiner Bio) and monitored for between 10 min and 1 hr at 25°C using a Perkin-Elmer HTS 7000 Bio-Assay Reader or a Thermo Scientific Varioskan Multimode Reader. For *EcPanK_I* and *SaPanK_{II}*, each 320 μl reaction contained ATP (1.5 mM), MgCl₂ (10 mM), KCl (20 mM), NADH (0.3 mM), phosphoenolpyruvate (0.5 mM), pyruvate kinase (5 units), and lactate dehydrogenase (5 units) in 50 mM HEPES buffer (pH 7.5). For *PaPanK_{III}*, each 300 μl contained ATP (5.0 mM), MgCl₂ (1 mM), NH₄Cl (60 mM), NADH (0.5 mM), phosphoenolpyruvate (2.0 mM), pyruvate kinase (2 units), and lactate dehydrogenase (2.75 units) in 100 mM HEPES buffer (pH 7.5). The concentration of pantothenate, CJ-15,801, and other substrate analogs was varied between 6.25 and 200 μM. Reactions were initiated by addition of *SaPanK_{II}* (3 μg), *EcPanK_I* (3.5 μg), or *PaPanK_{III}* (5 μg). Initial

velocities were calculated for each substrate concentration and fitted to the Michaelis-Menten equation using Prism software (Graphpad) or SigmaPlot 11.0 (Systat software). All measurements were obtained in triplicate.

PPCS Assay and Data Analysis

PPCS assays were performed according to the published procedure (Patrone et al., 2009; Yao et al., 2009). The PPCS reaction was observed in the forward reaction via an enzyme-linked assay in which the pyrophosphate that is released during transfer of CMP from CTP to the substrate is continuously detected; this is achieved using the commercially available pyrophosphate reagent from Sigma-Aldrich (Cat. # P7275). Each vial of the pyrophosphate reagent was resuspended in 4.5 ml of dH₂O. The assays were performed on a Biotek PowerWave microplate spectrophotometer at 37°C. All curve-fitting analyses were performed using SigmaPlot 11.0 (Systat software).

Molecular Modeling

Modeling studies were performed using Accelrys Discovery Studio 3.1 (DS 3.1). The coordinates for *EcPPCS* Asn210Asp containing P-Pan-CMP as a cocrystallized ligand were obtained from the Protein Data Bank (PDB code: 1U7Z). The structure was optimized prior to any receptor-ligand calculations (full details of the receptor preparation are given in the Supplemental Experimental Procedures). Docking of P-CJ-CMP was accomplished using CDocker (Wu et al., 2003), launched from within DS 3.1. Deviations from the default settings included generating 150 starting conformations of the ligands to adequately sample conformational space and 50 poses were selected for simulated annealing. The top scoring pose (CDOCKER_Energy) was visually inspected and found to mimic the binding of the co-crystallized P-Pan-CMP. To ensure that the optimized water bridging the connection between the Asn210 amide side chain and the phosphate of P-Pan-CMP was not biasing the pose found in the docking, the exercise was repeated without this water molecule, which resulted in a nearly identical pose being found. Similarly, docking of P-CJ-CMP in the original structure of the *EcPPCS* Asn210Asp mutant (1U7Z) again showed that P-CJ-CMP very closely mimics the binding pose of the P-Pan-CMP molecule cocrystallized in the active site (Figure S4).

Protein Melting Temperature Determinations and Analysis

Protein melting curves were determined by measuring the heat-induced unfolding of the PPCS proteins by circular dichroism (CD) at 220 nm in a 0.5 mm cuvette using an Applied Photophysics Chirascan-Plus CD spectrometer. Samples contained the PPCS protein (10 μM) and MgCl₂ (1 mM) in 50 mM Tris-HCl buffer (pH 7.6) and CTP (150 μM), CTP and P-Pan (150 μM each), or CTP and P-CJ (150 μM each).

SUPPLEMENTAL INFORMATION

Supplemental Information includes four figures, three tables, and Supplemental Experimental Procedures and can be found with this article online at doi:10.1016/j.chembiol.2012.03.013.

ACKNOWLEDGMENTS

We thank the following persons for assistance with various experiments: Leisl Brand for the preparation of the *SaCoaBC*-expression vector, Andrew Mercer for expression of the PanK biosynthetic enzymes, Leanne Barnard for PanK assays, and Andrew Smith for synthesis of CJ-15,801. This project was funded by grants from the National Research Foundation (NRF; FA2007041600013) and Medical Research Council (MRC) of South Africa to E.S., and from National Institutes of Health to V.N. (GM084350), J.C.H. (T32CA009523), and M.D.B. (R01GM086225). R.v.d.W. was supported by a scarce skills scholarship from the NRF. Author contributions: R.v.d.W. prepared the proteins, performed all the PPCS enzyme activity assays and inhibitor characterization studies, and prepared P-CJ-OMe; J.C.H. and J.L.M. prepared all other compounds; J.L.M. performed PanK kinetic assays; S.D. and V.N. performed the inhibition studies and analyzed the resulting data; W.J.A.M. performed the melting temperature determinations; S.C.P. was responsible for the modeling studies; M.D.B. and E.S. designed and directed the research, and E.S. wrote the paper with input from all the authors.

Received: December 21, 2011

Revised: March 13, 2012

Accepted: March 27, 2012

Published: May 24, 2012

REFERENCES

- Balibar, C.J., Hollis-Symynkywicz, M.F., and Tao, J. (2011). Pantothenate rescues phosphopantothenoylcysteine synthetase and phosphopantothenoylcysteine decarboxylase deficiency in *Escherichia coli* but not in *Pseudomonas aeruginosa*. *J. Bacteriol.* **193**, 3304–3312.
- Brand, L.A., and Strauss, E. (2005). Characterization of a new pantothenate kinase isoform from *Helicobacter pylori*. *J. Biol. Chem.* **280**, 20185–20188.
- Brownell, J.E., Sintchak, M.D., Gavin, J.M., Liao, H., Bruzzese, F.J., Bump, N.J., Soucy, T.A., Milhollen, M.A., Yang, X., Burkhardt, A.L., et al. (2010). Substrate-assisted inhibition of ubiquitin-like protein-activating enzymes: the NEDD8 E1 inhibitor MLN4924 forms a NEDD8-AMP mimetic in situ. *Mol. Cell* **37**, 102–111.
- Chen, J.J., Tsu, C.A., Gavin, J.M., Milhollen, M.A., Bruzzese, F.J., Mallender, W.D., Sintchak, M.D., Bump, N.J., Yang, X., Ma, J., et al. (2011). Mechanistic studies of substrate-assisted inhibition of ubiquitin-activating enzyme by adenosine sulfamate analogues. *J. Biol. Chem.* **286**, 40867–40877.
- Choudhry, A.E., Mandichak, T.L., Broskey, J.P., Egoif, R.W., Kinsland, C., Begley, T.P., Seefeld, M.A., Ku, T.W., Brown, J.R., Zalacain, M., and Ratnam, K. (2003). Inhibitors of pantothenate kinase: novel antibiotics for staphylococcal infections. *Antimicrob. Agents Chemother.* **47**, 2051–2055.
- Cisar, J.S., and Tan, D.S. (2008). Small molecule inhibition of microbial natural product biosynthesis—an emerging antibiotic strategy. *Chem. Soc. Rev.* **37**, 1320–1329.
- Clifton, G., Bryant, S.R., and Skinner, C.G. (1970). N'-(substituted) pantothenamides, antimetabolites of pantothenic acid. *Arch. Biochem. Biophys.* **137**, 523–528.
- Copeland, R.A. (2000). Tight binding inhibitors. In *Enzymes: A Practical Introduction to Structure, Mechanism, and Data Analysis* (New York: Wiley-VCH), pp. 305–317.
- Copeland, R.A. (2005). Tight binding inhibitors. In *Evaluation of Enzyme Inhibitors in Drug Discovery* (Hoboken, NJ: Wiley), pp. 179–213.
- delCardayre, S.B., and Davies, J.E. (1998). *Staphylococcus aureus* coenzyme A disulfide reductase, a new subfamily of pyridine nucleotide-disulfide oxidoreductase. Sequence, expression, and analysis of *cdr*. *J. Biol. Chem.* **273**, 5752–5757.
- Gulick, A.M. (2009). Conformational dynamics in the Acyl-CoA synthetases, adenylation domains of non-ribosomal peptide synthetases, and firefly luciferase. *ACS Chem. Biol.* **4**, 811–827.
- Han, C., Shen, R., Su, S., and Porco, J.A., Jr. (2004). Copper-mediated synthesis of *N*-acyl vinyllogous carbamic acids and derivatives: synthesis of the antibiotic CJ-15,801. *Org. Lett.* **6**, 27–30.
- Hollenhorst, M.A., Ntai, I., Badet, B., Kelleher, N.L., and Walsh, C.T. (2011). A head-to-head comparison of enamide and epoxyamide inhibitors of glucosamine-6-phosphate synthase from the dapdiamide biosynthetic pathway. *Biochemistry* **50**, 3859–3861.
- Hong, B.S., Yun, M.K., Zhang, Y.-M., Chohnan, S., Rock, C.O., White, S.W., Jackowski, S., Park, H.-W., and Leonardi, R. (2006). Prokaryotic type II and type III pantothenate kinases: the same monomer fold creates dimers with distinct catalytic properties. *Structure* **14**, 1251–1261.
- Imtiaz, U., Billings, E., Knox, J.R., Manavathu, E.K., Lerner, S.A., and Mobashery, S. (1993). Inactivation of class A beta-lactamases by clavulanic acid: the role of arginine-244 in a proposed nonconcerted sequence of events. *J. Am. Chem. Soc.* **115**, 4435–4442.
- Kim, S., Lee, S.W., Choi, E.C., and Choi, S.Y. (2003). Aminoacyl-tRNA synthetases and their inhibitors as a novel family of antibiotics. *Appl. Microbiol. Biotechnol.* **61**, 278–288.
- Kucharczyk, N., Denisot, M.A., Le Goffic, F., and Badet, B. (1990). Glucosamine-6-phosphate synthase from *Escherichia coli*: determination of the mechanism of inactivation by N3-fumaroyl-L-2,3-diaminopropionic derivatives. *Biochemistry* **29**, 3668–3676.
- Kupke, T. (2002). Molecular characterization of the 4'-phosphopantothenoylcysteine synthetase domain of bacterial dfp flavoproteins. *J. Biol. Chem.* **277**, 36137–36145.
- Kupke, T. (2004). Active-site residues and amino acid specificity of the bacterial 4'-phosphopantothenoylcysteine synthetase CoaB. *Eur. J. Biochem.* **271**, 163–172.
- Lee, J.M., Ahn, D.-S., Jung, D.Y., Lee, J., Do, Y., Kim, S.K., and Chang, S. (2006). Hydrogen-bond-directed highly stereoselective synthesis of Z-enamides via Pd-catalyzed oxidative amidation of conjugated olefins. *J. Am. Chem. Soc.* **128**, 12954–12962.
- Leonardi, R., Chohnan, S., Zhang, Y.-M., Virga, K.G., Lee, R.E., Rock, C.O., and Jackowski, S. (2005). A pantothenate kinase from *Staphylococcus aureus* refractory to feedback regulation by coenzyme A. *J. Biol. Chem.* **280**, 3314–3322.
- Mallett, T.C., Wallen, J.R., Karplus, P.A., Sakai, H., Tsukihara, T., and Claiborne, A. (2006). Structure of coenzyme A-disulfide reductase from *Staphylococcus aureus* at 1.54 Å resolution. *Biochemistry* **45**, 11278–11289.
- Manoj, N., Strauss, E., Begley, T.P., and Ealick, S.E. (2003). Structure of human phosphopantothenoylcysteine synthetase at 2.3 Å resolution. *Structure* **11**, 927–936.
- May, J.J., Finking, R., Wiegeshoff, F., Weber, T.T., Bandur, N., Koert, U., and Marahiel, M.A. (2005). Inhibition of the D-alanine:D-alanyl carrier protein ligase from *Bacillus subtilis* increases the bacterium's susceptibility to antibiotics that target the cell wall. *FEBS J.* **272**, 2993–3003.
- Mercer, A.C., and Burkart, M.D. (2007). The ubiquitous carrier protein—a window to metabolite biosynthesis. *Nat. Prod. Rep.* **24**, 750–773.
- Mercer, A.C., Meier, J.L., Torpey, J.W., and Burkart, M.D. (2009). In vivo modification of native carrier protein domains. *ChemBioChem* **10**, 1091–1100.
- Newton, G.L., Arnold, K., Price, M.S., Sherrill, C., Delcardayre, S.B., Aharonowitz, Y., Cohen, G., Davies, J., Fahey, R.C., and Davis, C. (1996). Distribution of thiols in microorganisms: mycothiol is a major thiol in most actinomycetes. *J. Bacteriol.* **178**, 1990–1995.
- Nicely, N.I., Parsonage, D., Paige, C., Newton, G.L., Fahey, R.C., Leonardi, R., Jackowski, S., Mallett, T.C., and Claiborne, A. (2007). Structure of the type III pantothenate kinase from *Bacillus anthracis* at 2.0 Å resolution: implications for coenzyme A-dependent redox biology. *Biochemistry* **46**, 3234–3245.
- Nicolaou, K.C., and Mathison, C.J.N. (2005). Synthesis of imides, *N*-acyl vinyllogous carbamates and ureas, and nitriles by oxidation of amides and amines with Dess-Martin periodinane. *Angew. Chem. Int. Ed. Engl.* **44**, 5992–5997.
- Orhan, G., Bayram, A., Zer, Y., and Balci, I. (2005). Synergy tests by E test and checkerboard methods of antimicrobial combinations against *Brucella melitensis*. *J. Clin. Microbiol.* **43**, 140–143.
- Padayatti, P.S., Helfand, M.S., Totir, M.A., Carey, M.P., Carey, P.R., Bonomo, R.A., and van den Akker, F. (2005). High resolution crystal structures of the trans-enamine intermediates formed by sulbactam and clavulanic acid and E166A SHV-1 β-lactamase. *J. Biol. Chem.* **280**, 34900–34907.
- Padayatti, P.S., Sheri, A., Totir, M.A., Helfand, M.S., Carey, M.P., Anderson, V.E., Carey, P.R., Bethel, C.R., Bonomo, R.A., Buynak, J.D., and van den Akker, F. (2006). Rational design of a β-lactamase inhibitor achieved via stabilization of the trans-enamine intermediate: 1.28 Å crystal structure of wt SHV-1 complex with a penam sulfone. *J. Am. Chem. Soc.* **128**, 13235–13242.
- Patrone, J.D., Yao, J., Scott, N.E., and Dotson, G.D. (2009). Selective inhibitors of bacterial phosphopantothenoylcysteine synthetase. *J. Am. Chem. Soc.* **131**, 16340–16341.
- Pope, A.J., Moore, K.J., McVey, M., Mensah, L., Benson, N., Osbourne, N., Broom, N., Brown, M.J.B., and O'Hanlon, P. (1998). Characterization of isoleucyl-tRNA synthetase from *Staphylococcus aureus*. II. Mechanism of inhibition by reaction intermediate and pseudomonic acid analogues studied using transient and steady-state kinetics. *J. Biol. Chem.* **273**, 31691–31701.
- Saliba, K.J., and Kirk, K. (2005). CJ-15,801, a fungal natural product, inhibits the intraerythrocytic stage of *Plasmodium falciparum* in vitro via an effect on pantothenic acid utilisation. *Mol. Biochem. Parasitol.* **141**, 129–131.

Chemistry & Biology

Mode of Action of the Antibiotic CJ-15,801

- Schimmel, P., Tao, J., and Hill, J. (1998). Aminoacyl tRNA synthetases as targets for new anti-infectives. *FASEB J.* *12*, 1599–1609.
- Sewell, A.L., Villa, M.V.J., Matheson, M., Whittingham, W.G., and Marquez, R. (2011). Fast and flexible synthesis of pantothenic acid and CJ-15,801. *Org. Lett.* *13*, 800–803.
- Sieber, S.A., and Marahiel, M.A. (2005). Molecular mechanisms underlying nonribosomal peptide synthesis: approaches to new antibiotics. *Chem. Rev.* *105*, 715–738.
- Spry, C., Kirk, K., and Saliba, K.J. (2008). Coenzyme A biosynthesis: an antimicrobial drug target. *FEMS Microbiol. Rev.* *32*, 56–106.
- Spry, C., van Schalkwyk, D.A., Strauss, E., and Saliba, K.J. (2010). Pantothenate utilization by Plasmodium as a target for antimalarial chemotherapy. *Infect. Disord. Drug Targets* *10*, 200–216.
- Stanitzek, S., Augustin, M.A., Huber, R., Kupke, T., and Steinbacher, S. (2004). Structural basis of CTP-dependent peptide bond formation in coenzyme A biosynthesis catalyzed by *Escherichia coli* PPC synthetase. *Structure* *12*, 1977–1988.
- Strauss, E. (2010). Coenzyme A biosynthesis and enzymology. In *Comprehensive Natural Products II Chemistry and Biology*, L. Mander and H.-W. Liu, eds. (Oxford: Elsevier), pp. 351–410.
- Strauss, E., and Begley, T.P. (2001). Mechanistic studies on phosphopantothenoylcysteine decarboxylase. *J. Am. Chem. Soc.* *123*, 6449–6450.
- Strauss, E., and Begley, T.P. (2002). The antibiotic activity of *N*-pentylpantothenamide results from its conversion to ethyldeithia-coenzyme a, a coenzyme a antimetabolite. *J. Biol. Chem.* *277*, 48205–48209.
- Strauss, E., Kinsland, C., Ge, Y., McLafferty, F.W., and Begley, T.P. (2001). Phosphopantothenoylcysteine synthetase from *Escherichia coli*. Identification and characterization of the last unidentified coenzyme A biosynthetic enzyme in bacteria. *J. Biol. Chem.* *276*, 13513–13516.
- Strauss, E., de Villiers, M., and Rootman, I. (2010). Biocatalytic production of coenzyme A analogues. *ChemCatChem* *2*, 929–937.
- Sugie, Y., Dekker, K.A., Hirai, H., Ichiba, T., Ishiguro, M., Shiomi, Y., Sugiura, A., Brennan, L., Duignan, J., Huang, L.H., et al. (2001). CJ-15,801, a novel antibiotic from a fungus, *Seimatosporium sp.* *J. Antibiot.* *54*, 1060–1065.
- Thomas, J., and Cronan, J.E. (2010). Antibacterial activity of *N*-pentylpantothenamide is due to inhibition of coenzyme a synthesis. *Antimicrob. Agents Chemother.* *54*, 1374–1377.
- van der Westhuyzen, R., and Strauss, E. (2010). Michael acceptor-containing coenzyme A analogues as inhibitors of the atypical coenzyme A disulfide reductase from *Staphylococcus aureus*. *J. Am. Chem. Soc.* *132*, 12853–12855.
- van Wyk, M., and Strauss, E. (2008). Development of a method for the parallel synthesis and purification of *N*-substituted pantothenamides, known inhibitors of coenzyme A biosynthesis and utilization. *Org. Biomol. Chem.* *6*, 4348–4355.
- Villa, M.V.J., Targett, S.M., Barnes, J.C., Whittingham, W.G., and Marquez, R. (2007). An efficient approach to the stereocontrolled synthesis of enamides. *Org. Lett.* *9*, 1631–1633.
- Virga, K.G., Zhang, Y.-M., Leonardi, R., Ivey, R.A., Hevener, K., Park, H.-W., Jackowski, S., Rock, C.O., and Lee, R.E. (2006). Structure-activity relationships and enzyme inhibition of pantothenamide-type pantothenate kinase inhibitors. *Bioorg. Med. Chem.* *14*, 1007–1020.
- Wu, G., Robertson, D.H., Brooks, C.L., 3rd, and Vieth, M. (2003). Detailed analysis of grid-based molecular docking: A case study of CDocker-A CHARMm-based MD docking algorithm. *J. Comput. Chem.* *24*, 1549–1562.
- Yang, K., Eyobo, Y., Brand, L.A., Martynowski, D., Tomchick, D., Strauss, E., and Zhang, H. (2006). Crystal structure of a type III pantothenate kinase: insight into the mechanism of an essential coenzyme A biosynthetic enzyme universally distributed in bacteria. *J. Bacteriol.* *188*, 5532–5540.
- Yang, K., Strauss, E., Huerta, C., and Zhang, H. (2008). Structural basis for substrate binding and the catalytic mechanism of type III pantothenate kinase. *Biochemistry* *47*, 1369–1380.
- Yao, J., and Dotson, G.D. (2009). Kinetic characterization of human phosphopantothenoylcysteine synthetase. *Biochim. Biophys. Acta* *1794*, 1743–1750.
- Yao, J., Patrone, J.D., and Dotson, G.D. (2009). Characterization and kinetics of phosphopantothenoylcysteine synthetase from *Enterococcus faecalis*. *Biochemistry* *48*, 2799–2806.
- Zhang, Y.-M., Frank, M.W., Virga, K.G., Lee, R.E., Rock, C.O., and Jackowski, S. (2004). Acyl carrier protein is a cellular target for the antibacterial action of the pantothenamide class of pantothenate antimetabolites. *J. Biol. Chem.* *279*, 50969–50975.